LUND UNIVERSITY

Twisted Loops and Models for Form-factors and the Muon g-2

Relefors, Johan

Published: 2016-01-01

Document Version
Publisher's PDF, also known as Version of record

Link to publication

Citation for published version (APA):
Relefors, J. (2016). Twisted Loops and Models for Form-factors and the Muon g-2 Lund: Lund University, Faculty of Science, Department of Astronomy and Theoretical Physics

General rights
Copyright and moral rights for the publications made accessible in the public portal are retained by the authors and/or other copyright owners and it is a condition of accessing publications that users recognise and abide by the legal requirements associated with these rights.

- Users may download and print one copy of any publication from the public portal for the purpose of private study or research.
- You may not further distribute the material or use it for any profit-making activity or commercial gain
- You may freely distribute the URL identifying the publication in the public portal ?

Take down policy
If you believe that this document breaches copyright please contact us providing details, and we will remove access to the work immediately and investigate your claim.

LUND UNIVERSITY

PO Box 117
221 00 Lund
+46 46-222 00 00

Twisted Loops and Models for Form-factors and the Muon g-2

Twisted Loops and Models for Form-factors and the Muon g-2

by Johan Relefors

LUND UNIVERSITY

Thesis for the degree of Doctor of Philosophy in Engineering in the subject of Theoretical Physics
Thesis advisor: Prof. Johan Bijnens
Faculty opponent: Prof. Joan Soto

To be presented, with the permission of the Faculty of Science of Lund University, for public criticism in the Lundmark lecture hall (Lundmarksalen) at the Department of Astronomy and Theoretical Physics on Friday, the 21st of October 2016 at 13:00.

DOKUMENTDATABLAD enl SIS 61 41 21

Organization
LUND UNIVERSITY

Department of Astronomy and Theoretical Physics
Sölvegatan 14A
SE-223 62 Lund
Sweden

Author(s)
Johan Relefors

Document name
DOCTORAL DISSERTATION

Date of issue
2016-10-21

Sponsoring organization

Title and subtitle
Twisted Loops and Models for Form-factors and the Muon g-2

Abstract
In this thesis we use effective field thory methods and models for low energy QCD in two different contexts. One is direct calculation of contributions to the anomalous magnetic moment of the muon, muon $g-2$. The other is estimates of systematic sources of uncertainty in lattice QCD simulations. The work is presented in five papers. Papers II, IV and V describe calculations for muon $g-2$ and papers I, III and V contain estimates of various systematic effects in lattice QCD simulations.

Paper I deals with the use of twisted boundary conditions. Using χPT we calculate one loop effects of twisted boundary conditions for a number of different observables. Furhtermore, we show how the direction dependence of masses, which shows up when using twisted boundary conditions, should be taken into account in order to fulfill Ward identities.

Twisted boundary conditions together with other effects are considered in papers III and V as well. In paper V we use partially twisted partially quenched χPT at two loops to estimate the systematic uncertainties in hadronic vacuum polarization which is relevant for muon $g-2$. In paper III we estimate systematic uncertainties for K_{l3} decays, which are relevant for the CKM matrix element V_{us}, using partially twisted partially quenched rooted staggered χPT at one loop.

In paper II we use several different models to compute the pion loop contribution to hadronic light-by-light scattering. Most models are inspired by vector meson dominance but we try to go beyond that and include also the lightest axial vector meson, a_1. We also present an estimate of the ratio of disconnected to connected contributions to hadronic light-by-light scattering relevant for lattice QCD.

In paper IV we use χPT to estimate the ratio between disconnected and connected contributions to hadronic vacuum polarization. This was studied in earlier work at one loop. We give an underlying reason for their result and show that the ratio holds for a large part of the higher loop corrections. We also discuss corrections to the ratio.

Key words
Chiral perturbation theory, Twisted boundary conditions, Phenomenological models, Muon g-2

Classification system and/or index terms (if any)

Supplementary bibliographical information

Language
English

ISSN and key title

ISBN
978-91-7623-975-9 (print)
978-91-7623-976-6 (pdf)

Recipient's notes

Number of pages
205

Price

Security classification

I, the undersigned, being the copyright owner of the abstract of the above-mentioned dissertation, hereby grant to all reference sources the permission to publish and disseminate the abstract of the above-mentioned dissertation.

Signature 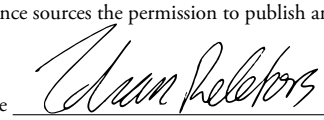 Date 2016-09-13

Twisted Loops and Models for Form-factors and the Muon g-2

by Johan Relefors

LUND
UNIVERSITY

A doctoral thesis at a university in Sweden takes either the form of a single, cohesive research study (monograph) or a summary of research papers (compilation thesis), which the doctoral student has written alone or together with one or several other author(s).

In the latter case the thesis consists of two parts. An introductory text puts the research work into context and summarizes the main points of the papers. Then, the research publications themselves are reproduced, together with a description of the individual contributions of the authors. The research papers may either have been already published or are manuscripts at various stages (in press, submitted, or in draft).

Cover illustration front: Giant torii gate at Itsukushima, also known as Miyajima, outside Hiroshima. One of Japan's three best views.

Cover illustration back: Background of key words.

© Johan Relefors 2016

Faculty of Science, Department of Astronomy and Theoretical Physics

ISBN: 978-91-7623-975-9 (print)
ISBN: 978-91-7623-976-6 (pdf)

Printed in Sweden by Media-Tryck, Lund University, Lund 2016

In memory of Martin and Max Pajuste

Contents

List of publications ii
Acknowledgments iii
Populärvetenskaplig sammanfattning på svenska v

Twisted Loops and Models for Form-factors and the Muon g-2 **1**
1 Introduction 1
2 Particle physics and the Standard Model 2
3 Quantum field theory 7
4 Effective field theory 16
5 QCD and symmetries 20
6 Chiral perturbation theory 31
7 Lattice QCD 39
8 Models for low energy QCD and the muon $g-2$ 51

Scientific publications **59**
Paper I: Masses, decay constants and electromagnetic form-factors with twisted boundary conditions 63
Paper II: Pion light-by-light contributions to the muon $g-2$ 89
Paper III: Partially quenched rooted staggered twisted finite volume corrections to K_{l3} decays 117
Paper IV: Connected, Disconnected and Strange Quark Contributions to HVP . 147
Paper V: Vector two point functions in finite volume using partially quenched chiral perturbation theory at two loops 165

List of publications

This thesis is based on the following publications, referred to by their Roman numerals:

I **Masses, decay constants and electromagnetic form-factors with twisted boundary conditions**

J. Bijnens, **J. Relefors**
JHEP **1405** (2014) 015 [arXiv:1402.1385 [hep-lat]]

II **Pion light-by-light contributions to the muon $g-2$**

J. Bijnens, **J. Relefors**
Accepted for publication by JHEP [arXiv:1608.01454 [hep-ph]], LU TP 16-44

III **Partially quenched rooted staggered twisted finite volume corrections to K_{l3} decays**

Claude Bernard, Johan Bijnens, Elvira Gámiz, **J. Relefors**
Draft, LU TP 16-50

IV **Connected, Disconnected and Strange Quark Contributions to HVP**

J. Bijnens, **J. Relefors**
Submitted to JHEP [arXiv:1609.01573 [hep-lat]], LU TP 16-49

V **Vector two point functions in finite volume using partially quenched chiral perturbation theory at two loops**

J. Bijnens, **J. Relefors**
Draft, LU TP 16-51

All papers are reproduced with permission of their respective publishers.

Publications not included in this thesis:

Masses, decay constants and electromagnetic form-factors with twisted boundary conditions

J. Bijnens, **J. Relefors**
PoS CD **15** (2016) 059 [arXiv:1509.07295 [hep-lat]]

Acknowledgments

The most important person to thank is the most important person in my life, my wife Jessica. The last few years have been tough in many ways and your support and belief in my ability has been invaluable. I love you and I couldn't have done this without you. During our time in Lund you have given birth to our awesome kids, Varja and Aron. While it is too early to tell the end result, they really are perfect. I hope that I have had a positive impact on them but I know you have.

I want to thank my parents and siblings. You are the most helpful when I need it the most. I wish that we didn't live so far from each other. I furthermore had great support from Jessica's family who also helped in taking care of Varja and Aron when I was working hard to get this thesis done.

I am grateful that I got the chance to do research in Lund. Hans, you are a great researcher and I have learned a lot from you. A special thanks for all the hard work during the last few months to get everything ready. Moreover, I want to thank Hans, and the rest of the department, for always keeping their doors open for questions.

In completing this book I have had great help from Torbjörn Sjöstrand who has read the introduction and papers giving valuable feedback. I wish I could read as carefully as you do. The introduction to the thesis was also improved by comments from Christian Bierlich, Ilkka Helenius, Jonas Wessén, Harsh Shah and Johan Rahtsman. The template which I have used was created by Daniel Michalik; thank you for helping me getting it up and running.

I want to thank all the PhD students at the department for a friendly atmosphere and for always listening. A special thanks to Jonas for all the discussions on quantum field theory and Harsh for all his questions and ideas; we should all be more open with what we don't know. I further take this opportunity to wish the new PhD students, Astrid Ordell and Nils Hermansson Truedsson, good luck! Too bad you will not be able to use the Thesis Maker like the Monte Carlo people!

I have had the good fortune of having two postdocs, Stefan Lanz and Alexey Vladimirov, as office mates. You both taught me much and I thoroughly enjoyed our time together. Stefan, too bad you had to move back to your home country, whichever it is. I really miss our movie nights. Alexey, too bad the GR project didn't work out, I'm glad that I got to work with you either way. Luckily for me, sharing an office is not the only way to meet postdocs. This gives me reason to thank Ilkka Helenius for teaching me all about finish culture, from acceptable sauna behavior to finish reggae. You could have said that I could play my own music on the car stereo on the way to Trysil, instead of when we were almost home already!

I've benefitted from the people upstairs as well. A special thanks to Carsten Peterson for interesting and entertaining conversations about everything and for helping me put my life in perspective. That your voice reminds me of the audio book version of "Bombibitt och jag" is a nice bonus. I also want to thank the runners at the department spearheaded by Anders Irbäck.

On the private side there are so many people that I want to thank. That we happened to move to an apartment two steps from people we met playing beach volleyball, and that these people turned out to be so fantastic, is one of the main reasons why Lund has been such a good place to live. Thank you for everything, except for stealing our estimated date of birth, Billing family. Although not living so close might be good for your blood sugar levels I do miss the time at Måsvägen.

Playing beach volleyball has been a great way of meeting people that we would otherwise not have met. Henric and Amanda Wilson Nilsson, life in Norra Fäladen was much better when you were around. Without you guys we will never make 50 vaniljbullar and eat them at once again. Don't know if that is a bad thing. I hope I never forget the magic day in Kalmar this summer. Note that you are the only family which I thank which does not yet have kids.

We also met Greger and Lina while playing beach volleyball. You guys are great to hang out with and I wish we would meet more often. One thing that I like in particular is that you are so earnest while still being a lot of fun.

There are people who we have met outside the context of beach volleyball. Our neighbors Anna and Jörgen with kids for example. Although we share many experiences you have so much more wisdom than we do. It is great to have older friends! I'm also happy that Jessica had the crazy idea of inviting Emelie and Jakob for dinner before we knew them. Together you seem to stand on your own four feet and discussing life's issues with you really puts them in perspective. Finally I come to the last little family, Malin and Warren with kids. Your hard training while having kids is really inspiring. I really enjoyed our trip to Härnösand and watching you race.

Populärvetenskaplig sammanfattning på svenska

Inom fysik försöker vi beskriva naturfenomen med matematiska modeller. Beroende på vilket system som ska beskrivas är olika modeller relevanta. På väldigt långa avstånd är gravitation den viktigaste kraften. Till exempel så beskrivs solsystemets dynamik av gravitation. På de kortaste avstånd som människan lyckats studera är det istället den elektromagnetiska, den svaga och den starka kraften som är viktigast. Till exempel så är det den elektromagnetiska kraften som binder negativt laddade elekroner vid positivt laddade atomkärnor, den svaga kraften som leder till neutronsönderfall och den starka kraften som sammanbinder kvarkar till neutroner och protoner.

Som tur är för naturvetenskapen så behöver vi nästan aldrig ta hänsyn till alla fyra krafterna. I praktiken så beskriver fysiken istället fenomen med hjälp av modeller som fångar det som är intressant för det system som studeras. Till exempel så beskrivs den kraft som håller samman atomkärnor ofta med potentialer mellan protoner och neutroner. Den underliggande fysiken domineras i det här fallet av den starka kraften men för att effektivt beskriva systemet så används en annan modell. Detta är en approximation som är användbar så länge växelverkan inte studeras vid alltför små avstånd. Generellt så kan man säga att vilka krafter och vilka andra frihetsgrader som är viktiga beror på typiska avstånd i det system som studeras.

Inom partikelfysik så studeras partiklar på korta avstånd där den elektromagnetiska, den svaga och den starka kraften dominerar. Dessa krafter beskriver växelverkan mellan elementarpartiklar. Elementarpartiklar är partiklar som, enligt vår nuvarande kunskap, inte går att dela upp i mindre beståndsdelar. Hur de olika krafterna påverkar elementarpartiklarna beror på partiklarnas laddningar. Till exempel så har en elektron elektromagnetisk och svag laddning, vilket ofta beskrivs som att elektronen växelverkar elektromagnetiskt och svagt. Den gällande beskrivningen av elementarpartiklar och deras växelverkan via den elektromagnetiska, svaga och starka kraften är Standardmodellen.

Ett mål inom partikelfysik är att beskriva alla fyra krafterna inom en och samma teori. Standardmodellen beskriver inte gravitation och måste således utökas för att nå detta mål. Det finns också astronomiska observationer som tyder på att det finns mörk materia som inte har någon naturlig förklaring inom Standardmodellen. För att nå vidare i strävan efter en mer komplett modell så behövs det observationer som Standardmodellen inte kan beskriva.

Ett sätt att testa Standardmodellen är att kollidera partiklar vid allt högre energier i hopp om att se spår av nya tunga partiklar. Ett annat sätt är att förbättra precisionen i teori och experiment vid lägre energier. Hittills okända partiklar kan påverka värdet av fysikaliska storheter vid låga energier genom kvanteffekter. En utmaning för sådan precisionsfysik är att det inte finns analytiska metoder för att göra beräkningar som involverar den starka kraften, som den beskrivs i Standardmodellen, vid låga energier.

En mycket vanlig analytisk metod, som inte fungerar för den starka kraften vid låga energier, är störningsräkning. I störningsräkning så utgår vi från en modell där vi kan göra beräkningar. Effekter som hindrar exakta beräkningar tas med som små störningar runt denna modell. För att detta ska vara en bra approximation så måste störningen vara liten, vilket inte är fallet för den starka växelverkan vid låga energier. Vid låga energier så är den starka kraften så stark att alla partiklar som har stark laddning, så kallad färgladdning, bildar bundna tillstånd. Dessa bundna tillstånd är färgneutrala, inga färgladdade tillstånd observeras.

För att göra förutsägelser vid låg energi så kan man använda störningsräkning för bundna tillstånd. Detta är en approximation som är användbar vid tillräckligt låga energier. I avhandlingen används denna typ av störningsräkning för att göra precisionsberäkningar av en del av myonens, en tyngre version av elektronen, växelverkan med magnetfält. Detta är en mycket precist uppmätt storhet och det finns sedan länge en skillnad mellan förutsägelser från Standardmodellen och det experimentella värdet. I våra beräkninar så försöker vi ta hänsyn till fler effekter än tidigare och gör en uppskattning av värdet genom att jämföra många olika modeller.

Ett annat sätt att göra beräkningar med den starka kraften vid låga energier är att göra numeriska beräkningar. I dessa simuleringar så ersätts rumtiden med ett gitter i en ändlig volym. Fysikaliska storheter som bestämms med denna metod har både statistiska och systematiska fel. För att uppskatta vissa systematiska fel så är återigen störningsräkning med bundna tillstånd användbart. Då de systematiska felen domineras av lätta tillstånd så är det möjligt för oss att använda kiral störningsräkning, en mycket väl underbyggd model, för att göra dessa uppskattningar.

I avhandlingen använder vi kiral störningsräkning för att uppskatta systematiska fel för gitterberäkningar relevanta för myonens växelverkan med magnetfält samt för svag växelverkan mellan bundna tillstånd, så kallade formfaktorer. Precis som med myonens växelverkan med magnetfält så används formfaktorer för att testa Standardmodellen.

Twisted Loops and Models for Form-factors and the Muon g-2

It is better to uncover a little than to cover a lot.
—Smart person

1 Introduction

In this introduction, as in any kind of writing, it is important to consider for whom I am writing. Since the actual research results are presented in the papers, I need not present these here, just give background to them. Therefore, I have decided to write as if to get myself from four, or maybe five, years ago up to speed on the topics. This was a time when I was a fresh PhD student with six chapters of Ref. [1] under my belt. My goal is to guide the reader from the theory of quantum chromodynamics (QCD) in the Standard Model (SM), describing interactions among quarks and gluons, to models of the low energy spectrum, describing interactions among bound states, ending up with how such models are used in the papers which constitute the main part of the thesis.

The work presented in the papers goes under the category of phenomenology. In the context of particle physics, phenomenology is the bridge between mathematical models and experiments. In other words, models are used to make predictions. The predictions presented in this thesis come in two kinds. One is using models of low energy QCD for calculation of (parts of) an observable physical quantity. The other is estimates of error sources when numerical simulations of QCD. In this case the actual physics is simulated elsewhere and our calculations are used to estimate part of the unphysical behavior in the simulations. In both these cases the practical work that we do is, to a large extent, algebraic manipulations of fairly large expressions. We do this using the algebraic manipulation software FORM [2] which, although not mentioned further in this introduction, has been an invaluable tool.

This introduction contains introductions to several topics which reflect the content of the

papers. First there is an introduction to the particles of the SM and unitary symmetry. Then there is an introduction to quantum field theory (QFT) and perturbation theory which is an important tool used in the papers. In the following section another important tool in contemporary particle physics, effective field theory (EFT), is briefly introduced. This is followed by an introduction to the symmetries of QCD and the low energy spectrum of QCD. In the section after that the combination of EFT ideas and the low energy symmetries of QCD, chiral perturbation theory (χPT), is introduced. The following section introduces χPT in the context of lattice QCD. The last section gives an introduction to other models for low energy QCD, specifically in the context of the muon anomalous magnetic moment, muon $g-2$.

Before moving on to introduce the SM I want to mention that if you are reading this from a popular science perspective I think it is appropriate to read section 2 up until around equation (1). I then recommend the introductory parts of sections 3, 4 and 8.

2 Particle physics and the Standard Model

The SM is our best description of the microscopic world. Microscopic is perhaps not the right word since the size of a proton is around one fermi[1] which is far from something studied in a microscope. The proton is in turn composed of quarks and gluons. These quarks and gluons are, to the best of our knowledge, not bound states but elementary particles.

The particles in the SM can be divided into different categories in many ways. As a first step we can separate fermions from bosons. Fermionic particles have the property that no two fermions can occupy the same state, this is known as Pauli's exclusion principle. Bosons on the other hand do not mind sticking together. Fermion fields are often associated with matter, the electron and the quarks are examples of fermions. Bosons are usually associated with force carriers, like the photon or gluon. The Higgs particle is also a boson but it plays a special role. The field associated with the Higgs boson gives mass to the other particles.

The forces in the SM are the electromagnetic (EM), the weak and the strong force. The association between bosons and forces is that the forces are a result of exchanging the associated bosons. Electrically charged objects interact through the EM force by exchanging photons. This can be formulated as that the photon couples to electric charge and thereby mediates the EM force. The weak bosons, $W^{\pm}$ and Z, couple to weak charge and mediate the weak force and the strong force is mediated by eight gluons, G^a, $a = 1, \ldots, 8$, which couple to the three strong charges called red, green and blue.

[1] 1 fermi = 1 fm = 10^{-15} meters

The behavior of the three forces is quite different. The photon is massless and carries no charge. This gives a long ranged force. The weak bosons are massive and carry weak charge. The mass of the bosons gives a short range force, explaining the weakness of the weak force at long distances. The gluons are massless and carry color charge. The combination of being massless and self interacting gives a radically different behavior from the other two forces. While the EM and weak forces grows weaker at long distances, the strong force is constant for long distances so that the energy between two color charges increases with distance. An experimental consequence of this is that only color neutral objects are observed, this is known as confinement[2].

The fermions in the SM are associated with matter. To describe most matter only a subset of the fermions are needed. Ordinary matter is well described as being composed of atoms. An atom is a positively charged nucleus surrounded by negatively charged electrons. The electrons are kept in place by the EM force so the electron carries EM charge. The nucleus is composed of nucleons; positively charged protons and neutral neutrons. The protons and neutrons consist of quarks and gluons, the latter is what keeps the nucleons together. Since quarks interact with gluons they must carry color charge. Moreover, the electric charge of the proton comes from the electric charge of the quarks. The main quark content of the nucleons is up and down quarks. This is enough to describe stable matter. However, some atoms decay by a mechanism where a neutron is turned into a proton and an electron and another particle is released. This other particle is called a neutrino. Neutron decay is described by quarks, electrons and neutrinos interacting via the weak force. To summarize, the fermions needed are the electron which carry EM and weak charge, the up and down quarks which carry color, EM and weak charge and the electron neutrino which carries weak charge. This collection of fermions make up the first generation of fermions. There are two additional generations which have the exact same charges as the first generation. The only difference is that the masses increase for every generation, possibly with the exception of neutrinos whose masses are not well known. The masses and some properties of the quarks in the SM are given in Table 1.

Most of this thesis concerns the strong force at low energies, hereafter referred to as low energy QCD. Low energy is in this case less than about 1 GeV. At these energies QCD describes color neutral particles which are bound states of quarks and gluons. The most common color neutral particles are mesons, bound states formed from a quark and an antiquark, and baryons, bound states formed from three quarks. Mesons are color neutral since the constituents carry color and anticolor while baryons are color neutral since the constituents carry a red, a green and a blue charge.

The interactions of the bound states should in principle follow from QCD. However, there are no analytical methods to make quantitative predictions for these interactions. Instead,

[2] A color neutral object carries a color and its anticolor or (anti) red, (anti) green and (anti) blue which mixes to white. This is why color is a good analogy in this case.

models are used. An important guiding principle when constructing models is that of symmetry. Symmetries is the topic of the next section.

Table 1: Quark properties from [3]. Isospin symmetry is a symmetry transformation which treats the up and down quarks the same. The isospin value in the table gives the isospin charge of the quarks determining how they transform. A value of 0 means no transformation. Strangeness is a property of the strange quark. Both of these numbers are used in the classification of bound states, see Table 2. The quark masses cited are the $\overline{MS}$ ones.

flavor	mass	charge	isospin	strangeness
u	$2.3^{+0.7}_{-0.5}$ MeV	$2/3$	$1/2$	0
d	$4.8^{+0.5}_{-0.3}$ MeV	$-1/3$	$-1/2$	0
c	1.275 ± 0.025 GeV	$2/3$	0	0
s	95 ± 5 MeV	$-1/3$	0	-1
t	160^{+5}_{-4} GeV	$2/3$	0	0
b	4.18 ± 0.03 GeV	$-1/3$	0	0

2.1 Unitary symmetry

Symmetry is an important tool in physics. For example, we expect that two identical experiments performed one hundred meters from each other should give the same result. This is formalized as translation invariance which is a symmetry related to spacetime. In particle physics there are also internal symmetries. This kind of symmetry corresponds to transformations in an internal space, not in spacetime. An example is if all physical observables are unaffected by rotating two degrees of freedom into each other. This is not a rotation in spacetime but a rotation in a two-dimensional internal space. It is also possible to have approximate internal symmetries where the theory acquires a real symmetry in some limit. The limits can be things like turning off electromagnetism or setting some approximately equal masses equal.

In QCD there is an approximate symmetry of this kind for the three lightest quarks. The approximate symmetry becomes exact when the masses of the three lightest quarks are set equal and the EM and weak interactions are turned off. These three quarks are enough to form the lightest bound states of QCD. The approximate symmetry of QCD will have consequences for the properties of the bound states. In this section we outline how the approximate symmetry of QCD would manifest itself at the level of bound states.

A way to study this is by formalizing the symmetry on the level of quarks by constructing explicit symmetry transformations. These transformation properties lead to transformation properties of the bound states which are consequences of the underlying symmetry. These consequences can then be compared with experimental information. In this section we focus on the eight lightest pseudoscalar mesons. Some of their properties are listed in Table 2.

Table 2: Light pseudoscalar meson properties from [3]. The charge, isospin and strangeness can be determined from the quark content. In the last four rows the η and η' are states with definite mass while η_0 and η_8 have definite quark content. The two are related by a rotation, we say that η_0 and η_8 mix to form η and η'. Since this difference has little effect on the results in the papers we identify η with η_8 and η' with η_0 in the following.

meson	quark content	mass	charge	isospin	strangeness
$\pi^{\pm}$	$u\bar{d}/d\bar{u}$	140 MeV	±1	1	0
π^0	$\frac{u\bar{u}-d\bar{d}}{\sqrt{2}}$	135 MeV	0	1	0
$K^{\pm}$	$u\bar{s}/s\bar{u}$	494 MeV	±1	0	±1
$K^0/\bar{K}^0$	$d\bar{s}/d\bar{u}$	498 MeV	0	0	$+1/-1$
η		548 MeV	0	0	0
η'		958 MeV	0	0	0
η_8	$\frac{u\bar{u}+d\bar{d}-2s\bar{s}}{\sqrt{6}}$		0	0	0
η_0	$\frac{u\bar{u}+d\bar{d}+s\bar{s}}{\sqrt{3}}$		0	0	0

To give the transformation properties of the quarks, q, and antiquarks, $\bar{q}$, we define the following vectors

$$q = \begin{pmatrix} u & d & s \end{pmatrix}^T, \qquad \bar{q} = \begin{pmatrix} \bar{u} & \bar{d} & \bar{s} \end{pmatrix}. \tag{1}$$

In QCD all the terms involving quarks can be written as $\bar{q}^i A_i^j q_j$, where repeated indices are summed over which is a convention used throughout this introduction. In the case of equal masses, A is proportional to the identity matrix and all the terms can be written as $A\bar{q}^i q_i$. The theory is then symmetric under unitary transformations of q and $\bar{q}$ given by

$$\begin{aligned} q_i &\to U_i^j q_j \\ \bar{q}^i &\to \bar{q}^j U^{\dagger i}{}_j \\ \bar{q}^i q_i &\to \bar{q}^i U^{\dagger j}{}_i U_j^k q_k = \bar{q}^i q_i. \end{aligned} \tag{2}$$

Unitary matrices can be written as

$$U = \exp\left(-i \sum_{a=0}^{8} \frac{T^a}{2} \phi^a\right) \tag{3}$$

where ϕ^a are numbers and the nine matrices T^a are

$$T^0 = \frac{\sqrt{2}}{\sqrt{3}}\begin{pmatrix}1 & 0 & 0\\ 0 & 1 & 0\\ 0 & 0 & 1\end{pmatrix}, \quad T^1 = \begin{pmatrix}0 & 1 & 0\\ 1 & 0 & 0\\ 0 & 0 & 0\end{pmatrix}, \quad T^2 = \begin{pmatrix}0 & -i & 0\\ i & 0 & 0\\ 0 & 0 & 0\end{pmatrix},$$
$$T^3 = \begin{pmatrix}1 & 0 & 0\\ 0 & -1 & 0\\ 0 & 0 & 0\end{pmatrix}, \quad T^4 = \begin{pmatrix}0 & 0 & 1\\ 0 & 0 & 0\\ 1 & 0 & 0\end{pmatrix}, \quad T^5 = \begin{pmatrix}0 & 0 & -i\\ 0 & 0 & 0\\ i & 0 & 0\end{pmatrix},$$
$$T^6 = \begin{pmatrix}0 & 0 & 0\\ 0 & 0 & 1\\ 0 & 1 & 0\end{pmatrix}, \quad T^7 = \begin{pmatrix}0 & 0 & 0\\ 0 & 0 & -i\\ 0 & i & 0\end{pmatrix}, \quad T^8 = \frac{1}{\sqrt{3}}\begin{pmatrix}1 & 0 & 0\\ 0 & 1 & 0\\ 0 & 0 & -2\end{pmatrix}. \tag{4}$$

The eight matrices $T^1, \ldots, T^8$ form a closed algebra under the commutator

$$\left[T^a, T^b\right] = i f^{abc} T^c. \tag{5}$$

This kind of algebra is called a Lie algebra. The matrix T^0 is proportional to the identity and thus commutes with all the others. The traceless generators $T^1, \ldots, T^8$ generate the Lie group of unitary 3×3 matrices with determinant one, $SU(3)$. The generator T^0 generates the group $U(1)$ acting on a three-dimensional vector space. The diagonal generators play a special role, they can be used to classify the states of the vector space. For example the electric charges of the quarks are the eigenvalues of $Q = \frac{1}{2}T^3 + \frac{1}{2\sqrt{3}}T^8$.

For each of the mesons in Table 2 there is an associated matrix B such that $\bar{q}^i B_i^j q_j$ gives the quark content of that meson. With the caveat that a quark field q_i is associated with a $\bar{q}_i$ quark in QFT, and vice versa, the matrices associated with each meson, written in terms of the generators T^a, are[3]

$$\pi^+ = \frac{T^1 + iT^2}{2}, \qquad \pi^- = \frac{T^1 - iT^2}{2}, \qquad \pi^0 = \frac{T^3}{\sqrt{2}},$$
$$K^+ = \frac{T^4 + iT^5}{2}, \qquad K^- = \frac{T^4 - iT^5}{2}, \qquad K^0 = \frac{T^6 + iT^7}{2},$$
$$\bar{K}^0 = \frac{T^6 - iT^7}{2}, \qquad \eta = \frac{T^8}{\sqrt{2}}, \qquad \eta' = \frac{T^0}{\sqrt{2}}. \tag{6}$$

Applying a unitary transformation to $\bar{q}^i \pi^{+j}_{\ i} q_j$ gives, to lowest order in ϕ^a,

$$\begin{aligned}\bar{q}\pi^+ q \to & \bar{q}\pi^+ q + i\bar{q}\phi^a\left[T^a, \pi^+\right]q \\ = & \bar{q}\pi^+ q - \sum_{B \in \pi^\pm, \pi^0, K^\pm, K^0, \bar{K}^0, \eta, \eta'} i\phi^a \bar{q} B q\end{aligned} \tag{7}$$

[3]Note the comment about η, η', η_0 and η_8 in Table 2.

The mesons transform into each other due to the underlying symmetry. If the underlying symmetry was exact this means that there would be an exact symmetry also from these rotations. The symmetry is broken by electromagnetism and the quark masses, as seen in Table 2 but up to these effect all states are the same.

From Table 2 this symmetry looks badly broken. Both the masses and the charges differ between the mesons. On the other hand, ignoring the η' and comparing with the mass of the nucleons which are about 1 GeV the largest mass differences are of the order of 30%. Perhaps $SU(3)$ is a more likely candidate for an underlying symmetry than $U(1) \times SU(3)$. While the η' stands out by being heavy the pions stand out by being light. The subgroup $SU(2)$ of $SU(3)$ which treats up and down quarks as identical particles, but does not involve the strange quark, looks like the best candidate for an approximate symmetry. Exploring approximate symmetries of QCD is a large part of this introduction. This is done in the language of quantum field theory which is introduced next.

3 Quantum field theory

There is a famous experiment[4] called Young's double slit experiment, which shows that even single particles can behave like waves. In the experiment there is a single particle source and a detector in the form of a sheet which can detect single particles. In between these two, there is a screen with two holes. The source emits single particles and, from experience of the everyday world, the expectation would be that each particle goes through either one hole or the other. However, as more and more particles are released, one by one, an interference pattern is detected. The single particles behave as a wave would. An illustration of the experiment is given in Figure 1.

The interference pattern comes from that the particles do not travel a distinct path; in some sense they pass through both holes. Attempts to measure which hole the particles passes through destroys the interference pattern. The experimental result can be described using quantum mechanics (QM). In this case, QM predicts the probability for a particle to land in a given region of the detector. This probability is the square of a probability amplitude, denoted amplitude from now on. The total amplitude for passing through either slit is the sum of the amplitudes for passing through each slit separately. Summing the two contributions and taking the square gives an interference pattern in the particle's probability to land in a specific region of the screen. It is the amplitude which is wave like.

One way of calculating the total amplitude is to sum over all possible paths from the source to the detector with a weight assigned to each path. A given path is described by a coordinate which depends on the time. Suppressing one space direction, a path, P, is described by

[4] This whole section is inspired by [4].

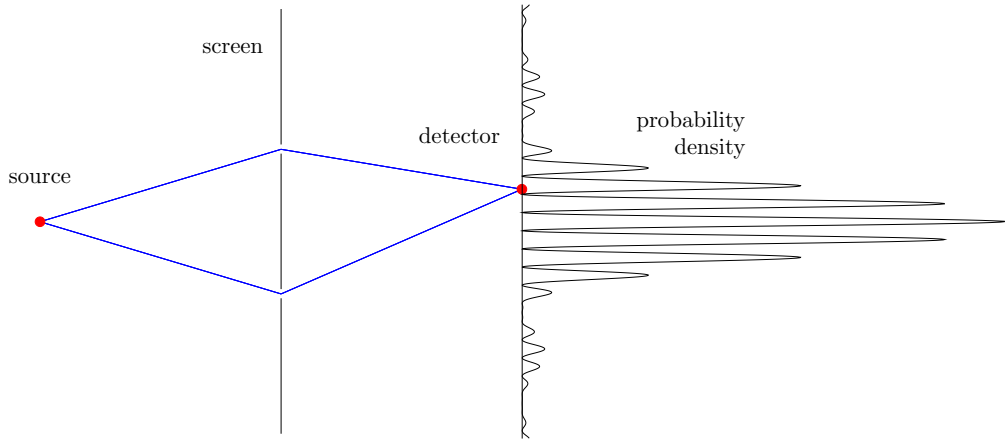

Figure 1: Double slit experiment experimental setup and probability density. The left most red point is the source. From the source, two possible paths through the double slit to a point on the detector are shown. On the right hand side of the detector the probability density for a single particle is shown. Given enough particles approximately this distribution is expected among the particles landing on the screen. Nothing is to scale.

$\vec{x}_P(t)$. A path always starts at the single particle source and ends on the detector. Choosing a specific point on the detector, the sum of all weighted paths from the source to that point gives the contribution to the amplitude from that point. The correct weight to assign to this path is

$$w_P = \frac{1}{N} \exp\left(i \int d\,t\, L(x_P(t), \partial_t x_P(t)) \right), \tag{8}$$

where L is a Lagrangian describing the dynamics of the particle, $\partial_t x_P(t)$ is the derivative of $x_P(t)$ and N is a normalization factor such that the total probability to end up in any point is 1. The collection of all paths with fixed starting and end points is then

$$\frac{1}{N} \sum_{P \in \text{paths}} w_P = \frac{1}{N} \sum_{P \in \text{paths}} \exp\left(i \int d\,t\, L(x_P(t), \partial_t x_P(t)) \right) \tag{9}$$

which gives the total amplitude.

The reason for introducing this experiment here is that the same reasoning applies with no screen in between the source and detector. Summing over all weighted paths between two points gives the probability amplitude. This idea generalizes directly to quantum field theory (QFT).

The QFT description is different in that the degrees of freedom are no longer a fixed number of particles with a wave function each. Instead, to each point in spacetime we assign a value, call it $\phi(x)$ where x includes both spatial and temporal coordinates. ϕ is then called a field.

All ϕ particles are excitations in the same field. In QFT the quantities we are interested in can be calculated from time ordered correlation functions[5] of the field in different spacetime points. An example is the two point function, related to the mass of the particle,

$$\langle 0|T\{\phi(x)\phi(0)\}|0\rangle = \frac{1}{N}\int D\phi\phi(x)\phi(0)\exp\left(i\int d^4y\mathscr{L}(\phi(y),\partial\phi(y)\right). \tag{10}$$

Here $\int D\phi$ means sum over all possible field configurations and

$$\exp\left(i\int d^4y\mathscr{L}(\phi(y),\partial\phi(y))\right) \tag{11}$$

gives the weight to assign to each field configuration. $\mathscr{L}$ is the Lagrangian density describing the dynamics of the system, which we assume is a local functional of the field and derivatives of the field. The Lagrangian and the Lagrangian density are related by

$$L = \int d^3x\mathscr{L} \tag{12}$$

but in the following the Lagrangian density will be referred to as only the Lagrangian. The normalization factor N is

$$N = \int D\phi\exp\left(i\int d^4y\mathscr{L}(\phi(y),\partial\phi(y))\right). \tag{13}$$

There are issues of convergence in the above. To discuss these we assume that the quantum mechanical version of the path integral works. There is then still the problem that it is not clear whether summing over all field configurations makes sense. To remedy the situation we can introduce spacetime as a lattice, with lattice spacing a, instead of a continuum. This means that each point is itself a well defined quantum mechanical system and we have a countable number of these systems.

The systems couple through derivatives. Going to momentum space using a Fourier transform the derivatives give energy and momentum. The effect of the lattice is to allow momenta only up to a cutoff π/a. This is reasonable also from a physics perspective, provided a is small enough. Physics at long distance scales does not depend on the precise dynamics at short distance scales. See [5] for more on this.

In a typical particle physics experiment it is not correlation functions which are measured. Instead there is a, more or less, well defined incoming state and what is interesting is the probability of ending up in a given outgoing state. The probabilities are, as in QM, given by

[5] $T\{\phi(t)\phi(0)\} = \theta(t)\phi(x)\phi(0) \pm \theta(-t)\phi(0)\phi(t)$ where $\theta(t>0)=1$, $\theta(t<)=0$ and the plus(minus) sign is for bosons(fermions).

the square of an amplitude. All possible amplitudes are collected in the S-matrix, defined as

$$S_{fi} = \langle f | i \rangle \,, \tag{14}$$

where $|i\rangle$ is the initial state and $\langle f|$ is the final state. S-matrix elements can be obtained from correlation functions using the LSZ theorem, see [6].

The path integral is one way to quantize a field theory. Another way is canonical quantization. In canonical quantization the field ϕ is an operator obeying the equal time commutation relations

$$\begin{aligned} [\phi(x), \phi(y)]_{\pm} &= 0 \\ [\Pi(x), \Pi(y)]_{\pm} &= 0 \\ [\phi(x), \Pi(y)]_{\pm} &= i\delta^{(3)}(\vec{x} - \vec{y}), \end{aligned} \tag{15}$$

where $\Pi(x)$ is the conjugate field to $\phi(x)$ defined by

$$\Pi(x) = \frac{\delta \mathscr{L}}{\delta \partial_0 \phi(x)} \tag{16}$$

and $[A, B]_{\pm} = AB \pm BA$. The minus sign is for bosons and the plus sign is for fermions.

The lattice introduced above makes sense also in canonical quantization. Each lattice point is a quantum mechanical system with its own set of commutation relations.

3.1 Perturbation theory

Perturbation theory is an important tool used in the papers. Here, we will give a very brief introduction to perturbation theory using a toy example consisting of an ordinary integral. The results from the toy example are then quickly translated into rules used in QFT for a scalar field. Finally, there is a very short introduction to renormalization.

Toy example

Let's start by defining

$$I_n = \int_{-\infty}^{\infty} d\phi \phi^n \exp\left(-\frac{k^2}{2}\phi^2 - \lambda\phi^4\right), \tag{17}$$

where ϕ is an ordinary real valued variable being integrated over. A correlation function would then be similar to

$$\langle 0 | \phi^n | 0 \rangle = \frac{I_n}{I_0}. \tag{18}$$

For small λ this can be calculated as an expansion in λ. To do this let us rewrite I_n as

$$\begin{aligned}
I_n &= \int d\phi \phi^n \exp\left(-\frac{k^2}{2}\phi^2 - \lambda\phi^4\right) \\
&= \int d\phi \phi^n \exp\left(-\frac{k^2}{2}\phi^2 - \lambda\phi^4 + J\phi\right)\Big|_{J=0} \\
&= \partial_J^n \int d\phi \exp\left(-\frac{k^2}{2}\phi^2 - \lambda\phi^4 + J\phi\right)\Big|_{J=0} \\
&= \partial_J^n \exp\left(-\lambda\partial_J^4\right) \int d\phi \exp\left(-\frac{k^2}{2}\phi^2 + J\phi\right)\Big|_{J=0}
\end{aligned} \tag{19}$$

where J is just an ordinary real valued variable and ∂_J is shorthand for derivative with respect to J. Making the change of variables

$$\phi \to \phi + \frac{J}{k^2} \tag{20}$$

brings the integral into the form

$$I_n = \partial_J^n \exp\left(-\lambda\partial_J\right) \exp\left(-J\frac{1}{2k^2}J\right)\Big|_{J=0} \times C. \tag{21}$$

Calculating correlation functions in perturbation theory is now a breeze, we don't even need the constant C. Just take

$$\langle 0|\phi^n|0\rangle = \frac{\partial_J^n \exp\left(-\lambda\partial_J\right) \exp\left(-J\frac{1}{2k^2}J\right)\Big|_{J=0}}{\exp\left(-\lambda\partial_J\right) \exp\left(-J\frac{1}{2k^2}J\right)\Big|_{J=0}}, \tag{22}$$

expand to the desired order in λ and take derivatives.

There is a diagrammatic interpretation of the above result. For each factor in ∂_J^n assign an external point. For each factor $-\lambda$ assign an internal vertex. Join the external points and vertices in every possible way, every vertex must have exactly four lines connected to it and every external point must have exactly one line connected to it. To each line assign a factor $-\frac{1}{k^2}$. A few examples are given in Figure 2.

The denominator contains only diagrams with no connection to external points. These can be factored out of the numerator, further simplifying the calculation. In order to do this, suppose that we are looking at diagrams with n vertices which are connected to external points, possibly via other vertices. If there are no disconnected pieces this comes from a term with $\left(-\lambda\partial_J^4\right)^n/n!$. If there are m vertices contributing to disconnected diagrams the

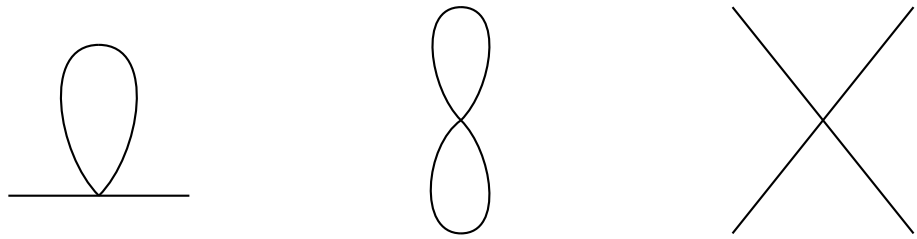

$12\frac{\lambda}{(k^2)^3}$ $\qquad$ $-3\frac{\lambda}{(k^2)^2}$ $\qquad$ $24\frac{\lambda}{(k^2)^4}$

Figure 2: A few example diagrams and their values in the toy example. The first diagram contributes to $\langle 0|\phi^2|0\rangle$, the second to $\langle 0|0\rangle$ and the third to $\langle 0|\phi^4|0\rangle$.

total diagram comes from $\left(-\lambda\partial_J^4\right)^{n+m}/(n+m)!$. Picking out n vertices for the connected part without considering order can be done in $(n+m)!/(n!m!)$ ways. Summing over the diagrams with $m = 0, 1, \ldots$ gives

$$\sum_{m=0}^{\infty}\left(-\lambda\partial_J^4\right)^{n+m}/(n+m)! = \left(-\lambda\partial_J^4\right)^n/n!\exp\left(-\lambda\partial_J^4\right). \tag{23}$$

This expression is acting on $\exp\left(-J\frac{1}{2k^2}J\right)$ but since no lines connect the disconnected and connected parts we have the result

$$\begin{aligned}&\left(-\lambda\partial_J^4\right)^n/n!\exp\left(-\lambda\partial_J^4\right)\exp\left(-J\frac{1}{2k^2}J\right)\\ =&\left(-\lambda\partial_J^4\right)^n/n!\exp\left(-J\frac{1}{2k^2}J\right)\exp\left(-\lambda\partial_J^4\right)\exp\left(-J\frac{1}{2k^2}J\right)\end{aligned} \tag{24}$$

where the equal sign holds under the assumption that the two parts are not allowed to be connected. The conclusion is that correlation functions consist of all diagrams where every vertex is connected to an external point, possibly via other vertices.

Perturbation theory in QFT

There are a few complications when going from the toy model to QFT but the diagrams appear in the same way. To relate QFT to the toy example we introduce a source term in the path integral and give a shorthand notation, Z, for the path integral with a source term,

$$Z[J] = \int D\phi\exp\left(i\int d^4x\left(\mathscr{L}(\phi(x),\partial\phi(x)) + J(x)\phi(x)\right)\right). \tag{25}$$

Correlation functions can then be written using functional derivatives[6] with respect to J, for example

$$\langle 0|T\{\phi(x)\phi(0)\}|\rangle = \delta_{J(x)}\delta_{J(0)}\frac{Z[J]}{Z[0]}\bigg|_{J=0}. \tag{26}$$

J is then interpreted as an external field which is a source for ϕ particles. $Z[J]$ is called the generating functional of correlation functions.

With the Lagrangian

$$\mathscr{L} = \frac{1}{2}\phi(x)\left(-\partial^2 - m^2 + i\epsilon\right)\phi(x) - \lambda\phi(x)^4 \tag{27}$$

the derivation from the previous section goes through almost unaltered given that a Fourier transform is performed[7]. To use diagrams in QFT construct them in the same way as above and translate according to

$$\begin{aligned} -\frac{1}{k^2} &\to \int \frac{d^4k}{(2\pi)^4}\frac{i}{k^2 - m^2 + i\epsilon} \\ -\lambda &\to -i\lambda\delta^{(4)}(p_1 + p_2 + p_3 + p_4) \end{aligned} \tag{28}$$

where the δ function ensures momentum conservation at each vertex.

3.2 Connection to measurements

The last stop in the QFT mini tour is the relation between parameters in the Lagrangian and measured, physical, quantities. For this purpose, suppose someone set up a scattering experiment for the fictitous ϕ particles described by the Lagrangian (27) but with $m = 0$. All the momenta in the experiment are of order q, this is the scale at which the experiment is performed. A measurement is performed which corresponds to a matrix element

$$\mathscr{M}_P = i\lambda_P. \tag{29}$$

The subscript P stands for physical since this is a measurement of something physical. It can be regarded as a prediction to all orders in perturbation theory. The question which will be answered in this section is how this measurement enters predictions at other scales.

If we calculate to first order in λ we only need to calculate the first diagram in Figure 3. This tree diagram gives

$$\mathscr{M}_{\text{tree}} = i\lambda = i\lambda_P, \tag{30}$$

[6] $\delta_{J(x)}J(y)$ is the functional derivative of $J(y)$ with respect to $J(x)$ given by $\delta_{J(x)}J(y) = \frac{\delta}{\delta J(x)}J(y) = \delta^{(4)}(x-y)$ where $\delta^{(4)}(x-y)$ is the four-dimensional delta function.

[7] Ok, it works without as well but this suits my purposes.

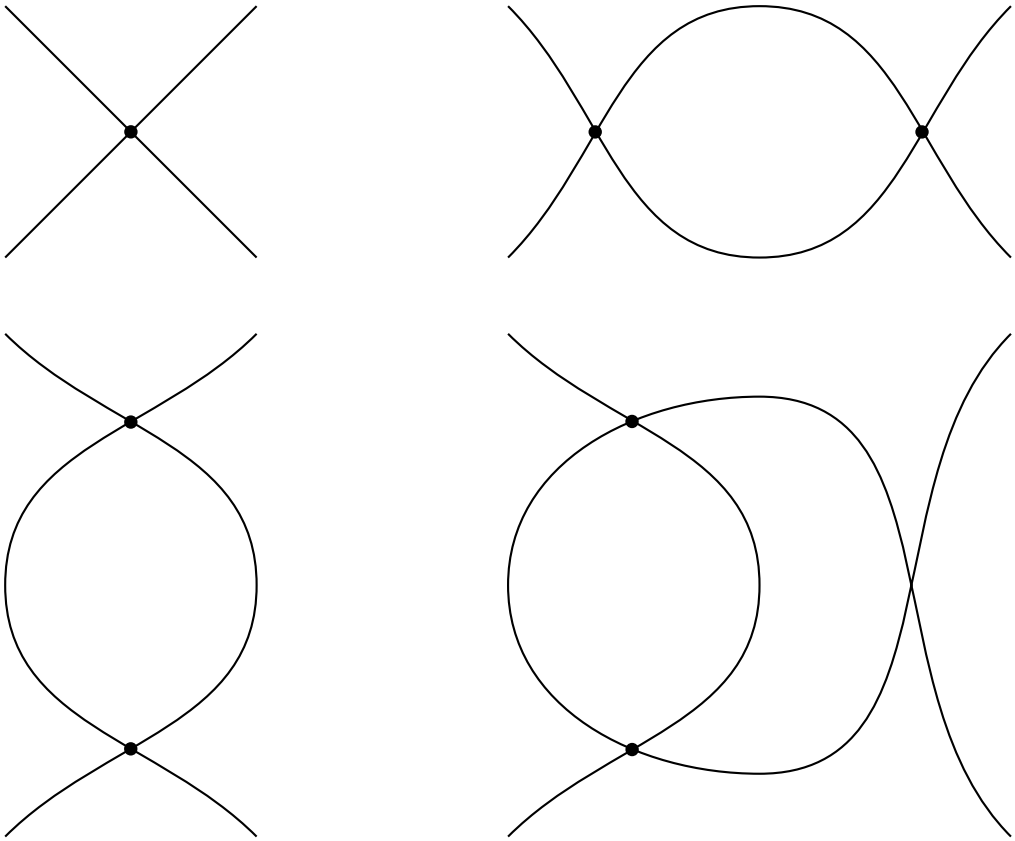

Figure 3: Diagrams needed for tree level and one loop calculations of $\phi\phi$ scattering. Vertices are marked with a filled circle for clarity. The top left diagram is the tree level diagram which contributes with a single factor of the coupling constant λ. The other three are one loop diagrams which contribute two factors of the coupling constant λ.

where we have identified the Lagrangian parameter λ with the measured parameter λ_P. To include effects of $\mathcal{O}(\lambda^2)$ the loop diagrams in Figure 3 are needed. Calculating at an arbitrary scale k, including these diagrams gives the general form of the matrix element as

$$\mathcal{M}_{\text{loop}}(k) = i\lambda + iK\lambda^2 \log(\Lambda/k) + C, \tag{31}$$

where K and C are two constants and Λ is the ultraviolet cutoff π/a. The Λ dependence follows from that the integral needed in calculating the loop diagrams is of the schematic form[8]

$$\int_{-\Lambda}^{\Lambda} \frac{d^4p}{(2\pi)^4} \frac{i}{p^2} \frac{i}{(k-p)^2} \tag{32}$$

[8]This integral diverges for small p but this is not important for the point I am trying to make.

which is proportional to the logarithm of Λ by dimensional analysis.

There are two issues with $\mathcal{M}_{\text{loop}}(k)$. First, setting $\lambda = \lambda_P$ and $k = q$ does not give the prediction (29). Second, Λ has appeared. The cutoff Λ was introduced in order to get rid of high energy effects that we do not know anything about. Now it has appeared in a prediction of $\phi\phi$ scattering. The solution to both problems is to set

$$\mathcal{M}_{\text{loop}}(q) = i\,\lambda_P. \tag{33}$$

Now there is no reference to Λ and we get the correct prediction! This gives

$$i\,\lambda + i K \lambda^2 \log(\Lambda/q) + C = i\,\lambda_P. \tag{34}$$

We can extract the parameter λ from the Lagrangian from this expression, up to corrections of $\mathcal{O}(\lambda^3)$,

$$\lambda(q) = \lambda_p - i K \lambda_p^2 \log(\Lambda/q) - C. \tag{35}$$

The coupling constant is no longer constant, it varies with the scale. Note that λ_P is defined through a measurement at a specific scale and so really is constant[9]. There is still reference to Λ but this drops out in $\mathcal{M}_{\text{loop}}(k)$ which is

$$\mathcal{M}_{\text{loop}}(k) = i\,\lambda_P + i K \lambda_P^2 \log(q/k). \tag{36}$$

It is now possible to make predictions as long as k is not too different from q. In the case where q and k are not of similar size there is a large logarithm which breaks the perturbative expansion in λ_P.

To get rid of these, note that the right hand side of (34) does not depend on q while the left hand side does. If we want to minimize the energy dependence in our predictions this is a good place to start. Taking a derivative with respect to q on both sides gives a differential equation for the coupling $\lambda(q)$

$$\frac{d\,\lambda}{d\,q} - K\frac{\lambda^2}{q} = \frac{d\,\lambda_P}{d\,q} = 0 \tag{37}$$

up to higher orders in λ. This equation is equivalent to taking one loop corrections as part of the coupling and the resulting coupling should be used at tree level. The solution must then satisfy $\lambda(q) = \lambda_P$ which gives

$$\lambda(k) = \frac{\lambda_P}{1 - K\,\lambda_P \log(q/k)}. \tag{38}$$

[9] Unless someone made a mistake!

This expression is much more well behaved and still reproduces (36) upon expansion in terms of λ. The coupling will still become large when the denominator goes to zero but the scale dependence of predictions is minimized. Note that the sign of K determines whether the coupling increases or decreases as k increases.

To summarize, the connection between parameters in the Lagrangian and measurements changes order by order. In order to reproduce a change of scale in an experiment, loop diagrams are needed and this redefines the parameters of the Lagrangian making them energy dependent. This is called renormalization. The energy dependence must satisfy differential equations coming from the fact that physical quantities must remain fixed when changing scale.

4 Effective field theory

An effective field theory is a field theory where only the relevant degrees of freedom are taken into account. All other physics is encoded in the coupling constants of the theory. As long as all energies in an experiment are $\mathcal{O}(m_\pi)$ the relevant degrees of freedom in QCD are the pions. The effects of heavy particle propagation can be encoded in the pion couplings to some approximation which should be valid up to $\mathcal{O}(m_\pi/m_K)$. If nature didn't work this way, it would be difficult to make progress in physics.

That effects of heavier states can be encoded in the couplings is essentially the same as that the effects of heavy particles are local. This essentially follows from the uncertainty principle, which tells us that in order to probe physics at small distances we need large momentum transfer. For small momentum, positions remain uncertain. Heavy states must be highly off shell for small momenta and can not propagate long distances and therefore appear effectively local.

From the above discussion it is not clear why EFTs are interesting when the underlying theory is known. In this thesis EFTs for low energy QCD are used since there is no known analytic way of making quantitative predictions directly from QCD if the energy is low enough. Perturbation theory in the strong coupling doesn't work since the strong coupling becomes large at low energies. With EFTs it is possible to make predictions without knowing exactly how quarks and gluons enter low energy QCD. In a more general sense EFTs are often useful when there are widely separated scales in a problem, see [7].

In constructing EFTs a guiding principle is Weinberg's folk theorem which states that "If one writes down the most general Lagrangian, including all terms consistent with assumed symmetry principles and then calculates matrix elements with this Lagrangian to any given order in perturbation theory, the result will simply be the most general possible S-matrix consistent with analyticity, perturbative unitarity, cluster decomposition, and the assumed

symmetry principles"[8]. This statement was shown to be correct in the case of χPT in [9].

Now, if the folk theorem was all we had there would be an infinite set of operators in the Lagrangian, each with a coupling constant which would have to be measured. This would not be a predictive model. A way to organize the operators in the Lagrangian as well as the Feynman diagrams was provided by Weinberg in the same paper as the folk theorem. This organizing principle will be addressed below.

4.1 Weinberg's power counting

To discuss power counting let's assume that we have written down the most general Lagrangian for a field, π, and it happens to be of the following schematic form

$$\mathscr{L} = -\pi(\partial^2 + m^2)\pi + \sum_{n=1}^{\infty} \pi^2 V_{2n} \frac{\partial^{2n}}{\Lambda^{2n-2}} H(\pi) \tag{39}$$

where $H(\pi)$ is a polynomial in π/Λ with Λ a dimensionful constant which is there to get the dimensions right, and V_{2n} is a dimensionless coupling constant assumed to be $\mathscr{O}(1)$. The form is schematic, the relevant part here is that all terms contain powers of derivatives yielding factors of momenta which are compensated by powers of Λ.

Λ is related to the cutoff where degrees of freedom which are not explicitly included enter. We assume that $p \sim m \ll \Lambda$ which would be the case if Λ represents a mass of a particle which is large when compared with p and m. Moreover, we assume that no positive powers of Λ can result from any part of calculating a diagram[10]. The schematic form of the Lagrangian together with the assumptions tell us the relative importance of a given diagram. For a given process every Feynman diagram has the same dimension of energy, we call this d. Each power of momentum or mass, except for the first d, in the expression for a specific diagram is compensated by a factor $1/\Lambda$. In order to calculate the number of suppression factors we rescale p and m by a factor t,

$$\begin{aligned} p &\to t\,p, \\ m &\to t\,m. \end{aligned} \tag{40}$$

A diagram which scales as t^D then has a $1/\Lambda^{D-d}$ suppression. To use this information to classify diagrams we need to work out the scaling of a generic diagram in terms of its parts.

A diagram consists of external lines, vertices, propagators and loops. In a diagram every propagator contributes t^{-2}, every loop contributes t^4 and every vertex with coupling V_{2n},

[10] This has to do with how momentum integrals are regularized, the cutoff introduced above does not satisfy this property, see section 4.2.

assumed $\mathcal{O}(1)$, contributes t^{2n}. In total a diagram with N_I propagators, N_L loops and N_{2n} vertices of type V_{2n} scales with t^D where

$$D = 4N_L - 2N_I + \sum_{n=1}^{\infty} N_{2n} 2n. \tag{41}$$

The number of vertices can be eliminated using the relations

$$\begin{aligned} N_L &= N_I - (N_V - 1) \\ N_V &= \sum_{n=0}^{\infty} N_{2n}, \end{aligned} \tag{42}$$

which follow from that every propagator contributes an integration over momentum and every vertex has a delta function but one delta function is needed for overall momentum conservation. This gives

$$D = 2 + 2N_L + \sum_{n=0}^{\infty} N_{2n}(2n-2), \tag{43}$$

which means that the relative importance of diagrams can be determined by the number of loops and the powers coming from vertices. Moreover, this information can be used to organize the terms in the Lagrangian according to the number of derivatives and masses. This means that for a given precision there are only a finite number of coupling constants to determine and the theory is predictive.

The assumption $V_{2n} \sim \mathcal{O}(1)$ was vital for this to work. If for some reason a specific coupling constant, V_{2i}, happens to be very large the above argument falls apart. Assuming that the couplings are of $\mathcal{O}(1)$ is the same as assuming that dimensional analysis works. In principle, only measurement of the couplings can show if this is a valid assumption[11].

As a more general comment, it is also possible to construct predictive EFTs when all couplings are not derivative couplings. One example is the SM EFT where higher-dimensional operators are added to the SM. The expansion scheme of choice is then a combination of an expansion in dimension as above and an expansion in the coupling constants of the SM.

4.2 Renormalization in EFT

In renormalizing the ϕ^4 interaction in section 3.2 it was possible to redefine λ in such a way that predictions come out with no reference to the cutoff Λ. If we would instead have had the interaction term

$$\lambda \frac{\partial^2}{\Lambda^2} \phi^4 \tag{44}$$

[11] This assumption can be used to estimate the size of unknown couplings, see for example [7]

we would have obtained one loop matrix elements such as

$$\mathcal{M} = i\lambda\frac{q^2}{\Lambda^2} + i\frac{\lambda^2}{16\pi^2\Lambda^4}C\left(\Lambda^4 + q^2\Lambda^2 + q^4\log(\Lambda/q)\right), \tag{45}$$

where $1/16\pi^2$ is a generic loop suppression factor which was not important until now. The first term from the loop diagrams is not suppressed by any factors of Λ. This is not a violation of power counting since the cutoff regulator violates the assumptions by giving positive powers of Λ. The factor $1/16\pi^2$ does not help because there are always q such that $q^2/\Lambda^2 < \lambda C/16\pi^2$.

A regulator that does satisfy the assumptions is dimensional regularization[12]. In this regulator loop integrals are evaluated in d dimensions instead of 4. Going from a cutoff regulator to dimensional regularization is accomplished by

$$\int_{-\Lambda}^{\Lambda}\frac{d^4p}{(2\pi)^4} \to \int_{-\infty}^{\infty}\mu^{2\epsilon}\frac{d^dp}{(2\pi)^d} \tag{46}$$

where $2\epsilon = d - 4$ and the factor $\mu^{2\epsilon}$ keeps the dimensions right. An example integral would be

$$\int \mu^{2\epsilon}\frac{d^dp}{(2\pi)^d}\frac{i}{p^2 - m^2} = -\frac{m^2}{16\pi^2}\left(\frac{1}{\bar{\epsilon}} - \log\frac{m^2}{\mu^2}\right) + \mathcal{O}(\epsilon) \tag{47}$$

where $1/\bar{\epsilon} = 1/\epsilon - (1 + \log 4\pi + \gamma_E)$ with γ_E the Euler–Mascheroni constant. The quadratically divergent integral has a pole in in $1/\epsilon = 2/(d-4)$ and a logarithm containing a scale. Generically in dimensional regularization any divergence shows up in this way. Moreover, since this integral is quadratically divergent in 4 dimensions it is logarithmically divergent in 2 dimensions and there would be poles for every $d \geq 2$. However, since we are only interested in $d = 4$ we see only that pole and the corresponding logarithm. To see that this really is a regulator which suppresses contributions far away from μ see [10].

With dimensional regularization the matrix element is schematically

$$\mathcal{M} = i\lambda\frac{q^2}{\Lambda^2} + i\frac{\lambda q^4}{16\pi^2\Lambda^4}D\left(\frac{1}{\bar{\epsilon}} + \log(\mu^2/q^2)\right), \tag{48}$$

with a new constant D. There is still one more point to address here, how to remove $1/\epsilon$.

In order to remove $1/\epsilon$ we have to modify a coupling constant from an operator of the form

$$\varkappa\frac{\partial^4}{\Lambda^4}\phi^4. \tag{49}$$

[12] There are ways of using cutoff regularization but using dimensional regularization is easier.

This is just what the power counting says, loops and extra derivatives in the Lagrangian are of the same order in the power counting. The most common way to do this is to define

$$\varkappa = \varkappa_R + \frac{E}{\bar{\epsilon}} \tag{50}$$

where $\varkappa_R$ is a numerical constant to be determined from experiment and E is such that $1/\bar{\epsilon}$ cancels. This scheme is called modified minimal subtraction ($\overline{MS}$). The constant, $\varkappa_R$, has to be $\mathcal{O}(1)$ for power counting to be consistent, if this is the case there really is a suppression by $\mathcal{O}(1)q^4/\Lambda^4$.

Note that it is not possible to resum logarithms in the way done in section 3.2 in this theory. The reason is that $\varkappa$ was needed to renormalize λ. There will then not be a differential equation for λ alone. The corresponding equation will instead result in relations between couplings with different numbers of derivatives. As a result the logarithms with power n in an n loop expansion can be obtained from calculating only one loop diagrams, see [11].

As a final comment on dimensional regularization it might seem strange that the integral is not cut off but instead is extended to infinity, albeit in d dimensions. The high energy modes in this integral would have to be highly off shell and so, by the uncertainty principle, appear local. Local terms can be absorbed in the coupling constants. This highlights the fact that the coupling constants are renormalization scheme dependent[13].

5 QCD and symmetries

With this short introduction to QFT and EFT we turn to the object under study, low energy QCD. As was noted in section 2 the degrees of freedom in low energy QCD are not the quarks and gluons but bound states. Using the EFT idea we want to develop a low energy theory for QCD. Symmetries play a central role in this analysis so a first step is to introduce QCD and the symmetries of QCD. However, to analyze the symmetries we must first introduce the QCD Lagrangian.

The Lagrangian for a single free quark is

$$\mathcal{L}_{free} = \bar{q}\left(i\gamma^\mu \partial_\mu - m\right)q \tag{51}$$

where $\bar{q}$ and q have four components. The matrices γ^μ are 4×4 matrices in this space and satisfy $\{\gamma^\mu, \gamma^\nu\} = 2\eta^{\mu\nu} I$ where $\eta^{\mu\nu}$ is the Minkowski metric and I is the 4×4 identity matrix. m is proportional to the identity matrix.

[13] In the ϕ^4 example above we renormalized by setting $\mathcal{M} = i\lambda_p$ at some scale, this is called momentum subtraction. This is very different from the subtraction scheme introduced here where the pole is subtracted. In the end both should predict $\mathcal{M} = i\lambda_p$.

The Lagrangian of QCD for a single flavor is given by

$$\mathscr{L}_{QCD} = \bar{q}^j \left(i\gamma_\mu D^{\mu k}_{\ j} - m\delta^k_j \right) q_k - \frac{1}{4} F^{a\mu\nu} F^a_{\mu\nu} \tag{52}$$

where

$$\begin{aligned} F^a_{\mu\nu} &= \partial_\mu G^a_\nu - \partial_\nu G^a_\mu + g_s f^{abc} G^b_\mu G^c_\nu, \\ D_\mu q_i &= \left(\delta^j_i \partial_\mu - i\, g_s G^a_\mu \frac{T^{aj}_{\ i}}{2} \right) q_j, \end{aligned} \tag{53}$$

g_s is the strong coupling constant and T^a are the matrices from (4). a, b, c are gluon color indices in the range $1, \ldots 8$ and i, j, k are quark color indices in the range $1, 2, 3$. Any repeated index is summed over. G^a_μ are the eight gluons.

This Lagrangian is invariant under the transformations

$$\begin{aligned} &q(x) \to U(x) q(x) \\ &\bar{q}(x) \to \bar{q}(x) U^\dagger(x) \\ &G_\mu(x) = \frac{T^a}{2} G^a_\mu(x) \to U(x) G_\mu(x) U^\dagger(x) - \frac{i}{g_s} \left(\partial_\mu U(x) \right) U^\dagger(x) \end{aligned} \tag{54}$$

where

$$U(x) = \exp\left(-i\phi_a(x) \frac{T^a}{2} \right) \tag{55}$$

with $\phi^a(x)$ parameterizing the local transformation and the color indices have been suppressed. Note that the parameters of the transformation is spacetime dependent. The Lagrangian has a local symmetry, or a gauge symmetry. Spacetime independent transformations are called global transformations and invariance under such a transformation is called a global symmetry. The $SU(3)$ group corresponding to the local transformation is called $SU(3)_C$ where C stands for color.

The QCD Lagrangian is written in terms of quarks and gluons. Due to confinement these are never directly observed. The observed states of QCD are color neutral bound states. The most common bound states are mesons and baryons. These are the degrees of freedom at low energies. Since the states are color neutral, any Lagrangian written in terms of these states is compatible with $SU(3)_C$. This means that color symmetry does not provide much useful input for a low energy EFT for QCD. There are, however, global symmetries which do give useful constraints.

5.1 Global symmetries

The low lying bound states in QCD are composed of up, down and strange quarks. These are the quarks which are most important at low energies. In this section the global symmetries of the QCD Lagrangian are described. Since the gluon part of the Lagrangian is symmetric under these symmetry transformations, it is not written explicitly.

The QCD Lagrangian for the three light quarks is

$$\mathscr{L}_{QCD} = \sum_{i=1,2,3} \bar{q}^i \left(i\gamma^\mu \partial_\mu - m_i \right) q_i, \tag{56}$$

where i is a flavor index as in section 2.1, not a color index, and

$$q = \begin{pmatrix} u & d & s \end{pmatrix}^T, \qquad \bar{q} = \begin{pmatrix} \bar{u} & \bar{d} & \bar{s} \end{pmatrix}. \tag{57}$$

The Lagrangian is the sum over three free quark fields with masses m_u, m_d, m_s. A symmetry of this Lagrangian is given by

$$q \to \exp(-i\theta)q, \quad \bar{q} \to \bar{q}\exp(i\theta). \tag{58}$$

This change of phase is a $U(1)$ symmetry. The Lagrangian is also symmetric under parity, time reversal and Lorentz transformations. To go further we make the assumption that the masses of the three lightest quarks can be treated as small and thus neglected as a first approximation. Any symmetry found in this limit is an approximate symmetry.

It is far from obvious that the concept of almost symmetric makes sense. To relate to it, think of a regular polygon which becomes more and more circle like as the number of vertices increases. There is a better and better approximate rotation symmetry. Importantly, in the limit where the number of vertices goes to infinity the polygon becomes a circle. The approximation is useful since the polygons can be used to approximate, for example, the area of the circle. For QCD the roles are reversed, QCD with quark masses is less symmetric than massless QCD. The similarity with the circle example is that there are still insights to be gained. The Lagrangian for massless QCD is

$$\mathscr{L}^{(0)}_{QCD} = \sum_{i=1,2,3} \bar{q}^i i\gamma^\mu \partial_\mu q_i. \tag{59}$$

There is now a global $SU(3)$ symmetry under the transformations

$$q_i \to \exp\left(-i\theta^a \frac{T^a}{2}\right)^j_i q_j, \quad \bar{q}^i \to \bar{q}^j \exp\left(i\theta^a \frac{T^a}{2}\right)^i_j. \tag{60}$$

The symmetry transforms the three quark flavors into each other as in section 2.1 and has nothing to do with the color indices of $SU(3)_C$. There is actually a larger symmetry than $SU(3) \times U(1)$ when left and right handed fields are considered.

The left and right handed quark fields are defined by

$$q_L = \frac{1-\gamma^5}{2}q, \quad q_R = \frac{1+\gamma^5}{2}q$$
$$\bar{q}_L = \bar{q}\frac{1+\gamma^5}{2}, \quad \bar{q}_R = \bar{q}\frac{1-\gamma^5}{2} \tag{61}$$

where γ^5 is a 4×4 matrix in spinor space which anti commutes with all the γ^μ. The fifth γ matrix is hermitian $(\gamma^5)^\dagger = \gamma^5$. The right and left handed fields live in different representations of the Lorentz group, they transform differently under rotations. The two are related by parity, $P\psi_R = \psi_L$. The right and left handed fields separate in the massless limit

$$\mathscr{L}^{(0)}_{QCD} = \sum_{i=u,d,s} \bar{q}^i_L i\gamma^\mu \partial_\mu q_{iL} + \bar{q}^i_R i\gamma^\mu \partial_\mu q_{iR}. \tag{62}$$

This Lagrangian has the symmetry

$$SU(3)_L \times SU(3)_R \times U(1)_L \times U(1)_R \tag{63}$$

together with parity, time reversal and Lorentz invariance. We now turn to consequences of the symmetries.

5.2 Noether's theorem

The invariance of the Lagrangian under a global symmetry gives that the action

$$S(\phi) = \int d^4x \mathscr{L}(\phi) \tag{64}$$

is also invariant. If the symmetry is parameterized in terms of a variable α we write this as

$$\delta S_\alpha(\phi) = 0. \tag{65}$$

If we now let α depend on x, the change in the action must be proportional to the derivative of $\alpha(x)$.

$$\delta S_{\alpha(x)}(\phi) = -\int d^4x \partial_\mu \alpha(x) j^\mu(x) \tag{66}$$

for some current $j^\mu(x)$[14]. However, the left hand side of this equation is zero when ϕ are solutions to the classical equations of motion which are derived from the action principle

$$\delta S(\phi) = 0 \tag{67}$$

[14]If there was no global symmetry to begin with there would be terms not involving derivatives of $\alpha(x)$ on the right hand side.

where any change in ϕ is now allowed. Integrating by parts in the right hand side of (66) and noting that we can choose $\alpha(x)$ arbitrarily, we conclude that

$$\partial_\mu j^\mu(x) = 0. \tag{68}$$

The quantity j^μ is called a conserved current. To each such conserved current there is a time independent charge,

$$Q = \int d^3x\, j^0(x). \tag{69}$$

The time independence isn't enforced but follows from (68),

$$\partial_0 \int d^3x\, j^0(x) = \int d^3x \partial_i j^i(x) = \int dS_i j^i(x) = 0 \tag{70}$$

where the divergence theorem has been used in the second equality and the current is assumed to vanish on the boundary.

Moving now to QCD and performing local versions of $SU(3)_L \times SU(3)_R \times U(1)_L \times U(1)_R$ in this manner gives the conserved currents

$$L^a_\mu = \bar{q}_L \gamma_\mu \frac{T^a}{2} q_L, \qquad R^a_\mu = \bar{q}_R \gamma_\mu \frac{T^a}{2} q_R, \tag{71}$$

where $a = 0$ corresponds to $U(1)_L$ and $U(1)_R$. In the canonical quantization picture there is a connection between the conserved charges and the symmetry transformations on the fields given by

$$\exp(-i\alpha^a_L Q^a_L) q_L(x) \exp(i\alpha^a_L Q^a_L) = \exp(-i\alpha^a_L \frac{T^a}{2}) q_L(x), \tag{72}$$

with a similar expression for $\bar{q}_L$. This follows from applying the commutation relations (15) to show that

$$[Q^a_L, q_L] = \frac{T^a}{2} q_L. \tag{73}$$

This connection makes it possible to discuss transformation properties of vacuum.

Transformations of the vacuum can be found if we require that arbitrary correlation functions should be invariant under the symmetry transformation of the fields. For this to hold, the vacuum transformation must undo the transformations of the field which gives that the vacuum must transform as

$$|0\rangle \to \exp(-i\alpha^a_L Q^a_L) |0\rangle. \tag{74}$$

For the vacuum to be invariant under the symmetry, the charge must annihilate the vacuum

$$Q_L^a |0\rangle = 0. \tag{75}$$

The vacuum must carry zero charge.

The conserved currents essentially follow from the symmetries of massless QCD. When constructing a low energy theory guided by symmetries the low energy theory should also provide corresponding conserved currents in the massless limit. Of course, since the particle content is different the current will be different but there should still be a corresponding conservation law.

There is a caveat to the above reasoning. While there are 18 conserved currents in the classical field theory this is no longer true in the quantum field theory. This will be discussed in the next section.

5.3 Ward identities

In QFT we are interested in symmetry constraints on correlation functions. These can be studied using the path integral,

$$I = \int Dq D\bar{q} \exp\left(iS_{QCD}\right), \tag{76}$$

where $Dq D\bar{q}$ is short hand for $\Pi_{q=u,d,s} Dq D\bar{q}$,.

The way to analyze symmetries in this case is to use a change of variables. The change of variables corresponding to a local version of $SU(3)_L$ is

$$q_L \to \exp\left(-i\theta_L^a(x)\frac{T^a}{2}\right) q_L, \qquad \bar{q}_L \to \bar{q}_L \exp\left(i\theta_L^a(x)\frac{T^a}{2}\right). \tag{77}$$

Performing this change of variables and expanding to first order in $\theta_L^a(x)$ gives

$$\begin{aligned} I &= \int Dq D\bar{q} \left(1 + \int d^4x \theta_L^a(x) \partial^\mu L_\mu^a(x)\right) \exp\left(iS_{QCD}\right)) \\ &= I + \int Dq D\bar{q} \left(\int d^4x \theta_L^a(x) \partial^\mu L_\mu^a(x)\right) \exp\left(iS_{QCD}\right)) \end{aligned} \tag{78}$$

canceling I on both sides and removing the integral over x since $\theta_L^a(x)$ is arbitrary gives

$$0 = \partial_x^\mu \int Dq D\bar{q} L_\mu^a(x) \exp\left(iS_{QCD}\right)). \tag{79}$$

Noether's theorem holds inside the path integral for this current. There are similar identities for other correlation functions which can be derived in the same way. This kind of identity is usually referred to as a Ward identity.

The derivation presented above is valid under the assumption that the path integral measure is invariant under the local change of variables. It is in the case above, but it is not for the change of variables

$$\begin{aligned} q_L &\to \exp(-i\theta(x))\, q_L, \quad \bar{q}_L \to \bar{q}_L \exp(i\theta(x)) \\ q_R &\to \exp(i\theta(x))\, q_R, \quad \bar{q}_R \to \bar{q}_R \exp(-i\theta(x)), \end{aligned} \tag{80}$$

that is a combination of $U(1)_L \times U(1)_R$ where $\theta_L = -\theta_R = \theta$. This combination of $U(1)_L \times U(1)_R$ is a symmetry at the classical level but not at the quantum level. The symmetry is called an anomalous symmetry. The left and right handed currents from $U(1)_L \times U(1)_R$ are therefore no longer conserved separately. There is still a conserved current corresponding to $\theta_L = \theta_R = \theta$. The symmetry group is called $U(1)_V$, where V stands for vector. The corresponding conserved current is $V_\mu = L_\mu + R_\mu$.

The symmetry group of massless QCD at the quantum level is $SU(3)_L \times SU(3)_R \times U(1)_V$, parity, time reversal and Lorentz invariance. The symmetry group $SU(3)_L \times SU(3)_R$ is usually called chiral symmetry since it treats left and right handed fields differently. The association of this symmetry with the massless limit justifies the name chiral limit for the massless limit. It is also common to refer to the group where the left and right handed fields transform with the same angle as $SU(3)_V$ and the other transformations, where the left and right handed fields transform oppositely as $SU(3)_A$, with A for axial. This is an abuse of notation since $SU(3)_A$ is not really a group. The commutator of two axial generators is a vector generator, $[T_L^a - T_R^a, T_L^b - T_R^b] = i f^{abc}(T_L^c + T_R^c)$, so there is no closed Lie algebra[15].

To get closer to the real world we need to include masses for the quarks and interactions with electroweak gauge bosons. These are effects that potentially break the symmetry group. This can be done using the external field method which will be introduced next.

5.4 Ward identities with external fields

As stated above the quark masses and couplings to electroweak bosons need to be included. Note that the goal is not to include more dynamical degrees of freedom, like a propagating W. The idea is rather to include interactions with the bosons to compute the strong part of matrix elements.

[15] A quick way to remember this is that switching left and right on the left hand side gives back the same expression, this means that the right hand side must satisfy the same and therefore has to be zero or a vector generator.

In the SM the W couples to L^a_μ. To introduce this interaction we start from the generating functional

$$Z[l^a_\mu] = \int Dq D\bar{q} \exp\left((iS_{QCD}) + \int d^4x\, l^a_\mu(x) L^\mu_a(x) \right) \tag{81}$$

where

$$L^a_\mu = \bar{q}_L \gamma_\mu \frac{T^a}{2} q_L \tag{82}$$

from (71) and l^a_μ are external fields. The new term breaks the Ward identity (79), and the information how this is done should be transferred to the low energy theory. Performing the same change of variables as in the previous section gives the identity

$$0 = \int Dq D\bar{q} \left(\partial^\mu L^a_\mu(x) - i\, l^b_\mu(x) f^{abc} L^c_\mu(x) \right) \exp\left(iS_{QCD} \right). \tag{83}$$

This relation should then be fulfilled in the low energy theory with whatever corresponds to $L^a_\mu(x)$.

The information in (83) can be transferred to constraints on the generating functional. Specifically, by demanding

$$Z[l^a_\mu] = Z[l^a_\mu + \partial^\mu \theta^a_L(x) - i\theta^b_L l^c_\mu(x) f^{abc}] \tag{84}$$

and expanding both sides to first order in θ_L gives (83). It is more convenient to write (84) in terms of $l_\mu = l^a_\mu \frac{T^a}{2}$ which gives

$$Z[l_\mu] = Z[U_L(x) l_\mu U^\dagger_L(x) + i\left(\partial_\mu U_L(x)\right) U^\dagger_L(x)] \tag{85}$$

where $U_L(x)$ is an $SU(3)_L$ matrix. Transformations will henceforth be written in this form, rather than the infinitesimal form used up until now.

This equivalent formulation of the Ward identities follows from that the right hand side of (81) is invariant under the substitutions

$$\begin{aligned} q &\to U_L(x) q, \\ \bar{q} &\to \bar{q} U^\dagger_L(x), \\ l_\mu &\to U_L(x) l_\mu U^\dagger_L(x) + (\partial^\mu U_L(x))\, U^\dagger_L(x). \end{aligned} \tag{86}$$

The left hand side of (81) is not invariant but should produce the same physics as the right hand side which is invariant, giving (85). To see the relation to the Ward identities on the right hand side, change variables of the quarks in a way which undoes the quark substitution. Such a change of variables is precisely what gives Ward identities but now there is no

transformation on the quarks. The Ward identities must be contained in the change in the external fields which is what (85) says.

From a low energy perspective the virtue of the formulation in (85) is that there is no mention of the high energy degrees of freedom. Imposing (85) in the low energy theory is the same as imposing the symmetries and symmetry breakings of $SU(3)_L$ present in the high energy theory. The method is called the external field method and it works for including other symmetry breaking effects as well, such as the mass term.

The mass term in QCD has the form

$$\mathscr{L}_{mass} = -\bar{q}^i m_i^j q_j \tag{87}$$

where

$$m = \begin{pmatrix} m_u & 0 & 0 \\ 0 & m_d & 0 \\ 0 & 0 & m_s \end{pmatrix}. \tag{88}$$

It is conventional to introduce a scalar external field, s, through which the mass term can be introduced. The relevant part of the QCD Lagrangian is

$$\mathscr{L}_s = -\bar{q}_L^i s^{\dagger j}{}_i q_{Rj} - \bar{q}_R^i s_i^j q_{Lj}. \tag{89}$$

Quark masses are introduced by setting $s = m$.

The external scalar field breaks $SU(3)_L \times SU(3)_R$ symmetry. However, the added term is invariant under the substitutions

$$\begin{aligned} q_L &\to U_L(x) q_L, & \bar{q}_L &\to \bar{q}_L U_L^\dagger(x) \\ q_R &\to U_R(x) q_R, & \bar{q}_R &\to \bar{q}_R U_R^\dagger(x) \\ s &\to U_R(x) s U_L^\dagger(x), & s^\dagger &\to U_L(x) s^\dagger U_R^\dagger(x). \end{aligned} \tag{90}$$

The corresponding constraint on the generating functional is then

$$Z[s] = Z[U_R(x) s U_L^\dagger(x)], \tag{91}$$

where the transformation on $s^\dagger$ is understood.

Checking how a specific term would have to transform in order to be invariant under a symmetry is called a spurion analysis. Table 3 includes all the external fields that are needed in low energy QCD and how these transform. There is also an external field, p, which couples to the pseudoscalar term $\bar{q}\gamma_5 q$, included even though there are no such terms in QCD. However, Ward identities relate this field to the others and these are useful.

Table 3: Transformation properties of the external fields. $U_L(x)$ is a local transformation in $SU(3)_L$ and $U_R(x)$ is a local transformation in $SU(3)_R$. Note that all the external fields are 3×3 matrices.

Term in $\mathscr{L}$	external field	transformed external field
$\bar{q}_L \gamma_\mu l^\mu q_L$	l^μ	$U_L(x) l^\mu U_L^\dagger(x) + i\,(\partial^\mu U_L(x))\, U_L^\dagger(x)$
$\bar{q}_R \gamma_\mu r^\mu q_R$	r^μ	$U_R(x) r^\mu U_R^\dagger(x) + i\,(\partial^\mu U_R(x))\, U_R^\dagger(x)$
$\bar{q}_R s\, q_L$	s	$U_R(x) s\, U_L^\dagger(x)$
$\bar{q}_R \gamma_5 p\, q_L$	p	$U_R(x) p\, U_L(x)$

As mentioned above, the transformation properties of the external fields are needed to determine the correct low energy theory.

So far we have described the global continuous symmetries of massless QCD and how to include symmetry breaking terms. It is time to see if the spectrum of QCD can be explained in terms of these symmetry considerations.

5.5 The QCD spectrum and $SU(3)_L \times SU(3)_R$

If the quark masses can be seen as a small perturbation on top of an underlying $SU(3)_L \times SU(3)_R$ symmetry, the spectrum should show traces of the underlying symmetry, similarly to the $SU(3)$ symmetry in section 2.1. Massless QCD on the other hand produces two $SU(3)$ groups. The consequence of this is that for each parity odd bound state in the spectrum there should be a parity even bound state with the same quantum numbers, up to symmetry breaking effects.

The reasoning, following [12], is as follows. Denote a single particle hadron state with definite parity by $|h\rangle$. If we apply the combination of charges $Q_A^a = Q_L^a - Q_R^a$, for some a, to this state we get a state of opposite parity given by

$$Q_A^a |h\rangle \,. \tag{92}$$

Applying the Hamiltonian to this state, to calculate the energy, and noticing that Q_A^a commutes with the Hamiltonian due to the symmetry, gives

$$H Q_A^a |h\rangle = E_h Q_A^a |h\rangle \,. \tag{93}$$

The state has the same energy as the hadron state alone. Taking the hadron to be at rest the conclusion is that for each state there should be a state of opposite parity with the same mass.

This parity doubling is not present in the QCD spectrum. There is still a way to save the massless approximation as a good place to start for low energy QCD. If we assume that the lightest pseudoscalar multiplet becomes massless in the massless limit and that Q_A^a creates

such states at rest. Note that the lightest pseudoscalar octet and the operator Q_A^a share the same quantum numbers. Denoting the state created by Q_A^a by π^a we get

$$H Q_A^a |h\rangle = E_h \left|h\pi^a\right\rangle. \tag{94}$$

Energy conservation requires that π^a is massless.

The assumption that

$$Q_A^a |0\rangle \neq 0 \tag{95}$$

means that although the action is invariant under the symmetry, the vacuum is not. This is known as spontaneous symmetry breaking. The massless states created by Q_A^a are called Goldstone bosons. There is one such Goldstone boson for each charge corresponding to a broken generator. The lightest pseudoscalar octet would then be pseudo Goldstone bosons. That is, Goldstone bosons due to the breaking of an approximate symmetry.

Since the pseudo Goldstone bosons are Goldstone bosons in the limit of massless quarks, their masses have to be proportional to the quark masses through some proportionality constant. Looking at the quark masses in Table 1 and the masses of the lightest pseudoscalar mesons in Table 2 what is needed is $m_{i\bar{j}}^2 \propto m_i + m_j$ for $m_{i\bar{j}}$ the mass of a meson with flavor content $i\bar{j}$ and $m_{i(j)}$ the quark mass for an $i(j)$ quark. In words, the squared masses of the lightest pseudoscalar mesons must be proportional to the quark masses through some dimensionful constant.

Given that the symmetry is broken the axial charges create Goldstone bosons,

$$Q_A^a |0\rangle = \left|\phi^a\right\rangle. \tag{96}$$

Such Goldstone bosons must be annihilated by the charges and the charges can be seen as the zero component of the axial current at zero momentum. Combining this with Lorentz invariance gives

$$\left\langle 0|A_\mu^a(0)|\phi^b(p)\right\rangle = i\, p_\mu F_0 \delta^{ab}, \tag{97}$$

where F_0 is the Goldstone boson decay constant in the chiral limit. As is shown in for example [13], one possible way to break the symmetry in this way is if

$$\langle 0|\bar{q}q|0\rangle = \langle 0|\bar{q}_L q_R|0\rangle + \langle 0|\bar{q}_R q_L|0\rangle = v \neq 0. \tag{98}$$

In this case $\langle 0|\bar{q}q|0\rangle$ is called an order parameter for the spontaneous symmetry breaking.

5.6 The spectrum of low energy QCD and spontaneous symmetry breaking

The above analysis is rather more complicated than saying that the $SU(3)$ present in the QCD spectrum comes from setting the light quark masses equal. Spontaneous symmetry breaking does have some explanatory benefits, however.

One virtue of spontaneous symmetry breaking is that it gives an explanation to why the lightest meson states are so much lighter than the lightest baryon states. Pions are made of pairs of up and down quarks while the proton and neutron are made out of three such particles. A naive expectation would be that the mass ratio should be around $2:3$. Instead the pions have masses around 135 MeV and the nucleons have masses around 1 GeV. This unexpected behavior is explained if most of the mass of the nucleons are from QCD binding energy while the pion mass is forced to be proportional to the quark mass due to symmetry.

This perspective would also explain why the $SU(3)_V$ symmetry is a good approximation. If most of the mass of the more massive particles originate from dynamical effects and the $SU(3)_V$ symmetric part with $m_u = m_d = m_s$, then the symmetry breaking part is causing only the differences in the spectrum[16]. With only $SU(2)$ symmetry it is especially clear since the nucleon masses are about 1 GeV and the mass difference is about 1 MeV. The relevant scale to compare the quark mass differences with would then be Λ_{QCD} which is a few hundred MeV [3]. Another reasonable scale to compare with is the average contribution to the nucleon masses per quark, which should be related to $SU(3)_V$. This is about 330 MeV. Predictions based on $SU(2)$ symmetry should then be expected to hold at around the percent level, whereas predictions from $SU(3)$ symmetry should be good to about 30% [14].

Using a low energy model which incorporates the symmetry breaking effects, it is be possible to improve the predictions in powers of m/Λ_{QCD}, which is the next topic.

6 Chiral perturbation theory

"A chiral symmetry can only hold if the baryon masses are neglected altogether; it is automatically a bad approximation."
—Sidney Coleman's PhD thesis from 1962 [15]

The goal in constructing a low energy theory of QCD is to produce the correct correlation functions. Written in terms of the generating functional, the goal is

$$Z_{\text{QCD}}[v, a, s, p] = Z_{(\text{low energy})}[v, a, s, p], \tag{99}$$

[16] Electromagnetism would also play a role.

where v, a, s, p are the vector, axial vector, scalar and pseudoscalar external fields respectively. The left hand side of (99) contains all the information about low energy QCD but we can not access it with analytical techniques. One way to make predictions in low energy QCD is to construct an EFT which approximates the right hand side of (99) to some precision.

To do this we will assume that the $SU(3)_L \times SU(3)_R$ symmetry of massless QCD is spontaneously broken to $SU(3)_V$. The squared masses of the lightest pseudoscalar mesons would be linearly proportional to the quark masses, while the baryon states could still be massive in the massless limit. The theory described below, starting from this assumption, is χPT [16, 17]. The success of χPT is in itself an indication that this spontaneous symmetry breaking takes place. However, as with any effective field theory there is a limited range of validity[17].

The validity range of χPT should be dictated by the lightest particles which are not included in the low energy theory; the σ and the ρ. While the σ is lighter it is also broader. The σ might also be a $\pi\pi$ bound state. Moreover, model calculations suggest that the most important effects on the χPT coupling constants come from the ρ meson [18]. This indicates that χPT should be valid up to somewhere around the ρ mass, but in the end the range of validity depends on the process being studied. The question might then arise why these particles are not included so that the range of validity is increased. It turns out that it is difficult to find a unique theory with these states, see section 8.

To build a theory which is invariant under $SU(3)_L \times SU(3)_R$, with the eight lightest mesons as degrees of freedom, we need to know how they transform. This is the first task below. Then the lowest order χPT Lagrangian is developed. The next section after that discusses the nature of χPT predictions.

6.1 Transformation properties of the fields

From Table 3 we know the external field transformation properties. The goal now is to use this information to build a Lagrangian for χPT which reproduces low energy QCD. However, to do this the transformation properties of the light pseudoscalar octet must be determined. The formalism to determine this, referred to as the CCWZ formalism, was introduced in [19, 20]. The presentation here closely follows [21]. We start with a toy example.

[17] The range of validity for the SM is being explored at the LHC and other experiments around the world.

CCWZ toy example

Assume that we have a field theory with three scalar fields ϕ_1, ϕ_2, ϕ_3 and that the Lagrangian can be written in terms of $\vec{\phi} \cdot \vec{\phi}$ where

$$\vec{\phi} = \begin{pmatrix} \phi_1 \\ \phi_2 \\ \phi_3 \end{pmatrix}. \tag{100}$$

There is then an $O(3)$ rotational symmetry in the Lagrangian. Suppose further that the potential of the theory enforces $\vec{\phi} \cdot \vec{\phi} = v$. At least one of the fields is forced to have a non zero value in vacuum. Any choice of non zero fields which satisfy $\vec{\phi} \cdot \vec{\phi} = v$ is ok, the particular choice will not affect the physics. Making the choice $\phi_3 = \sqrt{v}$ means that the only remnant of the rotation symmetry are rotations around the 3-axis. We denote elements of this unbroken subgroup by h. The charges corresponding to the other generators do not annihilate the vacuum. By Goldstone's theorem, two broken generators leads to two massless particles. The question is, how to parameterize these?

The fields which satisfy $\vec{\phi} \cdot \vec{\phi} = v$ form a sphere and the condition $\phi_3 = \sqrt{v}$ is a specific point on the sphere. Fluctuations in the radial direction are massive since the potential has degenerate minima on the sphere. The massless excitations lie on the sphere. The coordinates on the sphere should be a way to describe the massless states.

Any point on the sphere, and therefore any field configuration for the massless fields, can be described by

$$\vec{\phi} = u \begin{pmatrix} 0 \\ 0 \\ v \end{pmatrix} = \exp(i J_s \pi_s) \begin{pmatrix} 0 \\ 0 \\ v \end{pmatrix} \tag{101}$$

where u is a group element of $O(3)$ and J_s are the generators of $O(3)$. A possible choice of parameterization of the massless excitation is given by x-dependent coordinates $\pi_s(x)$. There are three generators and therefore three coordinates which means that there would be degeneracy in the description of the sphere. A simpler choice follows from the observation that any point on the sphere can be reached using only the broken generators[18],

$$u(x) = \exp(i J_1 \pi_1(x) + i J_2 \pi_2(x)). \tag{102}$$

This is the prescription from [19, 20] in this case.

[18] This parameterization is unique close to the identity which is all that is needed in perturbation theory.

To see how this field transforms under $g \in G$, note that the field configurations $u(x)$ and $u(x)h$ are equivalent when h is a rotation around the three axis. This follows from

$$h \begin{pmatrix} 0 \\ 0 \\ v \end{pmatrix} = \begin{pmatrix} 0 \\ 0 \\ v \end{pmatrix}. \tag{103}$$

Under a symmetry transformation with $g \in G$, $\vec{\phi}$ transforms as $\vec{\phi} \to g\vec{\phi}$. The transformation on u is then $u(x) \to g\,u(x)$. The matrix $g\,u(x)$ is no longer in the form of (102). However, since every point on the sphere can be reached by transformations of the form of (102) and g is just a rotation, it must be possible to write $g\,u(x)$ in terms of broken generators times a transformation $h \in H$,

$$g\,u(x) = u'(x)h. \tag{104}$$

Multiplying with the inverse of h on both sides gives the transformed matrix $u'(x)$ in terms of g, $u(x)$ and h. Importantly, multiplying with h^{-1} on the right does not change the field configuration since the field configuration is invariant under right multiplication with $h \in H$. This gives the transformation

$$u(x) \to u'(x) = g\,u(x)h^{-1}(g, u(x)). \tag{105}$$

The transformation h is called a compensator field since it makes sure that the matrix $u'(x)$ is in the form (102). The compensator field depends on both g and $u(x)$ since transformations on a sphere are complicated objects.

The jargon which is sometimes used to describe this situation is that the symmetry of the theory is given by a group $G = O(3)$, but only a subgroup $H = O(2)$ is realized in the ground state. We parameterize the field configurations using $u(x)$ which gives the same field configuration as $u(x)h$ for all $h \in H$. Each field configuration is in this way associated with the set $u(x)h$ for all $h \in H$, written $u(x)H$. Such sets are called left cosets[19] and the set of all such sets is denoted G/H. The specific choice $u(x)$ given here is a choice of representative from $u(x)H$. In this case G/H describes a sphere. Note that any point on the sphere is a potential vacuum configuration. The choice of vacuum should not affect the physics. The specific field configuration in a single point should not matter. This means that we should expect interactions which depend on the differences in field configurations between different points in spacetime. In a local Lagrangian such differences enter through derivatives. This implies that the Goldstone bosons should couple through derivatives.

[19] It is also possible to use right cosets.

CCWZ for QCD

In QCD the symmetry $SU(3)_L \times SU(3)_R$ is broken to $SU(3)_V$. A general transformation $g \in SU(3)_L \times SU(3)_R$ can be written in block diagonal form as

$$g = \begin{pmatrix} U_R & 0 \\ 0 & U_L \end{pmatrix} = \begin{pmatrix} \exp(i\frac{T_R^a}{2}\theta_R^a) & 0 \\ 0 & \exp(i\frac{T_L^a}{2}\theta_L^a) \end{pmatrix} \tag{106}$$

the unbroken subgroup is

$$h = \begin{pmatrix} U_V & 0 \\ 0 & U_V \end{pmatrix} \tag{107}$$

where $U_V = U_L = U_R$ when $\theta_L = \theta_R = \theta$. The Goldstone modes can be parameterized through the broken generators as

$$\begin{pmatrix} u(x) & 0 \\ 0 & u(x)^\dagger \end{pmatrix} = \begin{pmatrix} \exp(i\frac{T_R^a}{2}\pi^a(x)) & 0 \\ 0 & \exp(-i\frac{T_L^a}{2}\pi^a(x)) \end{pmatrix}, \tag{108}$$

which follows from setting $\theta_R = -\theta_L = \pi(x)$.

From the preceeding section we get the transformation behavior

$$\begin{pmatrix} u(x) & 0 \\ 0 & u(x)^\dagger \end{pmatrix} \to \begin{pmatrix} U_R & 0 \\ 0 & U_L \end{pmatrix} \begin{pmatrix} u(x) & 0 \\ 0 & u(x)^\dagger \end{pmatrix} \begin{pmatrix} U_V^{-1} & 0 \\ 0 & U_V^{-1} \end{pmatrix}. \tag{109}$$

The transformation law for $u(x)$ is then

$$u(x) \to u'(x) = U_R u(x) h^{-1}(U_R, u(x)) = h(U_L, u(x)) u(x) U_L^\dagger, \tag{110}$$

where, in a slight abuse of notation, we have set $h = U_V$. The unbroken subgroup transform the left and right handed fields in the same way. For this reason we get $h(U_R, u(x)) = h(U_L, u(x))$. We can use this fact to construct another parameterization of the pions as

$$U(x) = u(x)u(x) = \exp\left(i T^a \pi^a\right) \tag{111}$$

This field transforms as

$$U(x) \to U'(x) = U_R U(x) U_L^\dagger \tag{112}$$

and as long as no other fields are introduced which transform with h, this is sufficient for building the low energy Lagrangian.

While the geometrical structure in this case is not as clear as in the case of $O(3) \to O(2)$, the fields $\pi^a(x)$ are coordinates of the coset space $SU(3)_L \times SU(3)_R / SU(3)_V$. The space is isomorphic to $SU(3)$, which explains why we can parameterize the field configurations in terms of an $SU(3)$ matrix.

6.2 Lowest order Lagrangian

From the previous section we know that the eight lightest pseudoscalar mesons can be collected in a spacetime dependent $SU(3)$ matrix, U, which transforms as $U \to U_R U U_L^\dagger$ under $SU(3)_L \times SU(3)_R$. In section 2.1 we described how the generators can be associated to the particles. With this knowledge we parameterize the mesons as

$$U = \exp\left(i\sqrt{2}\frac{M}{F_0}\right), \quad M = \begin{pmatrix} \frac{1}{\sqrt{2}}\pi^0 + \frac{1}{\sqrt{6}}\eta & \pi^+ & K^+ \\ \pi^- & -\frac{1}{\sqrt{2}}\pi^0 + \frac{1}{\sqrt{6}}\eta & K^0 \\ K^- & \bar{K}^0 & -\frac{2}{\sqrt{6}}\eta \end{pmatrix}. \tag{113}$$

where the pion decay constant in the chiral limit, F_0, has been inserted to yield a dimensionless argument for the exponential. The matrix M is traceless. If this was not the case the trace of M would correspond to the η'. Due to the anomaly, η' is heavy and this is the reason why M is traceless.

Using the matrix U and the external fields we should now construct a theory which has the same constraints on the generating functional as QCD. To enforce these constraints we demand that the Lagrangian should satisfy local invariance under separate $SU(3)_L \times SU(3)_R$ transformations. Furthermore, the invariance should follow from including the same external fields as in QCD transforming in the same way as in QCD.

To accomplish this we start by finding the possible building blocks constructed from U and the external fields. In order to take derivatives on U, or any field transforming like U, we define a covariant derivative by

$$D_\mu U \equiv \partial_\mu U - i\, r_\mu U + i\, l_\mu U. \tag{114}$$

With the transformations of l_μ and r_μ this satisfies $D_\mu U \to U_R D_\mu U U_L^\dagger$. We can also have pieces involving only the external fields l_μ and r_μ,

$$\begin{aligned} f^R_{\mu\nu} &\equiv \partial_\mu r_\nu - \partial_\nu r_\mu - i[r_\mu, r_\nu] \\ f^L_{\mu\nu} &\equiv \partial_\mu l_\nu - \partial_\nu l_\mu - i[l_\mu, l_\nu], \end{aligned} \tag{115}$$

these are called the field strengths and transform as $f^R_{\mu\nu} \to U_R f^R_{\mu\nu} U_R^\dagger$ and $f^L_{\mu\nu} \to U_L f^L_{\mu\nu} U_L^\dagger$. It is possible to construct covariant derivatives for the field strengths which satisfy $D_\beta f^R_{\mu\nu} \to U_R D_\beta f^R_{\mu\nu} U_R^\dagger$ with a similar expression for the left handed field strength. The external fields s and p are often introduced in the combination

$$\chi = 2B_0(s + i\,p). \tag{116}$$

This combination transforms as $\chi \to U_R \chi U_L^\dagger$.

Using these building blocks the most general effective Lagrangian can be constructed. Weinberg's power counting tells us that if every term in the Lagrangian has at least two powers of momentum, or some quantity which we assign as the same order of magnitude as the momentum, we can order the effective Lagrangian in powers of momentum. To see if this is the case we need to state how the external fields should be counted in a momentum expansion. The standard counting is

$$U \sim p^0,\, D_\mu U \sim p^1,\, r_\mu, l_\mu \sim p^1,\, \chi \sim p^2. \tag{117}$$

The use of $r_\mu, l_\mu \sim p^1$ is consistent with that these show up in the derivatives. As an underlying reason they should be small in the counting as they are symmetry breaking effects. $\chi \sim p^2$ follows from the observation that the mesons are linear in the quark masses so that this term should give the meson masses which are $\mathcal{O}(p^2)$ on shell.

Any term which is $\mathcal{O}(p^0)$ must involve only the meson field U. The simplest combination would be

$$\left\langle U U^\dagger \right\rangle \tag{118}$$

where $\langle \ldots \rangle$ denotes the trace of $\ldots$ in flavor space. This term, however, is a constant since U is unitary. At $\mathcal{O}(p)$ there is also no term possible, The attempt

$$\left\langle U D_\mu U^\dagger \right\rangle \tag{119}$$

is zero which follows from that $\det U = 1$. There are no terms at $\mathcal{O}(p^0)$ or $\mathcal{O}(p)$. This means that the condition that the effective Lagrangian starts at $\mathcal{O}(p^2)$ for Weinberg's power counting to work is fulfilled.

At $\mathcal{O}(p^2)$ there are several possibilities,

$$\left\langle D_\mu U (D^\mu U)^\dagger \right\rangle, \left\langle \chi U^\dagger \right\rangle, \left\langle U \chi^\dagger \right\rangle, \left\langle f^R_{\mu\nu} \right\rangle, \left\langle f^L_{\mu\nu} \right\rangle. \tag{120}$$

The last two are not Lorentz invariant and vanish. The first term is one of three terms which look different but are the same upon expansion. The terms involving χ must appear in the combination $\left\langle U \chi^\dagger + \chi U^\dagger \right\rangle$. This follows from parity. Under parity U and χ become $U^\dagger$ and $\chi^\dagger$, respectively. The $\mathcal{O}(p^2)$ Lagrangian is then

$$\mathcal{L}_2 = \frac{F_0^2}{4} \left\langle D_\mu U (D^\mu U)^\dagger \right\rangle + \frac{F_0^2}{4} \left\langle U \chi^\dagger + \chi U^\dagger \right\rangle, \tag{121}$$

where the factors of F_0 are needed to get the dimensions right and the $1/4$ are there to give canonically normalized kinetic terms. F_0 is the pion decay constant and B_0, hiding inside χ, is related to the scalar quark condensate.

Inserting quark masses in the isospin limit, $m_u = m_d = \hat{m}$, using $s = \mathrm{diag}(\hat{m}, \hat{m}, m_s)$ and expanding U to find mass terms gives the meson masses as

$$\begin{aligned} m_\pi^2 &= 2B_0 \hat{m} \\ m_K^2 &= B_0 (\hat{m} + m_s) \\ m_\eta^2 &= \frac{2B_0}{3} (\hat{m} + 2m_s). \end{aligned} \tag{122}$$

The meson masses squared are linear in the quark masses. The correct dimension is obtained since B_0 is dimensionful. The reason for going to the isospin limit is that otherwise π^0 and η mix, giving more complicated expressions. The quantity B_0 is related to the symmetry breaking in the sense that

$$\begin{aligned} \delta_s Z_{QCD}[v, a, s, p]|_{v=0,a=0,s=0,p=0} &= \langle 0|\bar{q}q|0\rangle , \\ \delta_s Z_{\chi PT}[v, a, s, p]|_{v=0,a=0,s=0,p=0} &= -3F_0^2 B_0 + \mathcal{O}(p^4). \end{aligned} \tag{123}$$

As a final note on the construction of χPT , it is common to assume that the external fields l^μ, r^μ are traceless, since this is enough for considering possible interactions in the SM[20]. However, in order to consider single components of the electromagnetic field the trace must be included. We needed to do this in papers IV and V. It turns out that the trace does not couple to mesons until $\mathcal{O}(p^6)$.

6.3 Predictions and renormalization

The derivation of $\mathcal{L}_4$ follows similar lines although the complexity increases. At $\mathcal{O}(p^2)$ there are two quantities, apart from the quark masses, that need to be determined from experiment, F_0 and B_0. Constants appearing in the chiral Lagrangian are called low energy constants (LECs). At $\mathcal{O}(p^4)$ there are 10 LECs, usually denoted L_i in the three flavor case. Note that not every coupling constant is needed for every prediction, most processes require at least some of the 10 couplings for $\mathcal{O}(p^4)$ accuracy. It is also good to keep in mind that while the constants are called low energy constants, they really parameterize high energy physics, as discussed in section 4.

The $\mathcal{O}(p^4)$ LECs also serve to renormalize one loop contributions where vertices are $\mathcal{O}(p^2)$. As discussed in section 4.2 the renormalization scheme of choice is dimensional regularization and $\overline{MS}$, poles and some finite parts from loops are absorbed in higher order coupling constants. The remaining part of the LECs are expected to be suppressed with a factor $\mathcal{O}\left(1/\Lambda^2\right)$ when compared with coupling constants in $\mathcal{L}_2$.

[20] A coupling to the electromagnetic field is included via $r_\mu = l_\mu = eA_\mu \times \mathrm{diag}(2/3, -1/3, -1/3)$.

The predictions of χPT are then twofold. First, the same coupling constants are used in all processes. Second, the light pseudoscalar mesons propagate and interact. This gives rise to both logarithms and constant parts. Both of these predictions essentially follow from approximate symmetries of QCD.

Now that standard χPT has been introduced, we move on to modifications needed for using χPT to estimate corrections for quantities calculated using lattice QCD.

7 Lattice QCD

Correlation functions in QFT can be calculated as

$$\langle 0|T\left\{\phi(x,t)\phi(x,0)\right\}|0\rangle = \frac{1}{N}\int D\phi\phi(x,t)\phi(x,0)\exp(iS). \tag{124}$$

One way to do this would be to select the most important field configurations and sum over only these. However, due to the i in the exponential, it is difficult to find the most important configurations. Contributions from different configurations cancel due to phase differences, which is not something which can be judged easily from a single configuration. A solution to this problem is to switch from Minkowski space to Euclidean space

$$\langle 0|\phi(x,t)\phi(x,0)|0\rangle_E = \frac{1}{N}\int D\phi\phi(x,t)\phi(0,0)\exp(-S_E) \tag{125}$$

where S_E is the same as S except for the change $t \to it$. As long as S_E stays positive the most important field configurations are the ones where S_E is small. The correlation function can now be calculated using techniques from statistical mechanics.

The correlation functions calculated in Minkowski and Euclidean space are not the same but they are related. Inserting a complete set of states in the Minkowski correlation function and Fourier transforming at $p = 0$, which is the same as integrating over x, gives

$$\begin{aligned}
&\int dx \sum_n \langle 0|\phi(x,t)|n\rangle \langle n|\phi(x,0)|0\rangle \\
&= \int dx \sum_n \langle 0|\exp(-iHt)\phi(x,0)\exp(iHt)|n\rangle \langle n|\phi(x,0)|0\rangle \\
&= \sum_n c_n \exp(im_n t)
\end{aligned} \tag{126}$$

where in the first equality we have used that the Hamiltonian is the generator of time translation and in the second equality that at zero momentum the eigenvalues of the Hamiltonian are the masses. Changing $t \to it$ gives the Euclidean correlation function as

$$\int dx \langle 0|\phi(x,t)\phi(x,0)|0\rangle_E = \sum_n c_n \exp(-m_n t). \tag{127}$$

This follows since the same Hamiltonian shows up in both cases. Calculating correlation functions in Euclidean space gives information about the states in Minkowski space.

In QCD, a similar analysis goes through with some complications. One is that quarks are fermions, not really numbers that can be sampled. This can be dealt with by integrating out the quarks from the generating functional.

$$\begin{aligned} Z &= \int DGDqD\bar{q} \exp\left(-\int d^4x \bar{q}\left(\gamma^\mu D_\mu + m\right)q - S_{gluon}\right) \\ &= \int DGDqD\bar{q} \exp\left(-\bar{q}Mq - S_{gluon}\right) \\ &= \int DG \det M \exp\left(-S_{gluon}\right) = \int DG \exp\left(-S_{gluon} + \ln\det M\right) \end{aligned} \tag{128}$$

where the second equal sign defines the Dirac operator M. Note that it depends on the gluon field configuration.

Meson masses can be accessed through correlation functions as

$$\begin{aligned} &\left\langle 0|\bar{u}(t)\gamma^5 d(t)\bar{d}(0)\gamma^5 u(0)|0\right\rangle \\ &= \sum_n \left\langle 0|\bar{u}(0)\gamma^5 d(0)\exp(-Ht)|n\right\rangle \left\langle n|\bar{d}(0)\gamma^5 u(0)|0\right\rangle \\ &= \sum_n c_n \exp(-m_n t). \end{aligned} \tag{129}$$

Where all the states n must have the same quantum numbers as $\bar{u}\gamma^5 d$. This can be evaluated as

$$\begin{aligned} &\left\langle 0|\bar{u}(t)\gamma^5 d(t)\bar{d}(0)\gamma^5 u(0)|0\right\rangle \\ &= \int DGDqD\bar{q}\,\bar{u}(t)\gamma^5 d(t)\bar{d}(0)\gamma^5 u(0) \exp\left(-\int d^4x \bar{q}\left(\gamma^\mu D_\mu + m\right)q - S_{gluon}\right) \\ &= \int DG \left\langle M^{-1}_{u(0,t)}\gamma^5 M^{-1}_{d(t,0)}\gamma^5\right\rangle \det M \exp\left(-S_{gluon}\right) \end{aligned} \tag{130}$$

where $\langle\ldots\rangle$ is a trace over color and spin. The matrix M really deserves a bit more attention. Every field q contains 4 spinors and 3 colors. There are as many such fields as there are flavors. Each of these also depend on x, y, z, t. The matrix M is a collection of all these different labels into a matrix. The notation M_u means that the flavor should be kept fixed in the trace. The notation $M_{(0,t)}$ means that the left index should be chosen so that time is zero and the right index such that time is t.

Lattice QCD is a way to do the above in practice. Spacetime is divided into a lattice in a finite volume. The lattice is a regulator for high energy modes as described in section 3. In

this case there is then a finite, but very large, number of variables. Importance sampling can then be used to determine the most important field configurations.

Using importance sampling to estimate a physical observable leads to a statistical uncertainty. In lattice QCD there are also systematic uncertainties. Some of the papers deal with estimating such systematic uncertainties using χPT . The systematic uncertainties considered are

- Finite volume
- Twisted boundary conditions
- Unphysical quark masses
- Different masses for sea and valence quarks
- Finite lattice spacing for staggered quarks[21]

χPT is useful in estimating these error sources since they are dominated by light states and the underlying effects can be systematically included. Calculating physical observables to high enough precision on the other hand, requires taking effects from heavier states into account which is done in lattice QCD simulations.

7.1 Discretizing QCD

In section 5 $SU(3)_C$ gauge invariance was introduced. The quark fields were allowed to transform in a spacetime dependent way under gauge transformations. The gluons then transformed in a way which canceled the quark transformations rendering an invariant Lagrangian. When discretizing QCD it is beneficial to look at this from a slightly different perspective.

The transformations of quark fields under a gauge transformation take place in an internal space. For simplicity, let us call the transformations rotations in an internal space. The spacetime dependence of gauge transformations means that each spacetime point has its own internal space which is rotated independently of the rotations in all other spacetime points. In order to take derivatives, quark fields in different spacetime points are compared. For a gauge invariant theory, the rotations applied in each spacetime point can not have physical consequences. The covariant derivative is introduced in order to be able to compare different spacetime points in a way which is independent of the rotations. The role of the gluons, and their transformations, is then to enable comparison of quarks at different

[21] A particular type of formulation of lattice quarks, see rest of section 7.3

spacetime points in a gauge invariant way. With this short detour we can discuss how to discretize QCD.

We now treat spacetime as a lattice and define the quark fields only on the points of the lattice. The next step is to define a discretized version of the Dirac operator M. The Dirac operator contains derivatives and in order to take derivatives on the lattice, fields at different points are compared. Derivatives, and therefore gluons, are then associated with the links connecting different points. In the following we will assume that the kinetic term for the gluons is somehow discretized. In this case the most straightforward way of discretizing the quark part of the QCD action is

$$S = \sum_x \bar{q}(x)\left(\gamma_\mu \Delta^\mu(U) + m\right) q(x) \tag{131}$$

where the sum is over all points in spacetime and

$$\Delta_\mu(U)q(x) = \frac{1}{2a}\left(U_\mu(x)q(x + a\hat{\mu}) - U^\dagger(x - \hat{\mu})q(x - a\hat{\mu})\right) \tag{132}$$

with $U_\mu(x)$ the gluon link field, a the lattice spacing and m the bare quark mass. This action has the correct continuum limit and has chiral symmetry when $m = 0$. The propagator in the massless limit is

$$\frac{a}{i\sum_\mu \gamma_\mu \sin(p_\mu a)} \tag{133}$$

which has 16 poles. This means that there are 16 quarks present on the lattice. This problem is known as fermion doubling.

One solution to this problem, proposed by Kenneth Wilson, is based on that physical predictions are extracted from lattice QCD in the continuum limit, where the lattice spacing goes to zero, $a \to 0$. Wilson added an extra term term which doesn't effect the continuum limit but gives the doubler quarks masses proportional to $1/a$. These would then decouple in the continuum limit. Unfortunately, this term breaks chiral symmetry. Chiral symmetry protects the fermion masses from additive shifts from quantum effects. The pions can still be made light, but this requires tuning of the bare parameters.

There are other ways of dealing with doublers. However, there is a theorem showing that, under certain assumptions, the doublers can not be removed without breaking chiral symmetry. One way to deal with the doubling problem, the rooted staggered quark formulation, is introduced below. This formulation does not have full chiral symmetry but there is a symmetry which protects the quark masses from additive mass shifts from quantum effects. From a χPT perspective, it is easier to develop the concept of partially quenched (PQ) QCD before discussing staggered quarks so we now turn to PQQCD.

7.2 Partially quenched QCD

"Physical results from unphysical simulations"
—Title of [22]

Quarks are included in lattice ensembles by integrating them out which gives a determinant of the Dirac operator, M. When evaluating correlation functions, inverses of the Dirac operator are calculated. Although unnatural from a physics perspective, there is nothing stopping that the Dirac operators used in the different cases be different. This is the idea behind PQQCD where the masses are taken different in the two evaluations. This is useful since light quarks are expensive to simulate and it also gives an extra handle on the systematic errors. In order to get quantitative results from PQ simulations, the errors introduced must be quantified. This can be done using PQ χPT . Using this technique it is possible to get physical results from unphysical simulations [22].

Continuum description

The lattice is not needed to show how PQQCD can be formulated. Suppose that the quark part of the Lagrangian is

$$\mathscr{L}^{PQ}_{quark} = \bar{q}_v M_v q_v + \bar{\tilde{q}}_v \tilde{M}_v \tilde{q}_v + \bar{q}_s M_s q_s \tag{134}$$

where q_v and q_s are fermionic Dirac fields and $\tilde{q}_v$ is a bosonic Dirac field. Integrating out the three Dirac fields as in (128) gives

$$Z = \int DG \frac{\det M_v}{\det \tilde{M}_v} \det(M_s) \exp\left(-S_{gluon}\right). \tag{135}$$

Setting $\tilde{M}_v = M_v$ then gives that the fraction of determinants is equal to one. This gives that the fermionic and bosonic quarks with subscript v have the same mass. Effectively only the fermionic quark field q_s is needed in the generation of ensembles. When later evaluating correlation functions these can be taken with q_v instead which gives powers of M_v^{-1} in (130).

The above example introduces a bosonic Dirac field in order to get a determinant in the denominator. This violates spin-statistics and thus the theory is sick. The sickness doesn't disqualify it from a statistical mechanics treatment, it just means that this is no longer a good QFT. There exists a subspace in $\{m_v, m_s\}$ where the theory is no longer sick. With the help PQχPT , it is possible to estimate the effect of the sickness and compensate for it.

Partially quenched χPT

There are, at least, three ways of implementing PQχPT , the supersymmetric method, the replica method and the quark flow method. The supersymmetric method draws upon the description above with fermionic and bosonic quarks yielding fermionic and bosonic mesons. It was developed in the quenched[22] case in [23, 24] and for the partially quenched case in [22, 25, 26]. The replica method has only fermionic quarks but keeps a variable number of valence quarks. Sea quark contributions correspond to summing over all quarks and partial quenching is achieved by setting the number of valence quarks to zero in such sums [27]. Here, I will briefly describe the third method since this is the method we have used in the papers.

For the quark flow method we start from $SU(3)$ χPT with the difference that the trace of M is not integrated out,

$$U = \exp\left(i\sqrt{2}\frac{M}{F_0}\right), \quad M = \begin{pmatrix} U & \pi^+ & K^+ \\ \pi^- & D & K^0 \\ K^- & \bar{K}^0 & S \end{pmatrix}. \tag{136}$$

The mesons on the diagonal are single flavor neutral mesons, for example U stands for a $\bar{u}u$ meson. In order to enforce that the trace of M, corresponding to the η', should be heavy a mass term is introduced in $\mathscr{L}_2$ as

$$\mathscr{L}_2 = \frac{F^2}{4}\left\langle D_\mu U (D^\mu U)^\dagger \right\rangle + \frac{F^2}{4}\left\langle U\chi^\dagger + \chi U^\dagger \right\rangle + \frac{m_0^2}{3}\left\langle U + D + S \right\rangle^2. \tag{137}$$

η' is removed from the model by letting $m_0 \to \infty$ at a later stage [26]. Note that the LECs are the same in PQχPT as in χPT , since these are defined in the chiral limit.

The virtue of this parameterization is that the indices on M can be interpreted directly as flavor indices [28, 29]. Every meson is a single flavor anti-flavor combination. In Feynman diagrams these can be written using a double line notation as in Figure 4. In these diagrams each line corresponds to a quark and each double line corresponds to a single meson. In diagrams of this sort there will be lines which are connected to some external line and there will be lines which go in a loop. Lines that connect to external lines have their flavor determined by the external flavors. These lines describe valence quarks. Lines that form loops can take on any flavor, giving a sum over flavor. These lines describe sea quarks. PQ is then implemented by giving different masses to mesons depending on the valence and sea properties of the quark constituents.

The mass term for the η' in the Lagrangian gives a slight complication. Diagrammatically the mass term gives rise to a disconnected vertex between flavor neutral mesons, see Figure 5.

[22] In the quenched approximation QCD is simulated without sea quarks.

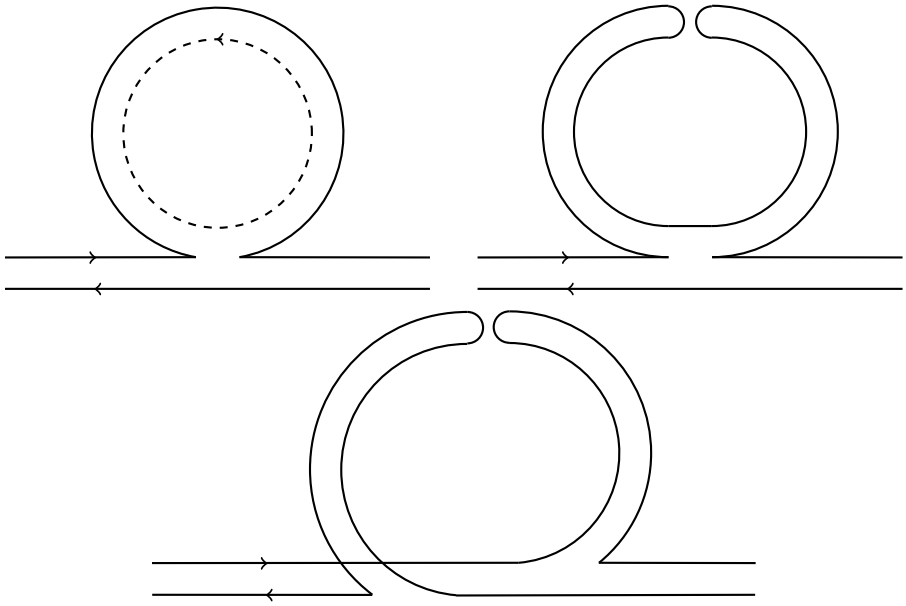

Figure 4: Examples of diagrams in double line notation for meson mass correction. Each line corresponds to a quark and each double line corresponds to a meson. The dashed loop indicates a sea quark contribution whereas the other diagrams contain only valence quark contributions. The disconnected pieces in the last two diagrams indicate the second term of the diagonal propagator in (138).

These diagrams can be resummed giving a slightly complicated propagator for the neutral mesons as

$$\mathscr{D}_{AB} = \frac{i\,\delta_{AB}}{p^2 - m_A^2} + \frac{i\,m_0^2}{3}\frac{(p^2 - m_U^2)(p^2 - m_D^2)(p^2 - m_S^2)}{(p^2 - m_A^2)(p^2 - m_B^2)(p^2 - m_\eta^2)(p^2 - m_{\pi^0}^2)(p^2 - m_{\eta'}^2)}, \tag{138}$$

where A and B signify flavor neutral mesons, sea or valence, m_U, m_D, m_S are masses for the flavor neutral sea mesons and $m_\pi, m_\eta, m_{\eta'}$ are masses for sea mesons. The mass of the η' is proportional to m_0. Taking the limit $m_0 \to \infty$ effectively removes η' from the theory. Note that there are double poles present when $A = B$ unless there are cancellations with the numerator. We can now move on to the effects of staggered quarks.

7.3 Staggered quarks

One partial solution to the doubling problem of lattice quarks is to use staggered quarks. This formulation is equivalent to using naive quarks but in a way where the 16-fold degeneracy is lifted to a 4-fold degeneracy, see [30]. This is done by constructing a change of

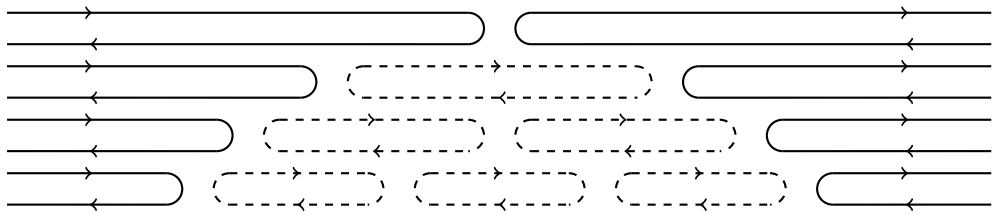

Figure 5: Disconnected propagator contributions due to the vertex from the η' mass term. The dashed loops are sea quark loops. The sum over all such contributions gives the second term in the diagonal propagator in (138).

variables which gives an action which is diagonal in spinor space. That is,

$$\mathscr{L} = \bar{q}(x)\left(\gamma_\mu \partial^\mu + I_{\text{spinor}} m\right) q(x) = \bar{\chi}(x) I_{\text{spinor}} \left(\alpha_\mu(x)\partial^\mu + m\right)\chi(x), \tag{139}$$

where I_{spinor} is the identity matrix in spinor space and $\alpha_\mu(x)$ are functions from the transformations. Due to the diagonal structure of the Dirac operator the spinor components are equivalent and do not mix in this basis. The propagator for the fields χ then reads

$$\langle \chi(x)\bar{\chi}(y)\rangle = s(x,y) I_{\text{spinor}}. \tag{140}$$

All the components of the spinor are equivalent and only one component has to be simulated, this is the staggered quark formulation. It is then possible to reassemble the staggered quarks into 4-fold degenerate Dirac spinors by considering a 2^4 block on the lattice. The 4 quarks corresponding to a single flavor are usually referred to as 4 tastes. This implementation of Dirac spinors yields intricate symmetry properties for the action, see [31]. For more information on the most common implementation of staggered quarks in contemporary lattice QCD, see [30].

In order to deal with the 4-fold degeneracy the 4th root of the determinant is taken in (128). A motivation is that in the continuum theory each quark contributes a determinant, here there is only one determinant for 4 quarks and taking the 4th root should then reduce the number of quarks to one. That this procedure works as intended is not proven non-perturbatively. However, the procedure seems to produce good physical results and attempts to disprove it have been refuted. For the interested reader I refer to [31].

Rooted staggered χPT

χPT for a single flavor staggered quark was derived in [32]. That result was generalized to multiple flavors in [33]. Before getting into describing staggered χPT I want to emphasize what it is that we want to describe. As noted in section 6 χPT is an expansion in masses and momenta. Here we want to add an additional expansion parameter which is the lattice spacing. To illustrate how this is done we will focus on the single flavor, or 4 taste case.

According to section 4 on EFT the symmetries of the underlying theory must be identified. To start we note that the continuum limit of the staggered lattice action is the QCD action with 4 quarks of the same mass. The action in the continuum limit, suppressing the gluon part, is then

$$S_{\text{continuum}} = \int d^4x \left[\bar{Q}^i \left(\gamma^\mu D_\mu - m \right) \delta_i^j Q_j \right] \tag{141}$$

$i, j = 1, \ldots, 4$ in taste space. This action has an $SU(4)$ taste symmetry, analogous to the $SU(3)$ symmetry in QCD with $m_u = m_d = m_s$. In analogy with $SU(3)$ χPT we then expect there to be 15 degenerate pseudoscalars, referred to as pions below, in the low energy theory. As stated above, the lattice spacing will be treated as a small parameter which may reduce the symmetry group and break the degeneracy of the pions.

The reduction of the symmetry group $SU(4)$ due to the finite lattice spacing can be taken into account using an effective action, valid for $p \ll \Lambda \sim 1/a$, with higher-dimensional operators with coefficients proportional to the lattice spacing[23]. These higher-dimensional operators come from integrating out modes near the cut-off. These modes must respect the symmetries of the lattice action. In this case, there are no operators of dimension five that are consistent with all the lattice symmetries. The action including the leading correction in a is then

$$S_{\text{eff}} = S_4 + a^2 S_6, \tag{142}$$

where S_4 and S_6 contain operators of dimension 4 and 6, respectively. The symmetries of this action were analyzed in [32].

Presenting the full analysis of S_6 is not interesting in this context. However, I want to point out that any term which breaks $SU(4)$ symmetry would have something like

$$\bar{Q}^i A_i^j Q_j \tag{143}$$

where i, j are taste indices and A is a matrix in taste space which is not proportional to the unit matrix. These terms do occur in S_6 and break the $SU(4)$ symmetry down to the lattice symmetry, except for a continuous translation symmetry[24].

A naive expectation on the low energy effective theory is then that it should have the same symmetry as S_{eff}, no more and no less. At $\mathcal{O}(a^2)$ this turns out, however, not to be the case. In particular the low energy effective theory has an $SO(4)$ symmetry at this order. The effective Lagrangian is, ignoring vector and axial source terms,

$$\mathcal{L}_2 = \frac{F^2}{4} \left\langle \partial_\mu U (\partial^\mu U)^\dagger \right\rangle - \frac{F^2}{2} B_0 m \left\langle U^\dagger + U^\dagger \right\rangle + \frac{m_0^2}{3} \langle U + D + S \rangle^2 + \mathcal{L}_2^{break}. \tag{144}$$

[23] This is an EFT technique and we should expect effects of $\mathcal{O}\left(\frac{p}{\Lambda}\right)$, heavy quarks must be treated differently.

[24] This might be interpreted as that low energy modes are somewhat less sensitive to the lattice spacing.

The matrices U are $U(4)$ matrices, since we have kept the η' like state, transforming analogously to the $SU(3)$ matrices in section 6.1. The Lagrangian $\mathscr{L}_2^{break}$ is

$$\begin{aligned}\mathscr{L}_2^{break} =& a^2 C_1 \operatorname{Tr}\left(\xi_5 U \xi_5 U^\dagger\right) \\ &+ a^2 C_2 \frac{1}{2} \operatorname{Tr}\left(U^2 - \xi_5 U \xi_5 U + \text{h. c.}\right) \\ &+ a^2 C_3 \frac{1}{2} \operatorname{Tr}\left(\xi_\nu U \xi_\nu U + \text{h. c.}\right) \\ &+ a^2 C_4 \frac{1}{2} \operatorname{Tr}\left(\xi_{5\nu} U \xi_{5\nu} U + \text{h. c.}\right) \\ &+ a^2 C_5 \frac{1}{2} \operatorname{Tr}\left(\xi_\nu U \xi_\nu U^\dagger - \xi_{\nu 5} U \xi_{\nu 5} U^\dagger\right) \\ &+ a^2 C_6 \operatorname{Tr}\left(\xi_{\mu\nu} U \xi_{\nu\mu} U^\dagger\right). \end{aligned} \tag{145}$$

Where the 16 matrices in the set $S^a = \{\xi_5, i\xi_{\mu 5}, i\xi_{\mu\nu}(\mu < \nu), \xi_\mu, I\}$ are generators of $U(4)$. Note that these are in taste space. The fact that all indices match up implies an $SO(4)$ taste symmetry[25]. Writing

$$U = \exp\left(i\frac{\phi}{F}\right), \qquad \phi = \sum_{a=1}^{16} \phi^a S^a \tag{146}$$

a calculation of the masses shows that pions associated with the same group of generators are degenerate, giving five groups of mesons. In contrast the $U(4)$ symmetry falls into eight groups in the lattice formulation [34]. When including N_f flavors the matrix U is a $U(4N_f)$ matrix. Only the taste singlet flavor singlet meson gets a mass term from the anomaly and is integrated out.

The description of SχPT above has not yet touched on the subject of rooting. The whole idea with rooting is to remove unwanted sea quark degrees of freedom, the valence quarks do not enter the functional determinant. In section 7.2 the quark flow method was used to sum over sea quarks. Using the same technique together with staggered χPT it is possible to simply divide by 4 for every sea quark sum. From this perspective, the effect of rooting is not to remove three out of 4 quarks but rather to weight each sea quark by a factor $1/4$.

7.4 Finite volume and twisted boundary conditions

Lattice QCD simulations necessarily take place in a finite volume. In order to avoid boundary effects, simulations are performed with boundary conditions which eliminate

[25] If taste indices would be summed with lorentz indices this would imply that we had an invariance under simultaneous taste and Lorentz transformations.

the boundary. One example is the use of periodic boundary conditions where, for spatial extent L and working in one dimension for notational convenience, the fields must satisfy

$$\phi(x+L) = \phi(x). \tag{147}$$

Fourier transforming both sides gives that the momentum of the field must satisfy

$$p = n\frac{2\pi}{L},\ n \in \mathbb{Z}. \tag{148}$$

For $L = 5$ fm, which is rather large for lattice QCD simulations, momentum is quantized in steps of about 250 MeV. Whether the steps are to be considered large is process dependent. For quantities such as hadronic vacuum polarization used for calculating muon $g-2$ or hadronic form-factors relevant for the determination of CKM elements the steps are large, see paper III and V.

One way around the problem is to use twisted boundary conditions defined by

$$\phi(x+L) = \phi(x)\exp(i\theta) \tag{149}$$

for an arbitrary angle θ. Fourier transforming this expression yields

$$p = n\frac{2\pi}{L} + \frac{\theta}{L},\ n \in \mathbb{Z}. \tag{150}$$

In this way arbitrary momenta can be considered. Only complex fields can be twisted in this way since $\phi^\dagger = \phi$ enforces $\theta = 0$.

An alternative way to describe twisted boundary conditions is to redefine new fields which satisfy periodic boundary conditions. Such a field is

$$\acute{\phi}(x) = \phi(x)\exp\left(-\theta\frac{x}{L}\right). \tag{151}$$

Any derivative acting on $\phi(x)$ will give the result

$$\partial_x\phi(x) = \partial_x\left(\acute{\phi}(x)\exp\left(\theta\frac{x}{L}\right)\right) = \exp\left(\theta\frac{x}{L}\right)\left(\partial_x + i\frac{\theta}{L}\right)\acute{\phi}(x). \tag{152}$$

Considering the case when all terms in the Lagrangian are real, which is enough for our purposes, all exponentials of θ vanish. The remnant of the twisted boundary conditions is that derivatives are shifted. This is exactly how the external fields enter covariant derivatives and the twisted boundary condition can be interpreted as a constant external field [35].

From a χPT perspective finite volume changes every loop integral into a sum over allowed momenta [36],

$$\int\frac{d^dp}{(2\pi)^d} \to \int_V\frac{d^dp}{(2\pi)^d} = \int\frac{d^{d-3}p}{(2\pi)^{d-3}}\frac{1}{L^3}\sum_{p\in\text{allowed momenta}}. \tag{153}$$

The integral is in d dimensions since it will still have to be regularized. The sums can be evaluated with the help of the Poisson summation formula. Using notation where $f(k)$ stands for some integrand in a loop calculation, for example $f(k) = i/(k^2 - m^2)$, and where $\hat{g}$ is the Fourier transform of g, the sum, in one dimension for simplicity, is evaluated as

$$\begin{aligned}
\frac{1}{L}\sum_{n\in\mathbb{Z}} f\left(\frac{2\pi}{L}n + \frac{\theta}{L}\right) &= \frac{1}{L}\sum_{n\in\mathbb{Z}} g(n) \\
&= \frac{1}{L}\sum_{l\in\mathbb{Z}} \hat{g}(l) \\
&= \frac{1}{L}\sum_{l\in\mathbb{Z}} \int dy\, f\left(\frac{2\pi}{L}y + \frac{\theta}{L}\right)\exp(-2\pi i l y) \\
&= \sum_{l\in\mathbb{Z}} \int \frac{dk}{2\pi} f(k)\exp(-i l k L)\exp(i\theta l)
\end{aligned} \tag{154}$$

where the Poisson summation formula was used in the second equality and where the last equality is from a change of variables, $\frac{2\pi}{L}y + \frac{\theta}{L} = k$. The sum over l has the striking feature that $l = 0$ corresponds to the infinite volume expression. It is then possible to sum over $l \neq 0$ to isolate the finite volume effects.

In QCD it is the quark fields which can be twisted. A quark field with twist angle θ leads to an anti-quark field with twist angle $-\theta$. Mesons get their twist angle from the quarks. A meson $\phi_{\bar{q}q'}$, where $\bar{q}q'$ indicates the quark content, satisfies

$$\phi_{\bar{q}q'}(x + L) = \phi_{\bar{q}q'}(x)\exp(i(\theta_{q'} - \theta_q)), \tag{155}$$

where $\theta_{q'}$ and θ_q are the twists of the q' and q quark fields, respectively. For flavor neutral mesons it is not possible to enforce twisted boundary conditions. One effect that we found in paper 1 is that the meson masses become momentum dependent when twisted boundary conditions are considered. The momentum dependence of the masses were needed in order to fulfill Ward identities related to form-factors.

7.5 Connected and disconnected diagrams

Flavor neutral mesons do not twist. In cases where arbitrary momentum for a flavor neutral meson is needed it is possible to use symmetry to relate flavor neutral processes to flavor charged ones, using the Wigner Eckhart theorem. There is a little problem with using the Wigner Eckhart theorem in this way. The assumed symmetry is broken by the twisted boundary conditions. Moreover, in lattice QCD there are both connected and disconnected contributions to flavor neutral external states. For flavor charged external states there are only connected contributions. This is explained further in Figure 6. The evaluation of

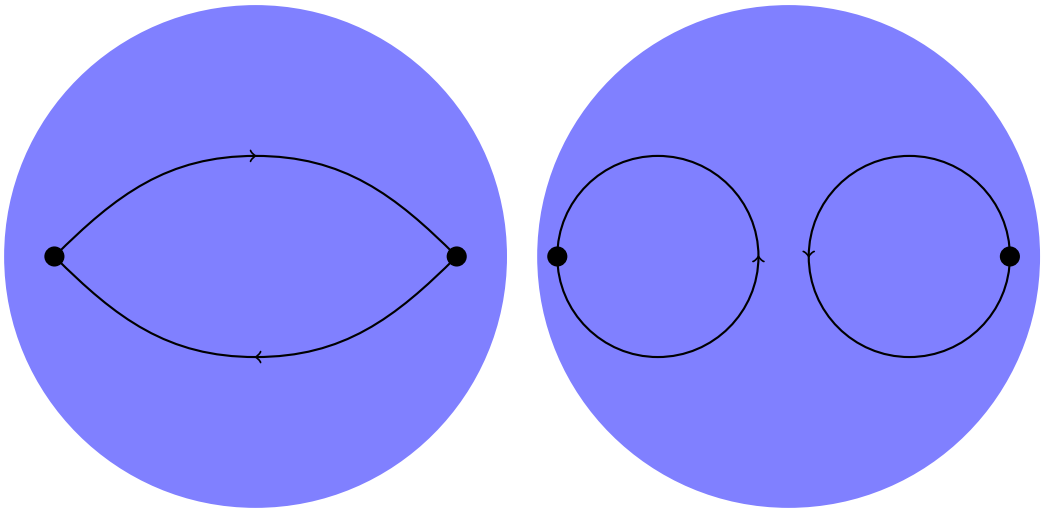

Figure 6: Example of a connected and a disconnected diagram. The lines are valence quark lines and the background color indicates a sea of quarks and gluons which interact with the valence quarks. Correlation functions between flavor charged operators such as $\bar{u}d$ give only connected diagrams. Flavor neutral operators with different flavor content such as the pair $\bar{u}u$ and $\bar{d}d$ give only disconnected diagrams. Flavor neutral operators with the same quark content like a pair of $\bar{u}u$ give both types of diagrams. Twisted boundary conditions can not be used to adjust the momentum of neutral operators. Using the Wigner-Eckhart theorem to relate flavor neutral and flavor charged correlation functions only catches the connected contributions.

the disconnected parts can not be done using twisted boundary conditions. Whether this is a problem or not depends on the accuracy required. In paper IV, we used χPT to estimate the ratio between connected and disconnected diagrams for the electromagnetic two point function at NNLO, extending a previous analysis in [37].

8 Models for low energy QCD and the muon $g-2$

"You can plan a pretty picnic. But you can't predict the weather"
—Ms. Jackson by Outkast

The muon anomalous magnetic moment, muon $g-2$, describes the strength of the muon's interaction with external magnetic fields. The energy of a muon from interacting with a magnetic field is $E = \vec{m}\cdot\vec{B}$, where $\vec{B}$ is the magnetic field and $\vec{m}$ is the magnetic moment of the muon. The value of $\vec{m}$ is proportional to $\vec{L}+g\vec{S}$, where $\vec{L}$ is the angular momentum of the muon, $\vec{S}$ is the spin of the muon and g is the gyromagnetic ratio. The understanding of g has been an important part in the development of quantum mechanics. The progression can be summarized as

- Classical mechanics $g = 0$
- Quantum mechanics $g = 2$ from experiment
- Relativistic quantum mechanics $g = 2$ understood from theory
- Quantum field theory $g = 2(1 + a_\mu)$, where a_μ parameterizes deviations from 2, understood from theory

The quantity which is most often quoted in the literature is the relative deviation from 2,

$$a_\mu \equiv \frac{g-2}{2}. \tag{156}$$

The muon $g - 2$ continues to be an important quantity for testing our understanding of nature, as it is ever more precisely measured and calculated. There appears to be a discrepancy between SM prediction and experimental measurement of this quantity. The world average of the measured value is [3]

$$a_\mu^{\text{exp}} = 116592091(54)(33) \times 10^{-11} \tag{157}$$

where the first error is statistical and the second is systematic. The SM prediction from the same source is

$$a_\mu^{\text{SM}} = 116591803(1)(41)(26) \times 10^{-11} \tag{158}$$

where the errors are from the electroweak, lowest order hadronic and higher order hadronic contributions, respectively. The discrepancy between the SM prediction and experiment is about 3.6σ. The hadronic contributions contribute the most to the uncertainty in the SM prediction.

The hadronic vacuum polarization contribution can be calculated from $e^+e^- \to$ hadrons using dispersion relations, see the introduction to paper IV. Calculations using lattice QCD are also competitive. Predictions of the hadronic light by light (HLbL) contributions have, at least until recently, had to rely on modeling of low energy QCD. In this context modeling does not refer to the model χPT but instead to more phenomenologically motivated models taking for example ρ mesons as active degrees of freedom. Calculations using lattice QCD are also becoming available although it is a very difficult problem in that context as well.

The reason why χPT is not a good enough model in this case is that while it produces perfectly finite predictions for the light by light scattering part, these finite parts integrate to an infinite contribution, which can not be remedied by renormalization, when attaching the muon line[26].

[26] At least up to two loops in χPT .

One of the main obstacles in developing phenomenological models is that it is difficult to retain some notion of power counting. In χPT , meson masses and momenta are in the numerators and compensated for by $1/4\pi F$ from loop integrals or by suppressed couplings. A general feature for many ways of including matter fields is that terms with $1/m_V^2$ shows up. If momenta are larger than m_V, which is desirable for models extending χPT , this leads to problems in the power counting.

Another issue is that the existence of a good looking power counting scheme doesn't mean that the model captures the correct physics. One common approach which doesn't rely on power counting is to look at which additional states, beyond the lightest pseudoscalar mesons, that are the most important and include these. Something like phenomenological power counting. Which states that are most important for low energy phenomenology is not clear a priori. One way that this has been studied is to see if the LECs of χPT can be predicted using a subset of all resonances in low energy QCD.

8.1 Resonance saturation

The LECs of χPT can be estimated using models for the lightest mesons not included in χPT . In Ref. [18] the strong interactions of low lying meson resonances with spin ≤ 1 with the eight lightest pseudoscalar mesons were considered. What was found was that the lowest lying resonances to a large extent saturate the measured values of the LECs. This provides a basis for building models which is known as lowest meson dominance (LMD). This concept goes back further to the idea of vector meson dominance (VMD) which states that the ρ meson dominates the coupling between pions and photons. Importantly, in the case of HLbL the vector meson ρ and, to some extent, the axial vector meson a_1 contribute to the relevant LECs. It is this line of thinking which led the authors of [38] to try include the a_1 meson in order to account for the pion polarizability.

While this line of reasoning provides a good start it does not pin down a unique model. There are many ways of adding additional mesons to the leading order χPT Lagrangian. Many of these ways are equivalent at tree level but differ when loops are considered. This will be discussed briefly in the next section.

8.2 Description of resonances

Chiral symmetry considerations gives good low energy predictions through χPT . One way of including matter fields in a way which is consistent with chiral symmetry is to have the fields in the adjoint representation

$$\rho_\mu = \rho_\mu^a T^a. \tag{159}$$

The CCWZ formalism then prescribes that the field should transform as

$$\rho_\mu \to h\rho_\mu h^\dagger \tag{160}$$

where h is the compensator field from section 6.1. The propagator for the ρ meson in such a formalism is

$$\frac{1}{p^2 - m_\rho^2}\left(g_{\mu\nu} - \frac{p_\mu p_\nu}{m_\rho^2}\right). \tag{161}$$

The factor $1/m_\rho^2$ will upset the power counting. An indication of this is that the limit $m_\rho \to 0$ is ill defined.

Another way, which we used in paper II, is to describe the vector mesons using an anti-symmetric tensor field

$$\rho_{\mu\nu} = \rho^a_{\mu\nu} T^a, \tag{162}$$

which transforms as in (160) with ρ_μ replaced by $\rho_{\mu\nu}$. The propagator is longer in this method but shares the property of containing inverse powers of m_ρ^2.

One way to include vector mesons which leads to successful power counting is hidden local symmetry (HLS)[39], see also [40]. This model assumes that along with $SU(3)_L \times SU(3)_R$ there is an additional $SU(3)_G$ symmetry. This symmetry group has quarks in the fundamental representation just like $SU(3)_L \times SU(3)_R$ but the left and right handed quarks are transformed with the same parameter. Moreover, the symmetry is assumed to be local. The symmetry breaking pattern is then $SU(3)_L \times SU(3)_R \times SU(3)_G \to SU(3)_V$ where in $SU(3)_V$ all three groups transform with the same parameter. This leads to 16 Goldstone bosons, 8 pseudoscalars and 8 scalars. Due to the local $SU(3)_G$ symmetry there must be massless vector gauge bosons in the unbroken phase. In the broken phase the scalars are eaten by the gauge fields which become massive and are identified as the lightest vector mesons, the lightest of these are ρ mesons. This leads to VMD as well as predictions for universality of the ρ coupling to pions from symmetry considerations.

The ρ meson propagator in this model in R_ξ gauge is

$$\frac{1}{p^2 - m_\rho^2}\left(g_{\mu\nu} - (1-\alpha)\frac{p_\mu p_\nu}{p^2 - \alpha m_\rho^2}\right), \tag{163}$$

which is well behaved in the limit $m_\rho \to 0$, see [41]. The reason why power counting works in HLS is the underlying local symmetry. However appealing this might be that does not make HLS the answer in low energy QCD model building. In the end, predictions must come out right and with HLS, as well as the other models, some do and some don't, see paper II.

In principle, all approaches which implement Weinberg's folk theorem should be equivalent. All of the models presented above are equivalent at tree level. Including loop effects and higher-dimensional operators the theories differ but this should be a truncation effect. Including all operators and all diagrams should give the same answer regardless of how the theory is implemented.

8.3 Additional constraints

In order to pin down a good model there are a lot of auxiliary constraints. One that is often imposed is that the model should reproduce the high energy behavior of QCD. To do this an operator product expansion is performed in QCD which gives the asymptotic behavior of some correlation function. This is then compared to the asymptotic behavior of the model. It is not clear that low energy models should respect high energy constraints from QCD, but if there is some intermediate region the models should overlap.

Another way to test a model is to test its predictions. If a model is to be used for HLbL calculations it should probably get the hadronic vacuum polarization, which is known to a larger relative precision, right. Checking whether a certain model saturates the LECs of χPT is another similar test. There are also sum rules which can be used to evaluate models.

Yet another possibility is to try several different models which all seem reasonable and see the spread in predictions as a theory error, as we did in paper II. There we also looked at which points in phase space that contribute to HLbL. All the models used in that analysis satisfy electromagnetic gauge invariance which is another important constraint.

In the end evaluating models for low energy QCD is hard. There are some conditions which must be satisfied and others which need to be given priority, depending on the observable under study. A uniquely determined model which offers systematic predictions is not yet available. Meanwhile, the lattice QCD community is progressing and many of the observables which previously required modeling will probably be computed with high precision numerical techniques. The discussion here has focused on Lagrangian models. There is also a possibility to use more data driven methods as dispersion relations, which provide a more direct link between experimental information and predictions.

References

[1] M. E. Peskin and D. V. Schroeder, "*An Introduction to quantum field theory*", Reading, USA: Addison-Wesley (1995) 842 p

[2] J. A. M. Vermaseren, "*New features of FORM*", math-ph/0010025

[3] K. A. Olive *et al.* [Particle Data Group Collaboration], "*Review of Particle Physics*", Chin. Phys. C **38** (2014) 090001.

[4] A. Zee, "*Quantum field theory in a nutshell*", Princeton, UK: Princeton Univ. Pr. (2010) 576 p

[5] G. 't Hooft, "*The Conceptual Basis of Quantum Field Theory*",

[6] M. D. Schwartz, "*Quantum Field Theory and the Standard Model*", ISBN-9781107034730.

[7] H. Georgi, "*Generalized dimensional analysis*", Phys. Lett. B **298** (1993) 187 [hep-ph/9207278].

[8] S. Weinberg, "*Phenomenological Lagrangians*", Physica A **96** (1979) 327.

[9] H. Leutwyler, "*On the foundations of chiral perturbation theory*", Annals Phys. **235** (1994) 165 [hep-ph/9311274].

[10] H. Georgi, "*Effective field theory*", Ann. Rev. Nucl. Part. Sci. **43** (1993) 209.

[11] J. Bijnens and A. A. Vladimirov, "*Leading logarithms for the nucleon mass*", Nucl. Phys. B **891** (2015) 700 [arXiv:1409.6127 [hep-ph]].

[12] S. Weinberg, "*The quantum theory of fields. Vol. 2: Modern applications*",

[13] S. Scherer and M. R. Schindler, "*A Chiral perturbation theory primer*", hep-ph/0505265

[14] H. Leutwyler, "*Foundations and scope of chiral perturbation theory*", Lect. Notes Phys. **452** (1995) 14 [hep-ph/9409423].

[15] S. R. Coleman, "*The structure of strong interaction symmetries*",

[16] J. Gasser and H. Leutwyler, "*Chiral Perturbation Theory to One Loop*", Annals Phys. **158** (1984) 142.

[17] J. Gasser and H. Leutwyler, "*Chiral Perturbation Theory: Expansions in the Mass of the Strange Quark*", Nucl. Phys. B **250** (1985) 465.

[18] G. Ecker, J. Gasser, A. Pich and E. de Rafael, "*The Role of Resonances in Chiral Perturbation Theory*", Nucl. Phys. B **321** (1989) 311.

[19] C. G. Callan, Jr., S. R. Coleman, J. Wess and B. Zumino, "*Structure of phenomenological Lagrangians. 2.*", Phys. Rev. **177** (1969) 2247.

[20] S. R. Coleman, J. Wess and B. Zumino, "*Structure of phenomenological Lagrangians. 1.*", Phys. Rev. **177** (1969) 2239.

[21] A. V. Manohar, "*Effective field theories*", Lect. Notes Phys. **479** (1997) 311 [hep-ph/9606222].

[22] S. R. Sharpe and N. Shoresh, "*Physical results from unphysical simulations*", Phys. Rev. D **62** (2000) 094503 [hep-lat/0006017].

[23] A. Morel, "*Chiral Logarithms in Quenched QCD*", J. Phys. (France) **48** (1987) 1111.

[24] C. W. Bernard and M. F. L. Golterman, "*Chiral perturbation theory for the quenched approximation of QCD*", Phys. Rev. D **46** (1992) 853 [hep-lat/9204007].

[25] C. W. Bernard and M. F. L. Golterman, "*Partially quenched gauge theories and an application to staggered fermions*", Phys. Rev. D **49** (1994) 486 [hep-lat/9306005].

[26] S. R. Sharpe and N. Shoresh, "*Partially quenched chiral perturbation theory without Phio*", Phys. Rev. D **64** (2001) 114510 [hep-lat/0108003].

[27] P. H. Damgaard and K. Splittorff, "*Partially quenched chiral perturbation theory and the replica method*", Phys. Rev. D **62** (2000) 054509 [hep-lat/0003017].

[28] S. R. Sharpe, "*Chiral Logarithms in Quenched M(π) and F(π)*", Phys. Rev. D **41** (1990) 3233.

[29] S. R. Sharpe, "*Quenched chiral logarithms*", Phys. Rev. D **46** (1992) 3146 [hep-lat/9205020].

[30] E. Follana *et al.* [HPQCD and UKQCD Collaborations], "*Highly improved staggered quarks on the lattice, with applications to charm physics*", Phys. Rev. D **75** (2007) 054502 [hep-lat/0610092].

[31] A. S. Kronfeld, "*Lattice Gauge Theory with Staggered Fermions: How, Where, and Why (Not)*", PoS LAT **2007** (2007) 016 [arXiv:0711.0699 [hep-lat]].

[32] W. J. Lee and S. R. Sharpe, "*Partial flavor symmetry restoration for chiral staggered fermions*", Phys. Rev. D **60** (1999) 114503 [hep-lat/9905023].

[33] C. Aubin and C. Bernard, "*Pion and kaon masses in staggered chiral perturbation theory*", Phys. Rev. D **68** (2003) 034014 [hep-lat/0304014].

[34] M. F. L. Golterman, "*Staggered Mesons*", Nucl. Phys. B **273** (1986) 663.

[35] C. T. Sachrajda and G. Villadoro, "*Twisted boundary conditions in lattice simulations*", Phys. Lett. B **609** (2005) 73 [hep-lat/0411033].

[36] J. Gasser and H. Leutwyler, "*Spontaneously Broken Symmetries: Effective Lagrangians at Finite Volume*", Nucl. Phys. B **307** (1988) 763.

[37] M. Della Morte and A. Juttner, "*Quark disconnected diagrams in chiral perturbation theory*", JHEP **1011** (2010) 154 [arXiv:1009.3783 [hep-lat]].

[38] K. T. Engel, H. H. Patel and M. J. Ramsey-Musolf, "*Hadronic light-by-light scattering and the pion polarizability*", Phys. Rev. D **86** (2012) 037502 [arXiv:1201.0809 [hep-ph]].

[39] M. Bando, T. Kugo, S. Uehara, K. Yamawaki and T. Yanagida, "*Is rho Meson a Dynamical Gauge Boson of Hidden Local Symmetry?*", Phys. Rev. Lett. **54** (1985) 1215. doi:10.1103/PhysRevLett.54.1215

[40] H. Georgi, "*Vector Realization of Chiral Symmetry*", Nucl. Phys. B **331** (1990) 311. doi:10.1016/0550-3213(90)90210-5

[41] M. Harada and K. Yamawaki, "*Hidden local symmetry at loop: A New perspective of composite gauge boson and chiral phase transition*", Phys. Rept. **381** (2003) 1 [hep-ph/0302103].

[42] S. Weinberg, "*What is quantum field theory, and what did we think it is?*", In *Boston 1996, Conceptual foundations of quantum field theory* 241-251 [hep-th/9702027].

Scientific publications

Paper I: Masses, decay constants and electromagnetic form-factors with twisted boundary conditions

We studied effects of twisted boundary conditions in lattice QCD using chiral perturbation theory. Twisted boundary conditions lead to broken reflection symmetry and gives new terms in the finite volume corrections. We presented results for masses, decay constants and electromagnetic form-factors. With twisted boundary conditions the masses become momentum dependent. We pointed out that this dependence must be taken into account in order for the Ward identities to be satisfied.

My contributions: We both performed all of the analytical and numerical calculations. My main contribution was to understand how the momentum dependent mass is needed for the Ward identities to be fulfilled as they should be. I wrote a draft of the paper which was modified by my supervisor.

Paper II: Pion light-by-light contributions to the muon $g-2$

There are two main topics in this paper. First we presented an argument for the relative size of connected and disconnected contributions to $g-2$ hadronic light-by-light contribution. Second we compared and evaluated different models for calculating the pion loop contribution. In particular we studied the contributions from different momentum regions and looked at how well the models live up to a QCD short distance constraint.

My contributions: In this paper both of us performed all of the analytical calculations. The calculations were independent to some extent. I did, however, rely a lot on my supervisor, especially in the early stages since this was our first project. We were both involved in trying to find finite solutions. Both of us also performed the numerical calculations. My supervisor wrote the paper.

Paper III: Partially quenched rooted staggered twisted finite volume corrections to K_{l3} decays

We calculated finite volume effects for K_{l3} decays in rooted staggered partially quenched lattice QCD with twisted boundary conditions using chiral perturbation theory. We gave analytical expressions and implemented these numerically. The estimate of the finite volume corrections when the specific lattice action is not taken into account were typically of the same order of magnitude as the estimate when the rooted staggered lattice action was taken into account. However, we found that the precise size and sign of the correction depends strongly on the extra effects.

My contributions: All collaborators have been involved in the analytical computations. Me and my supervisor did all of the analytical calculations independently and agreed with the other collaborators afterwards. We also implemented the needed numerics independently. In doing this I used my supervisors infinite volume integral expressions. I wrote the main draft for the paper which was modified by the other collaborators.

Paper IV: Connected, Disconnected and Strange Quark Contributions to HVP

We presented an argument showing why the ratio of disconnected to connected contributions to hadronic vacuum polarization is -1/2 for pions in two-loop chiral perturbation theory. We also pointed out what corrections are to be expected. The argument holds in the isospin limit up to corrections from higher orders in chiral perturbation and contributions from the strange quark. We checked these corrections at two loop in chiral perturbation theory. The corrections from strange quark contributions cancel to a large extent.

My contributions: The argument for the size of the ratio of disconnected to connected contributions was my supervisor's idea. The analytical and numerical calculations were performed independently by the two of us. I did all the comparison of our results. I wrote a draft for the paper which was modified by my supervisor.

Paper V: Vector two point functions in finite volume using partially quenched chiral perturbation theory at two loops

We calculated the vector two point functions in infinite and finite volume with twisted boundary conditions for partially quenched QCD using chiral perturbation theory. We presented analytical expressions and implemented them numerically. In the infinite volume case the two loop contribution dominates the one loop one. This is not the case for the finite volume corrections. We also used the partially quenched expressions to estimate the ratio of disconnected to connected contributions for the strange part of the electromagnetic

current. Finally, we suggested the use of different boundary conditions for testing finite volume effects using lattice data.

My contributions: We both performed all of the numerical and analytical calculations. We used quite different methods for the analytical part in this case but with the same result. I used my supervisors infinite volume integral expressions in my numerical work. I wrote a draft for the paper which we then worked on together.

Paper 1

Published for SISSA by Springer

Received: *February 7, 2014*
Accepted: *March 24, 2014*
Published: *May 5, 2014*

Masses, decay constants and electromagnetic form-factors with twisted boundary conditions

Johan Bijnens and Johan Relefors

Department of Astronomy and Theoretical Physics, Lund University, Sölvegatan 14A, SE - 223 62 Lund, Sweden

E-mail: bijnens@thep.lu.se, Johan.Relefors@thep.lu.se

Abstract: Using Chiral Perturbation Theory at one-loop we analyze the consequences of twisted boundary conditions. We point out that due to the broken Lorentz and reflection symmetry a number of unexpected terms show up in the expressions. We explicitly discuss the pseudo-scalar octet masses, axial-vector and pseudo-scalar decay constants and electromagnetic form-factors. We show how the Ward identities are satisfied using the momentum dependent masses and the non-zero vacuum-expectation-values values for the electromagnetic (vector) currents. Explicit expressions at one-loop are provided and an appendix discusses the needed one-loop twisted finite volume integrals.

Keywords: Lattice QCD, Chiral Lagrangians

ArXiv ePrint: 1402.1385

Open Access, © The Authors.
Article funded by SCOAP^3.

doi:10.1007/JHEP05(2014)015

JHEP05(2014)015

Contents

1 Introduction **1**

2 Chiral perturbation theory **3**

3 Finite volume with a twist **4**

4 Vector vacuum-expectation-value and two-point function **5**

5 Meson masses **6**

6 Decay constants **7**

7 Electromagnetic form-factor **11**
- 7.1 Analytic expressions 12
- 7.2 Ward identities 14
- 7.3 Numerical results 14

8 Comparison with earlier work **15**

9 Conclusions **18**

A Finite volume integrals with twist **19**
- A.1 Miscellaneous formulae 19
- A.2 Tadpole integral 19
- A.3 Two propagator integrals 21
- A.4 Integral relations 22

JHEP05(2014)015

1 Introduction

Lattice QCD calculations of hadronic quantities of necessity happen in a finite physical volume. In a box with periodic boundary conditions this leads to spatial momentum components $p^i = (2\pi/L)n_i$ which even for a large 4 fm lattice gives a minimum spatial momentum of about 300 MeV. In order to access smaller spatial momenta it has been suggested to use twisted boundary conditions [1–3]. This allows for more momenta to be sampled. Some early numerical tests were performed in [4].

It is well known that in a finite box Lorentz invariance is broken by the boundary conditions. In particular, the spatial part of the symmetry group becomes the cubic group

in case of periodic boundary conditions. Imposing twisted boundary conditions on a field ϕ in some spatial directions i via

$$\phi(x^i + L) = e^{i\theta_i L}\phi(x^i) \tag{1.1}$$

breaks the cubic symmetry down even further. In particular, reflection symmetry, $x^i \to -x^i$ in the i-direction is broken by (1.1).

In this paper we analyze the consequences of this for a number of quantities in Chiral Perturbation Theory (ChPT). In [2] ChPT for twisted boundary conditions was developed and they showed that finite volume corrections remain exponentially suppressed for large volumes. We use their method for masses, pseudo-scalar and axial-vector decay constants, the vector two-point function and electromagnetic form-factors. We have different expressions than those given in [2], the precise relation is discussed in more detail in section 8.

In general, form-factors and correlators can also have a much more general structure and this has consequences for the Ward identities. We discuss three examples of this. Another result is that vector currents get a vacuum-expectation-value (VEV), which leads to non-transverse vector two-point functions. The main goal of our paper is to study all this at one-loop order in ChPT.

Section 2 gives the lowest order Lagrangian in ChPT and defines a few other pieces of notation. We introduce twisted boundary conditions in section 3. The more technical derivation of the needed one-loop integrals is given in appendix A. As a first application we calculate the vacuum expectation value of vector currents and the two-point functions. We show how they do satisfy the Ward identities at finite volume. We find, in agreement with [5], that the two-point function is not transverse. The next two sections contain the results for the meson masses and the axial-vector and pseudo-scalar decay constants. Here again we see the occurrence of extra terms. The axial-vector matrix elements is not just described by the decay constant but there are other terms. The pseudo-scalar decay constants at infinite volume were not published earlier so we have included those expressions as well. We have explicitly checked that the Ward identities relating the axial-vector and pseudo-scalar matrix elements are satisfied. The extra terms in the axial-vector matrix element are needed to achieve this. We also add the mixed matrix elements due to the fact that the twisted boundary conditions break isospin. Numerical results are presented for all masses and the charged meson axial-vector decay constants.

Section 7 discusses the pion electromagnetic form-factor and related quantities. We show once more how finite volume and twisting allow for extra form-factors and have checked that with the inclusion of these the Ward identities are satisfied. We study in detail the finite volume corrections from the isospin current matrix element $\langle \pi^0(p')|\bar{d}\gamma_\mu u|\pi^+(p)\rangle$ which is used in lattice QCD to obtain information on the pion radius. We find that the corrections due to twisting can be sizable. Our main conclusions are summarized in section 9.

After finishing this work we became aware of the work in [6] where a number of the issues we discuss here were raised as well. The discussion there is in two-flavour theory but also includes partial twisting. We discuss the relation with our work in section 8.

JHEP05(2014)015

2 Chiral perturbation theory

ChPT is the effective field theory describing low energy QCD as an expansion in masses and momenta [7–9]. Finite volume ChPT was introduced in [10]. In this paper we work in the isospin limit for quark masses, i.e. $m_u = m_d = \hat{m}$, with three quark flavours. Results for two-quark flavours are obtained by simply dropping the integrals involving kaons and eta and replacing F_0, B_0 by F, B. We perform the calculations to next-to-leading order (NLO), or $\mathcal{O}(p^4)$. The Lagrangian to NLO is

$$\mathcal{L} = \mathcal{L}_2 + \mathcal{L}_4, \tag{2.1}$$

where $\mathcal{L}_{2n}$ is the $\mathcal{O}(p^{2n})$ Lagrangian. For the mesonic fields we use the exponential representation

$$U = e^{i\sqrt{2}M/F_0} \quad \text{with} \quad M = \begin{pmatrix} \frac{1}{\sqrt{2}}\pi^0 + \frac{1}{\sqrt{6}}\eta & \pi^+ & K^+ \\ \pi^- & -\frac{1}{\sqrt{2}}\pi^0 + \frac{1}{\sqrt{6}}\eta & K^0 \\ K^- & \bar{K}^0 & -\frac{2}{\sqrt{6}}\eta \end{pmatrix}. \tag{2.2}$$

We use the external field method [8, 9] to incorporate electromagnetism, quark masses as well as couplings to other quark-antiquark operators. To do this we introduce the field χ and the covariant derivative

$$\chi = 2B_0(s + ip), \quad D_\mu U = \partial_\mu U - ir_\mu U + iUl_\mu. \tag{2.3}$$

r_μ, l_μ, s and p are the external fields. Electromagnetism is included by setting

$$l_\mu = eA_\mu Q,\ r_\mu = eA_\mu Q, \tag{2.4}$$

where e is the electron charge, A_μ is the photon field and $Q = \mathrm{diag}(2/3, -1/3, -1/3)$. Masses are included by setting $s = \mathcal{M} = \mathrm{diag}(\hat{m}, \hat{m}, m_s)$ where $\hat{m} = (m_u + m_d)/2$.

With these definitions the lowest order Lagrangian $\mathcal{L}_2$ is

$$\mathcal{L}_2 = \frac{F_0^2}{4}\langle D_\mu U D^\mu U^\dagger + \chi U^\dagger + U\chi^\dagger \rangle \tag{2.5}$$

where the angular brackets denotes trace over flavour indices. The expression for $\mathcal{L}_4$ can be found in for example [8].

One problem at finite volume is the definition of asymptotic states, which we need to define the wave function renormalization and matrix elements. We assume the temporal direction to be infinite in extent and use the LSZ theorem to obtain the needed wave function renormalization by keeping the spatial momentum constant and taking the limit in $(p^0)^2$ to $p^2 = m^2$. We stick here to states with at most one incoming and outgoing particle so this is sufficient. Note that since Lorentz symmetry is broken the masses are different for the same particle with different spatial momenta.

We will not present the infinite volume expressions but only the corrections at finite volume using the quantity

$$\Delta^V X = X(V) - X(\infty), \tag{2.6}$$

where X is the object under discussion.

JHEP05(2014)015

3 Finite volume with a twist

Periodic boundary conditions on a finite volume implies that momenta become quantized. Adding a phase factor at the boundary shifts these discrete momenta. To see this, we impose for a field in one dimension at a fixed time

$$\psi(x+L) = e^{i\theta}\psi(x), \tag{3.1}$$

where L is the length of the dimension and θ is the twist angle. Developing both sides in a Fourier series we get

$$\sum_k \hat{\psi}_k e^{ik(x+L)} = \sum_k \hat{\psi} e^{ikx} e^{i\theta} \Rightarrow k = \frac{2\pi}{L}n + \frac{\theta}{L},\ n \in \mathbb{Z}. \tag{3.2}$$

The effect on anti-particles follows from the complex conjugate of (3.1); momenta are shifted in the opposite direction. It is possible to have different twists for different flavours and also different twists in different directions.

We impose now a condition like (3.1) on each quark field q in each spatial direction i

$$q(x^i + L) = e^{i\theta_q^i} q(x^i), \tag{3.3}$$

and collect the angles θ_q^i in a three vector $\vec{\theta}_q$ and a four-vector $\theta_q = (0, \vec{\theta}_q)$. The twist-angle vector for the anti-quark is minus the one for the quarks. For a meson field of flavour structure $\bar{q}'q$ this leads to a twisted boundary condition in direction i

$$\phi_{\bar{q}'q}(x^i + L) = e^{i(\theta_q^i - \theta_{q'}^i)} \phi_{\bar{q}'q}(x^i)\,. \tag{3.4}$$

We introduce the meson twist angle vector θ_ϕ in the same way as above and we will use the conventional $\pi^\pm, \ldots$ for labeling them... Note that flavour diagonal mesons are unaffected by twisted boundary conditions. A consequence of the boundary conditions (3.4) is that charge conjugation is broken since $\phi_{\bar{q}q'}$ and $\phi_{\bar{q}'q}$ have opposite twist. A particle with spatial momentum $\vec{p}$ corresponds to an anti-particle with momentum $-\vec{p}$.

In terms of loop integrals over the momentum of a meson M this means that we have to replace the infinite volume integral by a sum over the three spatial momenta and an integral over the remaining dimensions

$$\int \frac{d^d k_M}{(2\pi)^2} \to \int_V \frac{d^d k}{(2\pi)^d} \equiv \int \frac{d^{d-3}k}{(2\pi)^{d-3}} \frac{1}{L^3} \sum_{\substack{\vec{n}\in\mathbb{Z}^3 \\ \vec{k}=(2\pi\vec{n}+\vec{\theta}_M)/L}} . \tag{3.5}$$

It is explained in [2] how this ends up with the correct allowed momenta for each propagator in a loop. The allowed momenta $\vec{k} = (2\pi\vec{n} + \vec{\theta}_M)/L$ are not symmetric around zero and thus reflection symmetry is broken. An immediate consequence is that

$$\int_V \frac{d^d k}{(2\pi)^2} \frac{k^\mu}{k^2 - m^2} \neq 0\,. \tag{3.6}$$

Note also that a meson and its anti-meson carry different momenta and it is therefore important to keep track of which one is in a loop, as well as to be careful with using charge

JHEP05(2014)015

conjugation. The twist angles also bring in another source of explicit flavour symmetry breaking.

The one-loop integrals needed are worked out using the methods of [11, 12] and presented in detail in appendix A. The notation we use indicates the mass of the particle but implies also the corresponding twist vector in the expressions.

4 Vector vacuum-expectation-value and two-point function

Because of (3.6) the vacuum-expectation-value of a vector-current is non-zero and we obtain

$$\begin{aligned}
\langle \bar{u}\gamma_\mu u\rangle &= -2A^V_\mu(m^2_{\pi^+}) - 2A^V_\mu(m^2_{K^+})\\
\langle \bar{d}\gamma_\mu d\rangle &= 2A^V_\mu(m^2_{\pi^+}) - 2A^V_\mu(m^2_{K^0})\\
\langle \bar{s}\gamma_\mu s\rangle &= 2A^V_\mu(m^2_{K^+}) + 2A^V_\mu(m^2_{K^0})\\
\langle j^{em}_\mu\rangle &= -2A^V_\mu(m^2_{\pi^+}) - 2A^V_\mu(m^2_{K^+})\,.
\end{aligned} \tag{4.1}$$

We used here that $\theta_{\pi^-} = -\theta_{\pi^+}$, $\theta_{K^+} = -\theta_{K^-}$, $\theta_{K^0} = -\theta_{\overline{K}^0}$ and $\theta_{\pi^0} = \theta_\eta = 0$. This non-zero result can be understood better if we look at the alternative way of including twisting in ChPT [2]. The twisted boundary conditions can be removed by a field redefinition. However, then we get a non-zero external vector field which can be seen as a constant background field. Charged particle-anti-particle vacuum fluctuations are affected by this background field thus giving rise to a non-zero current even in the vacuum.

The two-point function of a current j^μ is defined as

$$\Pi^a_{\mu\nu}(q) \equiv i\int d^4x e^{iq\cdot x}\langle T(j^a_\mu(x)j^{a\dagger}_\nu(0))\rangle\,. \tag{4.2}$$

The current $j^{\pi^+}_\mu = \bar{d}\gamma_\mu u$ satisfies the Ward identity.

$$\partial^\mu\langle T(j^{\pi^+}_\mu(x)j^{\pi^-}_\nu(0))\rangle = \delta^{(4)}(x)\langle \bar{d}\gamma_\nu d - \bar{u}\gamma_\nu u\rangle\,. \tag{4.3}$$

We used here that $m_u = m_d$ with the usual techniques to derive Ward identities. A consequence is that with twisted boundary conditions the vector two-point function is no longer transverse. However, flavour diagonal currents like the electromagnetic one remain transverse. This does not mean that they are proportional to $q_\mu q_\nu - q^2 g_{\mu\nu}$ since Lorentz symmetry is broken. A more thorough discussion at the quark level and estimates using lattice calculations can be found in [5].

The infinite volume expressions we obtain agree with those of [13]. The finite-volume corrections for the $\bar{d}\gamma_\mu u$ and electromagnetic current are

$$\begin{aligned}
\Delta^V\Pi^{\pi^+}_{\mu\nu}(q) &= 2\widetilde{\Pi}_{\mu\nu}(m^2_{\pi^+}, m^2_{\pi^0}, q) + \widetilde{\Pi}_{\mu\nu}(m^2_{K^+}, m^2_{\overline{K}^0}, q)\,,\\
\Delta^V\Pi^{em}_{\mu\nu}(q) &= \widetilde{\Pi}_{\mu\nu}(m^2_{\pi^+}, m^2_{\pi^-}, q) + \widetilde{\Pi}_{\mu\nu}(m^2_{K^+}, m^2_{K^-}, q)\,,\\
\widetilde{\Pi}_{\mu\nu}(m^2_1, m^2_2, q) &= g_{\mu\nu}\left(4B^V_{22}(m^2_1, m^2_2, q) - A^V(m^2_1) - A^V(m^2_2)\right)\\
&\quad + q_\mu q_\nu\left(4B^V_{21}(m^2_1, m^2_2, q^2) - 4B^V_1(m^2_1, m^2_2, q^2) + B^V(m^2_1, m^2_2, q^2)\right)\\
&\quad + (q_\mu g^\alpha_\nu + q_\nu g^\alpha_\mu)(-2)B^V_{2\alpha}(m^2_1, m^2_2, q) + 4B^V_{23\mu\nu}(m^2_1, m^2_2, q)\,.
\end{aligned} \tag{4.4}$$

JHEP05(2014)015

Using the relations (A.16) it can be checked that the consequences of (4.3), namely $q^\mu \Pi^{\pi^+}_{\mu\nu} = \langle \bar{u}\gamma_\mu u - \bar{d}\gamma_\mu d\rangle$ and $q^\mu \Pi^{em}_{\mu\nu} = 0$ are satisfied.

We do not present numerical results here, the values of the vacuum expectation value are small compared to $\langle \overline{u}u\rangle$.

5 Meson masses

We define the mass here as the pole of the full propagator at fixed spatial momentum $\vec{p}$. $\vec{p}$ should be such that it satisfies the twisted boundary condition for the field under consideration. Lorentz and charge conjugation invariance are broken by the twisted boundary conditions. This leads to a mass that depends on all components of the spatial momentum $\vec{p}$. An anti-particle with spatial momentum $-\vec{p}$ has the same mass as the corresponding particle with spatial momentum $\vec{p}$.

The analytical results for the mass correction in terms of the integrals defined in appendix A are

$$\begin{aligned}
\Delta^V m^2_{\pi^\pm} &= \frac{\pm p^\mu}{F_0^2}[-2A^V_\mu(m^2_{\pi^+}) - A^V_\mu(m^2_{K^+}) + A^V_\mu(m^2_{K^0})] \\
&\quad + \frac{m^2_\pi}{F_0^2}\left(-\frac{1}{2}A^V(m^2_{\pi^0}) + \frac{1}{6}A^V(m^2_\eta)\right), \\
\Delta^V m^2_{\pi^0} &= \frac{m^2_\pi}{F_0^2}\left(-A^V(m^2_{\pi^+}) + \frac{1}{2}A^V(m^2_{\pi^0}) + \frac{1}{6}A^V(m^2_\eta)\right), \\
\Delta^V m^2_{K^\pm} &= \pm\frac{p^\mu}{F_0^2}[-A^V_\mu(m^2_{\pi^+}) - 2A^V_\mu(m^2_{K^+}) - A^V_\mu(m^2_{K^0})] - \frac{m^2_K}{F_0^2}\frac{1}{3}A^V(m^2_\eta), \\
\Delta^V m^2_{K^0(\overline{K}^0)} &= +(-)\frac{p^\mu}{F_0^2}[A^V_\mu(m^2_{\pi^+}) - A^V_\mu(m^2_{K^+}) - 2A^V_\mu(m^2_{K^0})] - \frac{m^2_K}{F_0^2}\frac{1}{3}A^V(m^2_\eta), \\
\Delta^V m^2_\eta &= -\frac{m^2_K}{F_0^2}\frac{2}{3}(A^V(m^2_{K^+}) + A^V(m^2_{K^0})) + \frac{m^2_\eta}{F_0^2}\frac{2}{3}A^V(m^2_\eta), \\
&\quad + \frac{m^2_\pi}{F_0^2}\frac{1}{6}(2A^V(m^2_{\pi^+}) + A^V(m^2_{\pi^0}) - A^V(m^2_\eta)).
\end{aligned} \tag{5.1}$$

The notation $K^0(\overline{K}^0)$ and $+(-)$ means $+$ for K^0 and $-$ for $\overline{K}^0$. We agree with the infinite volume expressions of [9] and the known untwisted finite-volume corrections [10, 11]. The relation to the results in [2, 6] is discussed in section 8.

In (5.1) the masses m^2_π, m^2_K and m^2_η can be replaced by the physical masses with or without finite volume correction, or lowest order masses. The differences are higher order. The same comment applies to F_0 in (5.1). The masses in the loop functions A^V are written as the physical masses. The notation $A^V(m^2_M)$ with M the meson includes includes the dependence on θ_M. We keep for example π^+ and π^0 as notation even if they have the same infinite volume and lowest order mass, since θ_{π^+} and θ_{π^0} are different.

Note that in the case where $\vec{p} = \vec{\theta}/L$ the different signs for A^V_μ between particle and anti-particle will be canceled by the sign difference in $\vec{p}$ originating from opposite twist angles. The same cancellation occurs for the higher momentum states if the change

JHEP05(2014)015

$2\pi\vec{n}/L \to -2\pi\vec{n}/L$ is taken. This is consistent with the fact that charge conjugation should be defined with a change of sign in momentum, as discussed above.

The twisted boundary conditions do break isospin and thus induce π^0-η mixing. This only affects the masses at next-to-next-to-leading-order (NNLO), i.e. higher order than NLO. The derivation follows the arguments as given in section 2.1 in [14] .

We now show the volume and twist angle dependence for the case with

$$m_\pi = 139.5 \text{ MeV}\,, \quad m_K = 495 \text{ MeV}\,, \quad m_\eta^2 = \frac{4}{3}m_K^2 - \frac{1}{3}m_\pi^2, \quad F_\pi = 92.2 \text{ MeV}\,. \tag{5.2}$$

We have used these masses in the one-loop expressions as well as the value of F_π for F_0 in the expressions. We show results for several values of the twist angle θ with

$$\vec{\theta}_u = (\theta, 0, 0)\,, \quad \vec{\theta}_d = \vec{\theta}_s = 0\,. \tag{5.3}$$

Note that this implies that for π^+ and K^+ there is a non-zero spatial momentum $\vec{p} = \vec{\theta}_u/L$, while $\vec{p}$ vanishes for π^0, K^0 and η. As can be seen in figure 1, the finite volume correction has a sizable dependence on the twist-angle. The correction for the K^0 does not depend on the twist angle here, since for the choice of angles in (5.3) there is only the η-loop contribution due to $\vec{p}_{K^0} = 0$. The relative correction to the kaon and eta masses remains small while for π^+ and π^0 it can become in the few % range.

6 Decay constants

We define the meson (axial-vector) decay constant in finite volume as

$$\langle 0|A_\mu^M|M(p)\rangle = i\sqrt{2}F_M p_\mu + i\sqrt{2}F_{M\mu}^V\,, \tag{6.1}$$

where $M(p)$ is a meson and $A_\mu = \bar{q}\gamma_\mu\gamma_5(\lambda^M/\sqrt{2})q$ is the axial current. The extra term is needed since the matrix element in finite volume is no longer proportional to p_μ. The first term in (6.1) can be identified by looking at the time component of the current. The second term has non-zero components only in the spatial directions and vanishes in infinite volume.

For the flavour charged mesons, the charge in the axial current and the meson is necessarily the same. In the isospin limit the same is true for the π^0 and the η. However the twisted boundary conditions do break isospin and thus the π^0 also couples to the octet current and the η to the triplet current. At NLO this coupling comes from two effects, the mixing between the isospin triplet π and the octet η as well as the direct transition to the other current. A derivation can be found in section 2.2 of [14].

We also consider decay through a pseudo-scalar current. We define this decay constant as

$$\langle 0|P^M|M(p)\rangle = \frac{G_M}{\sqrt{2}} \tag{6.2}$$

where $P = \bar{q}i\gamma_5(\lambda^M/\sqrt{2})q$ is the pseudo-scalar current corresponding to the meson M. A similar comment to above about π^0 and η applies.

JHEP05(2014)015

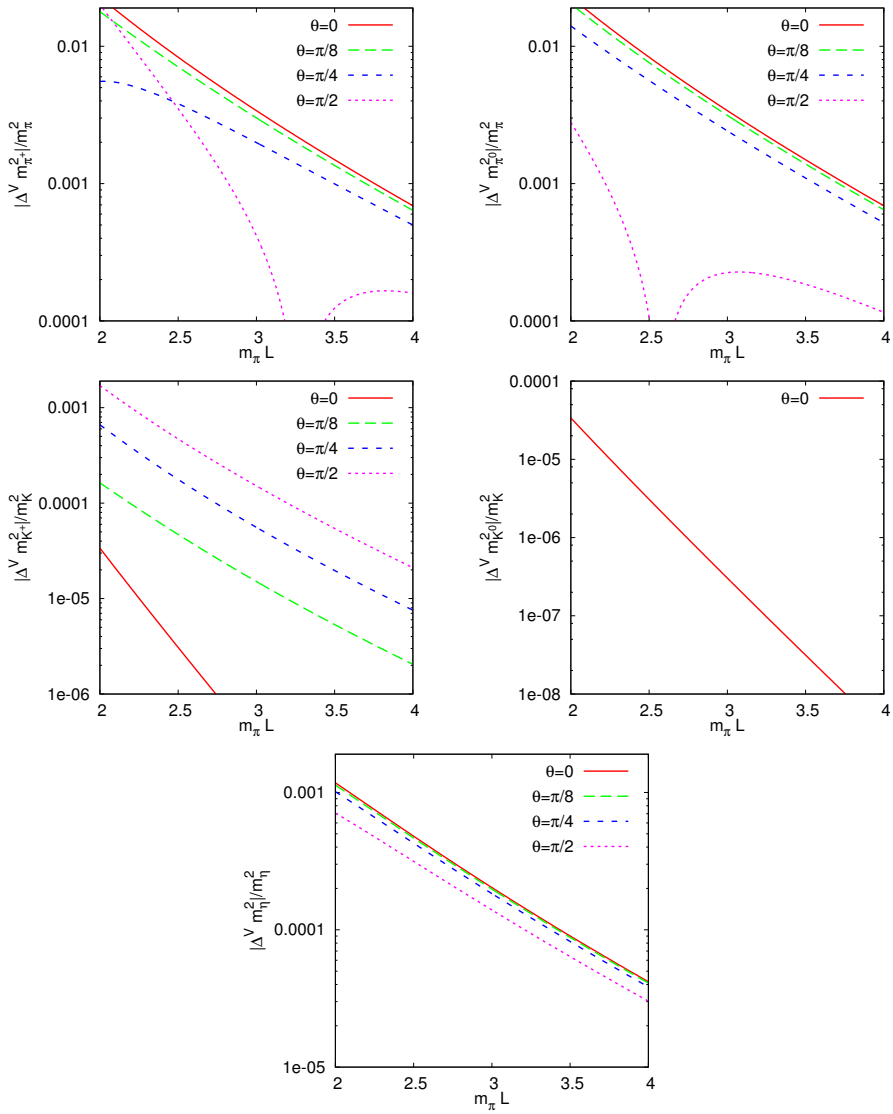

Figure 1. Absolute value of the relative finite volume correction to the masses of the light pseudoscalar mesons as a function of the box size for various twist angles. The twist is for all cases on the up quark. The input values are specified in (5.2) and (5.3). The dip in the top two plots is where the correction goes through zero

JHEP05(2014)015

These two matrix elements satisfy the Ward identity

$$\partial^\mu \left\langle 0|A^M_\mu|M(p)\right\rangle = (m_q + m_{q'}) \left\langle 0|P^M|M(p)\right\rangle \,, \tag{6.3}$$

valid for flavour charged mesons of composition $\bar{q}q'$. This leads to

$$p^2 F_M + p^\mu F^V_{M\mu} = \frac{1}{2}(m_q + m_{q'})G_M \,. \tag{6.4}$$

We have checked that our expressions for the charged mesons agree with this. An important part in this agreement is the use of the correct momentum-dependent mass of the meson. For the neutral mesons a somewhat more complicated relation is needed since they are sums of terms with different quark masses.

The analytical results for the finite volume effects on the axial-vector decay constants are given below in terms of the integrals defined in appendix A. For the π^0 and η we listed the matrix-elements with A^3_μ and A^8_μ separately, indicating which decay is which with an extra subscript. The isospin breaking decay vanishes if the up and down quarks have the same twist angles.

Again we agree with the infinite volume results of [9]. The finite volume corrections for the axial current decay constants for the flavour charged mesons are

$$\begin{aligned}
\Delta^V F_{\pi^\pm} &= \frac{1}{F_0}\left(\frac{1}{2}A^V(m^2_{\pi^+}) + \frac{1}{2}A^V(m^2_{\pi^0}) + \frac{1}{4}A^V(m^2_{K^+}) + \frac{1}{4}A^V(m^2_{K^0})\right) \,, \\
F^V_{\pi^\pm\mu} &= \pm\frac{1}{F_0}\left[2A^V_\mu(m^2_{\pi^+}) + A^V_\mu(m^2_{K^+}) - A^V_\mu(m^2_{K^0})\right] \,, \\
\Delta^V F_{K^\pm} &= \frac{1}{F_0}\left(\frac{1}{4}A^V(m^2_{\pi^+}) + \frac{1}{8}A^V(m^2_{\pi^0}) + \frac{1}{2}A^V(m^2_{K^+}) + \frac{1}{4}A^V(m^2_{K^0}) + \frac{3}{8}A^V(m^2_\eta)\right) \,, \\
F^V_{K^\pm\mu} &= \pm\frac{1}{F_0}\left[A^V_\mu(m^2_{\pi^+}) + 2A^V_\mu(m^2_{K^+}) + A^V_\mu(m^2_{K^0})\right] \,, \\
\Delta^V F_{K^0(\bar{K}^0)} &= \frac{1}{F_0}\left(\frac{1}{4}A^V(m^2_{\pi^+}) + \frac{1}{8}A^V(m^2_{\pi^0}) + \frac{1}{4}A^V(m^2_{K^+}) + \frac{1}{2}A^V(m^2_{K^0}) + \frac{3}{8}A^V(m^2_\eta)\right) \,, \\
F^V_{K^0(\overline{K}^0)\mu} &= +(-)\frac{1}{F_0}\left[-A^V_\mu(m^2_{\pi^+}) + A^V_\mu(m^2_{K^+}) + 2A^V_\mu(m^2_{K^0})\right] \,.
\end{aligned} \tag{6.5}$$

They agree with the untwisted finite volume results of [11]. The relation to the results given in [2] is discussed in section 8. The flavour neutral expressions include the effects of mixing.

$$\begin{aligned}
F^V_{\pi^0 3\mu} &= F^V_{\pi^0 8\mu} = F^V_{\eta 3\mu} = F^V_{\eta 8\mu} = 0 \,, \\
\Delta^V F_{\pi^0 3} &= \frac{1}{F_0}(A^V(m^2_{\pi^+}) + \frac{1}{4}A^V(m^2_{K^+}) + \frac{1}{4}A^V(m^2_{K^0})) \,, \\
\Delta^V F_{\pi^0 8} &= \frac{3m^2_\eta - m^2_\pi}{2\sqrt{3}F_0(m^2_\eta - m^2_\pi)}(A^V(m^2_{K^+}) - A^V(m^2_{K^0})) \,, \\
\Delta^V F_{\eta 8} &= \frac{3}{4F_0}(A^V(m^2_{K^+}) + A^V(m^2_{K^0})) \,, \\
\Delta^V F_{\eta 3} &= \frac{-m^2_\pi}{\sqrt{3}F_0(m^2_\eta - m^2_\pi)}(A^V(m^2_{K^+}) - A^V(m^2_{K^0})).
\end{aligned} \tag{6.6}$$

to simplify the expressions.

JHEP05(2014)015

The masses and F_0 in these expressions can be chosen in different ways as discussed earlier for the masses.

The lowest order value for the pseudo-scalar decay constants is $G_0 = 2F_0B_0$. We are not aware of published results for the NLO corrections at infinite volume, we thus quote those for completeness and add a superscript (4) to indicate the NLO infinite volume correction. Note that isospin is valid at infinite volume such that the mixed ones vanish and there is only an expression for the π, K and η_8 case.

$$\begin{aligned}
G_\pi^{(4)} &= \frac{G_0}{F_0^2}\left(4K_{46} + 4m_\pi^2(4L_8^r - L_5^r) + \frac{1}{2}\overline{A}(m_\pi^2) + \frac{1}{2}\overline{A}(m_K^2) + \frac{1}{6}\overline{A}(m_\eta^2)\right) , \\
G_K^{(4)} &= \frac{G_0}{F_0^2}\left(4K_{46} + 4m_K^2(4L_8^r - L_5^r) + \frac{3}{8}\overline{A}(m_\pi^2) + \frac{3}{4}\overline{A}(m_K^2) + \frac{1}{24}\overline{A}(m_\eta^2)\right) , \\
G_{\eta 8}^{(4)} &= \frac{G_0}{F_0^2}\left(4K_{46} + 4m_\eta^2(4L_8^r - L_5^r) + \frac{1}{2}\overline{A}(m_\pi^2) + \frac{1}{6}\overline{A}(m_K^2) + \frac{1}{2}\overline{A}(m_\eta^2)\right) , \\
K_{46} &= (2m_K^2 + m_\pi^2)(4L_6^r - L_4^r) . \qquad (6.7)
\end{aligned}$$

The integral is

$$\overline{A}(m^2) = -\frac{m^2}{16\pi^2}\log\frac{m^2}{\mu^2} . \qquad (6.8)$$

The finite volume effects for the pseudo-scalar decay constants for the flavour charged mesons are

$$\begin{aligned}
\Delta^V G_{\pi^\pm}^V &= \frac{G_0}{F_0^2}\left(\frac{1}{2}A^V(m_{\pi^+}^2) + \frac{1}{4}A^V(m_{K^+}^2) + \frac{1}{4}A^V(m_{K^0}^2) + \frac{1}{6}A^V(m_\eta^2)\right) , \\
\Delta^V G_{K^\pm} &= \frac{G_0}{F_0^2}\left(\frac{1}{4}A^V(m_{\pi^+}^2) + \frac{1}{8}A^V(m_{\pi^0}^2) + \frac{1}{2}A^V(m_{K^+}^2) + \frac{1}{4}A^V(m_{K^0}^2) + \frac{1}{24}A^V(m_\eta^2)\right) , \\
\Delta^V G_{K^0(\overline{K}^0)} &= \frac{G_0}{F_0^2}\left(\frac{1}{4}A^V(m_{\pi^+}^2) + \frac{1}{8}A^V(m_{\pi^0}^2) + \frac{1}{4}A^V(m_{K^+}^2) + \frac{1}{2}A^V(m_{K^0}^2) + \frac{1}{24}A^V(m_\eta^2)\right) . \qquad (6.9)
\end{aligned}$$

For the flavour neutral cases we need to take into account mixing and obtain

$$\begin{aligned}
\Delta^V G_{\pi^0 3} &= \frac{G_0}{F_0^2}\left(\frac{1}{2}A^V(m_{\pi^0}^2) + \frac{1}{4}A^V(m_{K^+}^2) + \frac{1}{4}A^V(m_{K^0}^2) + \frac{1}{6}A^V(m_\eta^2)\right) , \\
\Delta^V G_{\pi^0 8} &= \frac{G_0}{F_0^2}\frac{m_\eta^2 + m_\pi^2}{2\sqrt{3}(m_\eta^2 - m_\pi^2)}\left(A^V(m_{K^+}^2) - A^V(m_{K^0}^2)\right) , \\
\Delta^V G_{\eta 8} &= \frac{G_0}{F_0^2}\left(\frac{1}{3}A^V(m_{\pi^+}^2) + \frac{1}{6}A^V(m_{\pi^0}^2) + \frac{1}{12}A^V(m_{K^+}^2) + \frac{1}{12}A^V(m_{K^0}^2) + \frac{1}{2}A^V(m_\eta^2)\right) , \\
\Delta^V G_{\eta 3} &= \frac{G_0}{F_0^2}\frac{-m_\eta^2}{\sqrt{3}(m_\eta^2 - m_\pi^2)}\left(A^V(m_{K^+}^2) - A^V(m_{K^0}^2)\right) . \qquad (6.10)
\end{aligned}$$

At this order $G_{\pi^0 8}$ and $G_{\eta 3}$ only arise from π^0-η mixing.

We present now some numerics for the same inputs as used for the masses given in (5.2) and (5.3).

In figure 2 we show the size of the finite volume corrections to the charged meson decay constants with both terms in (6.1) shown separately. We use the same input parameters

JHEP05(2014)015

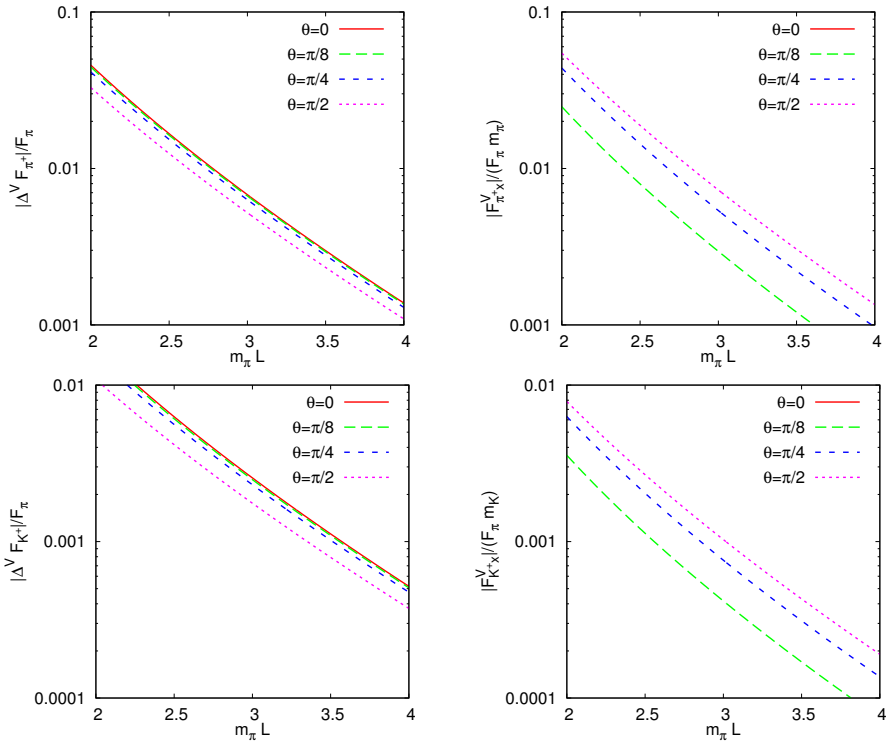

Figure 2. Relative finite volume correction for the two terms in the decay constant matrix element (6.1). On the left hand side we have plotted $\Delta^V F_M/F_\pi$ and on the right hand side $F^V_{Mx}/(F_\pi m_M)$, i.e. the x-component compared to the size of the zero-component. For the input chosen the x-component is the only non-zero one for the second term in (6.1). The top row is $M = \pi^+$ and the bottom row for $M = K^+$. Input values as in (5.2) and (5.3).

as for the masses of (5.2) and (5.3). The first term in (6.1) is shown in the left plots normalized to F_π for the charged pion and kaon. The right plots shows the x-component of the second term in (6.1), which is the only non-zero component for our choice of input. It vanishes identically for $\theta = 0$. We have normalized here to the value of $F_\pi m_K$ which is roughly the value of the t-component in infinite volume. Note that the finite volume corrections can be sizable and the second term is not always negligible.

7 Electromagnetic form-factor

The electromagnetic form-factor in infinite volume is defined as

$$\langle p'|j^{em}_\mu|p\rangle = F(q^2)(p+p')_\mu \tag{7.1}$$

JHEP05(2014)015

where $q = p - p'$ and j^μ is the electromagnetic current for the light quark flavours

$$j_\mu^{em} = \frac{2}{3}\bar{u}\gamma_\mu u - \frac{1}{3}(\bar{d}\gamma_\mu d + \bar{s}\gamma_\mu s). \tag{7.2}$$

The electromagnetic form-factor in twisted lattice QCD is not the same as in infinite volume or finite volume with periodic conditions. Instead it has the more general form

$$\begin{aligned}\left\langle M'(p')|j_\mu^I|M(p)\right\rangle &= f_{IMM'\mu} \\ &= f_{IMM'+}(p_\mu + p'_\mu) + f_{IMM'-}q_\mu + h_{IMM'\mu}\,.\end{aligned} \tag{7.3}$$

In addition to the electromagnetic current we will use

$$j_\mu^q = \bar{q}\gamma_\mu q, \qquad\qquad j_\mu^{\pi^+} = \bar{d}\gamma_\mu u\,. \tag{7.4}$$

We will also suppress the M' in the subscripts when initial and final meson are the same and sometimes the IMM'. In the infinite volume limit the functions f_- and h must go to zero and f_+ must go to $F(q^2)$ so that eq. (7.1) is recovered. We only work with currents where the quark and anti-quark have the same mass. The result in infinite volume can be found in [15]. Results at finite volume with periodic boundary conditions are in [16, 17].

The main reason for using twisted boundary conditions is to extract physical quantities for small momenta. In the case of the electromagnetic form-factor the twist does not help when applied to correlators such as

$$\left\langle \pi^+(p')|j_\mu^q|\pi^+(p)\right\rangle \tag{7.5}$$

since the same twist is applied to the incoming and outgoing particles we get $p_i - p'_i = 2\pi n_i/L$. However, as was pointed out in [4], it is possible to extract information using isospin symmetry. To analyze this more carefully requires calculations in partially quenched ChPT and this will be the topic of forthcoming work. Here we are satisfied with noting that in the isospin limit with $m_u = m_d$ and $\theta_u = \theta_d$ we have the relation (in our sign conventions)

$$\left\langle \pi^+(p')|\bar{u}\gamma_\mu u|\pi^+(p)\right\rangle = -\left\langle \pi^+(p')|\bar{d}\gamma_\mu d|\pi^+(p)\right\rangle = -\frac{1}{\sqrt{2}}\left\langle \pi^0(p')|\bar{d}\gamma_\mu u|\pi^+(p)\right\rangle. \tag{7.6}$$

The relation (7.6) can in principle be used to evaluate the main part, excluding $\bar{s}\gamma_\mu s$, of the electromagnetic form-factor of the pion for arbitrary momenta. The current $\bar{d}\gamma_\mu u$ is referred to as $\bar{d}u$ in the equations below. In practice π^0 gives rise to difficulties on the lattice, and the twisted boundary conditions explicitly break isospin. The corrections due to the latter are one of the goals of this work.

7.1 Analytic expressions

The split in f_+, f_- and h in (7.3) is not unique. The functions can depend on all components of the momenta and twist-vectors. However, we stick to the splitting among f_+, f_- and h which naturally emerges from the one-loop calculation. The integrals appearing are defined in appendix A.

JHEP05(2014)015

The results for f_+^V are most easily given in terms of the finite volume generalization of the function $\mathcal{H}$ in [15, 18].

$$H^V(m_1^2, m_2^2, q) = \frac{1}{4}A^V(m_1^2) + \frac{1}{4}A^V(m_2^2) - B_{22}^V(m_1^2, m_2^2, q) \tag{7.7}$$

The effects of π^0-η mixing appear earliest at NNLO for the form-factors listed here. The form-factors f_+ we consider are:

$$\begin{aligned}
\Delta^V f_{em\pi^\pm +} &= \frac{\pm 1}{F_0^2}\left(2H^V(m_{\pi^+}^2, m_{\pi^-}^2, q) + H^V(m_{K^+}^2, m_{K^-}^2, q)\right) , \\
\Delta^V f_{emK^\pm +} &= \frac{\pm 1}{F_0^2}\left(H^V(m_{\pi^+}^2, m_{\pi^-}^2, q) + 2H^V(m_{K^+}^2, m_{K^-}^2, q)\right) , \\
\Delta^V f_{emK^0(\overline{K}^0)+} &= \frac{\pm 1}{F_0^2}\left(-H^V(m_{\pi^+}^2, m_{\pi^-}^2, q) + H^V(m_{K^+}^2, m_{K^-}^2, q)\right) , \\
\Delta^V f_{em\pi^0 +} &= 0 , \\
\Delta^V f_{\bar{d}u\pi^+\pi^0 +} &= \frac{-\sqrt{2}}{F_0^2}\left(2H^V(m_{\pi^+}^2, m_{\pi^0}^2, q) + H^V(m_{K^+}^2, m_{\overline{K}^0}^2, q)\right) .
\end{aligned} \tag{7.8}$$

The f_- form-factors for the same cases are:

$$\begin{aligned}
\Delta^V f_{em\pi^+(\pi^-)-} &= \frac{p'^\nu(-p^\nu)}{F_0^2}\left(2B_{2\nu}^V(m_{\pi^+}^2, m_{\pi^-}^2, q) + B_{2\nu}^V(m_{K^+}^2, m_{K^-}^2, q)\right) , \\
\Delta^V f_{emK^+(K^-)-} &= \frac{p'^\nu(-p^\nu)}{F_0^2}\left(B_{2\nu}^V(m_{\pi^+}^2, m_{\pi^-}^2, q) + 2B_{2\nu}^V(m_{K^+}^2, m_{K^-}^2, q)\right) , \\
\Delta^V f_{emK^0(\overline{K}^0)-} &= \frac{1}{F_0^2}\left(-(p^\nu(-p'^\nu))B_{2\nu}^V(m_{\pi^+}^2, m_{\pi^-}^2, q) + p'^\nu(-p^\nu)B_{2\nu}^V(m_{K^+}^2, m_{K^-}^2, q)\right) , \\
\Delta^V f_{em\pi^0 -} &= \frac{1}{F_0^2}\Bigg(m_\pi^2\left(B^V(m_{\pi^+}^2, m_{\pi^-}^2, q) - 2B_1^V(m_{\pi^+}^2, m_{\pi^-}^2, q)\right) \\
&\qquad - q^\nu\left(2B_{2\nu}^V(m_{\pi^+}^2, m_{\pi^-}^2, q) + \frac{1}{2}B_{2\nu}^V(m_{K^+}^2, m_{K^-}^2, q)\right)\Bigg) , \\
\Delta^V f_{\bar{d}u\pi^+\pi^0 -} &= \frac{\sqrt{2}}{F_0^2}\Bigg(m_\pi^2\left(B^V(m_{\pi^+}^2, m_{\pi^0}^2, q) - 2B_1^V(m_{\pi^+}^2, m_{\pi^0}^2, q)\right) \\
&\qquad - \left(2p^\nu B_{2\nu}^V(m_{\pi^+}^2, m_{\pi^-}^2, q) + \frac{1}{2}(p+p')^\nu B_{2\nu}^V(m_{K^+}^2, m_{\overline{K}^0}^2, q)\right)\Bigg) ,
\end{aligned} \tag{7.9}$$

Finally, the h_μ at finite volume are

$$\begin{aligned}
\Delta^V h_{em\pi^\pm\mu} = \frac{1}{F_0^2}\Bigg(&2A_\mu^V(m_{\pi^+}^2) + A_\mu^V(m_{K^+}^2) - A_\mu^V(m_{K^0}^2) \\
&+ q^2 B_{2\mu}^V(m_{\pi^+}^2, m_{\pi^-}^2, q) + \frac{q^2}{2}B_{2\mu}^V(m_{K^+}^2, m_{K^-}^2, q) \\
&\mp (p+p')^\nu\left(2B_{23\mu\nu}^V(m_{\pi^+}^2, m_{\pi^-}^2, q) + B_{23\mu\nu}^V(m_{K^+}^2, m_{K^-}^2, q)\right)\Bigg) ,
\end{aligned}$$

JHEP05(2014)015

$$
\begin{aligned}
\Delta^V h_{emK^\pm\mu} &= \frac{1}{F_0^2}\Bigg(A_\mu^V(m_{\pi^+}^2) + 2A_\mu^V(m_{K^+}^2) + A_\mu^V(m_{K^0}^2) \\
&\qquad + \frac{q^2}{2} B_{2\mu}^V(m_{\pi^+}^2, m_{\pi^-}^2, q) + q^2 B_{2\mu}^V(m_{K^+}^2, m_{K^-}^2, q) \\
&\qquad \mp (p+p')^\nu \left(B_{23\mu\nu}^V(m_{\pi^+}^2, m_{\pi^-}^2, q) + 2B_{23\mu\nu}^V(m_{K^+}^2, m_{K^-}^2, q) \right) \Bigg), \\
\Delta^V h_{emK^0(\overline{K}^0)\mu} &= \frac{1}{F_0^2}\Bigg(\frac{q^2}{2} B_{2\mu}^V(m_{\pi^+}^2, m_{\pi^-}^2, q) + \frac{q^2}{2} B_{2\mu}^V(m_{K^+}^2, m_{K^-}^2, q) \\
&\qquad + (-)(p+p')^\nu \left(B_{23\mu\nu}^V(m_{\pi^+}^2, m_{\pi^-}^2, q) - B_{23\mu\nu}^V(m_{K^+}^2, m_{K^-}^2, q) \right) \Bigg), \\
\Delta^V h_{em\pi^0\mu} &= \frac{1}{F_0^2}\Bigg(2(q^2 - m_\pi^2) B_{2\mu}^V(m_{\pi^+}^2, m_{\pi^-}^2, q) + \frac{q^2}{2} B_{2\mu}^V(m_{K^+}^2, m_{K^-}^2, q) \Bigg), \\
\Delta^V h_{\bar{d}u\pi^+\pi^0\mu} &= \frac{\sqrt{2}}{F_0^2}\Bigg(- A_\mu^V(m_{\pi^+}^2) - \frac{1}{2} A_\mu^V(m_{K^+}^2) + \frac{1}{2} A_\mu^V(m_{K^0}^2) \\
&\qquad + (q^2 - 2m_\pi^2) B_{2\mu}^V(m_{\pi^+}^2, m_{\pi^0}^2, q) \\
&\qquad + (p+p')^\nu \left(2B_{23\mu\nu}^V(m_{\pi^+}^2, m_{\pi^0}^2, q) + B_{23\mu\nu}^V(m_{K^+}^2, m_{\overline{K}^0}^2, q) \right) \Bigg).
\end{aligned}
\tag{7.10}
$$

We used in these formulas that the π^0 and η have no twist and that particle and anti-particle have opposite twists. Both f_- and h vanish in infinite volume.

7.2 Ward identities

All the form-factors we discuss have the same mass for the quark and anti-quark in the vector current. As a consequence they obey, even at finite volume, the Ward identity

$$
q^\mu f_{IMM'\mu} = (p^2 - p'^2) f_{IMM'+} + q^2 f_{IMM'-} + q^\mu h_{IMM'\mu} = 0\,. \tag{7.11}
$$

We have used this as a check on our results. This standard check requires a bit of caution when using twisted boundary conditions. The issue is that masses are momentum dependent when twist is applied, see section 5. When performing a one loop calculation part of the mass correction is different for ingoing and outgoing meson, this means that $p^2 - p'^2 \neq 0$ even when the incoming and outgoing particle are the same. Comparing equations for the mass corrections, we see that these cancel the parts coming from A_μ^V in $h_{IMM'\mu}$. The remainder cancels between $q^2 f_{IMM'-}$ and $q^\mu h_{IMM'\mu}$ when using the identities in appendix A.4.

7.3 Numerical results

Let us first remind here why twisting is useful for form-factors with the example of the pion form-factor and a lattice size of $m_\pi L = 2$. The smallest spatial momentum that can be produced is $2\pi/L = \pi m_\pi$ and the corresponding q^2 is $q^2_{\text{min}} = -0.089\ \text{GeV}^2 = -(0.3\ \text{GeV})^2$. Twisting allows for q^2 continuously varying from zero.

JHEP05(2014)015

In this section we concentrate on the quantity

$$f_\mu = \left(1 + f_+^\infty + \Delta^V f_+\right)(p+p')_\mu + \Delta^V f_- q_\mu + \Delta^V h_\mu = -\frac{1}{\sqrt{2}} f_{\bar{d}u\pi^+\pi^0\mu}\,. \tag{7.12}$$

This is the form-factor corresponding to the right hand side of (7.6) normalized to 1 at $q^2 = 0$ in infinite volume. The finite volume parts are what is needed to obtain the pion electromagnetic form-factor, neglecting the s-quark contribution, at infinite volume. We have separated the lowest order value of 1, the infinite volume and finite volume correction to f_+ as well as the f_- and h_μ parts defined earlier.

Again we look at the case with $\vec{\theta}_u = (\theta, 0, 0)$. This means that the incoming π^+ four-momentum p, the outgoing π^0 momentum p' and q^2 are

$$\begin{aligned} p &= \left(\sqrt{m_{\pi^+}^{V2} + (\theta/L)^2}, \theta/L, 0, 0\right)\,, \\ p' &= \left(m_{\pi^0}^{V2}, 0, 0, 0\right)\,, \\ q^2 &= m_{\pi^+}^{V2} + m_{\pi^0}^{V2} - 2m_{\pi^0}^V \sqrt{m_{\pi^+}^{V2} + (\theta/L)^2}\,. \end{aligned} \tag{7.13}$$

Note that the masses at finite volume that come in here, not the infinite volume ones. We have indicated this with the superscript V in the masses. To plot the corrections we use $m_M^{V2} = m_M^2 + \Delta^V m_M^2$ in the numerics with $\Delta^V m_M^2$ given in (5.1). The size of this effect is shown in the left plot of figure 3. We plot the value of q^2 at finite and infinite volume and the deviation of the ratio from 1 as a function of θ/L. The endpoint of the curve is for $\theta = 2\pi$. The right plot in figure 3 shows the effect on the form-factor of this change in q^2. We plotted there the one-loop contribution at infinite volume to the pion electromagnetic form-factor, $f_+^\infty(q^2)$, as a function of the two different q^2 discussed here. The extra input values used are $L_9^r = 0$ and $\mu = 0.77$ GeV. The total effect of this correction is rather small.

In the remainder we will use the q^2 as calculated with the finite volume masses. In figure 4 we plot the different parts of the form-factor as defined in (7.12). Plotted are the infinite volume one-loop part of f_+^∞, the finite volume corrections $\Delta^V f_+$, $\Delta^V f_-$ and the two non-zero components of $\Delta^V h^\mu$. As one can see, the finite volume corrections are not small and the parts due to the extra form-factors can definitely not be neglected. The units are GeV for the two components of $\Delta^V h^\mu$.

The more relevant quantities for comparison are the components with $\mu = 0$ and $\mu = 1$. We have plotted the form-factor as defined with upper index μ. The left plot in figure 5 shows $\mu = 0$ and the right plot $\mu = 1$. Units are in GeV. The finite volume correction is of a size similar to the infinite volume pure one-loop contribution and the correction due to the extra terms at finite volume and twist are not negligible.

8 Comparison with earlier work

The one and two-point Green functions of vector currents are discussed in section 4. These issues were discussed in a more lattice oriented way in [5]. Here we have provided the ChPT expressions for them.

JHEP05(2014)015

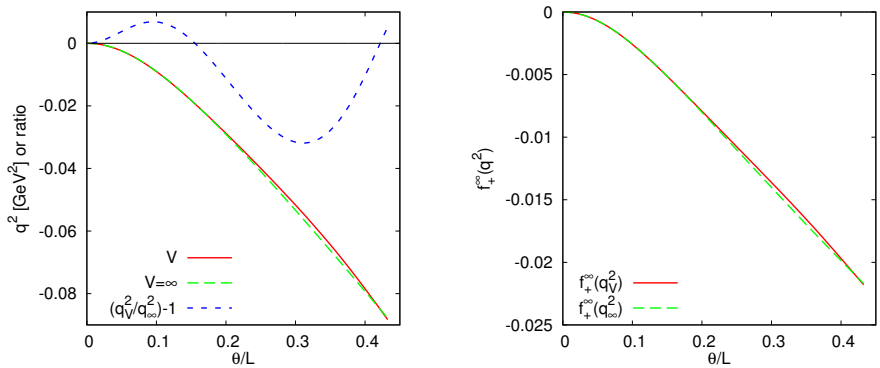

Figure 3. Left: the dependence of q^2 at a fixed $\vec{q} = (\theta/L, 0, 0)$ for the finite volume with $m_\pi L = 2$ and infinite volume as well as the difference ratio from one. The curves end at $\theta = 2\pi$. Right: the effect of this change in q^2 on the infinite volume corrections of $f_+^V(q^2)$ with $L_9^r = 0$.

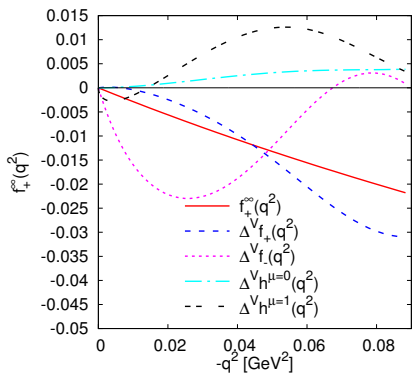

Figure 4. The various parts of the form-factor defined in (7.12). See text for a more detailed explanation.

For the masses the comparison with earlier work is more subtle. In this work, we have consistently used the formulation with non-zero twist angle and no induced background field. This implies that the allowed meson momenta are of the form $\vec{p}_{BR} = (2\pi\vec{n}+\vec{\theta})/L$, with $\vec{n}$ a three-vector with integer components and $\vec{\theta}$ the twist vector for the field corresponding to the meson. As mentioned in section 2 we define asymptotic states as those where there is at fixed $\vec{p}$ a pole at a value, E_0, of the energy. The LSZ theorem can then be used for these single particle states to obtain matrix elements by taking the limit $E \to E_0$ allowing for the usual method with wave function renormalization and possibly mixing of external states to take into account external leg corrections. Our definition of the mass used is

$$m_{BR}^2 = E_0^2 - \vec{p}_{BR}^2 \,. \tag{8.1}$$

JHEP05(2014)015

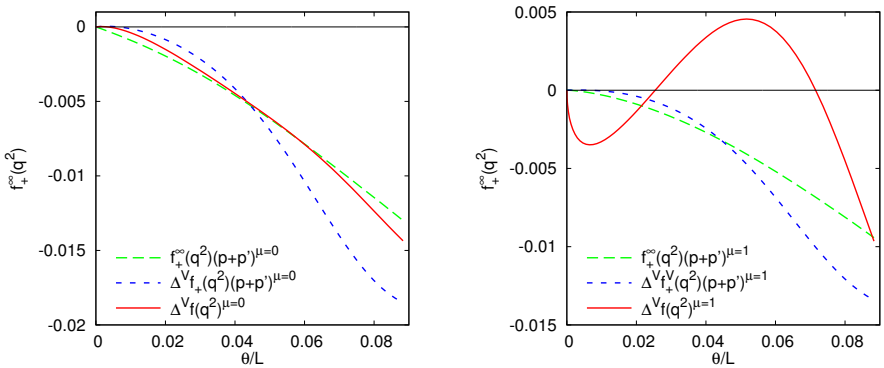

Figure 5. Left: $\mu = 0$ Right: $\mu = 1$. Plotted are those due to the one-loop infinite volume correction, $f_+^\infty(q^2)$, the finite volume correction to f_+, $\Delta^V f_+$, and the full finite volume correction, $\Delta^V f^\mu = \Delta^V f_+(p+p')^\mu + \Delta^V f_- q^\mu + \Delta^V h^\mu$.

The mass can depend on all components of $\vec{p}$ since there is no rotation invariance and even cubic invariance[1] is no longer present. We have used the expression "momentum-dependent mass" in the text to indicate this dependence. The relation between E and $\vec{p}$ for states is called dispersion relation in some other references, see e.g. [6].

[6] discussed the pion mass, both neutral and charged, in two-flavour ChPT on the lattice. They work in the version of ChPT where the fields satisfy periodic boundary conditions but there are background fields $\vec{B} = \vec{\theta}/L$. They have periodic momenta $\vec{p}_p = (2\pi\vec{n})/L$ and define kinematical momenta $\vec{p}_k = \vec{p}_p + \vec{B}$ which coincide with our definition $\vec{p}_{BR}$. However when they define the mass they write the result in the form[2]

$$m_{JT}^2 = E_0^2 - \left(\vec{p}_p + \vec{B} + \vec{K}\right)^2 = E_0^2 - \left(\vec{p}_p + \vec{B}\right)^2 - 2\left(\vec{p}_p + \vec{B}\right)\cdot\vec{K} + \text{NNLO}. \tag{8.2}$$

$\vec{K}$ is NLO, thus we can neglect $\vec{K}^2$ as indicated. Comparing (8.1) and (8.2), the parts containing the integral A_μ^V in (5.1) can be written in the form $-2(\vec{p}_p + \vec{B})\cdot\vec{K}$. [6] expresses this that the meson field (spatial) momentum is renormalized. When comparing the expressions, keep in mind we have also a twist on the sea quarks while [6] does not.

Comparing with the results of [2] is not obvious. The masses are not defined there. The discussion of loop diagrams in the main text indicates that they used momenta of the form $\vec{p}_p + \vec{B}$ everywhere and if one assumes that their mass is defined as

$$m_{SV1}^2 = E_0^2 - \left(\vec{p}_p + \vec{B}\right)^2 , \tag{8.3}$$

then they missed the terms with A_μ^V. If instead a definition of the mass similar to (8.2) is assumed we are in agreement. The expression corresponding to $\vec{K}$ is not present in [2].

[1] We assume here that the t direction is infinite.

[2] We have changed their notation and conventions to make the comparison more clearly.

JHEP05(2014)015

For the decay constants a similar issue arises. They are not fully defined in [2]. If one defines the decay constant from the time component of the axial current then only the parts $\Delta^V F_M$ are relevant and we are in full agreement, if, as is natural, the neutral pion and eta decay constants in [2] are defined with the isospin and octet axial currents. It turns out that to NLO the decay constants can be defined with a shift in momentum $\vec{K}'$ similar to what was done for the masses, i.e. the full matrix element has the form

$$\langle 0|A_\mu^M|M(p)\rangle = i\sqrt{2}F_M\left(p_\mu + K'_\mu\right) + \text{NNLO}\,. \tag{8.4}$$

However, the needed shift vector is different in the two cases,

$$\vec{K} \neq \vec{K}'\,. \tag{8.5}$$

The pion form-factors as discussed in section 7 were treated in the two-flavour case in [6]. They discussed the time component only but added partial twisting and quenching. The extra terms in the matrix element (7.3) are seen in (19) of [6] as well. The terms in (19) in [6] containing $G_{FV}, G_{FV}^{\text{iso}}, \mathbf{G}_{FV}^{\text{iso}}$ correspond to our $\Delta^V f_+, \Delta^V f_-, \Delta^V h_\mu$ of (7.8), (7.9) and (7.10). We have included the spatial components as well and checked that the expected Ward identity following from current conservation is satisfied when all effects of the boundary condition are taken into account. It should be noted that here the matrix element cannot be rewritten in terms of one form-factor f_+ and momenta rescaled with a shift $\vec{K}''$.

9 Conclusions

In this paper we discussed the one-loop tadpole and bubble integrals in finite volume and at non-zero twist.

We have worked out the expressions in one-loop ChPT for masses, axial-vector and pseudo-scalar decay constants as well as the vacuum expectation value and the two-point function for the electromagnetic current. We also discussed how the vector form-factors behave at finite twist angle. In particular we showed how one needs more form-factors than in the infinite volume limit and obtained expressions for those at one-loop order. We discussed how the extra terms are needed in order for the Ward identities to be satisfied.

Explicit formulas are provided for a large number of cases. We have given numerical results for all masses and the axial-vector decay constant of the charged mesons. We found that for the vector form-factor there are nontrivial finite volume effects due to the extra form-factors and have discussed the size of these effects on the form-factors. In particular, we have taken care to precisely define what all quantities are.

Work is in progress for including the effects due to partial quenching and twisting as well as the effects from staggered fermions [19].

Acknowledgments

This work is supported, in part, by the European Community SP4-Capacities "Study of Strongly Interacting Matter" (HadronPhysics3, Grant Agreement number 283286) and the Swedish Research Council grants 621-2011-5080 and 621-2013-4287.

JHEP05(2014)015

A Finite volume integrals with twist

The basic method to do finite volume integrals with twist can be found in [2]. The discussion below follows [12] closely.

A.1 Miscellaneous formulae

The first ingredient is the Poisson summation formula which is in one dimension

$$\frac{1}{L}\sum_{\substack{k=2\pi n/L+\theta/L\\ n\in\mathbb{Z}}} f(k) = \sum_{m\in\mathbb{Z}}\int\frac{dk}{2\pi}f(k)e^{iLmk}e^{-im\theta}. \tag{A.1}$$

The $\sum_{m\in\mathbb{Z}} e^{ima}$ projects on $a = 2\pi n$. $k-\theta/L$ is of this form, hence the sign in $e^{-im\theta}$ in (A.1).

The results for loop integrals with twist are expressed with the third Jacobi theta function and its derivatives w.r.t. to u. The definitions are

$$\Theta_3(u,q) = \sum_{n=-\infty}^{\infty} q^{n^2}e^{2\pi iun}\,, \quad \Theta_3'(u,q) = \sum_{n=-\infty}^{\infty} q^{n^2}2\pi ine^{2\pi iun},$$
$$\Theta_3''(u,q) = -\sum_{n=-\infty}^{\infty} q^{n^2}4\pi^2n^2e^{2\pi iun}. \tag{A.2}$$

Some useful properties can be found in [12].

A.2 Tadpole integral

We define the tadpole integral in finite volume with twist as

$$A^{\{\,,\mu,\mu\nu\}}(m_M^2,n) = \frac{1}{i}\int_V\frac{d^dk}{(2\pi)^d}\frac{\{1,k^\mu,k^\mu k^\nu\}}{(k^2-m_M^2)^n}\,. \tag{A.3}$$

The blank in the superscript indicates no superscript. $\int_V d^dk/(2\pi)^d$ is defined in (3.5). The momentum $\vec{k}$ which is summed over must be such that the boundary condition for the propagating meson M is satisfied,

$$\vec{k} = \frac{2\pi}{L}\vec{n} + \frac{\vec{\theta}_M}{L}\,, \quad \vec{\theta}_M = (\theta_M^x,\theta_M^y,\theta_M^z)\,. \tag{A.4}$$

We also introduce a fourvector $\theta_M = (0,\vec{\theta})$. Note that this implies that the tadpole integral is not invariant under $\vec{k}\to-\vec{k}$ since $-\vec{k}$ does not satisfy the boundary conditions for non-zero twist. The direction of propagation is important. We drop the subscript M below for clarity.

To describe the evaluation of these integrals, we restrict to the case $\{1\}$ and then quote the results for the other cases. We Wick rotate to Euclidean space and apply Poisson's summation formula from eq. (A.1), giving

$$A(m^2,n) = (-1)^n\sum_{\vec{l}\in\mathbb{Z}^3}\int\frac{d^dk_E}{(2\pi)^d}\frac{1}{(k_E^2+m^2)^n}e^{iL\vec{l}\cdot\vec{k}-i\vec{l}\cdot\vec{\theta}}\,. \tag{A.5}$$

JHEP05(2014)015

The term with $\vec{l} = 0$ gives the infinite volume result. We focus on the finite volume part and use a prime on the sum to indicate that we sum over $\vec{l} \neq 0$. Using $1/a^n = (1/\Gamma(n)) \int_0^\infty d\lambda \lambda^{n-1} e^{-a\lambda}$, we get

$$A^V(m^2, n) = (-1)^n \sum_{\vec{l}\in\mathbb{Z}^3}' \int \frac{d^d k_E}{(2\pi)^d} \int \frac{d\lambda}{\Gamma(n)} \lambda^{n-1} e^{-\lambda(k^2+m^2)} e^{iL\vec{l}\cdot\vec{k} - i\vec{l}\cdot\vec{\theta}}. \tag{A.6}$$

The shift of integration variable via $k = \bar{k} + iLl/(2\lambda)$, with $l = (0, \vec{l})$, completes the square:

$$A^V(m^2, n) = (-1)^n \sum_{\vec{l}\in\mathbb{Z}^3}' \int \frac{d^d \bar{k}_E}{(2\pi)^d} \int \frac{d\lambda}{\Gamma(n)} \lambda^{n-1} e^{-\lambda(\bar{k}^2+m^2)} e^{-L^2\vec{l}^2/(4\lambda) - i\vec{l}\cdot\vec{\theta}}. \tag{A.7}$$

We can now perform the Gaussian integral and we end up with

$$A^V(m^2, n) = (-1)^n \sum_{\vec{l}\in\mathbb{Z}^3}' \int \frac{d\lambda}{\Gamma(n)} \frac{\lambda^{n-1-d/2}}{(4\pi)^{d/2}} e^{-\lambda m^2} e^{-L^2\vec{l}^2/(4\lambda) - i\vec{l}\cdot\vec{\theta}}. \tag{A.8}$$

Changing variables $\lambda \to \lambda L^2/4$ and using the Jacobi theta function of (A.2), we arrive at

$$A^V(m^2, n) = (-1)^n \left(\frac{L^2}{4}\right)^{n-2} \int \frac{d\lambda}{\Gamma(n)} \frac{\lambda^{n-3}}{(4\pi)^2} e^{-\lambda m^2 L^2/4} \left(\prod_{j=x,y,z} \Theta_3\left(\frac{-\theta^j}{2\pi}, e^{-1/\lambda}\right) - 1 \right). \tag{A.9}$$

The -1 removes the case with $\vec{l} = 0$ and the triple product comes from the triple sum and we set $d = 4$.

Performing the same operations using the other elements in X gives for the finite volume corrections

$$\begin{aligned} A^{V\mu}(m^2, n) = (-1)^n \frac{1}{\pi L} \left(\frac{L^2}{4}\right)^{n-2} \int \frac{d\lambda}{\Gamma(n)} \frac{\lambda^{n-4}}{(4\pi)^2} e^{-\lambda m^2 L^2/4} \\ \times \Theta_3'\left(\frac{-\theta^\mu}{2\pi}, e^{-1/\lambda}\right) \prod_{\substack{j=x,y,z \\ j\neq\mu}} \Theta_3\left(\frac{-\theta^j}{2\pi}, e^{-1/\lambda}\right). \end{aligned} \tag{A.10}$$

Note that the component $\mu = 0$ vanishes.

$$A^{V\mu\nu}(m^2, n) = g^{\mu\nu} A_{22}^V(m^2, n) + A_{23}^{V\mu\nu}(m^2, n)\,,$$

$$A_{22}^V(m^2, n) = \frac{(-1)^{n-1}}{2} \left(\frac{L^2}{4}\right)^{n-3} \int \frac{d\lambda}{\Gamma(n)} \frac{\lambda^{n-4}}{(4\pi)^2} e^{-\lambda m^2 L^2/4} \left(\prod_{j=x,y,z} \Theta_3\left(\frac{-\theta^j}{2\pi}, e^{-1/\lambda}\right) - 1 \right),$$

$$\begin{aligned} A_{23}^{V\mu\nu}(m^2, n) = \frac{(-1)^n}{4\pi^2} \left(\frac{L^2}{4}\right)^{n-3} \int \frac{d\lambda}{\Gamma(n)} \frac{\lambda^{n-5}}{(4\pi)^2} e^{-\lambda m^2 L^2/4} \\ ((a)\mu = 0 \text{ or } \nu = 0) \;\; \times 0 \\ ((b) 0 \neq \mu \neq \nu \neq 0) \;\; \times \Theta_3'\left(\frac{-\theta^\mu}{2\pi}, e^{-1/\lambda}\right) \Theta_3'\left(\frac{-\theta^\nu}{2\pi}, e^{-1/\lambda}\right) \prod_{\substack{j=x,y,z \\ j\neq\mu,\nu}} \Theta_3\left(\frac{-\theta^j}{2\pi}, e^{-1/\lambda}\right) \end{aligned}$$

JHEP05(2014)015

$$((c)\mu=\nu\neq 0) \qquad \times\,\Theta_3''\left(\frac{-\theta^\mu}{2\pi},e^{-1/\lambda}\right)\prod_{\substack{j=x,y,z\\ j\neq\mu}}\Theta_3\left(\frac{-\theta^j}{2\pi},e^{-1/\lambda}\right) \tag{A.11}$$

$A_{23}^{V\mu\nu}$ vanishes for $\mu=0$ or $\nu=0$, case (a). For $\mu\neq\nu$ one uses the line (b), otherwise (c). $A_{23}^{V\mu\nu}$ is from the $l^\mu l^\nu$ part after the shift of k to $\bar{k}$. The sign conventions are Minkowski with upper indices as indicated. In the main text we have dropped the argument n, we only need $n=1$.

A.3 Two propagator integrals

We define two propagator integrals as

$$B^{\{,\mu,\mu\nu\}}(m_1^2,m_2^2,n_1,n_2)=\frac{1}{i}\int_V\frac{d^dk}{(2\pi)^d}\frac{\{1,k^\mu,k^\mu k^\nu\}}{(k^2-m_1^2)^{n_1}((q-k)^2-m_2^2)^{n_2}}. \tag{A.12}$$

As in the tadpole case, the direction of the propagators is important. We use the convention that the particles propagate in the direction of the momentum indicated in the propagator. We thus write k and $q-k$ in the propagators to indicate this, even if the sign in the denominator at first sight is not relevant.

We have in principle a twist angle vector for each of the two particles in the denominators. However, it is sufficient to specify only the twist vector for the first propagator, with m_1^2, and the external momentum q. The latter must be such that $q-k$ automatically produces the correct boundary conditions for the particle corresponding to m_2^2. This is discussed in detail in [2].

We first do the Poisson summation trick to get full integrals over k. We combine the two propagators in (A.12) using a Feynman parameter x and shift integration variable by $k=\tilde{k}+xq$. We then have expressions of the form of the previous subsection but with $\tilde{k}$ as integration variable and $\tilde{m}^2=(1-x)m_1^2+xm_2^2-x(1-x)q^2$ instead of m^2, as well as $\vec{\tilde{\theta}}=\vec{\theta}_1-x\vec{q}$.

The final result is

$$\begin{aligned}
B^V(m_1^2,m_2^2,n_1,n_2,q)&=\frac{\Gamma(n_1+n_2)}{\Gamma(n_1)\Gamma(n_2)}\int_0^1 dx(1-x)^{n_1-1}x^{n_2-1}A^V(\tilde{m}^2,n_1+n_2)\,,\\
B^{V\mu}(m_1^2,m_2^2,n_1,n_2,q)&=\frac{\Gamma(n_1+n_2)}{\Gamma(n_1)\Gamma(n_2)}\int_0^1 dx(1-x)^{n_1-1}x^{n_2-1}\\
&\quad\times\left(A^{V\mu}(\tilde{m}^2,n_1+n_2)+xq^\mu A^V(\tilde{m}^2,n_1+n_2)\right),\\
B^{V\mu\nu}(m_1^2,m_2^2,n_1,n_2)&=\frac{\Gamma(n_1+n_2)}{\Gamma(n_1)\Gamma(n_2)}\int_0^1 dx(1-x)^{n_1-1}x^{n_2-1}\left(A^{V\mu\nu}(\tilde{m}^2,n_1+n_2)\right.\\
&\quad\left.+x(q^\mu g_\alpha^\nu+q^\nu g_\alpha^\mu)A^{V\alpha}(\tilde{m}^2,n_1+n_2)+x^2q^\mu q^\nu A^V(\tilde{m}^2,n_1+n_2)\right)\,.
\end{aligned} \tag{A.13}$$

The signs are for upper indices in Minkowski space as indicated. For the numerical evaluation it is useful to treat the integral over x and λ together. In the main text we have dropped the indices n_1 and n_2 and used the components as defined below in (A.15).

JHEP05(2014)015

A.4 Integral relations

It is possible to derive relations between integrals using the relation

$$2k \cdot q = (k^2 - m_1^2) - ((q-k)^2 - m_2^2) + m_1^2 - m_2^2 + q^2 \,. \tag{A.14}$$

These were done in infinite volume in [20] and in [13] in the same conventions as ours. The trick remains valid at finite volume. Care has to be taken in the shift of integration momentum for some of the tadpole integrals (from k to $q-k$) but that is consistent with the boundary conditions.

We define components

$$\begin{aligned} B^{V\mu}(m_1^2, m_2^2) &= q^\mu B_1^V(m_1^2, m_2^2, q) + B_2^{V\mu}(m_1^2, m_2^2, q) \\ B^{V\mu\nu}(m_1^2, m_2^2, q) &= q^\mu q^\nu B_{21}^V(m_1^2, m_2^2, q) + g^{\mu\nu} B_{22}^V(m_1^2, m_2^2, q) + B_{23}^{V\mu\nu}(m_1^2, m_2^2, q) \,. \end{aligned} \tag{A.15}$$

The relations we get from using (A.14) are, suppressing the arguments (m_1^2, m_2^2, q),

$$\begin{aligned} 2q^2 B_1^V &= -A^V(m_1^2) + A^V(m_2^2) + (q^2 + m_1^2 - m_2^2) B^V - 2B_2^{V\mu} q_\mu \,, \\ q_\mu B_{23}^{V\mu\nu} &= -q^2 q^\nu B_{21}^V - q^\nu B_{22}^V \\ &\quad + \frac{1}{2}\left(-A^{V\nu}(m_2^2) - A^{V\nu}(m_1^2) + q^\nu A(m_2^2) + (q^2 + m_1^2 - m_2^2) B^{V\nu}\right) \,. \end{aligned} \tag{A.16}$$

These are valid for $n_1 = n_2 = 1$ and $n = 1$ in the tadpole integrals. They are needed to prove the Ward identities in the main text. We have also used them to simplify the expressions.

Open Access. This article is distributed under the terms of the Creative Commons Attribution License (CC-BY 4.0), which permits any use, distribution and reproduction in any medium, provided the original author(s) and source are credited.

References

[1] P.F. Bedaque, *Aharonov-Bohm effect and nucleon nucleon phase shifts on the lattice*, *Phys. Lett.* **B 593** (2004) 82 [nucl-th/0402051] [INSPIRE].

[2] C.T. Sachrajda and G. Villadoro, *Twisted boundary conditions in lattice simulations*, *Phys. Lett.* **B 609** (2005) 73 [hep-lat/0411033] [INSPIRE].

[3] G.M. de Divitiis, R. Petronzio and N. Tantalo, *On the discretization of physical momenta in lattice QCD*, *Phys. Lett.* **B 595** (2004) 408 [hep-lat/0405002] [INSPIRE].

[4] UKQCD collaboration, J.M. Flynn, A. Juttner and C.T. Sachrajda, *A Numerical study of partially twisted boundary conditions*, *Phys. Lett.* **B 632** (2006) 313 [hep-lat/0506016] [INSPIRE].

[5] C. Aubin, T. Blum, M. Golterman and S. Peris, *The hadronic vacuum polarization with twisted boundary conditions*, *Phys. Rev.* **D 88** (2013) 074505 [arXiv:1307.4701] [INSPIRE].

[6] F.-J. Jiang and B.C. Tiburzi, *Flavor twisted boundary conditions, pion momentum and the pion electromagnetic form-factor*, *Phys. Lett.* **B 645** (2007) 314 [hep-lat/0610103] [INSPIRE].

JHEP05(2014)015

[7] S. Weinberg, *Phenomenological Lagrangians*, *Physica* **A 96** (1979) 327 [INSPIRE].

[8] J. Gasser and H. Leutwyler, *Chiral Perturbation Theory to One Loop*, *Annals Phys.* **158** (1984) 142 [INSPIRE].

[9] J. Gasser and H. Leutwyler, *Chiral Perturbation Theory: Expansions in the Mass of the Strange Quark*, *Nucl. Phys.* **B 250** (1985) 465 [INSPIRE].

[10] J. Gasser and H. Leutwyler, *Spontaneously Broken Symmetries: Effective Lagrangians at Finite Volume*, *Nucl. Phys.* **B 307** (1988) 763 [INSPIRE].

[11] D. Becirevic and G. Villadoro, *Impact of the finite volume effects on the chiral behavior of f_K and B_K*, *Phys. Rev.* **D 69** (2004) 054010 [hep-lat/0311028] [INSPIRE].

[12] J. Bijnens, E. Boström and T.A. Lähde, *Two-loop Sunset Integrals at Finite Volume*, *JHEP* **01** (2014) 019 [arXiv:1311.3531] [INSPIRE].

[13] G. Amoros, J. Bijnens and P. Talavera, *Two point functions at two loops in three flavor chiral perturbation theory*, *Nucl. Phys.* **B 568** (2000) 319 [hep-ph/9907264] [INSPIRE].

[14] G. Amoros, J. Bijnens and P. Talavera, *QCD isospin breaking in meson masses, decay constants and quark mass ratios*, *Nucl. Phys.* **B 602** (2001) 87 [hep-ph/0101127] [INSPIRE].

[15] J. Gasser and H. Leutwyler, *Low-Energy Expansion of Meson Form-Factors*, *Nucl. Phys.* **B 250** (1985) 517 [INSPIRE].

[16] T.B. Bunton, F.-J. Jiang and B.C. Tiburzi, *Extrapolations of Lattice Meson Form Factors*, *Phys. Rev.* **D 74** (2006) 034514 [*Erratum ibid.* **D 74** (2006) 099902] [hep-lat/0607001] [INSPIRE].

[17] K. Ghorbani, *Chiral and Volume Extrapolation of Pion and Kaon Electromagnetic form Factor within* SU(3) *ChPT*, arXiv:1112.0729 [INSPIRE].

[18] J. Bijnens and P. Talavera, *Pion and kaon electromagnetic form-factors*, *JHEP* **03** (2002) 046 [hep-ph/0203049] [INSPIRE].

[19] C. Bernard, J. Bijnens, E. Gámiz and J. Relefors, work in progress.

[20] G. Passarino and M.J.G. Veltman, *One Loop Corrections for e^+e^- Annihilation Into $\mu^+\mu^-$ in the Weinberg Model*, *Nucl. Phys.* **B 160** (1979) 151 [INSPIRE].

JHEP05(2014)015

Paper II

LU TP 16-44
August 2016

Pion light-by-light contributions to the muon $g-2$

Johan Bijnens and Johan Relefors

Department of Astronomy and Theoretical Physics, Lund University,
Sölvegatan 14A, SE 223-62 Lund, Sweden

Abstract

This paper contains some new results on the hadronic light-by-light contribution (HLbL) to the muon $g-2$. The first part argues that we can expect large effects from disconnected diagrams in present and future calculations by lattice QCD of HLbL. The argument is based on the dominance of pseudo-scalar meson exchange.

In the second part, we revisit the pion loop HLbL contribution to the muon anomalous magnetic moment. We study it in the framework of some models studied earlier, pure pion loop, full VMD and hidden local symmetry for inclusion of vector mesons. In addition we study possible ways to include the axial-vector meson. The main part of the work is a detailed study of how the different momentum regions contribute. We derive a short distance constraint on the $\gamma^*\gamma^* \to \pi\pi$ amplitude and use this as a constraint on the models used for the pion loop. As a byproduct we present the general result for integration using the Gegenbauer polynomial method.

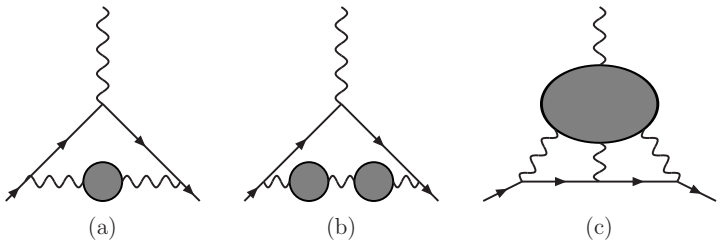

Figure 1: The thee main hadronic contributions to the muon anomalous magnetic moment. (a)The lowest order hadronic vacuum polarization. (b) An example of a higher order hadronic vacuum polarization contribution. (c) The light-by-light scattering contribution. In all three cases the shaded regions represent the hadronic part.

1 Introduction

The muon anomalous magnetic moment is one of the most precise measured quantities in high energy physics. The muon anomaly measures the deviation of the magnetic moment away from the prediction of a Dirac point particle

$$a_\mu \equiv \frac{g_\mu - 2}{2} \,. \tag{1}$$

where g_μ is the gyromagnetic ratio $\vec{M} = g_\mu (e/2m_\mu)\vec{S}$. The most recent experiment at BNL [1–4] obtains the value

$$a_\mu = 11\ 659\ 208.9(5.4)(3.3)\ 10^{-10} \,, \tag{2}$$

an impressive precision of 0.54 ppm (or 0.3 ppb on g_μ). The new experiment at Fermilab aims to improve this precision to 0.14 ppm [5] and there is a discussion whether a precision of 0.01 ppm is feasible [6]. In order to fully exploit the reach of these experiments an equivalent precision needs to be reached by the theory. The theoretical prediction consist of three main parts, the pure QED contribution, the electroweak contribution and the hadronic contribution.

$$a_\mu = a_\mu^{\rm QED} + a_\mu^{\rm EW} + a_\mu^{\rm had} \,. \tag{3}$$

An introductory review of the theory is [7] and more comprehensive review are [8, 9]. Recent results can be found in the proceedings of the conferences [10, 11].

The hadronic part has two different contributions, those due to hadronic vacuum polarization, both at lowest and higher orders, and the light-by-light scattering contributions.

$$a_\mu^{\rm had} = a_\mu^{\rm LO\text{-}HVP} + a_\mu^{\rm HO\text{-}HVP} + a_\mu^{\rm HLbL} \,. \tag{4}$$

These are depicted symbolically in Fig. 1.

The hadronic vacuum polarization contributions can be related to the experimentally measured cross-section $e^+e^- \to$ hadrons. Here the accuracy can thus in principle be improved as needed for the experimental measurements of a_μ.

The more difficult light-by-light contribution has no such simple relation to experimentally measurable quantities. A first comprehensive calculation appeared in [12]. One of the main problems there was the possibility of double counting when comparing quark-loop, hadron-loop and hadron exchange contributions. A significant step forward was done when it was realized [13] that the different contributions start entering at a different order in the expansion in the number of colours N_c and in the chiral power counting, order in momentum p. This splitting was then used by two groups to estimate the light-by-light contribution [14–16](HKS) and [17–19](BPP). After correcting a sign mistake made by both groups for different reasons and discovered by [20] the results are

$$a_\mu^{\rm HLbL} = 8.96(1.54)\ 10^{-10}\ \ (HKS), \qquad 8.3(3.2)\ 10^{-10}\ \ (BPP)\,. \tag{5}$$

A new developments since then have been the inclusion of short distance constraints on the full correction [21](MV) which indicated a larger contribution

$$a_\mu^{HLbL} = 13.6(2.5)\ 10^{-10}\ \ (MV)\,. \tag{6}$$

Comparisons in detail of the various contributions in these three main estimates can be found in [22] and [23]. An indication of a possibly larger quark-loop contribution are the recent Schwinger-Dyson estimates of that contribution [24–27]. First results of using dispersion relations to get an alternative handle on HLbL have also appeared [28–31]. Lattice QCD has now started to contribute to HLbL as well, see e.g. [32, 33] and references therein.

In this paper we add a number of new results to the HLbL discussion. First, in Sect. 2 we present an argument why in the lattice calculations the disconnected contribution is expected to be large and of opposite sign to the connected contribution. This has been confirmed by the first lattice calculation [34]. The second part is extending the Gegenbauer polynomial method to do the integration over the photon momenta [9, 20] to the most general hadronic four-point function. This is the subject of Sect. 3. The third and largest part is about the charged pion and kaon loop. These have been estimated rather differently in the the three main evaluations

$$a_\mu^{\pi loop} = -0.45(0.81)\,10^{-10}\,(HKS), \quad -1.9(1.3)\,10^{-10}\,(BPP), \quad 0.0(1.0)\,10^{-10}\,(MV). \tag{7}$$

The numerical result is always dominated by the charged pion-loop, the charged kaon loop is about 5% of the numbers quoted in (7). The errors in all cases were mainly the model dependence. The main goal of this part is to show how these differences arise in the calculation and include a number of additional models. Given the uncertainties we will concentrate on the pion-loop only.

There are several improvements in this paper over the previous work on the pion loop. First, we use the Gegenbauer polynomial method of [9, 20] to do two more of the integrals analytically compared to the earlier work. Second, we study more models by including the vector mesons in a number of different ways and study the possible inclusion of axial-vector mesons. That the latter might introduce some uncertainty has been emphasized in

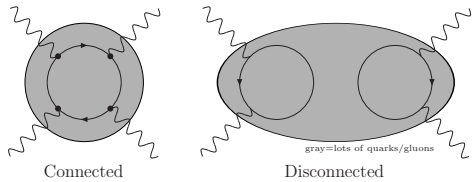

Figure 2: The connected contribution where all photons couple to a single quark-loop and an example of a disconnected diagram where the photons couple to different quark-loops.

[35, 36]. We present as well a new short-distance constraint that models have to satisfy for the underlying $\gamma\gamma\pi\pi$ vertex.

Our main tool for understanding the different results is to study the dependence on the virtualities of the three internal photons in Fig. 1(c). The use of this as a method to understand contributions was started in [22] for the main pion exchange. One aspect that will become clear is that one must be very careful in simply adding more terms in a hadronic model. In general, these models are non-renormalizable and there is thus no guarantee that there is a prediction for the muon anomaly in general. In fact, we have not found a clean way to do it for the axial vector meson as discussed in Sect. 4. However, using that the results should have a decent agreement with ChPT at low energies and the high-energy constraint and only integrating up to a reasonable hadronic scale we obtain the result

$$a_\mu^{HLbL\ \pi loop} = -(2.0 \pm 0.5) \cdot 10^{-10}\,. \tag{8}$$

This is discussed in Sect. 4.

A short summary is given in Sect. 5. Some of the results here have been presented earlier in [10, 37, 38] and [39].

2 Large disconnected contributions

Lattice calculations of HLbL are starting to give useful results. One question here is how to calculate the full contribution including both connected and disconnected contributions. The latter is more difficult to calculate, see e.g. [40], and many calculations so far have only presented results for the connected contribution. In this section we present an argument why the disconnected contribution is expected to be large and of opposite sign to the connected contribution. The connected contribution is the one where the four photons present in Fig. 1(c) all connect to the same quark line, the disconnected contribution where they connect to different quark lines. This is depicted schematically in Fig. 2. The argument below is presented for the case of two-flavours and has been presented shortly in [38].

A large part of the HLbL contribution comes from pseudo-scalar meson exchange. For that part of the contribution we can give some arguments on the relative size of the disconnected and connected contribution. An example of a limit where the connected

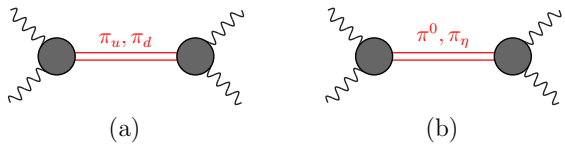

Figure 3: The meson-exchange picture. (a) With π_u and π_d exchange. (b) With π^0 and π_η exchange.

contribution is the only one is the large N_c limit. One important consequence of this limit is that the anomalous breaking of the $U(1)_A$ symmetry disappears and the flavour singlet pseudo-scalar meson becomes light as well. This also applies to exchanges of other multiplets, but there the mass differences between the singlet and non-singlet states are much smaller.

Let us first look at the quark-loop case with two flavours. The connected diagram has four photon couplings, thus each quark flavour gives a contribution proportional to its charge to the power four. The connected contribution has thus a factor of $q_u^4 + q_d^4 = (2/3)^4 + (-1/3)^4 = 17/81$. For the disconnected contribution we have instead charge factors of the form $(q_u^2 + q_d^2)$ for each quark-loop, so the final result has a factor of $(q_u^2 + q_d^2)^2 = 25/81$. However, this does not give any indication of the relative size since the contributions are very different.

In the large N_c limit the mesons are the flavour eigenstates. We then have two light neutral pseudo-scalars, one with flavour content $\bar{u}u$, π_u and one with $\bar{d}d$, π_d. In the meson exchange picture, shown in Fig. 3(a) the coupling of π_u to two photons is proportional to q_u^2, thus π_u exchange has factor of q_u^4. The same argument goes for the π_u exchange and we obtain a factor of q_d^4. The total contribution is thus proportional to $q_u^4 + q_d^4 = 17/81$ in agreement with the quark-loop argument for the same contribution.

We can also work with the isospin eigenstates instead. These are the π^0 with flavour content $(\bar{u}u - \bar{d}d)/\sqrt{2}$ and the flavour singlet π_η with flavour content $(\bar{u}u + \bar{d}d)/\sqrt{2}$. In the large N_c limit we should obtain the same result as with π_u and π_d. The π^0 coupling to 2 photons is proportional to $\delta_{\pi^0} = (q_u^2 - q_d^2)/\sqrt{2} = 3/(9\sqrt{2})$. The π_η coupling to two photons is $\delta_{\pi_\eta} = (q_u^2 + q_d^2)/\sqrt{2} = 5/(9\sqrt{2})$. The exchange of π^0 and π_η leads to a contribution proportional to $\delta_{\pi^0}^2 + \delta_{\pi_\eta}^2 = 17/81$ in agreement with the argument from the quark-loop or π_u, π_d exchange.

What happens now if we turn on the disconnected contribution or remove the large N_c limit. The physical eigenstates are now π_η and π^0 and they no longer have the same mass. In effect, from the breaking of the $U(1)_A$ the singlet has gotten a large mass and its contribution becomes much smaller. In the limit of being able to neglect π_η-exchange completely the sum of connected and disconnected contributions is reproduced by π^0 exchange alone which is proportional to $\delta_{\pi^0}^2 = (9/2)/81$. So in this limit we expect the total contribution is $\delta_{\pi^0}^2$ times a factor A. From the discussion in the previous paragraph follows that the connected part is $\delta_{\pi^0}^2 + \delta_{\pi_\eta}^2$ times the same factor A. The disconnected part must thus cancel the δ_π^2 part of the connected contribution and must be $-\delta_{\pi_\eta}^2$ times again the

factor A. We thus expect a large and negative disconnected contribution with a ratio of disconnected to connected of $-25/34$.

There are really three flavours u, d, s to be considered but the argument generalizes straightforward to that case with case $\delta_{\pi^0} = 3/(9\sqrt{2})$, $\delta_\eta = 3/(9\sqrt{6})$ and $\delta_{\eta'} = 6/(9\sqrt{3})$. In the equal mass case the ratio of disconnected to connected is for three flavours $-\delta\eta'^2/(\delta_{\pi^0}^2 + \delta_\eta^2 + \delta_{\eta'}^2) = -2/3$.

The above argument is valid in the equal mass limit, assuming the singlet does not contribute after $U(1)_A$ breaking is taken into account and only for the pseudo-scalar meson-exchange. There are corrections following from all of these. For most other contributions the disconnected effect is expected to be smaller. The ratio of disconnected to connected of $-2/3$ is thus an overestimate but given that π^0 exchange is the largest contribution we expect large and negative disconnected contributions.

Note that the above argument was in fact already used in the pseudo-scalar exchange estimate of [17–19], the comparison of the large N_c estimate and π^0, η, η' exchange is in Table 2 and the separate contributions in Table 3 of [18], up to the earlier mentioned overall sign.

Lattice QCD has been working hard on including disconnected contributions [40]. Using the same method of [32] at physical pion mass preliminary results were shown at Lattice 2016 [34] of 11.60(96) for the connected and $-6.25(80)$ for the disconnected in units of 10^{-10}. This is in good agreement with the arguments given above.

3 The Gegenbauer polynomial method

The hadronic light-by-light contribution to the muon anomalous magnetic moment is given by [41]

$$a_\mu^{LbL} = \frac{-1}{48 m_\mu} \mathrm{tr}\left[(\not{p} + m_\mu)\, M^{\lambda\beta}(0)\, (\not{p} + m_\mu)\, [\gamma_\lambda, \gamma_\beta] \right] , \tag{9}$$

with

$$M^{\lambda\beta}(p_3) = e^6 \int \frac{d^4p_1}{(2\pi)^4} \frac{d^4p_2}{(2\pi)^4} \frac{\gamma_\nu\, (\not{p}_4 + m)\, \gamma_\mu\, (\not{p}_5 + m)\, \gamma_\alpha}{q^2 p_1^2 p_2^2\, (p_4^2 - m^2)\, (p_5^2 - m^2)} \left[\frac{\partial}{\partial p_{3\lambda}} \Pi^{\mu\nu\alpha\beta}\, (p_1, p_2, p_3) \right] . \tag{10}$$

Here m is the muon mass, p is the muon momentum, $q = p_1 + p_2 + p_3$, $p_4 = p - p_1$ and $p_5 = p + p_2$. The momentum routing in the diagram is shown in Fig. 4. Note that because of charge conjugation the integration in (10) is symmetric under the interchange of p_1 and p_2. The symmetry under the full interchange of $-q, p_1, p_2$ is only explicitly present if the other permutations of the photons on the muon line are also added and then averaged. In this manuscript we stick to using only the permutation shown. The integral gives still the full contribution because the different permutations are included in the hadronic four-point function $\Pi^{\mu\nu\alpha\beta}(p_1, p_2, p_3)$.

The hadronic four-point function is

$$\Pi^{\mu\nu\alpha\beta}(p_1, p_2, p_3) = i^3 \int d^4x d^4y d^4z e^{i(p_1\cdot x + p_2\cdot y + p_3\cdot z)} \langle 0 | T\left(V^\mu(0) V^\nu(x) V^\alpha(y) V^\beta(z) \right) | 0 \rangle . \tag{11}$$

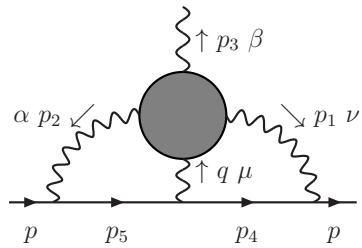

Figure 4: The momentum routing for the muon line and through the hadronic four-point function as used in (10).

The current is $V_\mu = \sum_q Q_q \bar{q}\gamma_\mu q$ with q denoting the quarks and Q_q the quark charge in units of $|e|$. The four-point function has a rather complicated structure and we discuss this in more detail Sect. 3.1.

The partial derivative in (10) was introduced by [41] to make each photon leg permutation of the fermion-loop finite which allows to do the numerical calculation at $p_3 = 0$. It used $p_{3\beta}\Pi^{\mu\nu\alpha\beta} = 0$ to obtain via $\partial/\partial p_{3\lambda}$

$$0 = \Pi^{\mu\nu\alpha\lambda} + p_{3\beta}\frac{\partial}{\partial p_{3\lambda}}\Pi^{\mu\nu\alpha\beta}\,. \tag{12}$$

The integral in (10) contains 8 degrees of freedom. After projecting on the muon magnetic moment with (9) it can only depend on $p_1^2, p_2^2, p_1 \cdot p_2, p \cdot p_1, p \cdot p_2$. The earlier work in [14–19] relied on doing all these integrals numerically and in [17–19] this was done after an additional rotation to Euclidean space. For the pion exchange contribution a method was developed to reduce the number of integrals from 5 to 2 using the method of Gegenbauer polynomials [20]. The assumptions made there about the behaviour of the hadronic four-point function are not valid for the parts we study in this paper. However, in [9] for the pion and scalar exchange contributions the same method has been used to explicitly perform the integrals over the $p \cdot p_1$ and $p \cdot p_2$ degrees of freedom. The same method can be used to perform the integral over these two degrees of freedom also in the case for the most general four-point function. This leads to an expression of about 260 terms expressed in the combinations [18] of the four point function that contribute to the muon $g-2$. We have checked that our calculation reproduces for the pion exchange the results quoted in [9].

3.1 The general four-point function

The four-point functions defined in (11) contains 138 different Lorentz-structures [18][1]

$$\begin{aligned}\Pi^{\mu\nu\alpha\beta}(p_1,p_2,p_3) \equiv\ & \Pi^1(p_1,p_2,p_3)g^{\mu\nu}g^{\alpha\beta} + \Pi^2(p_1,p_2,p_3)g^{\mu\alpha}g^{\nu\beta} \\ & + \Pi^3(p_1,p_2,p_3)g^{\mu\beta}g^{\nu\alpha} \\ & + \Pi^{1jk}(p_1,p_2,p_3)g^{\mu\nu}p_j^\alpha p_k^\beta + \Pi^{2jk}(p_1,p_2,p_3)g^{\mu\alpha}p_j^\nu p_k^\beta \\ & + \Pi^{3jk}(p_1,p_2,p_3)g^{\mu\beta}p_j^\nu p_k^\alpha + \Pi^{4jk}(p_1,p_2,p_3)g^{\nu\alpha}p_j^\mu p_k^\beta \\ & + \Pi^{5jk}(p_1,p_2,p_3)g^{\nu\beta}p_j^\mu p_k^\alpha + \Pi^{6jk}(p_1,p_2,p_3)g^{\alpha\beta}p_j^\mu p_k^\nu \\ & + \Pi^{ijkm}(p_1,p_2,p_3)p_i^\mu p_j^\nu p_k^\beta p_m^\alpha\,, \end{aligned} \tag{13}$$

where $i,j,k,m = 1,\ 2$ or 3 and repeated indices are summed. The functions are scalar functions of all possible invariant products $p_i \cdot p_j$.

The four point function satisfies the Ward-Takahashi identities

$$q_\mu \Pi^{\mu\nu\alpha\beta} = p_{1\nu}\Pi^{\mu\nu\alpha\beta} = p_{2\alpha}\Pi^{\mu\nu\alpha\beta} = p_{3\beta}\Pi^{\mu\nu\alpha\beta} = 0\,. \tag{14}$$

These identities allow to show that there are 43 independent functions in general. Of course, since the four-point function is symmetric under the interchange of the external legs many of these are related by permutations.

In practice it is easier not to do this reduction, but only the partial step up to reducing them to the 64 functions Π^{ijkm}. This can be done such that the powers of p_3 appearing explicitly never decrease. Not all of these contribute to a_μ, in fact at most 32 combinations can contribute [18]. These are the $\Pi^{3jkm}, \Pi^{i3km}, \Pi^{ij3m}$ and the Π^{Dijk}, all with $i,j,k = 1,2$. The Π^{Dijk} come from derivatives of the Π^{ijkm} w.r.t. $p_{3\lambda}$ at $p_3 = 0$

$$\begin{aligned}\frac{\partial}{\partial p_{3\lambda}}\Pi^{ijkm} &= p_1^\lambda \Pi^{1ijkm} + p_2^\lambda \Pi^{2ijkm} \\ \Pi^{Dijk} &= \Pi^{1ijk2} - \Pi^{2ijk1}\,. \end{aligned} \tag{15}$$

3.2 The Gegenbauer method

The simplification introduced in [20] was that the Gegenbauer polynomial method can be used to average over all directions of the muon momentum. After this averaging is done there is only dependence on the invariant quantities p_1^2, p_2^2 and $p_1 \cdot p_2$ left. The method is fully explained in [9]. One can apply it to the full four-point function or to the one where one has reduced the number of components by using the Ward identities to the 64 Π^{ijkl}.

So we first take (9) and (10) and rotate everything to Euclidean momenta P_1, P_2 and P with $Q = P_1 + P_2$, $P_4 = P - P_1$ and $P_5 = P + P_2$. We see that the muon momentum P

[1]Note that this is the most general case also valid in other dimensions. For four dimensions there are some additional constraints leading to only 136 independent components [27]. This is not relevant for the work presented here.

shows up in denominators with $p_4^2 - m^2 = -(P_4^2 + m^2)$ and $p_5^2 - m^2 = -(P_5^2 + m^2)$ only. After taking the Dirac trace only scalar products of momenta are present in the numerator. Removing the products $P \cdot P_1$ and $P \cdot P_2$ by completing them to the full $P_4^2 + m^2$ and $P_5^2 + m^2$, the angular averaging over muon momenta can be performed using [9]

$$\begin{aligned}
\left\langle \frac{1}{(P_4^2+m^2)(P_5^2+m^2)} \right\rangle_\mu &= \delta X\,, \\
\left\langle \frac{P \cdot P_1}{P_5^2+m^2} \right\rangle_\mu &= \frac{1}{8}\delta P_1 \cdot P_2 r_2^2\,, \\
\left\langle \frac{P \cdot P_2}{P_4^2+m^2} \right\rangle_\mu &= \frac{1}{8}\delta P_1 \cdot P_2 r_2^2\,, \\
\left\langle \frac{1}{P_4^2+m^2} \right\rangle_\mu &= \frac{1}{2}\delta r_1\,, \\
\left\langle \frac{1}{P_5^2+m^2} \right\rangle_\mu &= \frac{1}{2}\delta r_2\,.
\end{aligned} \tag{16}$$

Here we used the notation

$$\begin{aligned}
\delta &= \frac{1}{m^2}\,, \\
r_i &= 1 - \sqrt{1 + \frac{4m^2}{P_i^2}} \\
X &= \frac{1}{P_1 P_2 \sin\theta} \mathrm{atan}\left(\frac{z \sin\theta}{1 - z\cos\theta}\right) \\
\cos\theta &= \frac{P_1 \cdot P_2}{P_1 P_2} \\
z &= \frac{P_1 P_2}{4m^2} r_1 r_2\,.
\end{aligned} \tag{17}$$

The final contribution to the muon anomaly is given by

$$a_\mu = \frac{\alpha^3}{2\pi^2} \int P_1^2 dP_1^2 P_2^2 dP_2^2 \sin\theta d\cos\theta A_\Pi(P_1, P_2, \cos\theta)\,. \tag{18}$$

The quantity A_Π is given by

$$\begin{aligned}
&\Pi^{1131}(-1/6\,\rho_3^2 r_2^2\delta - 2/3\,\rho_1\rho_3 r_2\delta + 8/3\,\rho_1\rho_3 X - \rho_1^2 r_1\delta - 4/3\,\rho_1^2\rho_3 X\delta - 2\,\rho_1^2\rho_2 X\delta) \\
&+\Pi^{1132}(+2/3\rho_3 + 1/3\rho_2\rho_3 r_2\delta - 1/6\rho_2\rho_3 r_2^2\delta - 2/3\rho_1\rho_3 r_1\delta - 1/6\rho_1\rho_3 r_1^2\delta - 2/3\rho_1\rho_2 r_2\delta \\
&\qquad + 1/3\rho_1\rho_2 r_1\delta + 8/3\rho_1\rho_2 X - 4/3\rho_1\rho_2\rho_3 X\delta + 2/3\rho_1\rho_2^2 X\delta - 4/3\rho_1^2\rho_2 X\delta) \\
&+\Pi^{1231}(-2/3\rho_3^2 r_2\delta - 1/6\rho_2\rho_3 r_2^2\delta - 2/3\rho_1\rho_3 r_1\delta - 4/3\rho_1\rho_3^2 X\delta + 1/3\rho_1\rho_2 r_2\delta \\
&\qquad + 8/3\rho_1\rho_2 X - 4/3\rho_1\rho_2\rho_3 X\delta + 2/3\rho_1^2\rho_2 X\delta) \\
&+\Pi^{1232}(-2/3\rho_3^2 r_1\delta - 2/3\rho_2 - 2/3\rho_2\rho_3 r_2\delta + 8/3\rho_2\rho_3 X - 4/3\rho_2\rho_3^2 X\delta - 1/3\rho_2^2 r_2\delta
\end{aligned}$$

$$
\begin{aligned}
&\quad - 1/3\rho_1\rho_2 r_1\delta - 4/3\rho_1\rho_2\rho_3 X\delta - 2/3\rho_1\rho_2^2 X\delta) \\
&+\Pi^{1311}(+1/3\rho_1\rho_3 r_2\delta + 1/3\rho_1^2 r_1\delta + 2/3\rho_1^2\rho_3 X\delta + 2/3\rho_1^2\rho_2 X\delta) \\
&+\Pi^{1312}(-2/3\rho_3^2 r_2\delta + 4/3\rho_3^2 X - 1/12\rho_2\rho_3 r_2^2\delta - 4/3\rho_1\rho_3 r_1\delta - 1/12\rho_1\rho_3 r_1^2\delta \\
&\quad - 4/3\rho_1\rho_3^2 X\delta + 1/2\rho_1\rho_2 r_2\delta + 1/6\rho_1\rho_2 r_1\delta + 4/3\rho_1\rho_2 X - 8/3\rho_1\rho_2\rho_3 X\delta \\
&\quad + 1/3\rho_1\rho_2^2 X\delta + \rho_1^2\rho_2 X\delta) \\
&+\Pi^{1322}(-2/3\rho_2 - 2/3\rho_2\rho_3 r_2\delta + 8/3\rho_2\rho_3 X - 1/3\rho_2^2 r_2\delta - 2\rho_1\rho_2 r_1\delta \\
&\quad - 4/3\rho_1\rho_2\rho_3 X\delta - 4\rho_1\rho_2^2 X\delta) \\
&+\Pi^{2131}(-2/3\rho_1 - 2/3\rho_1\rho_3 r_1\delta + 8/3\rho_1\rho_3 X - 2\rho_1\rho_2 r_2\delta - 4/3\rho_1\rho_2\rho_3 X\delta - 1/3\rho_1^2 r_1\delta \\
&\quad - 4\rho_1^2\rho_2 X\delta) \\
&+\Pi^{2231}(-2/3\rho_3^2 r_1\delta + 4/3\rho_3^2 X - 4/3\rho_2\rho_3 r_2\delta - 1/12\rho_2\rho_3 r_2^2\delta - 4/3\rho_2\rho_3^2 X\delta - 1/12\rho_1\rho_3 r_1^2\delta \\
&\quad + 1/6\rho_1\rho_2 r_2\delta + 1/2\rho_1\rho_2 r_1\delta + 4/3\rho_1\rho_2 X - 8/3\rho_1\rho_2\rho_3 X\delta + \rho_1\rho_2^2 X\delta + 1/3\rho_1^2\rho_2 X\delta) \\
&+\Pi^{2232}(+1/3\rho_2\rho_3 r_1\delta + 1/3\rho_2^2 r_2\delta + 2/3\rho_2^2\rho_3 X\delta + 2/3\rho_1\rho_2^2 X\delta) \\
&+\Pi^{2311}(-2/3\rho_3^2 r_2\delta - 2/3\rho_1 - 2/3\rho_1\rho_3 r_1\delta + 8/3\rho_1\rho_3 X - 4/3\rho_1\rho_3^2 X\delta - 1/3\rho_1\rho_2 r_2\delta \\
&\quad - 4/3\rho_1\rho_2\rho_3 X\delta - 1/3\rho_1^2 r_1\delta - 2/3\rho_1^2\rho_2 X\delta) \\
&+\Pi^{2312}(-2/3\rho_3^2 r_1\delta - 2/3\rho_2\rho_3 r_2\delta - 4/3\rho_2\rho_3^2 X\delta - 1/6\rho_1\rho_3 r_1^2\delta + 1/3\rho_1\rho_2 r_1\delta + 8/3\rho_1\rho_2 X \\
&\quad - 4/3\rho_1\rho_2\rho_3 X\delta + 2/3\rho_1\rho_2^2 X\delta) \\
&+\Pi^{2321}(+2/3\rho_3 - 2/3\rho_2\rho_3 r_2\delta - 1/6\rho_2\rho_3 r_2^2\delta + 1/3\rho_1\rho_3 r_1\delta - 1/6\rho_1\rho_3 r_1^2\delta + 1/3\rho_1\rho_2 r_2\delta \\
&\quad - 2/3\rho_1\rho_2 r_1\delta + 8/3\rho_1\rho_2 X - 4/3\rho_1\rho_2\rho_3 X\delta - 4/3\rho_1\rho_2^2 X\delta + 2/3\rho_1^2\rho_2 X\delta) \\
&+\Pi^{2322}(-1/6\rho_3^2 r_1^2\delta - 2/3\rho_2\rho_3 r_1\delta + 8/3\rho_2\rho_3 X - \rho_2^2 r_2\delta - 4/3\rho_2^2\rho_3 X\delta - 2\rho_1\rho_2^2 X\delta) \\
&+\Pi^{3111}(+1/6\rho_3^2 r_2^2\delta - 2/3\rho_1 - 4/3\rho_1\rho_3 r_2\delta + 1/2\rho_1\rho_3 r_2^2\delta - 1/3\rho_1\rho_2 r_2\delta - \rho_1^2 r_2\delta \\
&\quad - 1/3\rho_1^2 r_1\delta - 8/3\rho_1^2\rho_3 X\delta - 2/3\rho_1^2\rho_2 X\delta - 2\rho_1^3 X\delta) \\
&+\Pi^{3112}(+4/3\rho_3 + 2/3\rho_2\rho_3 r_2\delta + 1/6\rho_2\rho_3 r_2^2\delta + 2/3\rho_1 + 2/3\rho_1\rho_3 r_1\delta - 1/3\rho_1\rho_3 r_1^2\delta \\
&\quad - 8/3\rho_1\rho_3 X + 2/3\rho_1\rho_2 r_1\delta - 8/3\rho_1\rho_2 X + 4/3\rho_1\rho_2\rho_3 X\delta + 4/3\rho_1\rho_2^2 X\delta + 1/3\rho_1^2 r_1\delta) \\
&+\Pi^{3121}(+2\rho_1 + \rho_1^2 r_1\delta) \\
&+\Pi^{3122}(+2\rho_2 + \rho_2^2 r_2\delta) \\
&+\Pi^{3211}(+4/3\rho_3 - 8/3\rho_3^2 X + 2/3\rho_2\rho_3 r_2\delta + 2/3\rho_1 + 2/3\rho_1\rho_3 r_1\delta - 1/6\rho_1\rho_3 r_1^2\delta \\
&\quad - 8/3\rho_1\rho_3 X + 1/3\rho_1\rho_2 r_2\delta + 1/3\rho_1\rho_2 r_1\delta + 4/3\rho_1\rho_2\rho_3 X\delta + 2/3\rho_1\rho_2^2 X\delta \\
&\quad + 1/3\rho_1^2 r_1\delta + 2/3\rho_1^2\rho_2 X\delta) \\
&+\Pi^{3212}(+4/3\rho_3 - 8/3\rho_3^2 X + 2/3\rho_2 + 2/3\rho_2\rho_3 r_2\delta - 1/6\rho_2\rho_3 r_2^2\delta - 8/3\rho_2\rho_3 X \\
&\quad + 1/3\rho_2^2 r_2\delta + 2/3\rho_1\rho_3 r_1\delta + 1/3\rho_1\rho_2 r_2\delta + 1/3\rho_1\rho_2 r_1\delta + 4/3\rho_1\rho_2\rho_3 X\delta \\
&\quad + 2/3\rho_1\rho_2^2 X\delta + 2/3\rho_1^2\rho_2 X\delta) \\
&+\Pi^{3221}(+4/3\rho_3 + 2/3\rho_2 + 2/3\rho_2\rho_3 r_2\delta - 1/3\rho_2\rho_3 r_2^2\delta - 8/3\rho_2\rho_3 X + 1/3\rho_2^2 r_2\delta + 2/3\rho_1\rho_3 r_1\delta \\
&\quad + 1/6\rho_1\rho_3 r_1^2\delta + 2/3\rho_1\rho_2 r_2\delta - 8/3\rho_1\rho_2 X + 4/3\rho_1\rho_2\rho_3 X\delta + 4/3\rho_1^2\rho_2 X\delta) \\
&+\Pi^{3222}(+1/6\rho_3^2 r_1^2\delta - 2/3\rho_2 - 4/3\rho_2\rho_3 r_1\delta + 1/2\rho_2\rho_3 r_1^2\delta - 1/3\rho_2^2 r_2\delta - \rho_2^2 r_1\delta - 8/3\rho_2^2\rho_3 X\delta \\
&\quad - 2\rho_2^3 X\delta - 1/3\rho_1\rho_2 r_1\delta - 2/3\rho_1\rho_2^2 X\delta)
\end{aligned}
$$

$$
\begin{aligned}
&+\Pi^{D111}(-1/3\rho_1\rho_3+2/3\rho_1\rho_3^2X-1/6\rho_1\rho_2\rho_3r_2\delta+1/24\rho_1\rho_2\rho_3r_2^2\delta-1/6\rho_1^2\rho_3r_1\delta\\
&\quad+1/24\rho_1^2\rho_3r_1^2\delta-1/12\rho_1^2\rho_2r_2\delta-1/12\rho_1^2\rho_2r_1\delta-2/3\rho_1^2\rho_2X-1/3\rho_1^2\rho_2\rho_3X\delta\\
&\quad-1/6\rho_1^2\rho_2^2X\delta-1/6\rho_1^3\rho_2X\delta)\\
&+\Pi^{D121}(+1/3\rho_3^2-2/3\rho_3^3X+1/6\rho_2\rho_3^2r_2\delta-1/24\rho_2\rho_3^2r_2^2\delta+1/6\rho_1\rho_3^2r_1\delta-1/24\rho_1\rho_3^2r_1^2\delta\\
&\quad+1/12\rho_1\rho_2\rho_3r_2\delta+1/12\rho_1\rho_2\rho_3r_1\delta+2/3\rho_1\rho_2\rho_3X+1/3\rho_1\rho_2\rho_3^2X\delta+1/6\rho_1\rho_2^2\rho_3X\delta\\
&\quad+1/6\rho_1^2\rho_2\rho_3X\delta)\\
&+\Pi^{D122}(+2/3\rho_2\rho_3-4/3\rho_2\rho_3^2X+1/3\rho_2^2\rho_3r_2\delta-1/12\rho_2^2\rho_3r_2^2\delta+1/3\rho_1\rho_2\rho_3r_1\delta\\
&\quad-1/12\rho_1\rho_2\rho_3r_1^2\delta+1/6\rho_1\rho_2^2r_2\delta+1/6\rho_1\rho_2^2r_1\delta+4/3\rho_1\rho_2^2X+2/3\rho_1\rho_2^2\rho_3X\delta\\
&\quad+1/3\rho_1\rho_2^3X\delta+1/3\rho_1^2\rho_2^2X\delta)\\
&+\Pi^{D211}(-2/3\rho_1\rho_3+4/3\rho_1\rho_3^2X-1/3\rho_1\rho_2\rho_3r_2\delta\\
&\quad+1/12\rho_1\rho_2\rho_3r_2^2\delta-1/3\rho_1^2\rho_3r_1\delta+1/12\rho_1^2\rho_3r_1^2\delta-1/6\rho_1^2\rho_2r_2\delta-1/6\rho_1^2\rho_2r_1\delta\\
&\quad-4/3\rho_1^2\rho_2X-2/3\rho_1^2\rho_2\rho_3X\delta-1/3\rho_1^2\rho_2^2X\delta-1/3\rho_1^3\rho_2X\delta)\\
&+\Pi^{D221}(-1/3\,\rho_3^2+2/3\,\rho_3^3X-1/6\,\rho_2\rho_3^2r_2\delta+1/24\,\rho_2\rho_3^2r_2^2\delta-1/6\,\rho_1\rho_3^2r_1\delta+1/24\,\rho_1\rho_3^2r_1^2\delta\\
&\quad-1/12\,\rho_1\rho_2\rho_3r_2\delta-1/12\,\rho_1\rho_2\rho_3r_1\delta-2/3\,\rho_1\rho_2\rho_3X-1/3\,\rho_1\rho_2\rho_3^2X\delta\\
&\quad-1/6\,\rho_1\rho_2^2\rho_3X\delta-1/6\,\rho_1^2\rho_2\rho_3X\delta)\\
&+\Pi^{D222}(+1/3\,\rho_2\rho_3-2/3\,\rho_2\rho_3^2X+1/6\,\rho_2^2\rho_3r_2\delta-1/24\,\rho_2^2\rho_3r_2^2\delta+1/6\,\rho_1\rho_2\rho_3r_1\delta\\
&\quad-1/24\,\rho_1\rho_2\rho_3r_1^2\delta+1/12\,\rho_1\rho_2^2r_2\delta+1/12\,\rho_1\rho_2^2r_1\delta+2/3\,\rho_1\rho_2^2X+1/3\,\rho_1\rho_2^2\rho_3X\delta\\
&\quad+1/6\,\rho_1\rho_2^3X\delta+1/6\,\rho_1^2\rho_2^2X\delta)\,. \qquad (19)
\end{aligned}
$$

Here we used the abbreviations $\rho_1 = P_1^2$, $\rho_2 = P_2^2$ and $\rho_3 = P_1 \cdot P_2$. in addition to those defined above.

A more general formula without using the Ward identities can also be derived. Quoting this one would be too long. In practice for many models, the method without using Ward identities leads to shorter but equivalent results. We have used both options for the bare pion loop, the full VMD (Vector Meson Dominance) model and the hidden local symmetry (HLS) model and only the latter method for the antisymmetric field model for the vector and axial vector mesons.

4 The pion-loop contribution to HLbL

The pion loop contribution is depicted in Fig. 5. In the models we consider all the diagrams depicted can appear. The shaded blob indicates the presence of form-factors. In this section we will only discuss models and not include rescattering and a possible ambiguity in distinguishing two-pion contributions from scalar-exchanges. The dispersive method [28–30] will include this automatically but at present no full numerical results from this approach are available.

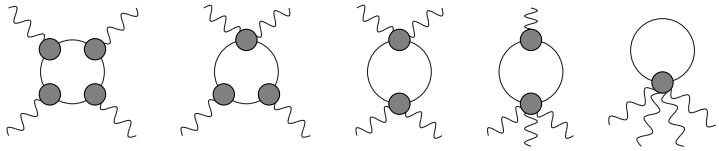

Figure 5: The pion-loop contributions to the vector four-point function of Eq. 11. The modeling is in the expressions for the form-factors designated by the shaded blobs.

4.1 VMD versus HLS

The simplest model is a point-like pion or scalar QED (sQED). This gives a contribution of $a_\mu^{\pi loop} \approx -4 \cdot 10^{-10}$. However, at high energies a pion is clearly not point-like. A first step is to include the pion form-factor in the vertices with a single photon. Gauge invariance then requires the presence of more terms with form-factors. The simplest gauge-invariant addition is to add the pion form-factor also to both legs of the $\pi\pi\gamma^*\gamma^*$ vertices and neglect vertices with three or more photons. For the pion form-factor one can use either the VMD expression or a more model/experimental inspired version. Using a model for the form-factor, is what was called full VMD [17, 18] and using the experimental data corresponds to what is called the model-independent or FsQED part of the two-pion contribution in [28–30]. The ENJL model used for the form-factor of [17, 18] led to $a_\mu^{\pi loop} \approx -1.9 \cdot 10^{-10}$. A form-factor parametrization of the form $m_V^2/(m_V^2 - q^2)$, a VMD parametrization, leads to $a_\mu^{\pi loop} \approx -1.6 \cdot 10^{-10}$ and using the experimental data FsQED gives $a_\mu^{\pi loop} \approx -1.6 \cdot 10^{-10}$ [42].

We study which momentum regions contribute most to a_μ by rewriting Eq. (18) with integration variables the (Euclidean) off-shellness of the three photons, P_1^2, P_2^2, Q^2. In fact to see the regions better we use [22] $l_P = (1/2)\ln(P^2/\mathrm{G}eV^2)$ for $P = P_1, P_2, Q$. With these variables we define

$$a_\mu = \int dl_{P_1} dl_{P_2} dl_Q \, a_\mu^{\mathrm{LLQ}} \, . \tag{20}$$

As a first example we show $-a_\mu^{LLQ}$ along the plane with $P_1 = P_2$ for the bare pion-loop or sQED and the full VMD in Fig. 6. The minus sign is included to make the plots easier to see. The contribution to a_μ as shown is proportional to the volume under the surfaces. It is clearly seen how the form-factors have little effect at low energies but are much more important at high momenta. We have three variables in principle but we only show plots with $P_1 = P_2$. The reason is that one can see in all our figures that the results are concentrated along the line $Q = P_1 = P_2$ and fall off fast away from there. The plots with $P_1 \neq P_2$ look similar but are smaller and do not show anything new qualitatively.

The other main evaluation of the pion-loop in [14, 15] (HKS) used a different approach. It was believed then that the full VMD approach did not respect gauge invariance. HKS therefore used the hidden local symmetry model with only vector mesons (HLS) [43] and obtained -0.45×10^{-10}. The only difference with full VMD is in the $\pi\pi\gamma^*\gamma^*$ as discussed in [18]. In [18] it was shown that the full VMD approach is gauge invariant. However, the

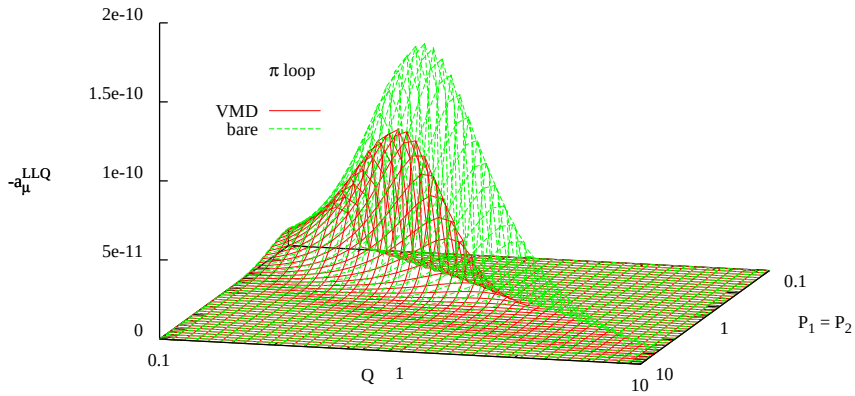

Figure 6: The momentum dependence of the pion loop contribution. Plotted is a_μ^{LLQ} of (20) as a function of $P_1 = P_2$ and Q. Top surface: sQED, bottom surface:full VMD.

large spread in the results for models that are rather similar was puzzling, both have a good description of the pion form-factor. We can make a similar study of the momentum range contributions, shown in Fig. 7. It is clearly visible that the two models agree very well for low momenta but there is a surprisingly large dip of the opposite sign for the HLS model at higher momenta, above and around 1 GeV. This is the reason for the large difference in the final number for $a_\mu^{\pi loop}$. A comparison as a function of the cut-off can be found in [39].

4.1.1 Short distance constraint: VMD is better

In QCD we know that the total hadronic contribution to the muon anomalous magnetic moment must be finite. This is however not necessarily true when looking at non-renormalizable models that in addition only describe part of the total hadronic contribution. For these one has too apply them intelligently, i.e. only use them in momentum regions where they are valid.

One tool to study possible regions of validity is to check how well the models do in reproducing short-distance constraints following directly from QCD. Examples of these are the Weinberg sum rules but there are also some applicable to more restricted observables. Unfortunately it is known that in general one cannot satisfy all QCD constraints with a finite number of hadrons included as discussed in detail in [44]. Still one wants to include as much as possible of QCD knowledge in the models used.

One constraint on the amplitude for $\gamma^*\gamma^* \to \pi\pi$ can be easily derived analoguously to the short-distance constraint of [21] for the pion exchange contribution. If we take both photons to be far off-shell and at a similar Q^2 then the leading term in the operator product expansion of the two electromagnetic currents is proportional to the axial current. However, a matrix element of the axial current with two pions vanishes so we have the

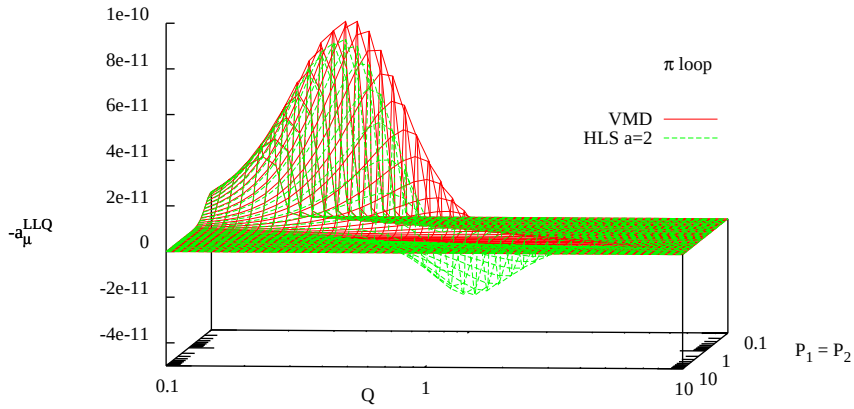

Figure 7: $-a_\mu^{LLQ}$ of (20) as a function of $P_1 = P_2$ and Q. Top surface: full VMD, bottom surface: HLS.

constraint

$$\lim_{Q^2\to\infty} A(\gamma^*(q_1 = Q + k)\gamma^*(q_2 = -Q + k) \to \pi(p_1)\pi(p_2)) \propto \frac{1}{Q^2} \tag{21}$$

when all scalar products involving k, p_1, p_2 and at most one power of Q are small compared to Q^2.

In scalar QED the amplitude for $\gamma^*\gamma^* \to \pi\pi$ is

$$ie^2\left[2g^{\mu\nu} + \frac{(k^\mu + Q^\mu - 2p_1^\mu)(k^\nu - Q^\nu - 2p_2^\nu)}{(Q + k - p_1)^2 - m_\pi^2} + \frac{(k^\mu + Q^\mu - 2p_2^\mu)(k^\nu - Q^\nu - 2p_1^\nu)}{(Q - k + p_1)^2 - m_\pi^2}\right] \tag{22}$$

which to lowest order in $1/Q^2$ is

$$2ie^2\left[g^{\mu\nu} - \frac{Q^\mu Q^\nu}{Q^2}\right]. \tag{23}$$

This amplitude does not vanish in the large Q^2 limit. sQED does not satsify the short distance constraint.

In full VMD the $\gamma\pi\pi$ and $\gamma\gamma\pi\pi$ vertices of scalar QED are multiplied by a factor

$$\frac{m_\rho^2 g^{\mu\nu} - q^\mu q^\nu}{m_\rho^2 - q^2} \tag{24}$$

for each photon line, where q is the momentum of the photon. The $(Q^2)^0$ term in the $\gamma^*\gamma^* \to \pi\pi$ amplitude is then zero. The full VMD model does respect the short distance constraint.

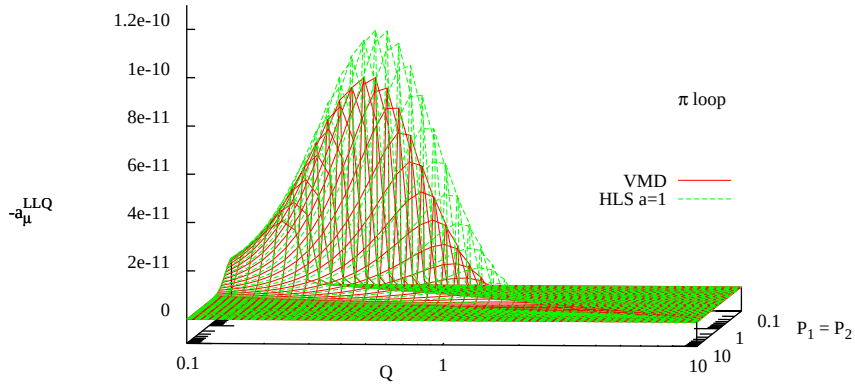

Figure 8: The momentum dependence of the pion loop contribution. $-a_\mu^{LLQ}$ of (20) as a function of $P_1 = P_2$ and Q. Top surface: HLS a=1, bottom surface: full VMD.

In HLS the $\gamma\pi\pi$ vertex of scalar QED is multiplied by

$$g^{\mu\nu} - \frac{a}{2}\frac{q^2 g^{\mu\nu} - q^\mu q^\nu}{q^2 - m_\rho^2} \tag{25}$$

and the $\gamma\gamma\pi\pi$ vertex is multiplied by

$$g^{\mu\alpha} g^{\nu\beta} - g^{\mu\alpha}\frac{a}{2}\frac{q^2 g^{\nu\beta} - q^\nu q^\beta}{q^2 - m_\rho^2} - g^{\nu\beta}\frac{a}{2}\frac{p^2 g^{\mu\alpha} - p^\mu p^\alpha}{p^2 - m_\rho^2}. \tag{26}$$

To lowest order in $1/Q^2$ the amplitude for $\gamma^*\gamma^* \to \pi\pi$ is

$$2ie^2\left[g^{\mu\nu} - \frac{Q^\mu Q^\nu}{Q^2}\right](1-a). \tag{27}$$

The HLS model with its usual value of $a = 2$ does not satisfy the short distance constraint.

It was also noticed [22] in a similar vein that the ENJL model, that essentially has full VMD, lives up to the Weinberg sum rules but the HLS does not.

In fact, using the HLS with an unphysical value of the parameter $a = 1$ satisfies the short-distance constraint (21) and lives up to the first Weinberg sum rule. The total result for that model is $a_\mu^{\pi loop} = -2.1 \cdot 10^{-10}$, similar to the ENJL model. A comparison for different momentum regions between the full VMD model and a HLS model with $a = 1$ is shown in Fig. 8. Notice in particular that the part with the opposite sign from Fig. 7 has disappeared.

From this we conclude that a number in the range $a_\mu^{\pi loop} = -(1.5\text{-}2.1) \times 10^{-10}$ would be more appropriate.

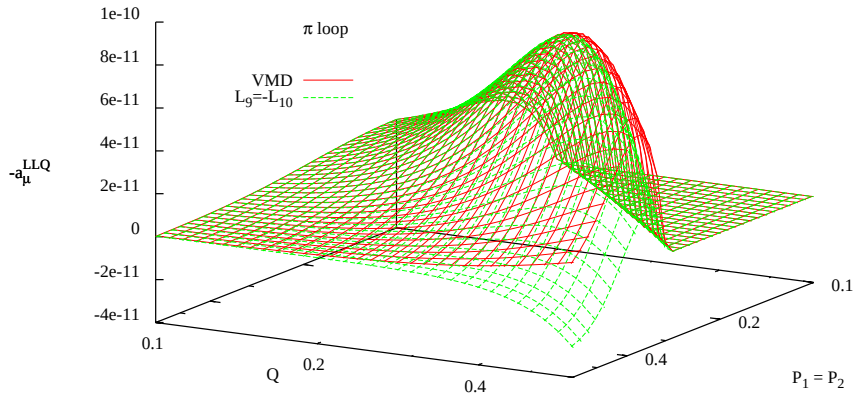

Figure 9: $-a_\mu^{LLQ}$ of (20) as a function of $P_1 = P_2$ and Q. Top surface: full VMD, bottom surface: ChPT with $L_9 = -L_{10}$ so the charge radius is included but no polarizability.

4.2 Including polarizability at low energies

It was pointed out that the effect of pion polarizability was neglected in the estimates of the pion-loop in [14, 15, 17, 18] and a first estimate of this effect was given using the Euler-Heisenberg four photon effective vertex produced by pions [35] within Chiral Perturbation Theory. This approximation is only valid below the pion mass. In order to check the size of the pion radius effect and the polarizability, we have implemented the low energy part of the four-point function and computed a_μ^{LLQ} for these cases in Chiral Perturbation Theory (ChPT). First results were shown in [37, 39]. The plots shown include the p^4 result which is the same as the bare pion-loop and we include in the vertices the effect of the terms from the L_9 and L_{10} terms in the p^4 ChPT Lagrangian. The effect of the charge radius is shown in Fig. 9 compared to the VMD parametrization of it, notice the different momentum scales compared to the earlier Figs. 6-8. The polarizability we have set to zero by setting $L_9 + L_{10} = 0$. As expected, the charge radius effect is included in the VMD result since the latter gives a good description of the pion form-factor. Including the effect of the polarizability can be done in ChPT by using experimentally determined values for L_9 and L_{10}. The latter can be determined from $\pi^+ \to e\nu\gamma$ or the hadronic vector two-point functions. Both are in good agreement and lead to a prediction of the pion polarizability confirmed by the Compass experiment [45]. The effect of including this in ChPT on a_μ^{LLQ} is shown in Fig. 10. An increase of 10-15% over the VMD estimate can be seen.

ChPT at lowest order, or p^4, for a_μ is just the point-like pion loop or sQED. At NLO pion exchange with point-like vertices and the pion-loop calculated at NLO in ChPT are needed. Both give divergent contributions to a_μ, so pure ChPT is of little use in predicting a_μ. If we had tried to extend the plots in Figs. 9 and 10 to higher momenta the bad high energy behaviour would have been clearly visible. We therefore need to go beyond ChPT. This is done in the next subsection.

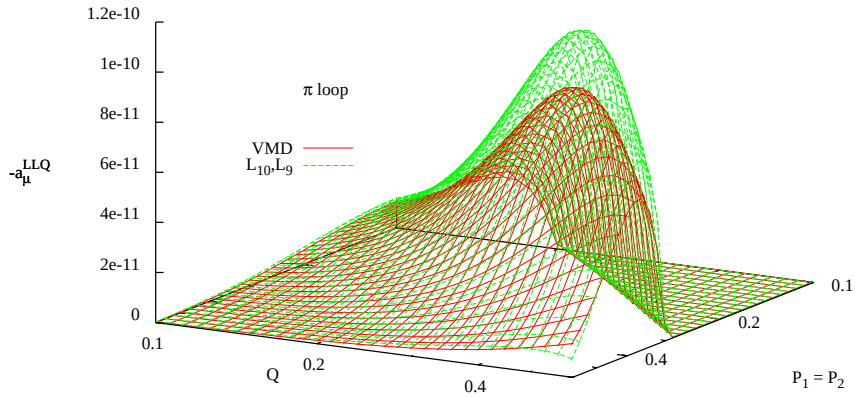

Figure 10: $-a_\mu^{LLQ}$ of (20) as a function of $P_1 = P_2$ and Q. Bottom surface: full VMD, top surface: ChPT with $L_9 \neq -L_{10}$ so the charge radius and the polarizability are included.

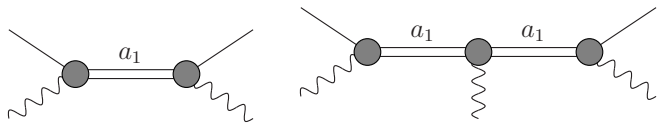

Figure 11: Left: the a_1-exchange that produces the pion polarizability. Right: an example of a diagram that is required by gauge invariance.

4.3 Including polarizability at higher energies

If we want to see the full effect of the polarizability we need to include a model that can be extended all the way, or at least to a cut-off of about 1 GeV. For the approach of [35] this was done in [36] by including a propagator description of a_1 and choosing it such that the full contribution of the pion-loop to a_μ is finite. They obtained a range of $-(1.1\text{-}7.1)\times 10^{-10}$ for the pion-loop contribution. This seems a very broad range when compared with all earlier estimates. One reason is that the range of polarizabilities used in [36] is simply not compatible with ChPT. The pion polarizability is an observable where ChPT should work and indeed the convergence is excellent. The ChPT prediction has also recently been confirmed by experiment [45]. Our work discussed below indicates that $-(2.0\pm 0.5)\times 10^{-10}$ is a more appropriate range for the pion-loop contribution.

The polarizability comes from $L_9 + L_{10}$ in ChPT [46, 47]. Using [48], we notice that the polarizability is produced by a_1-exchange depicted in Fig. 11. This is depicted in the left diagram of Fig. 11. However, once such an exchange is there, diagrams like the right one in Fig. 11 lead to effective $\pi\pi\gamma\gamma\gamma$ vertices and are required by electromagnetic gauge invariance. This issue can be dealt with in several ways. Ref. [36] introduced modifications of the a_1 propagator that introduces one form of the extra vertices. We deal with them

via effective Lagrangians incorporating vector and axial-vector mesons.

If one studies Fig. 11 one could raise the question "Is including a π-loop but no a_1-loop consistent?" The answer is yes with the following argument. We can first look at a tree level Lagrangian including pions ρ and a_1. We then integrate out the ρ and a_1 and calculate the one-loop pion diagrams with the resulting all order Lagrangian. In the diagrams of the original Lagrangian this corresponds to only including loops with at least one pion propagator present. Numerical results for cases including full a_1 loops are presented as well below. As a technicality, we use anti-symmetric vector fields for the vector and axial-vector mesons. This avoids complications due to π-a_1 mixing. We add vector $V_{\mu\nu}$ and axial-vector $A_{\mu\nu}$ nonet fields. The kinetic terms are given by [48]

$$-\frac{1}{2}\left\langle \nabla^\lambda V_{\lambda\mu}\nabla_\nu V^{\nu\mu} - \frac{M_V^2}{2}V_{\mu\nu}V^{\mu\nu}\right\rangle + V \leftrightarrow A\,. \tag{28}$$

We add first the terms that contribute to the L_i [48]

$$\frac{F_V}{2\sqrt{2}}\left\langle f_{+\mu\nu}V^{\mu\nu}\right\rangle + \frac{iG_V}{\sqrt{2}}\left\langle V^{\mu\nu}u_\mu u_\nu\right\rangle + \frac{F_A}{2\sqrt{2}}\left\langle f_{-\mu\nu}A^{\mu\nu}\right\rangle \tag{29}$$

with $L_9 = \frac{F_V G_V}{2M_V^2}$, $L_{10} = -\frac{F_V^2}{4M_V^2} + \frac{F_A^2}{4M_A^2}$. The Weinberg sum rules in the chiral limit imply $F_V^2 = F_A^2 + F_\pi^2$, $F_V^2 M_V^2 = F_A^2 M_A^2$ and requiring VMD behaviour for the pion form-factor $F_V G_V = F_\pi^2$. We have used input values for the L_9 and L_{10} consistent with this in the previous subsection.

Calculating the $\gamma^*\gamma^* \to \pi\pi$ amplitude in this framework using antisymmetric tensor notation to lowest order in $1/Q^2$ gives the amplitude

$$\begin{aligned}
&2ie^2\frac{F_A^2}{Q_1^2 m_a^2 F^2}(-p_1^\mu Q_1^\nu p_1\cdot Q_1 - p_1^\nu Q_1^\mu p_1\cdot Q_1 + Q_1^\mu Q_1^\nu m_\pi^2 + g^{\mu\nu}(p_1\cdot Q_1)^2)\\
&+2ie^2\frac{F_A^2}{m_a^2 F^2}(p_1^\mu p_1^\nu - g^{\mu\nu}m_\pi^2)\\
&+2ie^2(F_A^2 + F^2 - F_V^2)\left(\frac{g^{\mu\nu}}{F^2} - \frac{Q_1^\mu Q_1^\nu}{Q_1^2 F^2}\right).
\end{aligned} \tag{30}$$

The last line vanishes for $F_A^2 + F^2 - F_V^2 = 0$ which is one of Weinberg's sum rules. However, the first two lines give the additional requirement $F_A^2 = 0$. In this model it is not possible to incorporate the a_1 meson and satisfy the short distance constraint (21).

First, we take the model with only π and ρ, i.e. we only keep the first two terms of (28) and (29). The one-loop contributions to $\Pi^{\rho\nu\alpha\beta}$ are not finite. They were also not finite for the HLS model of HKS, but the relevant $\delta\Pi^{\rho\nu\alpha\beta}/\delta p_{3\lambda}$ was. However, in the present model, the derivative can be made finite only for $G_V = F_V/2$. With this value of the parameters the result for a_μ is identical to that of the HLS model and suffers as a consequences from the same defects discussed above.

Next we do add the a_1 and require $F_A \neq 0$. After a lot of work we find that $\delta\Pi^{\rho\nu\alpha\beta}/\delta p_{3\lambda}|_{p_3=0}$ is finite only for $G_V = F_V = 0$ and $F_A^2 = -2F_\pi^2$ or, if including a full a_1-loop $F_A^2 = -F_\pi^2$. These solutions are clearly unphysical.

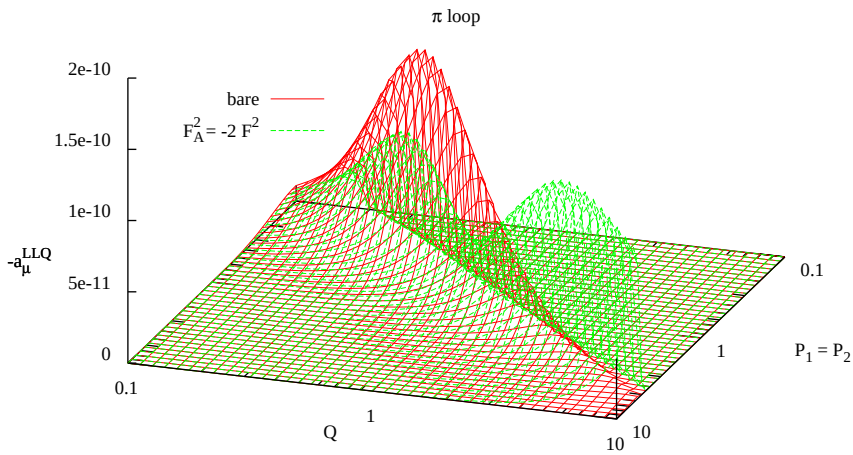

Figure 12: $-a_\mu^{LLQ}$ as defined in (20) as a function of $P_1 = P_2$ and Q with a_1 but no full a_1-loop, $F_A^2 = -2F_\pi^2$ and $F_V = G_V = 0$. The bare pion loop is shown for comparison.

We then add all $\rho a_1 \pi$ vertices given by

$$\begin{aligned}
&\lambda_1 \langle [V^{\mu\nu}, A_{\mu\nu}]\, \chi_- \rangle + \lambda_2 \langle [V^{\mu\nu}, A_{\nu\alpha}]\, h_\mu{}^\nu \rangle \\
&+ \lambda_3 \langle i\, [\nabla^\mu V_{\mu\nu}, A_{\nu\alpha}]\, u_\alpha \rangle + \lambda_4 \langle i\, [\nabla_\alpha V_{\mu\nu}, A_{\alpha\nu}]\, u^\mu \rangle \\
&+ \lambda_5 \langle i\, [\nabla^\alpha V_{\mu\nu}, A_{\mu\nu}]\, u_\alpha \rangle + \lambda_6 \langle i\, [V^{\mu\nu}, A_{\mu\nu}]\, f_-{}^\alpha{}_\nu \rangle \\
&+ \lambda_7 \langle i V_{\mu\nu} A^{\mu\rho} A^\nu{}_\rho \rangle \ . \qquad (31)
\end{aligned}$$

These are not all independent due to the constraints on $V_{\mu\nu}$ and $A_{\mu\nu}$ [49], there are three relations. After a lot of work, we found that no solutions with $\delta\Pi^{\rho\nu\alpha\beta}/\delta p_{3\lambda}|_{p_3=0}$ exists except those already obtained without Λ_i terms. The same conclusions holds if we look at the combination that shows up in the integral over P_1^2, P_2^2, Q^2. We thus find no reasonable model that has a finite prediction for a_μ for the pion-loop including a_1. In the remainder we therefore stick to $\lambda_i = 0$ for the numerical results.

Let us first show the result for one of the finite cases, no a_1 loop, $F_V = G_V = 0$ and $F_A^2 = -2F_\pi^2$. The resulting contribution from the different momentum regimes is shown in Fig. 12 The high-energy behaviour is by definition finite but there is a large bump at rather high energies. The other finite solution, including a full a_1-loop and $F_A = -F_\pi^2, F_V = G_V = 0$ is shown in Fig. 13. Here the funny bump at high energies has disappeared but the behaviour is still unphysical. The high-energy behaviour is good by definition since we enforced a finite a_μ.

We can now look at the cases where $a_\mu^{\pi loop}$ was not finite but that include a good low-energy behaviour. I.e. they have $F_V^2 = F_\pi^2/2$, $F_V G_V = F_\pi^2$, $F_A^2 = F_\pi^2/2$ and $M_A^2 = 2M_V^2$. The resulting model then satisfies the Ward identities and the VMD behaviour of the pion-form factor. For the case with no a_1-loop we obtain $-a_\mu^{LLQ}$ as shown in Fig. 14. The bad

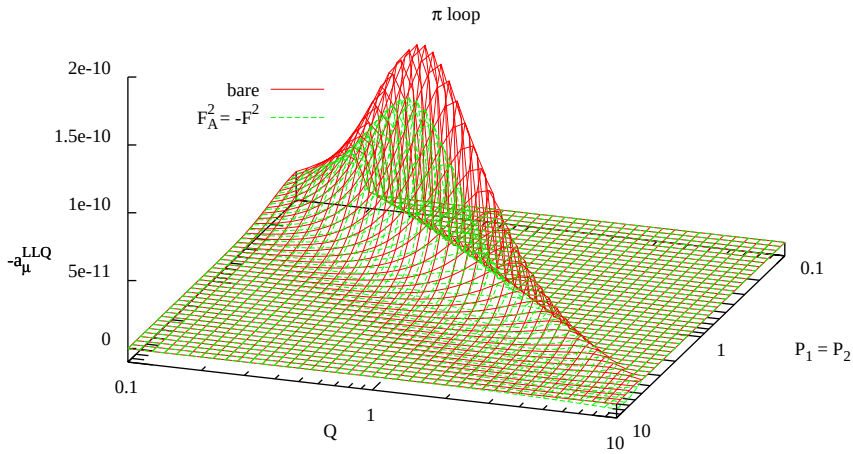

Figure 13: $-a_\mu^{LLQ}$ as defined in (20) as a function of $P_1 = P_2$ and Q with a_1 with a full a_1-loop, $F_A^2 = -F_\pi^2$ and $F_V = G_V = 0$. The bare pion loop is shown for comparison.

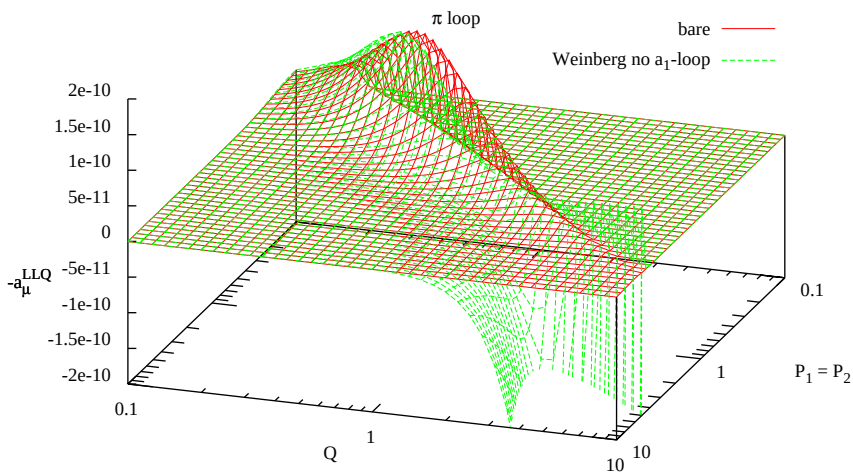

Figure 14: $-a_\mu^{LLQ}$ as defined in (20) as a function of $P_1 = P_2$ and Q with a_1 but no full a_1-loop. Parameters determined by the Weinberg sum rules.

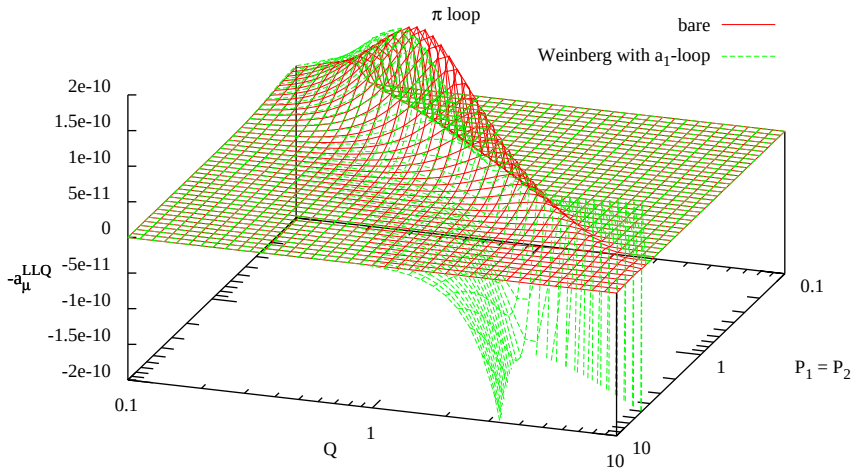

Figure 15: $-a_\mu^{LLQ}$ as defined in (20) as a function of $P_1 = P_2$ and Q with a_1 but no full a_1-loop. Parameters determined by the Weinberg sum rules.

high energy behaviour is clearly visible, but it only starts above 1 GeV. The same input parameters but with a full a_1-loop leads to only small changes in the momentum regime considered as shown in Fig. 15 Again the bad high-energy behaviour is clearly visible.

As a last model, we take the case with $F_A^2 = +F_\pi^2$ and add VMD propagators also in the photons coming from vertices involving a_1. This makes the model satisfy the short-distance constraint (21). The contributions to $a_\mu^{\pi loop}$ are shown in Fig. 16. The same model but now with the full a_1-loop is shown in Fig. 17. Both cases are very similar and here is a good high energy behaviour due to the VMD propagators added. This model cannot be reproduced by the Lagrangians shown above, we need higher order terms to do so. However, the arguments of [18] showing that the full VMD model was gauge invariant also apply to this model.

Now how does the full contribution to $a_\mu^{\pi loop}$ of these various models look like. The integrated contribution up to a maximum Λ for the size of P_1, P_2 and Q is shown in Fig. 18. The models with good high energy behaviour are the ones with a horizontal behaviour towards the right. We see that the HLS is quite similar to the others below about 0.5 GeV but then drops due to the part with the sign as shown in Fig. 7. All physically acceptable models that show a reasonable enhancement over the full VMD result. In fact, all models except HLS end up with a value of $a_\mu = -(2.0 \pm 0.5) \times 10^{-10}$ when integrated up-to a cut-off of order 1-2 GeV. We conclude that that is a reasonable estimate for the pion-loop contribution.

We have not redone the calculation with the model of [36], however their large spread of numbers comes from considering a very broad range of pion polarizabilities and we suspect that the result might contain a large contribution from high energies similarly to the model

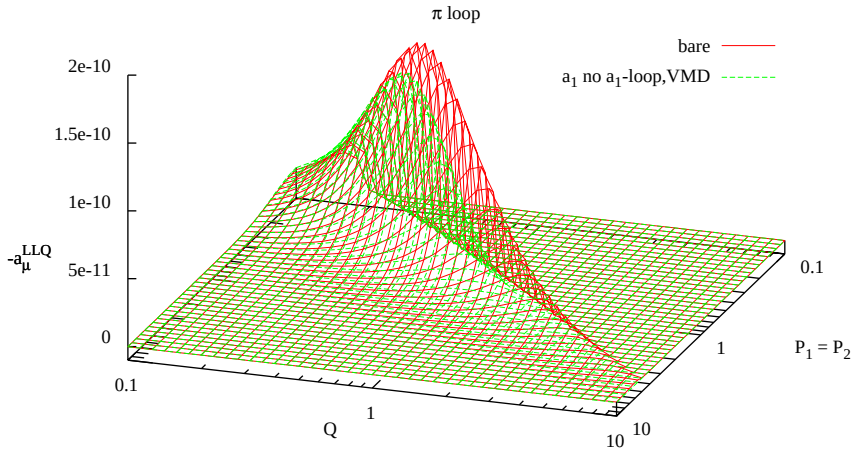

Figure 16: $-a_\mu^{LLQ}$ as defined in (20) as a function of $P_1 = P_2$ and Q with a_1 and $F_A^2 = F_\pi^2$ but no full a_1-loop. A VMD form-factor is added in all photon legs.

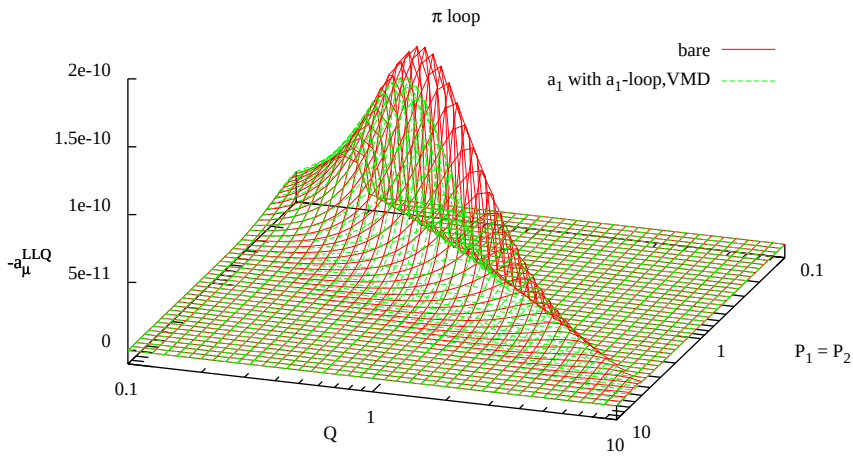

Figure 17: $-a_\mu^{LLQ}$ as defined in (20) as a function of $P_1 = P_2$ and Q with a_1 and $F_A^2 = F_\pi^2$ with a full a_1-loop. A VMD form-factor is added in all photon legs.

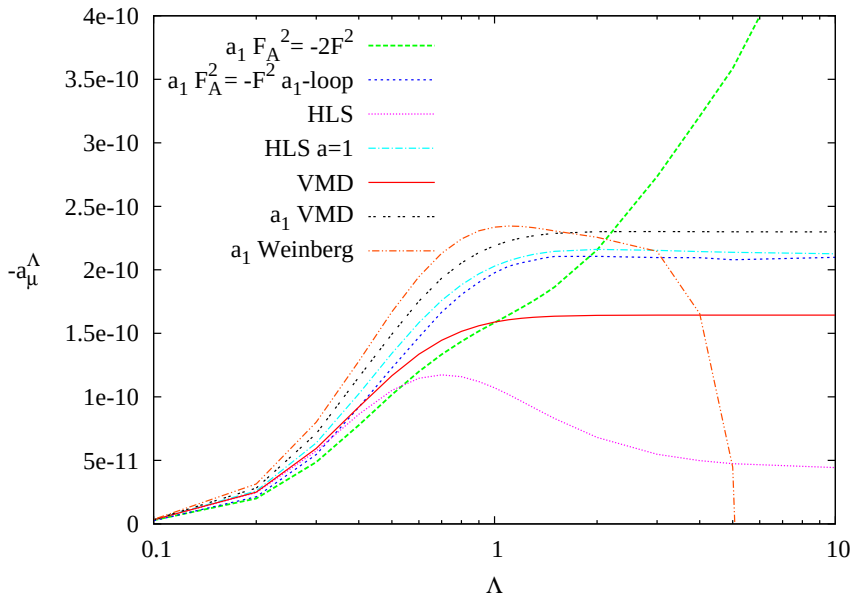

Figure 18: $-a_\mu$ using a variety of models for the pion loop as a function of Λ, the cut-off on the photon momenta. Units for Λ are GeV.

shown in Fig. 12. We therefore feel that their broad range should be discarded.

5 Summary and conclusions

In this paper we have two main results and two smaller ones. The first main result is that we expect large and opposite sign contribution from the disconnected versus the connected parts in lattice calculations of the HLbL contribution to the muon anomalous magnetic moment.

The second main result is that the estimate of the pion-loop is

$$a_\mu^{\pi loop} = -(2.0 \pm 0.5) \cdot 10^{-10} \,. \tag{32}$$

This contains the effects of the pion polarizability as well as estimates of other a_1 effects. The main constraints are that a realistic limit to low-energy ChPT seems to constrain the models enough to provide the result and range given in (32). We have given a number of arguments why the HLS number of [14, 15] should be considered obsolete. In this context we have also derived a short distance constraint on the underlying $\pi\pi\gamma^*\gamma^*$ amplitude.

As a minor result we have given the extension of the Gegenbauer polynomial method of [9, 20] to the most general hadronic vector four-point function.

Acknowledgements

We thank Mehran Zahiri Abyaneh who was involved in the early stages of this work. This work is supported in part by the Swedish Research Council grants contract numbers 621-2013-4287 and 2015-04089 and by the European Research Council (ERC) under the European Union's Horizon 2020 research and innovation programme (grant agreement No 668679).

References

[1] G. W. Bennett *et al.* [Muon g-2 Collaboration], Phys. Rev. Lett. **89** (2002) 101804 [Erratum-ibid. **89** (2002) 129903] [hep-ex/0208001].

[2] G. W. Bennett *et al.* [Muon g-2 Collaboration], Phys. Rev. Lett. **92** (2004) 161802 [hep-ex/0401008].

[3] G. W. Bennett *et al.* [Muon G-2 Collaboration], Phys. Rev. D **73** (2006) 072003 [hep-ex/0602035].

[4] J. Beringer *et al.* [Particle Data Group Collaboration], Phys. Rev. D **86** (2012) 010001.

[5] R. M. Carey, K. R. Lynch, J. P. Miller, B. L. Roberts, W. M. Morse, Y. K. Semertzides, V. P. Druzhinin and B. I. Khazin *et al.*, FERMILAB-PROPOSAL-0989.

[6] H. Iinuma [J-PARC New g-2/EDM experiment Collaboration], J. Phys. Conf. Ser. **295** (2011) 012032.

[7] M. Knecht, Lect. Notes Phys. **629** (2004) 37 [hep-ph/0307239].

[8] J. P. Miller, E. de Rafael and B. L. Roberts, Rept. Prog. Phys. **70** (2007) 795 [hep-ph/0703049].

[9] F. Jegerlehner and A. Nyffeler, Phys. Rept. **477** (2009) 1 [arXiv:0902.3360 [hep-ph]].

[10] M. Benayoun *et al.*, arXiv:1407.4021 [hep-ph].

[11] G. D'Ambrosio, M. Iacovacci, M. Passera, G. Venanzoni, P. Massarotti and S. Mastroianni, EPJ Web Conf. **118** (2016).

[12] T. Kinoshita, B. Nizic and Y. Okamoto, Phys. Rev. D **31** (1985) 2108.

[13] E. de Rafael, Phys. Lett. B **322** (1994) 239 [hep-ph/9311316].

[14] M. Hayakawa, T. Kinoshita and A. I. Sanda, Phys. Rev. Lett. **75** (1995) 790 [hep-ph/9503463].

[15] M. Hayakawa, T. Kinoshita and A. I. Sanda, Phys. Rev. D **54** (1996) 3137 [hep-ph/9601310].

[16] M. Hayakawa and T. Kinoshita, Phys. Rev. D **57** (1998) 465 [hep-ph/9708227] [Erratum-ibid. D **66** (2002) 019902, [hep-ph/0112102]].

[17] J. Bijnens, E. Pallante and J. Prades, Phys. Rev. Lett. **75** (1995) 1447 [Erratum-ibid. **75** (1995) 3781] [hep-ph/9505251].

[18] J. Bijnens, E. Pallante and J. Prades, Nucl. Phys. B **474** (1996) 379 [hep-ph/9511388].

[19] J. Bijnens, E. Pallante and J. Prades, Nucl. Phys. B **626** (2002) 410 [hep-ph/0112255].

[20] M. Knecht and A. Nyffeler, Phys. Rev. D **65** (2002) 073034 [hep-ph/0111058].

[21] K. Melnikov and A. Vainshtein, Phys. Rev. D **70** (2004) 113006 [hep-ph/0312226].

[22] J. Bijnens and J. Prades, Mod. Phys. Lett. A **22** (2007) 767 [hep-ph/0702170].

[23] J. Prades, E. de Rafael and A. Vainshtein, (Advanced series on directions in high energy physics. 20) [arXiv:0901.0306 [hep-ph]].

[24] C. S. Fischer, T. Goecke and R. Williams, Eur. Phys. J. A **47** (2011) 28 [arXiv:1009.5297 [hep-ph]].

[25] T. Goecke, C. S. Fischer and R. Williams, Phys. Rev. D **83** (2011) 094006 [arXiv:1012.3886 [hep-ph]].

[26] T. Goecke, C. S. Fischer and R. Williams, Phys. Rev. D **87** (2013) 034013 [arXiv:1210.1759 [hep-ph]].

[27] G. Eichmann, C. S. Fischer, W. Heupel and R. Williams, AIP Conf. Proc. **1701** (2016) 040004 doi:10.1063/1.4938621 [arXiv:1411.7876 [hep-ph]].

[28] G. Colangelo, M. Hoferichter, M. Procura and P. Stoffer, JHEP **1409** (2014) 091 doi:10.1007/JHEP09(2014)091 [arXiv:1402.7081 [hep-ph]].

[29] G. Colangelo, M. Hoferichter, B. Kubis, M. Procura and P. Stoffer, Phys. Lett. B **738** (2014) 6 doi:10.1016/j.physletb.2014.09.021 [arXiv:1408.2517 [hep-ph]].

[30] G. Colangelo, M. Hoferichter, M. Procura and P. Stoffer, JHEP **1509** (2015) 074 doi:10.1007/JHEP09(2015)074 [arXiv:1506.01386 [hep-ph]].

[31] V. Pauk and M. Vanderhaeghen, Phys. Rev. D **90** (2014) no.11, 113012 doi:10.1103/PhysRevD.90.113012 [arXiv:1409.0819 [hep-ph]].

[32] T. Blum, N. Christ, M. Hayakawa, T. Izubuchi, L. Jin and C. Lehner, Phys. Rev. D **93** (2016) no.1, 014503 doi:10.1103/PhysRevD.93.014503 [arXiv:1510.07100 [hep-lat]].

[33] J. Green, O. Gryniuk, G. von Hippel, H. B. Meyer and V. Pascalutsa, Phys. Rev. Lett. **115** (2015) no.22, 222003 doi:10.1103/PhysRevLett.115.222003 [arXiv:1507.01577 [hep-lat]].

[34] T. Blum *et al*, present by L. Jin at Lattice 2016

[35] K. T. Engel, H. H. Patel and M. J. Ramsey-Musolf, Phys. Rev. D **86** (2012) 037502 doi:10.1103/PhysRevD.86.037502 [arXiv:1201.0809 [hep-ph]].

[36] K. T. Engel and M. J. Ramsey-Musolf, Phys. Lett. B **738** (2014) 123 doi:10.1016/j.physletb.2014.09.006 [arXiv:1309.2225 [hep-ph]].

[37] J. Bijnens and M. Z. Abyaneh, EPJ Web Conf. **37** (2012) 01007 [arXiv:1208.3548 [hep-ph]].

[38] J. Bijnens, EPJ Web Conf. **118** (2016) 01002 doi:10.1051/epjconf/201611801002 [arXiv:1510.05796 [hep-ph]].

[39] M. Z. Abyaneh, "The Anatomy of the Pion Loop Hadronic Light by Light Scattering Contribution to the Muon Magnetic Anomaly," arXiv:1208.2554 [hep-ph], master thesis.

[40] M. Hayakawa, T. Blum, N. H. Christ, T. Izubuchi, L. C. Jin and C. Lehner, PoS LATTICE **2015** (2016) 104 [arXiv:1511.01493 [hep-lat]].

[41] J. Aldins, S. J. Brodsky, A. J. Dufner and T. Kinoshita, , Phys. Rev. D **1** (1970) 2378.

[42] M. Procura, G. Colangelo, M. Hoferichter and P. Stoffer, EPJ Web Conf. **118** (2016) 01030. doi:10.1051/epjconf/201611801030

[43] M. Bando, T. Kugo and K. Yamawaki, Phys. Rept. **164** (1988) 217. doi:10.1016/0370-1573(88)90019-1

[44] J. Bijnens, E. Gamiz, E. Lipartia and J. Prades, JHEP **0304** (2003) 055 [hep-ph/0304222].

[45] C. Adolph *et al.* [COMPASS Collaboration], Phys. Rev. Lett. **114**, 062002 (2015) [arXiv:1405.6377 [hep-ex]].

[46] J. F. Donoghue and B. R. Holstein, Phys. Rev. D **48** (1993) 137 doi:10.1103/PhysRevD.48.137 [hep-ph/9302203].

[47] J. Bijnens and F. Cornet, Nucl. Phys. B **296** (1988) 557. doi:10.1016/0550-3213(88)90032-6

[48] G. Ecker, J. Gasser, A. Pich and E. de Rafael, Nucl. Phys. B **321**, 311 (1989).

[49] S. Leupold, private communication.

Paper III

LU TP 16-50
September 2016

Partially quenched rooted staggered twisted finite volume corrections to K_{l3} decays

Claude Bernard[a], Johan Bijnens[b], Elvira Gámiz[c] and Johan Relefors[b]

[a]Department of Physics, Washington University, St. Louis, Missouri, USA

[b]Department of Astronomy and Theoretical Physics, Lund University, Lund, Sweden

[c]CAFPE and Departamento de Física Teórica y del Cosmos, Universidad de Granada, Granada, Spain

Abstract

The determination of $|V_{us}|$ from kaon semileptonic decays requires the value of the form factor $f_+(q^2 = 0)$ which can be calculated precisely on the lattice. We provide the one-loop partially quenched chiral perturbation theory expressions both with and without including the effects of staggered quarks for all form factors at finite volume and with partially twisted boundary conditions for both the vector current and scalar density matrix elements at all q^2. We point out that at finite volume there are more form factors than just f_+ and f_- for the vector current matrix element but that the Ward identity is fully satisfied. The size of the finite volume corrections at present lattice sizes is small.

We propose the use of partially twisted boundary conditions to determine the size of and test estimates of the finite volume corrections using only a single lattice ensemble.

1 Introduction

The elements of the Cabibbo-Kobayashi-Maskawa (CKM) quark-mixing matrix are fundamental parameters of the Standard Model (SM). The matrix is unitary in the SM. Any deviation from unitarity would be a clear signal for new physics. The first row, containing V_{ud}, V_{us} and V_{ub}, is the one best determined by experiment. For testing the unitarity relation $|V_{ud}|^2 + |V_{us}|^2 + |V_{ub}|^2 = 1$, the precision on $|V_{ud}|$ and $|V_{us}|$ are comparable [1], while $|V_{ub}|$ is negligible at the current level of precision. The determination of $|V_{us}|$ from semileptonic Kaon decays requires $f_+(q^2)$, see e.g. [2], the vector form factor of the K to π transition. The ratio $f_+(q^2)/f_+(0)$ can be extracted from experiment whereas theoretical input is needed for the absolute normalization given by the vector form factor at zero momentum transfer, $f_+(0)$.

The vector form factor is defined via

$$\langle \pi(p_\pi)|V_\mu|K(p_K)\rangle = (p_K + p_\pi)_\mu f_+(q^2) + (p_K - p_\pi)_\mu f_-(q^2) \tag{1}$$

where $q = p_k - p_\pi$ and $V_\mu = \bar{s}\gamma_\mu q$, with q the relevant light quark. The most precise way of calculating $f_+(0)$ at present is with numerical lattice QCD [3, 4, 5, 6, 7, 8]. In lattice QCD calculations, as well as experimentally, it is beneficial to introduce the scalar form factor

$$f_0(q^2) = f_+(q^2) + f_-(q^2)\frac{q^2}{m_K^2 - m_\pi^2} \tag{2}$$

which satisfies

$$f_0(0) = f_+(0). \tag{3}$$

The form factors f_+ and f_0 are less correlated than f_+ and f_- and therefore easier to disentangle experimentally. From a lattice perspective the scalar form factor can be calculated using an insertion of a scalar current instead of a vector current. Using a chiral Ward identity at zero momentum transfer we have

$$f_+(0) = f_0(0) = \frac{m_s - m_q}{m_K^2 - m_\pi^2}\,\langle \pi(p_\pi)|S|K(p_K)\rangle \tag{4}$$

where $S = \bar{s}q$. The scalar form factor is often easier to calculate on the lattice. Moreover, in the staggered formulation the local vector current is not a taste singlet and the added complications typically lead to larger statistical errors [9, 10, 11].

An important part in handling the errors introduced in calculating $f_+(0)$ is the use of chiral perturbation theory (ChPT) and various extensions involving discretization effects, finite volume and boundary conditions. In this paper we calculate the finite volume corrections to the vector and scalar form

factors in rooted staggered partially quenched ChPT with twisted boundary conditions, possibly different for valence and sea quarks. The infinite volume rooted staggered case is included in the calculation in the sense that these can be obtained from our expressions by exchanging finite volume integrals by infinite volume integrals, some of which are zero.

In a previous paper [12] some of us developed a mixed action formalism for staggered quarks. However, since the MILC collaboration has moved to using only the HISQ action no such results are presented here. Some previous work on vector form factors in finite volume is [13, 14, 15].

We point out that at finite volume there are more form factors than the usual f_+ and f_-, which means that care has to be taken while analysing Ward identities. In particular Eq. (4) has corrections at finite volume and twisted boundary conditions. We also point out that the finite volume corrections can be checked using only a single lattice ensemble by varying the twisted boundary conditions.

We have implemented the resulting expressions numerically and they will be made available in the CHIRON package [16]. We have applied the numerical programs to a few ensembles from the MILC collaboration's highly-improved-staggered-quarks (HISQ) ensembles [17] to show expected sizes of the corrections. The main conclusions are that the finite volume corrections are small for present lattices.

This paper is best read together with [12] and is organized as follows: section 2 establishes our conventions and introduces the various versions of ChPT that we use. Section 3 introduces our notation for the kaon semileptonic (K_{l3}) decays and specifies the corrections to Eq. (4) at finite volume. Our analytical expressions for the K_{l3} form factors are presented in section 4 and some numerical examples are given in section 5. Finally, section 6 contains our conclusions. The integral notation used in our results and a few integral identities can be found in the appendices.

2 ChPT and lattice extensions

This section establishes our conventions and describes the lattice effects that we take into account. We start by introducing SU(3) ChPT in the continuum and then give the additional features needed for partially quenched ChPT, rooted staggered ChPT and twisted boundary conditions. The conventions used are the same as in [12].

Continuum infinite volume ChPT describes low energy QCD as an expansion in momenta and masses [18, 19, 20]. It was first used in [21] to study meson form factors. The same Lagrangian can also be used in finite volume [22]. In this paper we perform calculations to next-to-leading order (NLO), or $\mathcal{O}(p^4)$. The Lagrangian up to NLO is

$$\mathcal{L} = \mathcal{L}_2 + \mathcal{L}_4 \tag{5}$$

where $\mathcal{L}_{2n}$ is the $\mathcal{O}(p^{2n})$ Lagrangian.

The effective degrees of freedom in the SU(3) case are the π, K, and η mesons. For the fields we use the exponential representation

$$\Sigma = \exp\left(i\frac{2\phi}{f}\right), \text{ with } \phi = \begin{pmatrix} U & \pi^+ & K^+ \\ \pi^- & D & K^0 \\ K^- & \bar{K}^0 & S \end{pmatrix}, \tag{6}$$

where f is the pion decay constant at LO and U, D and S are flavor neutral mesons with up, down and strange flavor respectively.

The lowest order ChPT Lagrangian with external sources [19, 20] is given by

$$\mathcal{L}_2 = \frac{f^2}{8}\mathrm{Tr}\left(D_\mu\Sigma D_\mu\Sigma^\dagger\right) - \frac{1}{4}\mu f^2\mathrm{Tr}\left(\chi^\dagger\Sigma + \chi\Sigma^\dagger\right) + \frac{m_0^2}{6}\mathrm{Tr}(\phi)^2 \tag{7}$$

where μ is a low energy constant (LEC) and $\chi = s + ip$ contains scalar and pseudo scalar external fields. The covariant derivative is given by

$$D_\mu\Sigma = \partial_\mu\Sigma - il_\mu\Sigma + i\Sigma r_\mu. \tag{8}$$

In order to include quark masses we let $s \to s + \mathrm{diag}(m_u, m_d, m_s)$. The last term in $\mathcal{L}_2$ is essentially an η' mass term allowed by the anomaly. The mass should be taken to infinity in order to integrate out the η'. This may be postponed until the final stage of the calculation [23]. Postponing the limit is useful when discussing lattice effects since there is then a one-to-one relation between indices on ϕ and the quark content of the mesons [24]. When $m_{\eta'} \to \infty$ the trace of ϕ decouples leaving π_0 and η in the diagonal elements of ϕ and the correspondence is lost as standard ChPT is recovered. An expression for $\mathcal{L}_4$ can be found in [19].

2.1 Partially quenched ChPT

In partially quenched QCD the masses of the valence quarks differ from the masses of the sea quarks. In ChPT this can be incorporated using the observation that the indices on the meson matrix ϕ are quark indices before taking the limit $m_{\eta'} \to \infty$. In a given diagram the indices which are determined by the external meson indices correspond to valence quarks and we refer to these indices as valence indices. Indices which are summed over in a given diagram correspond to sea quarks and we refer to these as sea indices. In this way there are sea-sea, sea-valence, valence-sea and valence-valence mesons.

From a technical point of view the partial quenching can be incorporated in ChPT using either the supersymmetric method [25], the replica method [26] or using quark flow. The three methods are equivalent but the quark flow method is more convenient with rooting in the Staggered theory as will

be explained below. For this reason we have used the quark flow method in our calculations.

From a calculational point of view one difference between standard ChPT and partially quenched ChPT is that the flavor neutral propagators have a more complicated structure. The flavor charged propagators have the standard form

$$G^C_{ef} = \frac{1}{p^2 + m^2_{ef}} \tag{9}$$

where e and f indicate the flavor content of the meson. The flavor neutral propagators on the other hand have the form

$$G^N_{EF} = G_{0,EF} + \mathcal{D}_{EF} \tag{10}$$

where

$$\begin{aligned} G_{0,EF} &= \frac{\delta_{EF}}{p^2 + m^2_E}, \\ \mathcal{D}_{EF} &= -\frac{m_0^2}{3(p^2 + m^2_E)(p^2 + m^2_F)} \frac{(p^2 + m^2_U)(p^2 + m^2_D)(p^2 + m^2_S)}{(p^2 + m^2_\pi)(p^2 + m^2_\eta)(p^2 + m^2_{\eta'})} \end{aligned} \tag{11}$$

where $m_{U,D,S}$ are the masses of the neutral sea mesons with quark content u, d, s and $m_{\pi,\eta,\eta'}$ are the masses of the π, η, η' sea mesons. E and F are quark indices of neutral mesons (sea or valence). Note that G^N_{EF} takes the form of a standard propagator plus a term due to the vertex proportional to m_0^2 of the type $\phi_E \phi_F$. We will refer to this type of vertex as a hairpin vertex. Letting $m_{\eta'} = m_0 \to \infty$ [23] gives

$$\mathcal{D}_{EF} = -\frac{1}{3(p^2 + m^2_E)(p^2 + m^2_F)} \frac{(p^2 + m^2_U)(p^2 + m^2_D)(p^2 + m^2_S)}{(p^2 + m^2_\pi)(p^2 + m^2_\eta)}. \tag{12}$$

2.2 Rooted staggered ChPT

We now introduce staggered quarks and rooting in ChPT. In the staggered formulation of lattice QCD each quark is fourfold degenerate. In lattice simulations this is compensated for by taking the fourth root of the quark determinant, the so called fourth root trick. A consequence of the fourfold degeneracy is that the number of mesons is increased 16 fold, giving 16 tastes for each flavor. In staggered ChPT the degeneracy is compensated for by dividing each sum over sea quarks by four, mimicking the fourth-root trick. This is the reason why having a direct correspondence between the indices of ϕ and the quark content of the corresponding meson is so useful when dealing with staggered quarks. Also, note that in the replica method any summed over flavor index is a sea index so that each sum should simply be divided by four.

In order to accommodate the 16 fold increase in the number of mesons in ChPT we use the representation

$$\Sigma = \exp\left(i\frac{\phi}{f}\right), \quad \text{with} \quad \phi = \begin{pmatrix} U & \pi^+ & K^+ & \dots \\ \pi^- & D & K^0 & \dots \\ K^- & \bar{K}^0 & S & \dots \\ \vdots & \vdots & \vdots & \ddots \end{pmatrix}, \tag{13}$$

where the extra space in the matrix ϕ can be used to accommodate partial quenching [26, 25]. Each entry in ϕ is a 4×4 matrix written as

$$\pi^a \equiv \sum_{\Xi=1}^{16} \pi^a_\Xi T_\Xi\,, \quad \text{where} \quad T_\Xi \in \{\xi_5, i\xi_{\mu 5}, i\xi_{\mu\nu}(\mu > \nu), \xi_\mu, I\} \tag{14}$$

are the taste generators, here taken as the Euclidean gamma matrices ξ_μ, with $\xi_{\mu\nu} = \xi_\mu\xi_\nu$, $\xi_{\mu 5} \equiv \xi_\mu\xi_5$ and $\xi_I \equiv I$ is the 4×4 identity matrix. These generate $U(4)$ which is the coset space of a single flavor staggered theory where the trace is not decoupled. The tastes will also be reffered to as P,A,T,V and I. As long as no discretization effects are taken into account all tastes with the same flavor have degenerate masses, this degeneracy is broken by discretization effects.

When including discretization effects we treat p^2, m_q and a^2 as the same order in our power counting. $\mathcal{L}_2$ will then contain corrections of $\mathcal{O}(a^2)$. Although such effects break the 16 fold degeneracy in the meson spectrum, it turns out [27] that at this order in the power counting there is still an $SO(4)$ symmetry, usually referred to as taste symmetry. The subgroup $SO(4)$ is the subgroup where the degeneracy of mass between the tastes P,A,T,V and I is lifted, giving five different masses for each meson flavor.

Using the conventions in Ref. [12], the Lee-Sharpe Lagrangian [27] generalized to multiple flavors [28] is written as

$$\mathcal{L} = \frac{f^2}{8}\mathrm{Tr}\left(D_\mu\Sigma D_\mu\Sigma^\dagger\right) - \frac{1}{4}\mu f^2 \mathrm{Tr}\left(\chi^\dagger\Sigma + \chi\Sigma^\dagger\right) + \frac{m_0^2}{24}\left(\mathrm{Tr}\left(\Phi^2\right)\right) + a^2\mathcal{V}. \tag{15}$$

where $\mathcal{V}$ is the taste violating potential found in [28]. The m_0^2 term is the contribution to the singlet-taste and singlet flavor meson, $\eta'_I \propto \mathrm{Tr}(\phi)$, which is the only mass term allowed by the anomaly. As in the continuum partially quenched case the limit $m_0 \to \infty$ can be taken at the end of the calculation in order to keep a correspondence between the indices of ϕ and the quark content of the mesons.

As in the continuum partially quenched theory the flavor neutral propagators are more complicated than in standard ChPT. In the staggered theory the m_0^2 terms generate hairpin vertices for the singlet taste flavor neutral mesons. There are also hairpin vertices for the axial and vector taste flavor

neutral mesons coming from double trace terms in the staggered Lagrangian. The neutral propagators for taste Ξ are in this case given by

$$G^N_{EF,\Xi} = G_{0,EF,\Xi} + \mathcal{D}^{\Xi}_{EF} \tag{16}$$

where

$$G_{0,EF,\Xi} = \frac{\delta_{EF}}{p^2 + m^2_{A,\Xi}}, \tag{17}$$

$$\mathcal{D}^{\Xi}_{EF} = -a^2 \delta_\Xi \frac{(p^2 + m^2_{U,\Xi})(p^2 + m^2_{D,\Xi})(p^2 + m^2_{S,\Xi})}{(p^2 + m^2_{E,\Xi})(p^2 + m^2_{F,\Xi})(p^2 + m^2_{\pi^0,\Xi})(p^2 + m^2_{\eta,\Xi})(p^2 + m^2_{\eta',\Xi})},$$

where δ_Ξ are the couplings appearing in the Lagrangian for the hairpin vertices, for tastes $\Xi = V, A, I$ respectively. In the limit $m_0 \to \infty$ the singlet taste disconnected flavor-neutral propagator simplifies to

$$\mathcal{D}^{I}_{EF} = -\frac{4}{3} \frac{(p^2 + m^2_{U,I})(p^2 + m^2_{D,I})(p^2 + m^2_{S,I})}{(p^2 + m^2_{A,I})(p^2 + m^2_{B,I})(p^2 + m^2_{\pi^0,I})(p^2 + m^2_{\eta,I})}. \tag{18}$$

The other tastes have no hairpin vertices and hence $\mathcal{D}^{T,P} = 0$.

2.3 Twisted boundary conditions

Twisted boundary conditions [29] in one dimension are defined by

$$\psi(x + L) = \exp(i\theta)\psi(x) \tag{19}$$

where L is the length of the dimension and θ is the twist angle. With twisted boundary conditions momenta are quantized as

$$p = \frac{2\pi}{L} n + \frac{\theta}{L}, \quad n \in \mathrm{Z}. \tag{20}$$

The twist angle can be choosen arbitrarily, so the momentum of the field ψ can be continuously varied. In the case $\theta = 0$, periodic boundary conditions are recovered. The twist of the anti-particle follows from complex conjugation of (19); momenta are shifted in the opposite direction.

Twist angles can be chosen independently in each spatial direction for each flavor and also independently for sea and valence quarks. For each quark q, either valence or sea, we define the twist angle, θ^q_i, in direction i via

$$q(x_i + L) = \exp(i\theta^q_i) q(x_i). \tag{21}$$

We collect the twist angles θ^q_i in a three vector $\vec{\theta}^q$ and in a four vector $\theta^q = (0, \vec{\theta}^q)$. The twist angle for an anti-quark is minus the twist angle for the corresponding quark.

The twist angles of the mesons follow from that of the quarks as [30]

$$\phi_{\bar{q}'q}(x_i + L) = \exp(i(\theta_i^q - \theta_i^{q'}))\phi_{\bar{q}'q}(x_i) \tag{22}$$

where $\phi_{\bar{q}'q}$ is a meson with quark content $\bar{q}'q$. It follows that flavor diagonal mesons have zero twist angle and that charge conjugate mesons have opposite twist. A particle with spatial momentum $\vec{p}$ has an anti-particle with spatial momentum $-\vec{p}$.

When computing loop integrals using twisted boundary conditions in a finite volume we have to make the replacement

$$\int \frac{d^d k}{(2\pi)^d} \to \int_V \frac{d^d k}{(2\pi)^d} \equiv \int \frac{d^{d-3}k}{(2\pi)^{d-3}} \frac{1}{L^3} \sum_{\substack{\vec{n}\in \mathrm{Z}^3 \\ \vec{k}=(2\pi\vec{n}+\vec{\theta})/L}} \tag{23}$$

where we allow for dimensional regularization by using a total of d dimensions. Note that the twisted boundary conditions lead to

$$\int_V \frac{d^d k}{(2\pi)^d} \frac{k_\mu}{k^2 + m^2} \neq 0 \tag{24}$$

since the sum is not symmetric around zero. This leads to momentum dependent masses and fewer constraints on form factors, which reflects the broken lattice symmetry. This also makes checking Ward identities more involved than in the usual case [14].

3 Parametrization of kaon semileptonic decays at finite volume

In this section we present our calculation of the finite volume corrections for the hadronic matrix element in K_{l3} decay. Although we use $K^0 \to \pi^- l^+ \nu$ as an example, our calculations can be used for any $K \to \pi l \nu$ decay. The decay $K^0 \to \pi^- l^+ \nu$ is at the quark level due to the vector current $\bar{s}\gamma_\mu u$. In order to keep the discussion general we follow Ref. [12] and define $\bar{y}$ and $\bar{x}$ to be the valence anti-quarks corresponding to $\bar{s}$ and $\bar{u}$ respectively. We also define x' to be the spectator valence quark corresponding to the d quark. The decay is then that of an $x'\bar{y}$ to an $x'\bar{x}$ pseudo scalar through the vector current $\bar{y}\gamma_\mu x$. We also introduce the notation X, X' and Y for the valance pseudo scalar mesons $x\bar{x}$, $x'\bar{x}'$ and $y\bar{y}$.

We parameterize the matrix element of the weak current between a kaon and a pion in finite volume as

$$\left\langle \pi(p_\pi)|V_\mu^{xy}|K(p_K)\right\rangle_V = f_+^{xy}(q)(p_K + p_\pi)_\mu + f_-^{xy}(q)(p_K - p_\pi)_\mu + h_\mu^{xy}(q), \tag{25}$$

where $q = (p_K - p_\pi)$ and V_μ^{xy} is the appropriate flavor changing vector current. In the various versions of ChPT presented above V_μ^{xy} share the same form given by

$$V_\mu^{xy} = \frac{if^2}{4}\mathrm{Tr}_t\left[\partial_\mu\Sigma\Sigma^\dagger - \Sigma^\dagger\partial_\mu\Sigma\right]_{xy}, \tag{26}$$

where the content of Σ will differ in the different versions and Tr_t is a trace over taste only (which simply gives one in the non-staggered theory). Our conventions are such that $f_+ = 1$ at leading order in ChPT. For zero twist angle the restored cubic symmetry means that the only first two terms are needed so that $h_\mu = 0$ in this case. For non-zero twist angle $h_\mu \neq 0$. Note that the split between different form factors is not unique in this case. For example, changing routings in a diagram will shift terms between f_- and h_μ. Also, the form-factors depend on the individual components of q through the twist angles which enter the integrals, see [14]. Nevertheless, altough the split is in some sense artificial when twisted boundary conditions are imposed, it is useful in order to relate to the infinite volume limit where there are well defined form factors depening only on q^2:

$$\langle\pi(p_\pi)|V_\mu|K(p_K)\rangle = f_+(q^2)(p_K + p_\pi)_\mu + f_-(q^2)(p_K - p_\pi)_\mu. \tag{27}$$

In practice it is advantageous to study the scalar form factor on the lattice and then relate the result to the vector form factor [31, 9]. In ChPT the scalar current is

$$S_{xy} = -\frac{f^2\mu}{4}\mathrm{Tr}_t\left(\Sigma + \Sigma^\dagger\right)_{xy}. \tag{28}$$

We parameterize the matrix element between a kaon and a pion as

$$\langle\pi(p_\pi)|S_{xy}|K(p_K)\rangle_V = \frac{\rho_{xy}(q)}{m_y - m_x}. \tag{29}$$

With these definitions the Ward-Takahashi identity relating the hadronic matrix elements leads to the following relation between the relevant form factors

$$(p_K^2 - p_\pi^2)f_+^{xy} + q^2 f_-^{xy} + q_\mu h_\mu^{xy} = -\rho^{xy}. \tag{30}$$

Note that $p_{K/\pi}^2$ must contain the full loop contribution, to the order at which the Ward identity is being checked, since $f_+ = 1$ at leading order. In all results presented below we have checked that this Ward identity holds.

Finally, setting $q^2 = 0$, which is important for $|V_{us}|$, we have the relation

$$f_+^{xy}(q^2 = 0) = \left.\frac{-\rho^{xy} - q_\mu h_\mu^{xy}}{(p_K^2 - p_\pi^2)}\right|_{q^2=0} \tag{31}$$

where h_μ^{xy} vanishes in the infinite volume limit, allowing for a determination of the vector form factor from the scalar form factor. In lattice calculations the term proportional to $q_\mu h_\mu$ is often dropped [1, 3, 4, 6, 7, 32, 9]. The left hand side of the equation is then not f_+ but a quantity which goes to f_+ in the infinite volume limit.

4 Finite volume corrections to f_+, f_-, h_μ and ρ

In this section we present finite volume corrections to the hadronic matrix elements needed for K_{l3} decays at NLO in ChPT. We present rooted staggered partially quenched ChPT (rSPQChPT) expressions for the partially twisted case (twisted boundary conditions different in the valence and sea sectors), as well as the corresponding continuum limit (PQChPT with partially twisted boundary conditions). The continuum limit can be derived from the staggered results, but we present both for clarity. The finite volume corrections can be used to derive the infinite volume expressions. To do this replace every finite volume integral by its infinite volume counterpart. The expressions are presented using the $\mathcal{D}$ notation of [12] which keep the diagonal propagators intact, see Appendix A. This is to keep the expressions of manageable length.

Taking the full QCD infinite volume and isospin limits of the PQ result produces a slightly different expression from the NLO results in [33]. The difference is of $\mathcal{O}(p^6)$. There is, however, no conflict in using our finite volume result with the infinite volume NLO+NNLO calculation of [33] since there is no overlap between the finite and infinite volume results.

Some complementary results have been moved to the Appendix. In Appendix C you will find expressions for the partially twisted and fully twisted $K^0 \to \pi^-$ form factors in the isospin limit, in which most of the current lattice calculations are performed. In Appendix B you will find expressions for the finite volume correction to the masses in the partially twisted partially quenched and partially twisted partially quenched rooted staggered cases. These are needed to check the Ward identity in Eq. (30).

The results presented below are the finite volume corrections needed for hadronic matrix elements of a vector and a scalar current. For a given quantity, X, the finite volume correction, $\Delta^V X$, is defined as

$$\Delta^V X = X^V - X^\infty \tag{32}$$

where X^V is X calculated in finite volume and X^∞ is X calculated in infinite volume. The way to use the finite volume corrections is to calculate X^V using lattice QCD and correct for finite volume effects using the appropriate expression for $\Delta^V X$ in order to get X^∞ , which is the quantity of interest. The case of h_μ^V is special in that the corresponding infinite volume expression is zero.

The finite volume expressions depend on the volume through the integrals A^V, B^V, etc. These integrals also depend on the masses and twist angles of both valence and sea quarks. In staggered ChPT there are additional low energy constants which enter through the relation between meson masses and quark masses and through hairpin couplings for the diagonal vector and axial propagators.

The quantity c_Ξ which shows up in the rooted staggered expressions is defined as

$$c_\Xi = \frac{1}{4}\mathrm{Tr}(\xi^5\xi^\Xi\xi^5\xi^\Xi). \tag{33}$$

We use the following two momentum variables,

$$\begin{aligned} q &= p_K - p_\pi, \\ p_{12} &= p_K + p_\pi \end{aligned} \tag{34}$$

4.1 Continuum Partially Quenched Partially Twisted ChPT

Below we include the finite volume corrections to the K_{l3} form factors, calculated using PQChPT at $\mathcal{O}(p^4)$, when the inserted current is a vector current (Sec. 4.1.1) and a scalar current (Sec. 4.1.2).

4.1.1 Finite volume corrections for the vector form factors

$$\begin{aligned} \Delta^V f_+^{xy} = -\frac{1}{2f^2}\Bigg(&\sum_{\mathcal{S}} \left(-A^V(m^2_{y\mathcal{S}}) - A^V(m^2_{x\mathcal{S}}) + 4B^V_{22}(m^2_{x\mathcal{S}}, m^2_{\mathcal{S}y})\right) \\ &+4\left(B^V_{22}(m^2_{xy}, \mathcal{D}_{YY}) - 2B^V_{22}(m^2_{xy}, \mathcal{D}_{YX}) + B^V_{22}(m^2_{xy}, \mathcal{D}_{XX})\right) \\ &-A^V(\mathcal{D}_{YY}) + 2A^V(\mathcal{D}_{YX}) - A^V(\mathcal{D}_{XX})\Bigg) \end{aligned} \tag{35}$$

$$\begin{aligned} \Delta^V f_-^{xy} = -\frac{1}{2f^2}\Bigg(&\sum_{\mathcal{S}} \Big(4\left(m^2_{x'y} - m^2_{x'x}\right)\Big(B^V_{21}(m^2_{x\mathcal{S}}, m^2_{\mathcal{S}y}) \\ &\qquad -B^V_1(m^2_{x\mathcal{S}}, m^2_{\mathcal{S}y})\Big) \\ &\qquad + 2q_\mu B^V_{2\mu}(m^2_{x\mathcal{S}}, m^2_{\mathcal{S}y}) + 2p_{12\mu}B^V_{2\mu}(m^2_{x\mathcal{S}}, m^2_{\mathcal{S}y})\Big) \\ &+ 4\left(m^2_{x'y} - m^2_{x'x}\right)\Big(B^V_{21}(m^2_{xy}, \mathcal{D}_{YY}) - 2B^V_{21}(m^2_{xy}, \mathcal{D}_{YX}) \\ &\qquad +B^V_{21}(m^2_{xy}, \mathcal{D}_{XX})\Big) \\ &+4B^V_1(m^2_{xy}, \mathcal{D}_{X'Y})\left(-2m^2_{x'x'} + 3m^2_{x'y} + m^2_{x'x}\right) \\ &+4B^V_1(m^2_{xy}, \mathcal{D}_{X'X})\left(2m^2_{x'x'} - m^2_{x'y} - 3m^2_{x'x}\right) \\ &-4\left(m^2_{x'y} - m^2_{x'x}\right)\left(B^V_1(m^2_{xy}, \mathcal{D}_{YY}) + B^V_1(m^2_{xy}, \mathcal{D}_{XX})\right) \\ &-4q_\mu B^V_{2\mu}(m^2_{xy}, \mathcal{D}_{X'Y}) + 4q_\mu B^V_{2\mu}(m^2_{xy}, \mathcal{D}_{X'X}) \end{aligned} \tag{36}$$

$$
\begin{aligned}
&+2q_\mu B^V_{2\mu}(m^2_{xy},\mathcal{D}_{YY}) - 2q_\mu B^V_{2\mu}(m^2_{xy},\mathcal{D}_{XX}) \\
&+2p_{12\mu} B^V_{2\mu}(m^2_{xy},\mathcal{D}_{YY}) - 4p_{12\mu} B^V_{2\mu}(m^2_{xy},\mathcal{D}_{YX}) \\
&+2p_{12\mu} B^V_{2\mu}(m^2_{xy},\mathcal{D}_{XX}) \\
&+4B^V(m^2_{xy},\mathcal{D}_{X'Y})\left(m^2_{x'x'} - m^2_{x'y} - m^2_{x'x}\right) \\
&+4B^V(m^2_{xy},\mathcal{D}_{X'X})\left(-m^2_{x'x'} + m^2_{x'y} + m^2_{x'x}\right) \Bigg)
\end{aligned}
$$

$$
\begin{aligned}
\Delta^V h^{xy}_\mu = -\frac{1}{2f^2}\Bigg(&\sum_{\mathcal{S}} \Big(-4p_{12\nu} B^V_{23\mu\nu}(m^2_{x\mathcal{S}}, m^2_{\mathcal{S}y}) \\
&\qquad + 2B^V_{2\mu}(m^2_{x\mathcal{S}}, m^2_{\mathcal{S}y})\left(-q^2 - m^2_{x'y} + m^2_{x'x}\right) \\
&\qquad - 4A^V_\mu(m^2_{x'\mathcal{S}}) + 2A^V_\mu(m^2_{y\mathcal{S}}) + 2A^V_\mu(m^2_{x\mathcal{S}})\ \Big) \\
&-4p_{12\nu}(B^V_{23\mu\nu}(m^2_{xy},\mathcal{D}_{YY}) + B^V_{23\mu\nu}(m^2_{xy},\mathcal{D}_{XX})) \\
&+8p_{12\nu} B^V_{23\mu\nu}(m^2_{xy},\mathcal{D}_{YX}) \\
&\quad +4B^V_{2\mu}(m^2_{xy},\mathcal{D}_{X'Y})\left(q^2 - m^2_{x'x'} + 2m^2_{x'y} + m^2_{x'x}\right) \\
&\quad +4B^V_{2\mu}(m^2_{xy},\mathcal{D}_{X'X})\left(-q^2 + m^2_{x'x'} - m^2_{x'y} - 2m^2_{x'x}\right) \\
&\quad +2B^V_{2\mu}(m^2_{xy},\mathcal{D}_{YY})\left(-q^2 - m^2_{x'y} + m^2_{x'x}\right) \\
&\quad +2B^V_{2\mu}(m^2_{xy},\mathcal{D}_{XX})\left(q^2 - m^2_{x'y} + m^2_{x'x}\right) \Bigg)
\end{aligned} \tag{37}
$$

4.1.2 Finite volume corrections for the scalar form factor

$$
\begin{aligned}
\frac{\Delta^V \rho_{xy}}{(m_K^2 - m_\pi^2)} = -\frac{1}{2f^2}\Bigg(&\sum_{\mathcal{S}} \Big(-2\left(m^2_{x'y} - m^2_{x'x}\right) B^V_1(m^2_{x\mathcal{S}}, m^2_{\mathcal{S}y}) \\
&\qquad + 2p_{12\mu} B^{V\mu}_2(m^2_{x\mathcal{S}}, m^2_{\mathcal{S}y}) \\
&\qquad + B^V(m^2_{x\mathcal{S}}, m^2_{\mathcal{S}y})\left(+q^2 + m^2_{x'y} - m^2_{x'x}\right)\Big) \\
&-2\left(m^2_{x'y} - m^2_{x'x}\right)\Big(B^V_1(m^2_{xy},\mathcal{D}_{YY}) \\
&\qquad - B^V_1(m^2_{xy},\mathcal{D}_{XX})\Big) \\
&+2p_{12\mu} B^{V\mu}_2(m^2_{xy},\mathcal{D}_{YY}) - 2p_{12\mu} B^{V\mu}_2(m^2_{xy},\mathcal{D}_{XX}) \\
&-2B^V(m^2_{xy},\mathcal{D}_{X'Y})\left(q^2 + m^2_{x'y} + m^2_{x'x}\right) \\
&-2B^V(m^2_{xy},\mathcal{D}_{X'X})\left(q^2 + m^2_{x'y} + m^2_{x'x}\right) \\
&+B^V(m^2_{xy},\mathcal{D}_{YY})\left(q^2 + m^2_{x'y} - m^2_{x'x}\right) \\
&+2B^V(m^2_{xy},\mathcal{D}_{YX})\left(q^2\right) \\
&+B^V(m^2_{xy},\mathcal{D}_{XX})\left(+q^2 - m^2_{x'y} + m^2_{x'x}\right) \\
&-2A(\mathcal{D}_{X'Y}) - 2A(\mathcal{D}_{X'X})\ \Bigg)
\end{aligned} \tag{38}
$$

4.2 Partially Quenched Partially Twisted Rooted Staggered ChPT

Below we include the finite volume corrections to the K_{l3} form factors, calculated using rSPQChPT at $\mathcal{O}(p^4)$, when the inserted current is a vector current (Sec. 4.2.1) and a scalar current (Sec. 4.2.2).

4.2.1 Finite volume corrections for the vector form factor

$$\begin{aligned}\Delta^V f_+^{xy} = -\frac{1}{2f^2}\sum_{\Xi}\Bigg(&\frac{1}{16}\sum_{\mathcal{S}}\Big(-A^V(m^2_{y\mathcal{S},\Xi}) - A^V(m^2_{x\mathcal{S},\Xi}) + \frac{1}{4}B^V_{22}(m^2_{x\mathcal{S},\Xi}, m^2_{\mathcal{S}y,\Xi})\Big)\\ &+ B^V_{22}(m^2_{xy,\Xi}, \mathcal{D}^{\Xi}_{YY}) - 2B^V_{22}(m^2_{xy,\Xi}, \mathcal{D}^{\Xi}_{YX})\\ &+ B^V_{22}(m^2_{xy,\Xi}, \mathcal{D}^{\Xi}_{XX})\\ &- \frac{1}{4}\left(A^V(\mathcal{D}^{\Xi}_{YY}) - 2A^V(\mathcal{D}^{\Xi}_{YX}) + A^V(\mathcal{D}^{\Xi}_{XX})\right)\Bigg)\end{aligned} \tag{39}$$

$$\begin{aligned}\Delta^V f_-^{xy} = -\frac{1}{2f^2}\sum_{\Xi}\Bigg(&\frac{1}{4}\sum_{\mathcal{S}}\Big(\left(m^2_{x'y,5} - m^2_{x'x,5}\right)\Big(B^V_{21}(m^2_{x\mathcal{S},\Xi}, m^2_{\mathcal{S}y,\Xi})\\ &\qquad - B^V_1(m^2_{x\mathcal{S},\Xi}, m^2_{\mathcal{S}y,\Xi})\Big)\\ &\quad + \frac{q_\mu}{2}B^V_{2\mu}(m^2_{x\mathcal{S},\Xi}, m^2_{\mathcal{S}y,\Xi})\\ &\quad + \frac{p_{12\mu}}{2}\,B^V_{2\mu}(m^2_{x\mathcal{S},\Xi}, m^2_{\mathcal{S}y,\Xi})\Big)\\ &+ \left(m^2_{x'y,5} - m^2_{x'x,5}\right)\Big(B^V_{21}(m^2_{xy,\Xi}, \mathcal{D}^{\Xi}_{YY}) - 2B^V_{21}(m^2_{xy,\Xi}, \mathcal{D}^{\Xi}_{YX})\\ &\qquad + B^V_{21}(m^2_{xy,\Xi}, \mathcal{D}^{\Xi}_{XX})\\ &+ B^V_1(m^2_{xy,\Xi}, \mathcal{D}^{\Xi}_{X'Y})\left(-2m^2_{x'x',5} + m^2_{x'y,5}(2+c_\Xi) + m^2_{x'x,5}c_\Xi\right)\\ &+ B^V_1(m^2_{xy,\Xi}, \mathcal{D}^{\Xi}_{X'X})\left(+2m^2_{x'x',5} - m^2_{x'y,5}c_\Xi - m^2_{x'x,5}(2+c_\Xi)\right)\\ &- \left(m^2_{x'y,5} - m^2_{x'x,5}\right)\left(B^V_1(m^2_{xy,\Xi}, \mathcal{D}^{\Xi}_{YY}) + B^V_1(m^2_{xy,\Xi}, \mathcal{D}^{\Xi}_{XX})\right)\\ &+ c_\Xi q_\mu\left(-B^V_{2\mu}(m^2_{xy,\Xi}, \mathcal{D}^{\Xi}_{X'Y}) + B^V_{2\mu}(m^2_{xy,\Xi}, \mathcal{D}^{\Xi}_{X'X})\right)\\ &+ \frac{1}{2}q_\mu\left(B^V_{2\mu}(m^2_{xy,\Xi}, \mathcal{D}^{\Xi}_{YY}) - B^V_{2\mu}(m^2_{xy,\Xi}, \mathcal{D}^{\Xi}_{XX})\right)\\ &+ \frac{1}{2}p_{12\mu}\Big(B^V_{2\mu}(m^2_{xy,\Xi}, \mathcal{D}^{\Xi}_{YY}) - 2B^V_{2\mu}(m^2_{xy,\Xi}, \mathcal{D}^{\Xi}_{YX})\\ &\qquad + B^V_{2\mu}(m^2_{xy,\Xi}, \mathcal{D}^{\Xi}_{XX})\Big)\\ &+ B^V(m^2_{xy,\Xi}, \mathcal{D}^{\Xi}_{X'Y})\left(m^2_{x'x',5} - m^2_{x'y,5} - m^2_{x'x,5}c_\Xi\right)\\ &+ B^V(m^2_{xy,\Xi}, \mathcal{D}^{\Xi}_{X'X})\left(-m^2_{x'x',5} + m^2_{x'y,5}c_\Xi + m^2_{x'x,5}\right)\Bigg)\end{aligned} \tag{40}$$

$$
\begin{aligned}
\Delta^V h_\mu^{xy} = -\frac{1}{2f^2}\sum_{\Xi}\Bigg(&\frac{1}{4}\sum_{\mathcal{S}}\Big(-p_{12\nu}B^V_{23\mu\nu}(m^2_{x\mathcal{S},\Xi}, m^2_{\mathcal{S}y,\Xi}) \\
&\qquad + \frac{1}{2}B^V_{2\mu}(m^2_{x\mathcal{S},\Xi}, m^2_{\mathcal{S}y,\Xi})\left(-q^2 - m^2_{x'y,5} + m^2_{x'x,5}\right) \\
&\qquad - \frac{1}{2}\left(2A^V_\mu(m^2_{x'\mathcal{S},\Xi}) - A^V_\mu(m^2_{y\mathcal{S},\Xi}) - A^V_\mu(m^2_{x\mathcal{S},\Xi})\right)\Bigg) \\
&-p_{12\nu}\left(B^V_{23\mu\nu}(m^2_{xy,\Xi}, \mathcal{D}^\Xi_{YY}) - 2B^V_{23\mu\nu}(m^2_{xy,\Xi}, \mathcal{D}^\Xi_{YX})\right. \\
&\qquad \left. + B^V_{23\mu\nu}(m^2_{xy,\Xi}, \mathcal{D}^\Xi_{XX})\right) \\
&+B^V_{2\mu}(m^2_{xy,\Xi}, \mathcal{D}^\Xi_{X'Y})\left(-m^2_{x'x',5} + m^2_{x'y,5}(1+c_\Xi) + m^2_{x'x,5}c_\Xi + q^2 c_\Xi\right. \\
&+B^V_{2\mu}(m^2_{xy,\Xi}, \mathcal{D}^\Xi_{X'X})\left(+m^2_{x'x',5} - m^2_{x'y,5}c_\Xi - m^2_{x'x,5}(1+c_\Xi) - q^2 c_\Xi\right. \\
&+\frac{1}{2}B^V_{2\mu}(m^2_{xy,\Xi}, \mathcal{D}^\Xi_{YY})\left(-q^2 - m^2_{x'y,5} + m^2_{x'x,5}\right) \\
&+\frac{1}{2}B^V_{2\mu}(m^2_{xy,\Xi}, \mathcal{D}^\Xi_{XX})\left(+q^2 - m^2_{x'y,5} + m^2_{x'x,5}\right)\Bigg)
\end{aligned}
\tag{41}
$$

4.2.2 Finite volume corrections for the scalar form factor

$$
\begin{aligned}
\frac{\Delta^V \rho_{xy}}{m_K^2 - m_\pi^2} = -\frac{1}{2f^2}\Bigg(&\frac{1}{8}\sum_{\mathcal{S}}\Big(-\left(m^2_{x'y,5} - m^2_{x'x,5}\right)B^V_1(m^2_{x\mathcal{S},\Xi}, m^2_{\mathcal{S}y,\Xi}) \\
&\qquad + p_{12\mu}B^V_{2\mu}(m^2_{x\mathcal{S},\Xi}, m^2_{\mathcal{S}y,\Xi}) \\
&\qquad + \frac{1}{2}B^V(m^2_{x\mathcal{S},\Xi}, m^2_{\mathcal{S}y,\Xi})\left(+q^2 + m^2_{x'y,5} - m^2_{x'x,5}\right)\Big) \\
&+\frac{1}{2}\left(m^2_{x'y,5} - m^2_{x'x,5}\right)\left(-B^V_1(m^2_{xy,\Xi}, \mathcal{D}^\Xi_{YY})\right. \\
&\qquad \left. + B^V_1(m^2_{xy,\Xi}, \mathcal{D}^\Xi_{XX})\right) \\
&+p_{12\mu}\frac{1}{2}\left(B^V_{2\mu}(m^2_{xy,\Xi}, \mathcal{D}^\Xi_{YY}) - B^V_{2\mu}(m^2_{xy,\Xi}, \mathcal{D}^\Xi_{XX})\right) \\
&-\frac{c_\Xi}{2}B^V(m^2_{xy,\Xi}, \mathcal{D}^\Xi_{X'Y})\left(m^2_{x'y,5} + m^2_{x'x,5} + q^2\right) \\
&-\frac{c_\Xi}{2}B^V(m^2_{xy,\Xi}, \mathcal{D}^\Xi_{X'X})\left(m^2_{x'y,5} + m^2_{x'x,5} + q^2\right) \\
&+\frac{1}{4}B^V(m^2_{xy,\Xi}, \mathcal{D}^\Xi_{YY})\left(+q^2 + m^2_{x'y,5} - m^2_{x'x,5}\right) \\
&+\frac{1}{2}B^V(m^2_{xy,\Xi}, \mathcal{D}^\Xi_{YX})q^2 \\
&+\frac{1}{4}B^V(m^2_{xy,\Xi}, \mathcal{D}^\Xi_{XX})\left(+q^2 - m^2_{x'y,5} + m^2_{x'x,5}\right) \\
&-\frac{c_\Xi}{2}\left(A^V(\mathcal{D}^\Xi_{X'Y}) + A^V(\mathcal{D}^\Xi_{X'X})\right)\Bigg)
\end{aligned}
\tag{42}
$$

Table 1: Parameters for the HISQ $N_f = 2+1+1$ MILC ensembles we have used in the numerical results [17]. The numbers not in that reference come from the on-going FNAL/MILC analysis [34]. The light (up,down) valence quark masses are the same as the light sea quark masses on each ensemble, but the strange quark can be different. We have quoted the kaon mass therefore with valence and with sea quarks. Below we refer to the different ensembles using m_π and $m_\pi L$ since these are the most relevant quantities in the finite volume calculation.

a (fm)	m_l/m_s	L (fm)	r_1/a	m_π (MeV)	m_K (MeV)	m_K(sea) (MeV)	$m_\pi L$
0.15	0.035	4.8	2.089	134	505	490	3.2
0.12	0.2	2.9	2.575	309	539	528	4.5
	0.1	2.9	2.5962	220	516	506	3.2
	0.1	3.8	2.5962	220	516	506	4.3
	0.1	4.8	2.5962	220	516	506	5.4
	0.035	5.7	2.608	135	504	493	3.9
0.09	0.2	2.9	3.499	312	539	534	4.5
	0.1	4.2	3.566	222	523	512	4.7
	0.035	5.6	3.565	129	495	495	3.7
0.06	0.2	2.8	5.342	319	547	547	4.5
	0.035	5.5	5.4424	134	491	491	3.7

5 Typical finite volume corrections to current lattice simulations

As an illustration of the numerical size of finite volume corrections in current lattice simulations we present an explicit calculation of these effects for the set of ensembles used by the FNAL/MILC collaboration in its on-going analysis of $K \to \pi\ell\nu$. The formulas in the previous section are of course more general.

The ensemble parameters we use are presented in Tables 1 and 2. They are originally described in [17]. The values of r_1/a were determined in [17] and then used with $r_1 = 0.3117$ fm to convert converted a to fm. The masses were determined in terms of of a and are preliminary results from the ongoing MILC K_{l3} analysis [34]. The values used for the taste splittings come from [17] and are averages over the light-light numbers for the same taste presented there. The hairpin couplings, $a^2\delta_V$ and $a^2\delta_A$ are from an unpublished MILC analysis for the 0.12 fm lattice and have been scaled by $\alpha_s^2 a^2$ for the other cases. Finally, we use $f = 130.41$ MeV.

The numerical evaluations needed will be implemented in CHIRON [16].

Table 2: Taste splittings and hairpin couplings for the HISQ $N_f = 2+1+1$ MILC ensembles we have used in the numerical results. Taste splittings from [17, 35] and the r_1/a in Table 1 and hairpin vertices from an unpublished MILC analysis. The correspondence between ensembles here and in Table 1 is given by the lattice spacing a since the splittings used are the same for all ensembles with a given lattice spacing.

a (fm)	$a^2\delta_V$ GeV^2	$a^2\delta_A$ GeV^2	$a^2\Delta_V$ GeV^2	$a^2\Delta_A$ GeV^2	$a^2\Delta_T$ GeV^2	$a^2\Delta_S$ GeV^2
0.15	0.042256	-0.058008	0.11464	0.041394	0.077496	0.1474
0.12	0.022844	-0.031341	0.062249	0.021744	0.041057	0.08288
0.09	0.0073091	-0.010034	0.019641	0.0072139	0.01334	0.025289
0.06	0.0013934	-0.0019131	0.003647	0.0013226	0.0024848	0.0051299

Next, we have to make a choice on which masses to use. From the pion and kaon masses in Table 1 we fix the lowest order masses[1] for the neutral particles (pseudo-scalar taste for staggered) via

$$\begin{aligned} m_{uu}^2 &= m_{dd}^2 = m_{UU}^2 = m_{DD}^2 = m_\pi^2 \\ m_{ss}^2 &= 2m_K^2 - m_\pi^2 \qquad\qquad m_{SS}^2 = 2m_K^2(\text{sea}) - m_\pi^2 \,. \end{aligned} \tag{43}$$

In the staggered theory we can determine the meson masses at LO in ChPT using the relation

$$m_{ab,\Xi}^2 = \frac{1}{2}\left(m_{aa}^2 + m_{bb}^2\right) + a^2\Delta_\Xi \,. \tag{44}$$

Alternatively we could have determined m_{ss}^2 and m_{SS}^2 from the neutral meson masses obtained from the lattice instead of from the kaon masses. We have checked that these two choices for the meson masses produces differences which are small, much below the expected size of higher orders of about 20%. All results presented here are calculated using the LO SChPT expression in Eq. (44), together with the values for masses and taste splittings in Tables 1 and 2 and Eq. (43).

The finite volume correction to K_{l3} decays is presented in a way that shows the relative size to the LO $f_+(0)^{LO} = 1$. We calculate each term in the Ward identity in Eq. (30) divided by the mass difference,

$$\frac{\Delta^V m_K^2 - \Delta^V m_\pi^2}{m_K^2 - m_\pi^2} + \Delta^V f_+(0) + \frac{q_\mu h_\mu}{m_K^2 - m_\pi^2} = \frac{\Delta^V \rho}{m_K^2 - m_\pi^2}, \tag{45}$$

[1]Corrections are higher order than we have used in ChPT.

Table 3: Values for the different parts in the Ward identity in Eq. (45) for the ensembles in Table 1. "mass", "f_+" and "h_μ" label the three terms in the left-hand side of Eq. (45) and "ρ" the right-hand side. The numbers are obtained with $\theta^u = (0, \theta, \theta, \theta)$ such that $q^2 = 0$ and the kaon at rest for the staggered case.

m_π	$m_\pi L$	"mass"	"f_+"	"h_μ"	"ρ"
134	3.2	0.00000	−0.00042	0.00007	−0.00036
309	4.5	0.00013	−0.00003	−0.00041	−0.00031
220	3.2	0.00054	−0.00048	−0.00084	−0.00077
220	4.3	−0.00007	−0.00009	−0.00005	−0.00021
220	5.4	−0.00005	−0.00003	0.00001	−0.00006
135	3.9	−0.00006	−0.00020	0.00005	−0.00021
312	4.5	0.00047	0.00023	−0.00068	−0.00001
222	4.7	−0.00000	0.00018	−0.00003	0.00014
129	3.7	−0.00013	−0.00004	0.00009	−0.00007
319	4.5	0.00052	0.00037	−0.00081	0.00008
134	3.7	−0.00016	0.00045	0.00013	0.00043

at $q^2 = 0$ and the results are presented in Tables 3-5. The needed twisting angle is determined by having $q^2 = 0$. While our results are for a fully general twisting, the results presented here are for the case where we only twist the valence up quark. This corresponds to a kaon at rest and a moving pion. We present results for three cases. The rooted staggered case with $\theta^u = (0, \theta, \theta, \theta)$, Table 3, and with $\theta^u = (0, \theta', 0, 0)$, Table 4. θ and θ' are chosen to have $q^2 = 0$. The third case we show is without effects from staggering with $\theta^u = (0, \theta', 0, 0)$, Table 5.

Looking at the tables one effect is very clear, for these lattices the finite volume corrections are all very small and clearly below the 0.2% used as error in the published MILC results [1]. The finite volume effects also decrease with increasing $m_\pi L$ as expected.

A second observation is that the finite volume effects are dependent on the precise way the twisting is done. The predictions for a twisting in all space directions or in one space direction only are quite different as a glance at Tables 3 and 4 shows. This opens up a relatively cheap way to check the rough size of finite volume effects and in particular also our predictions for them by doing the (lattice) calculations with different ways of partial twisting but using the same underlying lattice.

A third observation is that the finite volume correction is typically smaller for the case with staggered effects than for the unstaggered case and the differences can be of the same size as the actual corrections. We believe this is due to the fact that the non-pseudoscalar taste mesons have

Table 4: Values for the different parts in the Ward identity in Eq. (45) for the ensembles in Table 1. "mass", "f_+" and "h_μ" label the three terms in the left-hand side of Eq. (45) and "ρ" the right-hand side. The numbers are obtained with $\theta^u = (0, \theta', 0, 0)$ such that $q^2 = 0$ and the kaon at rest for the staggered case.

m_π	$m_\pi L$	"mass"	"f_+"	"h_μ"	"ρ"
134	3.2	−0.00003	−0.00066	0.00008	−0.00061
309	4.5	−0.00030	−0.00017	−0.00002	−0.00049
220	3.2	−0.00078	−0.00105	0.00036	−0.00148
220	4.3	−0.00033	−0.00034	0.00018	−0.00049
220	5.4	−0.00008	−0.00010	0.00003	−0.00015
135	3.9	−0.00002	−0.00032	0.00001	−0.00033
312	4.5	−0.00019	0.00002	−0.00009	−0.00026
222	4.7	−0.00024	−0.00018	0.00017	−0.00025
129	3.7	−0.00003	−0.00050	−0.00001	−0.00054
319	4.5	−0.00026	0.00013	−0.00012	−0.00025
134	3.7	−0.00005	−0.00058	0.00001	−0.00062

typically larger masses and thus have smaller finite volume effects.

The exponential decrease of the finite volume correction remains true also in this case. As an example we show for one of the lattice parameters the same parts of the Ward identity as shown in the Tables as a function of $m_\pi L$. We have used the parameters of the ensemble with $m_\pi = 129$ MeV and $m_\pi L = 3.7$ and vary m_π while keeping the valence and sea kaon mass fixed. The result is shown in Fig. 5.

6 Conclusions

In this paper we have calculated the finite volume corrections to K_{l3} decays in rooted staggered partially quenched ChPT with twisted boundary conditions allowing for different twists in the valence and sea sector as well. The analytical formulas in section 4 and the appendices are our main results. These formulas can be used to obtain also the corresponding infinite volume expressions. We presented results for the vector as well as scalar form factor and we have checked analytically and numerically that the relevant Ward identity is fulfilled.

Numerically, for representative parameters of current lattice simulations, the corrections are $\mathcal{O}(10^{-3})$, but often much smaller. The magnitude and sign of the corrections vary significantly between ensembles.

We suggested using the different ways include twist as a way to determine

Table 5: Values for the different parts in the Ward identity in Eq. (45) for the ensembles in Table 1. "mass", "f_+" and "h_μ" label the three terms in the left-hand side of Eq. (45) and "ρ" the right-hand side. The numbers are obtained with $\theta^u = (0, \theta', 0, 0)$ such that $q^2 = 0$ and the kaon at rest. This is the case without effects from staggering.

m_π	$m_\pi L$	"mass"	"f_+"	"h_μ"	"ρ"
134	3.2	−0.00049	−0.00124	0.00037	−0.00137
309	4.5	−0.00033	0.00014	−0.00004	0.00022
220	3.2	−0.00113	0.00077	0.00067	0.00031
220	4.3	−0.00062	−0.00011	0.00046	−0.00027
220	5.4	−0.00014	−0.00011	0.00010	−0.00016
135	3.9	0.00004	−0.00045	−0.00008	−0.00049
312	4.5	0.00031	0.00015	−0.00009	−0.00025
222	4.7	−0.00037	−0.00015	0.00027	−0.00025
129	3.7	−0.00000	−0.00066	−0.00005	−0.00071
319	4.5	−0.00031	0.00015	−0.00011	−0.00027
134	3.7	−0.00007	−0.00064	0.00001	−0.00070

and check finite volume corrections using the same underlying configurations as a relatively cheap way to check finite volume effects.

Acknowledgements

This work is supported in part by the Swedish Research Council grants contract numbers 621-2013-4287 and 2015-04089, by the European Research Council (ERC) under the European Union's Horizon 2020 research and innovation programme (grant agreement No 668679), by MINECO under grant number FPA2013-47836-C-1-P, by Junta de Andalucía grants FQM 101 and FQM 6552, and by the U.S. Department of Energy under Grant DE-FG02-91ER-40628.

A Integrals and relations

Our results can be written using slight additions to integrals found elsewhere in the literature. In this section we define the integrals we need and give references to where more detailed treatments can be found.

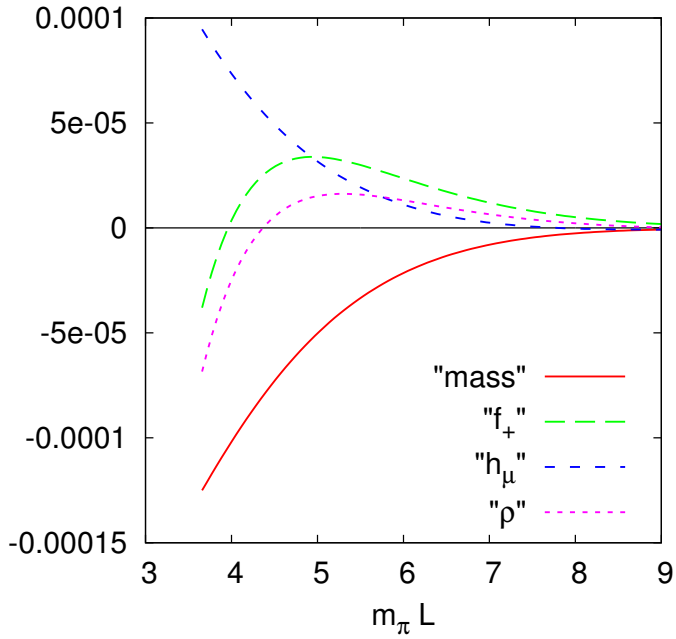

Figure 1: Values for the different parts in the Ward identity in Eq. (45) when varying the pion mass while keeping the kaon mass fixed with the staggered parameters from the ensemble with $m_\pi = 129$ and $m_\pi L = 3.7$ in in Table 1. "mass", "f_+" and "h_μ" label the three terms in the left-hand side of Eq. (45) and "ρ" the right-hand side. The numbers are obtained with $\theta^u = (0, \theta, \theta, \theta)$ such that $q^2 = 0$ and the kaon at rest.

A.1 One loop integrals with single poles

We will use the notation for finite volume integrals given in Eq. (23). Note that every integral below depends on the twist angles since these determine which momenta are sampled in the sum in Eq. (23). We use the mass to indicate which momenta are to be sampled in each integral. For example a momentum k^2 which shows up as $(k^2 + m^2_{\pi^+})$ will only assume the allowed values for a π^+ meson. For this reason $(q-k)^2 \neq (k-q)^2$ since they sample different momenta.

All our results are given in Euclidean space. We need the following integrals

$$\mathcal{A}(m^2) = -\int_V \frac{d^dk}{(2\pi)^d} \frac{1}{(k^2+m^2)} \tag{46}$$
$$\mathcal{A}_\mu(m^2) = -\int_V \frac{d^dk}{(2\pi)^d} \frac{k_\mu}{(k^2+m^2)}$$

$$\mathcal{B}(m_1^2, m_2^2, q) = \int_V \frac{d^d k}{(2\pi)^d} \frac{1}{(k^2+m_1^2)((q-k)^2+m_2^2)}$$
$$\mathcal{B}_\mu(m_1^2, m_2^2, q) = \int_V \frac{d^d k}{(2\pi)^d} \frac{k_\mu}{(k^2+m_1^2)((q-k)^2+m_2^2)}$$
$$\mathcal{B}_{\mu\nu}(m_1^2, m_2^2, q) = \int_V \frac{d^d k}{(2\pi)^d} \frac{k_\mu k_\nu}{(k^2+m_1^2)((q-k)^2+m_2^2)}$$

We split these integrals according to

$$\begin{aligned} \mathcal{B}_\mu(m_1^2, m_2^2, q) &= q_\mu \mathcal{C}_1(m_1^2, m_2^2, q) + \mathcal{C}_{2\mu}(m_1^2, m_2^2, q) \\ \mathcal{B}_{\mu\nu}(m_1^2, m_2^2, q) &= q_\mu q_\nu \mathcal{C}_{21}(m_1^2, m_2^2, q) \\ &\quad - \delta_{\mu\nu}\mathcal{C}_{22}(m_1^2, m_2^2, q) + \mathcal{C}_{23\mu\nu}(m_1^2, m_2^2, q). \end{aligned} \tag{47}$$

where $\mathcal{C}_{2\mu}$ and $\mathcal{C}_{23\mu\nu}$ are zero due to symmetry in the zero twist and infinite volume cases. The sign of $\mathcal{C}_{22}$ is chosen such that the corresponding Minkowski integral has plus signs for all three terms.

In this paper we are primarily interested in the finite volume part of the integrals. We denote the finite volume integrals by

$$\begin{aligned} \mathcal{C}_x &\to B_x^V, \\ \mathcal{A}_x &\to A_x^V \end{aligned} \tag{48}$$

Expressions for these integrals in terms of Jacobi theta functions can be found in [14].

A.2 One loop integrals for diagonal propagator

In partially quenched and staggered ChPT the diagonal propagators are more complicated than in standard ChPT, see sections 2.1 and 2.2. The non-standard part of the propagators takes the generic form

$$\mathcal{D}_{XY} = -\delta \frac{\prod_{i\in U,D,S}(p^2+m_i^2)}{(p^2+m_X^2)(p^2+m_Y^2)\prod_{j\in\pi^0,\eta,\eta'}(p^2+m_j^2)} \tag{49}$$

where δ is the hairpin coupling of the propagating particles. In the staggered theory δ is taste dependent and given by

$$\delta_\Xi = \begin{cases} a^2\delta_V \equiv 16a^2(C_{2V}-C_{5V})/f^2, & \Xi \in \{\xi_\mu\} \text{ (vector taste);} \\ a^2\delta_A \equiv 16a^2(C_{2A}-C_{5A})/f^2, & \Xi \in \{\xi_5\xi_\mu\} \text{ (axial taste);} \\ 4m_0^2/3, & \Xi = I \text{ (singlet taste);} \\ 0, & \text{otherwise.} \end{cases} \tag{50}$$

The coefficients $C_{2V}, \ldots$ are part of the taste breaking potential $\mathcal{V}$ and are defined in [28]. In the partially quenched theory δ is given by

$$\delta = m_0^2/3. \tag{51}$$

Taking the isospin limit for the sea quarks gives the diagonal propagators simplify to

$$\mathcal{D}_{XY} = -\delta \frac{\prod_{i\in U,S}(p^2+m_i^2)}{(p^2+m_X^2)(p^2+m_Y^2)\prod_{j\in\eta,\eta'}(p^2+m_j^2)}. \tag{52}$$

To evaluate integrals with diagonal propagators we use the residue notation described in [28]. Both single and double poles can be evaluated using this technique. Double poles are written as derivatives of single poles. Although this method works well for evaluation, it produces rather messy expressions. For this reason we allow for the replacement of any m^2 in the integrals above by $\mathcal{D}$ as in Ref. [12]. An example would be

$$A^V(\mathcal{D}^A_{XY}) = -\int_V \frac{d^dk}{(2\pi)^d}\left(-a^2\delta_A\right)\times \tag{53}$$
$$\left(\frac{(p^2+m_{U,A})(p^2+m_{D,A})(p^2+m_{S,A})}{(p^2+m_{X,A})(p^2+m_{Y,A})(p^2+m_{\pi^0,A})(p^2+m_{\eta,A})(p^2+m_{\eta',A})}\right).$$

A.3 Integral relations

There are relations among the integrals presented above. The relations valid when including twisted boundary conditions canbe found in [14]. In addition there are some relations which are useful for the neutral propagator given in [28]. Finally, we have used the relation

$$(m_a^2-m_b^2)\mathcal{D}_{ab}+(m_b^2-m_c^2)\mathcal{D}_{bc}+(m_c^2-m_a^2)\mathcal{D}_{ac}=0. \tag{54}$$

All of these relations are needed to get the result in the form presented above and they are necessary to show that the Ward identity is fulfilled.

There is also another class of relations among the integrals. These come from interchanging the masses in $\tilde{B}$ type integrals, which corresponds to changing the routings in the corresponding Feynman diagrams. The interchanges give the following behavior

$$\begin{aligned}
B(m_1^2,m_2^2,q) &= B(m_2^2,m_1^2,q) \\
B_1(m_1^2,m_2^2,q) &= B(m_2^2,m_1^2,q) - B_1(m_2^2,m_1^2,q) \\
B_{2\mu}(m_1^2,m_2^2,q) &= -B_{2\mu}(m_2^2,m_1^2,q) \\
B_{21}(m_1^2,m_2^2,q) &= B(m_2^2,m_1^2,q) - 2B_1(m_2^2,m_1^2,q) + B_{21}(m_2^2,m_1^2,q) \\
B_{22}(m_1^2,m_2^2,q) &= B_{22}(m_2^2,m_1^2,q) \\
B_{23\mu\nu}(m_1^2,m_2^2,q) &= B_{23\mu\nu}(m_2^2,m_1^2,q) \\
&\quad - q_\mu B_{2\nu}(m_2^2,m_1^2,q) - q_\nu B_{2\nu}(m_2^2,m_1^2,q).
\end{aligned} \tag{55}$$

The last of these relations shows that the split between f_- and h_μ is not unique.

All of the relations presented in this section are valid in both finite and infinite volume. In infinite volume some of the integrals are zero.

B Finite volume corrections for masses

In this appendix we give expressions for the finite volume correction for masses in partially twisted partially quenched ChPT and partially twisted partially quenched rooted staggered ChPT. The expressions are valid for a flavor charged meson with flavor content xy and, in the staggered case, pseudoscalar taste. Note that in comparing with [14] we see that the PQ expression neatly summarizes all flavor charged meson results into a single expression, valid both with and without isospin.

B.1 Partially Quenched Partially Twisted ChPT

$$\Delta^V m_{xy}^2 = -\frac{2}{f^2}\left(\sum_{\mathcal{S}} p_\mu \left(A_\mu^V(m_{y\mathcal{S}}^2) - A_\mu^V(m_{x\mathcal{S}}^2)\right) - m_{xy}^2 A^V(\mathcal{D}_{XY})\right) \tag{56}$$

B.2 Partially Quenched Partially Twisted Rooted Staggered ChPT

$$\Delta^V m_{xy,5}^2 = -\frac{1}{2f^2}\sum_{\Xi}\left(\sum_{\mathcal{S}} \frac{p_\mu}{4}\left(A_\mu^V(m_{y\mathcal{S},\Xi}^2) - A_\mu^V(m_{x\mathcal{S},\Xi}^2)\right) - m_{xy,5}^2 A^V(\mathcal{D}_{XY}^{\Xi})c_\Xi\right) \tag{57}$$

C $K^0 \to \pi^-$ isospin limit expressions

In this appendix we present expressions for the process $K^0 \to \pi^-$ with up and down masses set equal, note that isospin is still broken by the boundary conditions. We give expressions for when sea and valence quarks have the same twist, which we call fully twisted, and for the partially twisted case. In the partially twisted case the indices $1, 2, 3$ on the masses indicate valence quarks u, d, s respectively.

C.1 Fully twisted

$$\begin{aligned}\Delta^V f_+ = -\frac{1}{2f^2}\Big(&4B_{22}^V(m_{\pi^+}^2, m_{K^0}^2) + 6B_{22}^V(m_{K^+}^2, m_\eta^2) \\ &+2B_{22}^V(m_{\pi^0}^2, m_{K^+}^2) - A^V(m_{\pi^+}^2) - 2A^V(m_{K^+}^2) \\ &- A^V(m_{K^0}^2) - \frac{3}{2}A^V(m_\eta^2) - \frac{1}{2}A^V(m_{\pi^0}^2)\Big)\end{aligned} \tag{58}$$

$$\Delta^V f_- = -\frac{1}{2f^2}\Bigg((m_K^2 - m_\pi^2)\left(4B_{21}^V(m_{\pi^+}^2, m_{K^0}^2) + 6B_{21}^V(m_{K^+}^2, m_\eta^2)\right. \tag{59}$$
$$\left. + 2B_{21}^V(m_{\pi^0}^2, m_{K^+}^2) - 4B_1^V(m_{\pi^+}^2, m_{K^0}^2)\right)$$
$$-4B_1^V(m_{K^+}^2, m_\eta^2)(2m_K^2 - m_\pi^2)$$
$$-4m_K^2 B_1^V(m_{\pi^0}^2, m_{K^+}^2)$$
$$+2q_\mu B_{2\mu}^V(m_{\pi^+}^2, m_{K^0}^2) + 3q_\mu B_{2\mu}^V(m_{K^+}^2, m_\eta^2)$$
$$+3q_\mu B_{2\mu}^V(m_{\pi^0}^2, m_{K^+}^2) + 2p_{12\mu} B_{2\mu}^V(m_{\pi^+}^2, m_{K^0}^2)$$
$$+3p_{12\mu} B_{2\mu}^V(m_{K^+}^2, m_\eta^2) + 3p_{12\mu} B_{2\mu}^V(m_{\pi^0}^2, m_{K^+}^2)$$
$$+2m_K^2 B^V(m_{K^+}^2, m_\eta^2) + 2m_\pi^2 B^V(m_{\pi^0}^2, m_{K^+}^2)\Bigg)$$

$$\Delta^V h_\mu = -\frac{1}{2f^2}\Bigg(-4p_{12\nu} B_{23\mu\nu}^V(m_{\pi^+}^2, m_{K^0}^2) - 6p_{12\nu} B_{23\mu\nu}^V(m_{K^+}^2, m_\eta^2) \tag{60}$$
$$-4p_{12\nu} B_{23\mu\nu}^V(m_{\pi^0}^2, m_{K^+}^2) + 2p_{12\nu} B_{23\mu\nu}^V(m_{K^+}^2, m_{\pi^0}^2)$$
$$+2B_{2\mu}^V(m_{\pi^+}^2, m_{K^0}^2)(-q^2 + m_\pi^2 - m_K^2)$$
$$+B_{2\mu}^V(m_{K^+}^2, m_\eta^2)(-3q^2 + m_\pi^2 - 5m_K^2)$$
$$+B_{2\mu}^V(m_{\pi^0}^2, m_{K^+}^2)(-3q^2 + m_\pi^2 - 5m_K^2)$$
$$+6\left(A_\mu^V(m_{\pi^+}^2) - A_\mu^V(m_{K^0}^2)\right)\Bigg)$$

$$\frac{\Delta^V \rho_{xy}}{m_K^2 - m_\pi^2} = -\frac{1}{2f^2}\Bigg(-\left(m_K^2 - m_\pi^2\right)\left(2B_1^V(m_{\pi^+}^2, m_{K^0}^2)\right. \tag{61}$$
$$\left. +B_1^V(m_{K^+}^2, m_\eta^2) + B_1^V(m_{\pi^0}^2, m_{K^+}^2)\right)$$
$$+2p_{12\mu} B_{2\mu}^V(m_{\pi^+}^2, m_{K^0}^2)$$
$$+p_{12\mu} B_{2\mu}^V(m_{K^+}^2, m_\eta^2) + p_{12\mu} B_{2\mu}^V(m_{\pi^0}^2, m_{K^+}^2)$$
$$+B^V(m_{\pi^+}^2, m_{K^0}^2)(q^2 - m_\pi^2 + m_K^2)$$
$$+\frac{1}{2}B^V(m_{K^+}^2, m_\eta^2)(+q^2 - \frac{1}{3}m_\pi^2 + \frac{5}{3}m_K^2)$$
$$+2B^V(m_{\pi^0}^2, m_{K^+}^2)(3q^2 + m_\pi^2 + 3m_K^2)$$
$$+\frac{1}{3}A^V(m_\eta^2) + A^V(m_{\pi^0}^2)\Bigg)$$

C.2 Partially twisted

In the partially twisted result there is no difference between sea and valence indices for flavor-neutral mesons. We label these states with m_π, m_η and m_S where $m_S = m_{33}$.

$$\Delta^V f_+ = -\frac{1}{2f^2}\Bigg(\sum_{\mathcal{S}}\left(-A^V(m^2_{1\mathcal{S}}) - A^V(m^2_{3\mathcal{S}}) + 4B^V_{22}(m^2_{1\mathcal{S}}, m^2_{\mathcal{S}3})\right) \tag{62}$$
$$6B^V_{22}(m^2_{13}, m^2_\eta) - 4B^V_{22}(m^2_{13}, m^2_S)$$
$$-2B^V_{22}(m^2_{\pi^0}, m^2_{13})$$
$$+\frac{1}{2}\left(-3A^V(m^2_\eta) + A^V(m^2_{\pi^0}) + 2A^V(m^2_S)\right)\Bigg)$$

$$\Delta^V f_- = -\frac{1}{2f^2}\Bigg(\sum_{\mathcal{S}}\Big(-4(m^2_K - m^2_\pi)\left(B^V_{21}(m^2_{1\mathcal{S}}, m^2_{\mathcal{S}3}) + B^V_1(m^2_{1\mathcal{S}}, m^2_{\mathcal{S}3})\right) \tag{63}$$
$$+2(q_\mu + p_{12\mu})B^V_{2\mu}(m^2_{1\mathcal{S}}, m^2_{\mathcal{S}3})\Big)$$
$$+(m^2_K - m^2_\pi)\left(6B^V_{21}(m^2_{13}, m^2_\eta) - 4B^V_{21}(m^2_{13}, m^2_S)\right.$$
$$\left. - 2B^V_{21}(m^2_{\pi^0}, m^2_{13})\right.$$
$$-4B^V_1(m^2_{13}, m^2_\eta)(2m^2_K - m^2_\pi)$$
$$+4B^V_1(m^2_{13}, m^2_S)(m^2_K - m^2_\pi)$$
$$-4B^V_1(m^2_{\pi^0}, m^2_{13})m^2_\pi$$
$$+3q_\mu B^V_{2\mu}(m^2_{13}, m^2_\eta) - 2q_\mu B^V_{2\mu}(m^2_{13}, m^2_S)$$
$$+3q_\mu B^V_{2\mu}(m^2_{\pi^0}, m^2_{13}) + 3p_{12\mu}B^V_{2\mu}(m^2_{13}, m^2_\eta)$$
$$-2p_{12\mu}B^V_{2\mu}(m^2_{13}, m^2_S)$$
$$+p_{12\mu}B^V_{2\mu}(m^2_{\pi^0}, m^2_{13})$$
$$+2B^V(m^2_{13}, m^2_\eta)m^2_K + 2B^V(m^2_{\pi^0}, m^2_{13})m^2_\pi\Bigg)$$

$$\Delta^V h_\mu = -\frac{1}{2f^2}\Bigg(\sum_{\mathcal{S}}\Big(-4p_{12\nu}B^V_{23\mu\nu}(m^2_{1\mathcal{S}}, m^2_{\mathcal{S}3}) \tag{64}$$
$$+ 2B^V_{2\mu}(m^2_{1\mathcal{S}}, m^2_{\mathcal{S}3})(-q^2 + m^2_\pi - m^2_K)$$
$$+ 2B^V_{2\mu}(m^2_{1\mathcal{S}}, m^2_{\mathcal{S}3})(-q^2 + m^2_\pi - m^2_K)$$
$$+ 2\left(A^V_\mu(m^2_{1\mathcal{S}}) - 2A^V_\mu(m^2_{2i}) + A^V_\mu(m^2_{3i})\right)\Big)$$
$$-6p_{12\nu}B^V_{23\mu\nu}(m^2_{13}, m^2_\eta) + 4p_{12\nu}B^V_{23\mu\nu}(m^2_{13}, m^2_S)$$
$$+2p_{12\nu}B^V_{23\mu\nu}(m^2_{\pi^0}, m^2_{13})$$
$$+B^V_{2\mu}(m^2_{13}, m^2_\eta)(-3q^2 + m^2_\pi - 5m^2_K)$$
$$+2B^V_{2\mu}(m^2_{13}, m^2_S)(+q^2 - m^2_\pi + m^2_K)$$
$$+B^V_{2\mu}(m^2_{\pi^0}, m^2_{13})(-q^2 - 3m^2_\pi - m^2_K)\Bigg)$$

$$
\begin{aligned}
\frac{\Delta^V \rho_{xy}}{m_K^2 - m_\pi^2} = -\frac{1}{2f^2} \Bigg(\sum_{\mathcal{S}} \big(& -\left(m_K^2 - m_\pi^2\right) 2B_1^V(m_{1\mathcal{S}}^2, m_{\mathcal{S}3}^2) \\
& + 2p_{12\mu} B_{2\mu}^V(m_{1\mathcal{S}}^2, m_{\mathcal{S}3}^2) \\
& + B^V(m_{1\mathcal{S}}^2, m_{\mathcal{S}3}^2)(q^2 - m_\pi^2 + m_K^2)\big) \\
& \left(m_K^2 - m_\pi^2\right) \big(-B_1^V(m_{13}^2, m_\eta^2) + B_1^V(m_{13}^2, m_S^2) \\
& + B_1^V(m_{\pi^0}^2, m_{13}^2)\big) \\
& + p_{12\mu} B_{2\mu}^V(m_{13}^2, m_\eta^2) - 2p_{12\mu} B_{2\mu}^V(m_{13}^2, m_{3,3}^2) \\
& - p_{12\mu} B_{2\mu}^V(m_{\pi^0}^2, m_{13}^2) \\
& + \frac{1}{2} B^V(m_{13}^2, m_\eta^2)(q^2 - \frac{1}{3} m_\pi^2 + \frac{1}{3} m_K^2) \\
& + B^V(m_{13}^2, m_{3,3}^2)(-q^2 + m_\pi^2 - m_K^2) \\
& + \frac{1}{2} B^V(m_{\pi^0}^2, m_{13}^2)(q^2 + 3m_\pi^2 + m_K^2) \\
& + \frac{1}{3} A^V(m_\eta^2) + A^V(m_{\pi^0}^2) \Bigg)
\end{aligned}
\tag{65}
$$

References

[1] A. Bazavov *et al.*, Phys. Rev. Lett. **112** (2014) 112001 [arXiv:1312.1228 [hep-ph]].

[2] V. Cirigliano, G. Ecker, H. Neufeld, A. Pich and J. Portoles, Rev. Mod. Phys. **84** (2012) 399 [arXiv:1107.6001 [hep-ph]].

[3] T. Kaneko *et al.* [JLQCD Collaboration], PoS **LATTICE2012** (2012) 111 [arXiv:1211.6180 [hep-lat]].

[4] P. A. Boyle, J. M. Flynn, N. Garron, A. Jüttner, C. T. Sachrajda, K. Sivalingam, and J. M. Zanotti [RBC/UKQCD Collaboration], JHEP **1308** (2013) 132 [arXiv:1305.7217 [hep-lat]].

[5] E. Gámiz *et al.* [Fermilab Lattice and MILC Collaborations], PoS **LATTICE2013** (2013) 395 [arXiv:1311.7264 [hep-lat]].

[6] P. A. Boyle *et al.* [RBC/UKQCD Collaboration], JHEP **1506** (2015) 164 [arXiv:1504.01692 [hep-lat]].

[7] N. Carrasco, P. Lami, V. Lubicz, L. Riggio, S. Simula and C. Tarantino, Phys. Rev. D **93** (2016) 114512 [arXiv:1602.04113 [hep-lat]].

[8] S. Aoki *et al.*, arXiv:1607.00299 [hep-lat].

[9] A. Bazavov *et al.*, Phys. Rev. D **87** (2013) 073012 [arXiv:1212.4993 [hep-lat]].

[10] H. Na, C. T. H. Davies, E. Follana, P. Lepage and J. Shigemitsu, PoS LAT **2009** (2009) 247 [arXiv:0910.3919 [hep-lat]].

[11] J. Koponen *et al.* [HPQCD Collaboration], arXiv:1208.6242 [hep-lat].

[12] C. Bernard, J. Bijnens and E. Gámiz, Phys. Rev. D **89** (2014) 054510 [arXiv:1311.7511 [hep-lat]].

[13] K. Ghorbani, Chin. J. Phys. **51** (2013) 920 [arXiv:1112.0729 [hep-ph]].

[14] J. Bijnens and J. Relefors, JHEP **1405** (2014) 015 [arXiv:1402.1385 [hep-lat]].

[15] F.-J. Jiang and B. C. Tiburzi, Phys. Lett. B **645**, 314 (2007) [hep-lat/0610103].

[16] J. Bijnens, Eur. Phys. J. C **75** (2015) 27 [arXiv:1412.0887 [hep-ph]].

[17] A. Bazavov *et al.* [MILC Collaboration], Phys. Rev. D **87** (2013) 054505 [arXiv:1212.4768 [hep-lat]].

[18] S. Weinberg, Physica A **96** (1979) 327.

[19] J. Gasser and H. Leutwyler, Annals Phys. **158** (1984) 142;

[20] J. Gasser and H. Leutwyler, Nucl. Phys. B **250** (1985) 465.

[21] J. Gasser and H. Leutwyler, Nucl. Phys. B **250** (1985) 517.

[22] J. Gasser and H. Leutwyler, Nucl. Phys. B **307** (1988) 763.

[23] S. R. Sharpe and N. Shoresh, Phys. Rev. D **64** (2001) 114510 [hep-lat/0108003].

[24] S. R. Sharpe, Phys. Rev. D **46** (1992) 3146 [hep-lat/9205020].

[25] C. W. Bernard and M. F. L. Golterman, Phys. Rev. D **49** (1994) 486 [hep-lat/9306005].

[26] P. H. Damgaard and K. Splittorff, Phys. Rev. D **62** (2000) 054509 [hep-lat/0003017].

[27] W. J. Lee and S. R. Sharpe, Phys. Rev. D **60** (1999) 114503 [hep-lat/9905023].

[28] C. Aubin and C. Bernard, Phys. Rev. D **68** (2003) 034014 [hep-lat/0304014]; C. Aubin and C. Bernard, Phys. Rev. D **68** (2003) 074011 [hep-lat/0306026].

[29] P. F. Bedaque, Phys. Lett. B **593** (2004) 82 [arXiv:nucl-th/0402051]

[30] C. T. Sachrajda and G. Villadoro, Phys. Lett. B **609** (2005) 73 [arXiv:hep-lat/0411033].

[31] H. Na, C. T. H. Davies, E. Follana, G. P. Lepage and J. Shigemitsu, Phys. Rev. D **82** (2010) 114506 [arXiv:1008.4562 [hep-lat]].

[32] T. Kaneko *et al.* [JLQCD Collaboration], PoS LATTICE **2015** (2016) 325 [arXiv:1601.07658 [hep-lat]].

[33] J. Bijnens and P. Talavera, Nucl. Phys. B **669** (2003) 341 [hep-ph/0303103].

[34] A. Bazavov *et al.* [Fermilab Lattice and MILC Collaborations], in preparation.

[35] A. Bazavov *et al.* [MILC Collaboration], PoS LATTICE **2011** (2011) 107 [arXiv:1111.4314], and work in progress

Paper IV

LU TP 16-49
September 2016

Connected, Disconnected and Strange Quark Contributions to HVP

Johan Bijnens and Johan Relefors

Department of Astronomy and Theoretical Physics, Lund University,
Sölvegatan 14A, SE 223-62 Lund, Sweden

Abstract

We calculate all neutral vector two-point functions in Chiral Perturbation Theory (ChPT) to two-loop order and use these to estimate the ratio of disconnected to connected contributions as well as contributions involving the strange quark. We extend the ratio of $-1/10$ derived earlier in two flavour ChPT at one-loop order to a large part of the higher order contributions and discuss corrections to it. Our final estimate of the ratio disconnected to connected is negative and a few % in magnitude.

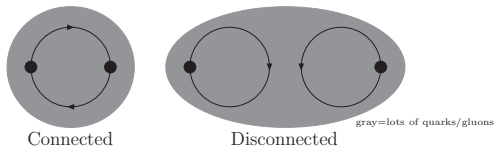

Figure 1: Connected (left) and disconnected (right) diagram for the two point vector function. The lines are valence quark lines in a sea of quarks and gluons.

1 Introduction

The muon anomalous magnetic moment is one of most precisely measured quantities around. The measurement [1] differs from the standard model prediction by about 3 to 4 sigma depending on precisely which theory predictions are taken. A review is [2] and talks on the present situation can be found in [3]. The main part of the theoretical error at present is from the lowest-order hadronic vacuum polarization (HVP). This contribution can be determined from experiment or can be computed using lattice QCD [4]. An overview of the present situation in lattice QCD calculations is given by [5].

The underlying object that needs to be calculated is the two-point function of electromagnetic currents as defined in (1). The contribution to $a_\mu = (g-2)/2$ is given by the integral in (9). There are a number of different contributions to the two-point function of electromagnetic currents that need to be measured on the lattice. First, if we only consider the light up and down quarks, there are connected and disconnected contributions depicted schematically in Fig. 1. If we add the strange quark to the electromagnetic currents then there are contributions with the strange electromagnetic current in both points and the mixed up-down and strange case. In this paper we provide estimates of all contributions at low energies using Chiral Perturbation Theory (ChPT).

The disconnected light quark contribution has been studied at one-loop order in Ref. [6] using partially quenched (PQChPT). They found that the ratio in the subtracted form factors, as defined in (5), is $-1/2$ in the case of valence quarks of a single mass and two degenerate sea quarks. They also found that adding the strange quark did not change the ratio much. Here we give an argument explaining the factor of $-1/2$ and extend their analysis to order p^6. We also present estimates for the contributions from the strange electromagnetic current.

The finite volume, partially quenched and twisted boundary conditions extensions to two loop order will be presented in [7].

In Sect. 2 we give the definitions of the two-point functions and currents we use. Sec. 3 discusses ChPT and the extra terms and low-energy-constants (LECs) needed for a singlet vector current. Our main analytical results, the two-loop order ChPT expressions for all needed vector two-point functions are in Sect. 4. Section 5 uses the observation given in Sect. 3 of the absence of singlet vector couplings to mesons until ChPT order p^6 to show for which contributions the ratio $-1/2$ is valid. Numerical results need an estimate of the

LECs involved, both old and new. This is done in Sect. 6 and applied there to the light connected and disconnected part. Because of the presence of the LECs we find a total disconnected contribution of opposite sign and size a few % of the connected contribution. The same type of estimates are then used for the strange quark contribution in Sect. 7. Here we find a very strong cancellation between p^4 and p^6 contributions, leaving the LEC part dominating strongly. A comparison with a number of lattice results is done in Sect. 8. We find a reasonable agreement in some cases. Our conclusions are summarized in Sect. 9.

2 The vector two point function

We define the two point vector function as

$$\Pi_{ab}^{\mu\nu} = i \int d^4x e^{iq\cdot x} \left\langle T(j_a^\mu(x) j_b^{\nu\dagger}(0)) \right\rangle \tag{1}$$

where the labels a, b specify the involved currents. We label the currents as

$$\begin{aligned}
j_{\pi^+}^\mu &= \bar{d}\gamma^\mu u\,, & j_U^\mu &= \bar{u}\gamma^\mu u\,, & j_D^\mu &= \bar{d}\gamma^\mu d\,, \\
j_S^\mu &= \bar{s}\gamma^\mu s\,, & j_{EM}^\mu &= \frac{2}{3}j_U^\mu - \frac{1}{3}j_D^\mu - \frac{1}{3}j_S^\mu\,, & j_{EM2}^\mu &= \frac{2}{3}j_U^\mu - \frac{1}{3}j_D^\mu\,, \\
j_{\pi^0}^\mu &= \frac{1}{\sqrt{2}}\left(j_U^\mu - j_D^\mu\right)\,, & j_{I2}^\mu &= \frac{1}{\sqrt{2}}\left(j_U^\mu + j_D^\mu\right)\,, & j_{I3}^\mu &= \frac{1}{\sqrt{3}}\left(j_U^\mu + j_D^\mu + j_S^\mu\right)\,.
\end{aligned} \tag{2}$$

The divergence of the vector current is given by

$$\partial_\mu \bar{q}_i \gamma^\mu q_j = i(m_i - m_j)\bar{q}_i q_j\,, \tag{3}$$

which means that any current involving equal mass quark and anti-quark is conserved. Assuming isospin for the π^+ current, Lorentz invariance then implies that we can parametrize the vector two-point functions given above as

$$\Pi_{ab}^{\mu\nu}(q) = (q^\mu q^\nu - q^2 g^{\mu\nu})\Pi_{ab}(q^2). \tag{4}$$

We also define the subtracted quantity

$$\hat{\Pi}_{ab}(q^2) = \Pi_{ab}(q^2) - \Pi_{ab}(0)\,. \tag{5}$$

For simplicity we also use $\Pi_a = \Pi_{aa}$ and $\hat{\Pi}_a = \hat{\Pi}_{aa}$

In this paper we work in the isospin limit. This immediately leads to a number of relations

$$\Pi_{\pi^+} = \Pi_{\pi^0}\,, \qquad \Pi_U = \Pi_D\,, \qquad \Pi_{US} = \Pi_{DS}\,. \tag{6}$$

With those one can derive

$$\begin{aligned}
\Pi_{EM} &= \frac{5}{9}\Pi_U + \frac{1}{9}\Pi_S - \frac{4}{9}\Pi_{UD} - \frac{2}{9}\Pi_{US}\,, \\
\Pi_{EM2} &= \frac{5}{9}\Pi_U - \frac{4}{9}\Pi_{UD}\,.
\end{aligned} \tag{7}$$

The two-point functions Π are themselves not directly observable. However, the vector current two-point function in QCD satisfies a once subtracted dispersion relation

$$\hat{\Pi}(q^2) = \Pi(q^2) - \Pi(0) = q^2 \int_{threshold}^{\infty} ds \frac{1}{s(s-q^2)} \frac{1}{\pi} \mathrm{Im}\Pi(s) \,. \tag{8}$$

The imaginary part can be measured in hadron production if there exists an external vector boson like $W^{\pm}$ or the photon coupling to the current. Thus $\hat{\Pi}(q^2)$ is an observable, but not $\Pi(0)$. $\Pi(0)$ depends on the precise definitions used in regularizing the product of two currents in the same space-time point. The two-point functions for the electromagnetic current can be determined in e^+e^- collisions and Π_{π^+} in τ-decays.

One main use has been the determination of the lowest order HVP part of the muon anomalous magnetic the electromagnetic two-point function[1]

$$\begin{aligned} a_\mu^{LOHVP} &= 4\alpha^2 \int_0^\infty dQ^2 \hat{\Pi}_{EM}(-Q^2) g(Q^2) \,, \\ g(Q^2) &= \frac{-16 m_\mu^4}{Q^6 \left(1 + \sqrt{1 + 4m_\mu^2/Q^2}\right)^4 \sqrt{1 + 4m_\mu^2/Q^2}} \,. \end{aligned} \tag{9}$$

3 Chiral perturbation theory and the singlet current

ChPT describes low-energy QCD as an expansion in masses and momenta [10, 11, 12]. The dynamical degrees of freedom are the pseudo-Goldstone bosons (GB) from the spontaneous breaking of the left- and right-handed flavor symmetry to the vector subgroup, $SU(3)_L \times SU(3)_R \to SU(3)_V$. The GB can be parameterized in the $SU(3)$ matrix

$$U = e^{i\sqrt{2}M/F_0} \quad \text{with} \quad M = \begin{pmatrix} \frac{1}{\sqrt{2}}\pi^0 + \frac{1}{\sqrt{6}}\eta & \pi^+ & K^+ \\ \pi^- & -\frac{1}{\sqrt{2}}\pi^0 + \frac{1}{\sqrt{6}}\eta & K^0 \\ K^- & \bar{K}^0 & -\frac{2}{\sqrt{6}}\eta \end{pmatrix} . \tag{10}$$

or with the 2×2 matrix with only the pions in the case of two-flavours. The Lagrangians, as well as the divergences, are known at order p^2 (LO), p^4 (NLO) and p^6(NNLO) in the ChPT counting [11, 12, 13, 14]. However, the vector currents defined in Sect. 2 contain also a singlet component and the Lagrangians including only this extension are not known. There is work when extending the symmetry to including the singlet GB as well as singlet vector and axial-vector currents at p^4 [15] and p^6 [16]. However this contains very many more terms than we need. If we only add the singlet vector current, in addition to simply extending the external vector field to include the singlet part, there are two extra terms relevant at order p^4:

$$H_3 \left(\langle F_{L\mu\nu} \rangle \langle F_L^{\mu\nu} \rangle + \langle F_{R\mu\nu} \rangle \langle F_R^{\mu\nu} \rangle \right) + H_4 \langle F_{R\mu\nu} \rangle \langle F_L^{\mu\nu} \rangle \,. \tag{11}$$

[1]The version mentioned here comes from [4] but the result essentially goes back to [8, 9]

Since we are only interested in two-point functions of vector currents these will always appear in the combination $2H_3 + H_4$. For the two-flavour case we get $H_3 \to h_4$ and $H_4 \to h_5$ but otherwise similar terms.

It should be noted that none of the terms in the extended p^4 Lagrangian contains couplings of the singlet vector-field to the GB. The singlet appearing in commutators vanishes and the terms involving field strengths vanish, except for the combinations above which do not contain GB fields.

At order p^6 there are many more terms, there are terms appearing that contain interactions of the singlet vector field with the GBs. Two examples are

$$\left\langle F_{R\mu\nu}\chi F_L^{\mu\nu}U^\dagger\right\rangle + \left\langle F_{L\mu\nu}\chi^\dagger F_R^{\mu\nu}U\right\rangle\,, \qquad \left\langle F_{L\mu\nu}+F_{R\mu\nu}\right\rangle\left\langle\left(\chi U^\dagger + U\chi^\dagger\right)D^\mu U D^\nu U^\dagger\right\rangle\,. \tag{12}$$

The extra terms that contribute to the vector two-point function at order p^6 always contain two field strengths and the extra p^2 needed can come from either two derivatives or quark masses. Setting all GB fields to zero, the only possible extra terms have a structure with $F_{V\mu\nu}$ the vector-field field strength and $\bar{\chi}$ the quark mass part of χ. This leads to the possible terms

$$D_1\left\langle F_{V\mu\nu}\right\rangle\left\langle F_V^{\mu\nu}\bar{\chi}\right\rangle + D_2\left\langle F_{V\mu\nu}\right\rangle\left\langle F_V^{\mu\nu}\right\rangle\left\langle\bar{\chi}\right\rangle + D_3\left\langle\partial_\rho F_{V\mu\nu}\right\rangle\left\langle\partial^\rho F_V^{\mu\nu}\right\rangle \tag{13}$$

The D_i are linear combinations of a number of LECs in the Lagrangian and one can check that they are all independent by writing down a few fully chiral invariant terms. A similar set with $D_i \to d_i$ exists for the two-flavour case.

There is a coupling of the singlet vector current to the GBs already at order p^4 via the WZW term. However, due to the presence of $\epsilon^{\mu\nu\alpha\beta}$ we need an even number of insertions of the WZW term or higher order terms from the odd-intrinsic-parity sector to get a contribution to the vector two-point functions.

4 ChPT results up to two-loop order

The vector two-point functions for neutral non-singlet currents were calculated in [17, 18]. We have reproduced their results and added the parts coming from the singlet currents.

The expressions for the two-point functions are most simply expressed in terms of the function

$$\mathcal{G}(m^2,q^2) \equiv \frac{1}{q^2}\left(\overline{B}_{22}(m^2,m^2,q^2) - \frac{1}{2}\overline{A}(m^2)\right) \tag{14}$$

The one-loop integrals here are defined in many places, see e.g. [18]. The explicit expression is

$$\begin{aligned}\mathcal{G}(m^2,q^2) &= \frac{1}{16\pi^2}\left[\frac{1}{36}+\frac{1}{12}\log\frac{m^2}{\mu^2}+\frac{q^2-4m^2}{12}\int_0^1 dx\log\left(1-x(1-x)\frac{q^2}{m^2}\right)\right]\\ &= \frac{1}{16\pi^2}\left(\frac{1}{12}+\frac{1}{12}\log\frac{m^2}{\mu^2}-\frac{q^2}{12m^2}-\frac{q^4}{1680m^4}+\cdots\right)\end{aligned} \tag{15}$$

We also need

$$\overline{A}(m^2) = -\frac{m^2}{16\pi^2}\log\frac{m^2}{\mu^2}\,. \tag{16}$$

μ is the ChPT subtraction scale. We always work in the isospin limit. The expressions we give are in the three flavour case with physical masses. We will quote the corresponding results with lowest order masses in [7].

The two-point functions only start at p^4. We therefore write the result as

$$\Pi = \Pi^{(4)} + \Pi^{(6)} + \cdots \tag{17}$$

in the chiral expansion. The p^4 results are

$$\begin{aligned}
\Pi^{(4)}_{\pi^+} &= -8\mathcal{G}(m_\pi^2,q^2) - 4\mathcal{G}(m_K^2,q^2) - 4(L_{10}^r + 2H_1^r)\,,\\
\Pi^{(4)}_{U} &= -4\mathcal{G}(m_\pi^2,q^2) - 4\mathcal{G}(m_K^2,q^2) - 4(L_{10}^r + 2H_1^r + 2H_3^r + H_4^r)\,,\\
\Pi^{(4)}_{S} &= -8\mathcal{G}(m_K^2,q^2) - 4(L_{10}^r + 2H_1^r + 2H_3^r + H_4^r)\,,\\
\Pi^{(4)}_{UD} &= 4\mathcal{G}(m_\pi^2,q^2) - 4(2H_3^r + H_4^r)\,,\\
\Pi^{(4)}_{US} &= 4\mathcal{G}(m_K^2,q^2) - 4(2H_3^r + H_4^r)\,,\\
\Pi^{(4)}_{EM} &= -4\mathcal{G}(m_\pi^2,q^2) - 4\mathcal{G}(m_K^2,q^2) - \frac{8}{3}(L_{10}^r + 2H_1^r)\,.
\end{aligned} \tag{18}$$

The obvious relations visible for the $\mathcal{G}$ terms will be discussed in Sect. 5. This result agrees with [6] when the appropriate limits are taken.

The results at p^6 are somewhat longer but still fairly short.

$$\begin{aligned}
F_\pi^2\Pi^{(6)}_{\pi^+} =& 4q^2\left(2\mathcal{G}(m_\pi^2,q^2) + \mathcal{G}(m_K^2,q^2)\right)^2 - 16q^2L_9^r\left(2\mathcal{G}(m_\pi^2,q^2) + \mathcal{G}(m_K^2,q^2)\right)\\
&- 8(L_9^r + L_{10}^r)\left(2\overline{A}(m_\pi^2) + \overline{A}(m_K^2)\right) - 32m_\pi^2C_{61}^r - 32(m_\pi^2 + 2m_K^2)C_{62}^r - 8q^2C_{93}^r\,,\\
F_\pi^2\Pi^{(6)}_{U} =& 8q^2\mathcal{G}(m_\pi^2,q^2)^2 + 8q^2\mathcal{G}(m_\pi^2,q^2)\mathcal{G}(m_K^2,q^2) + 8q^2\mathcal{G}(m_K^2,q^2)^2\\
&- 16q^2L_9^r\left(\mathcal{G}(m_\pi^2,q^2) + \mathcal{G}(m_K^2,q^2)\right) - 8(L_9^r + L_{10}^r)\left(\overline{A}(m_\pi^2) + \overline{A}(m_K^2)\right)\\
&- 32m_\pi^2C_{61}^r - 32(m_\pi^2 + 2m_K^2)C_{62}^r - 8q^2C_{93}^r - 4m_\pi^2D_1^r - 4(m_\pi^2 + 2m_K^2)D_2^r - 4q^2D_3^r\,,\\
F_\pi^2\Pi^{(6)}_{S} =& 24q^2\mathcal{G}(m_K^2,q^2)^2 - 32q^2L_9^r\mathcal{G}(m_K^2,q^2) - 16(L_9^r + L_{10}^r)\overline{A}(m_K^2)\\
&- 32(2m_K^2 - m_\pi^2)C_{61}^r - 32(m_\pi^2 + 2m_K^2)C_{62}^r - 8q^2C_{93}^r\\
&- 4(2m_K^2 - m_\pi^2)D_1^r - 4(m_\pi^2 + 2m_K^2)D_2^r - 4q^2D_3^r\,,\\
F_\pi^2\Pi^{(6)}_{UD} =& -8q^2\mathcal{G}(m_\pi^2,q^2)^2 - 8q^2\mathcal{G}(m_\pi^2,q^2)\mathcal{G}(m_K^2,q^2) + 4q^2\mathcal{G}(m_K^2,q^2)^2\\
&+ 16q^2L_9^r\mathcal{G}(m_\pi^2,q^2) + 8(L_9^r + L_{10}^r)\overline{A}(m_\pi^2) - 4m_\pi^2D_1^r - 4(m_\pi^2 + 2m_K^2)D_2^r - 4q^2D_3^r\,,\\
F_\pi^2\Pi^{(6)}_{US} =& -12q^2\mathcal{G}(m_K^2,q^2)^2 + 16q^2L_9^r\mathcal{G}(m_K^2,q^2) + 8(L_9^r + L_{10}^r)\overline{A}(m_K^2)\\
&- 4m_K^2D_1^r - 4(m_\pi^2 + 2m_K^2)D_2^r - 4q^2D_3^r\,.
\end{aligned} \tag{19}$$

For the two-flavour case the results can be derived from the above. First, only keep the integral terms with m_π^2, second replace L_9 by $-(1/2)l_6^r$, $L_{10}^r + 2H_1^r$ by $-4h_2^r$ and L_{10}^r

by l_5^r. In addition there are also extra counterterms for the singlet current appearing. The results are

$$\begin{aligned}
\Pi_{\pi^+}^{(4)} &= -8\mathcal{G}(m_\pi^2,q^2)+16h_2^r\,,\\
\Pi_{U}^{(4)} &= -4\mathcal{G}(m_\pi^2,q^2)+16h_2^r-4(2h_4^r+h_5^r)\,,\\
\Pi_{UD}^{(4)} &= 4\mathcal{G}(m_\pi^2,q^2)-4(2h_4^r+h_5^r)\,,\\
\Pi_{EM}^{(4)} &= -4\mathcal{G}(m_\pi^2,q^2)+\frac{32}{3}h_2^r-\frac{4}{9}(2h_4^r+h_5^r)\,,\\
F_\pi^2\Pi_{\pi^+}^{(6)} &= 16q^2\mathcal{G}(m_\pi^2,q^2)^2+16q^2l_6^r\mathcal{G}(m_\pi^2,q^2)-8(2l_5^r-l_6^r)\overline{A}(m_\pi^2)-32m_\pi^2c_{34}^r-8q^2c_{56}^r\,,\\
F_\pi^2\Pi_{U}^{(6)} &= 8q^2\mathcal{G}(m_\pi^2,q^2)^2+8q^2l_6^r\mathcal{G}(m_\pi^2,q^2)-4(2l_5^r-l_6^r)\overline{A}(m_\pi^2)\\
&\quad -32m_\pi^2c_{34}^r-8q^2c_{56}^r-4m_\pi^2(d_1^r+2d_2^r)-4q^2d_3^r\,,\\
F_\pi^2\Pi_{UD}^{(6)} &= -8q^2\mathcal{G}(m_\pi^2,q^2)^2-8q^2l_6^r\mathcal{G}(m_\pi^2,q^2)+4(2l_5^r-l_6^r)\overline{A}(m_\pi^2)-4m_\pi^2(d_1^r+2d_2^r)-4q^2d_3^r\,.
\end{aligned} \tag{20}$$

5 Connected versus disconnected contributions

If we look at the flavour content of the two-point functions in the isospin limit, it is clear that Π_{π^+} only contains connected contributions while Π_{UD} only contains disconnected contributions. This is derived by thinking of which quark contractions can contribute as shown in Fig. 1. In the same way Π_U contains both with

$$\Pi_U = \Pi_{\pi^+} + \Pi_{UD}\,. \tag{21}$$

Inspection of all the results in Sect. 4 shows that (21) is satisfied. From (7) we thus obtain

$$\Pi_{EM2} = \frac{5}{9}\Pi_{\pi^+} + \frac{1}{9}\Pi_{UD}\,, \tag{22}$$

and

$$\Pi_{EM} = \frac{5}{9}\Pi_{\pi^+} + \frac{1}{9}\Pi_{UD} - \frac{2}{9}\Pi_{US} + \frac{1}{9}\Pi_{S}\,. \tag{23}$$

Π_{US} is fully disconnected while Π_S has both connected and disconnected parts.

5.1 Two-flavour and isospin arguments

In [6], they found, using NLO two-flavour ChPT in the isospin limit, that

$$\frac{\hat{\Pi}_{EM2}^{Disc}}{\hat{\Pi}_{EM2}^{conn}} = -\frac{1}{10}\,. \tag{24}$$

They also calculated corrections to this ratio due to the inclusion of strange quarks. Their result is in our terms expressed via

$$\frac{\hat{\Pi}_{UD}^{(4)}}{\hat{\Pi}_{\pi^+}^{(4)}} = -\frac{1}{2} \tag{25}$$

which is clearly satisfied for the results shown in (20). Note that $\Pi(0)$, via the part coming from the LECs, does not satisfy a similar relation due to the extra terms possible for the singlet current. Inspection of (20) shows that the loop part at order p^6 also satisfies (25) but due to the part of the LECs, the relation is no longer satisfied even for the subtracted functions $\hat{\Pi}$.

The relation (25) can be derived in more general way. As noted in Sect. 3 the singlet current j^μ_{I2} only couples to GBs at order p^6 or at order p^4 via the WZW term and we need at least two of the latter for the vector two-point function. For those contributions, denoted by a prime, we get

$$\Pi'_{U(U+D)} = \Pi'_U + \Pi'_{UD} = 0\,, \tag{26}$$

which together with (21) immediately leads to (25) but for many more contributions. The ratio of disconnected to connected is $-1/2$ for all loop-diagrams only involving vertices from the lowest-order Lagrangian or from the normal NLO Lagrangian. So the ratio is true for a large part of all higher order loop diagrams and corrections start appearing only in loop diagrams at order p^8 with one insertion from the p^6-Lagrangian or at p^{10} with two insertions of a WZW vertex. The argument includes diagrams with four or more pions.

Using the isospin relations we can derive that

$$\Pi_{UD} = \frac{1}{2}\left(\Pi_{I2} - \Pi_{\pi^0}\right) \tag{27}$$

Looking at (27), one can see that the ratio $(-1/2)$ is exact for all contributions with isospin $I = 1$ and only broken due to $I = 0$ contributions. This can be used as well to estimate the size of the ratio, see below and [19]. A corollary is that two-pion intermediate state contributions obey (25) to all orders.

The contributions to order p^6 for $\hat{\Pi}$ satisfy the relation (26) up to the LEC contributions. Using resonance saturation, the LECs can be estimated from ρ and ω exchange. In the large N_c limit that combination will only contribute to the connected contribution. Since the ρ-ω mass splitting and coupling differences are rather small, we expect that the disconnected contribution from this source will be rather small. This will lower the ratio of disconnected to connected contributions compared to (25).

5.2 Three flavour arguments

It was already noted in [6] that kaon loops violate the relation (25) in NLO three-flavour ChPT and the same is rather visible in the results (18) and (19).

The argument for the singlet current coupling to mesons is just as true in three- as in two-flavour ChPT. However here one needs to use the three-flavour singlet current, j^μ_{I3}, instead. Again denoting with a prime superscript the contributions from loop diagrams involving only lowest order vertices or NLO vertices not from the WZW term, we have (after using isospin) two relations similar to (26)

$$\begin{aligned}\Pi'_{U(U+D+S)} &= \Pi'_U + \Pi'_{UD} + \Pi'_{US} = 0\,,\\ \Pi'_{S(U+D+S)} &= 2\Pi'_{US} + \Pi'_S = 0\,.\end{aligned} \tag{28}$$

Note that in this subsection we talk about the three-flavour ChPT expressions. Inspection of the expressions in (18) and (19) show that the relations (28) are satisfied.

In general we can write using (28)

$$\frac{\Pi'_{UD}}{\Pi'_{\pi^+}} = -\frac{1}{2} - \frac{\Pi'_{US}}{2\Pi'_{\pi^+}} \,. \tag{29}$$

This indicates that corrections to the $-1/2$ are expected to be small due to the strange quark being much heavier than the up and down quarks.

The second relation in (28) allows is a relation involving two-point functions with the strange quark current.

Note that a consequence of (28) in the equal mass limit is

$$m_u = m_d = m_s \implies \frac{\Pi'_{UD}}{\Pi'_{\pi^+}} = -\frac{1}{3} \,. \tag{30}$$

In this case the disconnected contribution to the electromagnetic two-point function vanishes identically since the charge matrix is traceless.

6 Estimate of the ratio of disconnected to connected

In order to estimate the ratio of disconnected to connected contributions in ChPT the inputs that appear must be determined. For the plots shown below we use

$$\begin{array}{lll} F_\pi = 92.2 \text{ MeV} & m_\pi = 135 \text{ MeV} & m_K = 495 \text{ MeV} \\ L_9^r = 0.00593 & L_{10}^r = -\,0.0038 & \mu = 770 \text{ MeV} \end{array} \tag{31}$$

The values for the decay constant and masses are standard ones. The values for the L_i^r were recently reviewed in [20] and we have taken the values for L_9^r [21] and L_{10}^r quoted there.

If we only consider $\hat{\Pi}$, the only other LECs we need are C_{93}^r and D_3^r. As first suggested in [22] LECs are expected to be saturated by resonances. For C_{93}^r and D_3^r the main contribution will be from the vector resonance multiplet. Here a nonet approach typically works well and that would suggest that $D_3^r \approx 0$. We will set it to zero in our estimates. The value for C_{93}^r was first determined using resonance saturation in [18] with a value of

$$C_{93}^r = -1.4\ 10^{-4} \tag{32}$$

If we use resonance saturation for the nonet and the constraints from short-distance as used in [23] we obtain for the two-point function

$$\Pi_{\pi^+}^{\rm VMD}(q^2) = \frac{4F_\pi^2}{m_V^2 - q^2} \,. \tag{33}$$

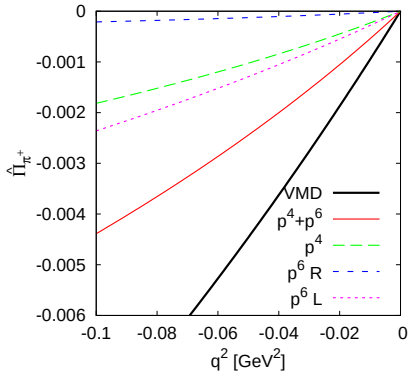

Figure 2: The subtracted two-point function $\hat{\Pi}_{\pi^+}(q^2)$ or the connected part. Plotted are the p^4 contribution of (18) labeled p^4 and the three parts of the higher order contribution: the pure two-loop contribution labeled p^6 R, the p^6 contribution from one-loop graphs labeled p^6 L and the pure LEC contribution as modeled by (33) labeled VMD.

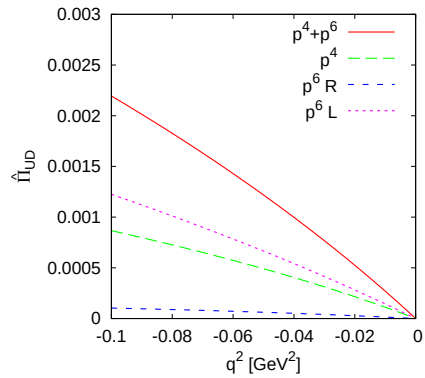

Figure 3: The subtracted two-point function $\hat{\Pi}_{UD}(q^2)$ or the disconnected part. Plotted are the p^4 contribution of (18) labeled p^4 and the two non-zero parts of the higher order contribution: the pure two-loop contribution labeled p^6 R and the p^6 contribution from one-loop graphs labeled p^6 L. The the pure LEC contribution is estimated to be zero here.

Assuming that the pure LEC parts reproduce (33), leads to the value

$$C_{93}^r = -1.02\ 10^{-4} \tag{34}$$

with $m_V = 770$ MeV. Finally fitting the expression for Π_{π^+} to a phenomenological form of the two-point function [24] gives

$$C_{93}^r = -1.33\ 10^{-4} \tag{35}$$

The three values are in reasonable agreement. The size can be compared to other vector meson dominated combinations of LECS, e.g. $C_{88}^r - C_{90}^r = -0.55\ 10^{-4}$ [21], which is of the same magnitude. In the numerical results we will use the full expression (33) for the contribution from higher order LECs rather than just the terms with C_{93}^r.

In Fig. 2 we have plotted the different contributions to $\hat{\Pi}_{\pi^+}$. This is what is usually called the connected contribution. As we see, the contribution from higher order LECs, as modeled by (33), is, as expected, dominant. The full result for $\hat{\Pi}$ is the sum of the VMD and the $p^4 + p^6$ lines. We see that the pure two-loop contribution is small compared to the one-loop contribution but there is a large contribution at order p^6 from the one-loop diagrams involving L_i^r.

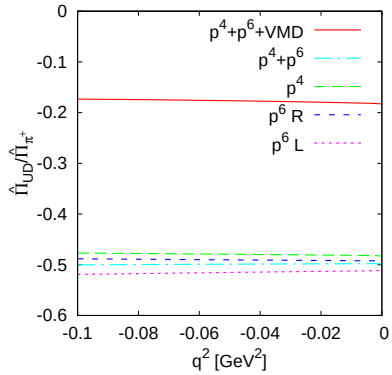

Figure 4: The ratio of the subtracted two-point functions $\hat{\Pi}_{UD}(q^2)/\hat{\Pi}_{\pi^+}(q^2)$ or ratio of the disconnected to the connected part. Plotted are the p^4 contribution of (18) labeled p^4, the parts of the higher order contribution: the pure two-loop contribution labeled p^6 R and the p^6 contribution from one-loop graphs labeled p^6 L as well as their sum. The ratio of the pure LEC contribution is estimated to be zero. The ratio for all contributions summed is the continuous line.

In Fig. 3 we have plotted the same contributions but now for $\hat{\Pi}_{UD}$ or the contribution from disconnected diagrams. Note that the scale is exactly half that of Fig. 2. The contributions are very close to $-1/2$ times those of Fig. 2 except for the pure LEC contribution which is here estimated to be zero.

How well do the estimates of the ratio now hold up. The ratio of disconnected to connected is plotted in Fig. 4. We see that the contribution at order p^4 has a ratio very close to $-1/2$ and the same goes for all loop contributions at order p^6. The effects of kaon loops is thus rather small. The deviation from $-1/2$ is driven by the estimate of the pure LEC contribution. Using the VMD estimate (33) we end up with a ratio of about 0.18 for the range plotted. Taking into account (22) we get an expected ratio for the disconnected to connected contribution to the light quark electromagnetic two-point function $\hat{\Pi}_{EM2}$ of about 3.5%. If we had used the other estimates for C_{93}^r (and assumed a similar ratio for higher orders) the number would have been about 3%.

An analysis using only the pion contributions, so no contribution from intermediate kaon states, would give essentially the same result.

7 Estimate of the strange quark contributions

The numerical results in the previous section included the contribution from kaons but only via the electromagnetic couplings to up and down quarks. In this section we provide

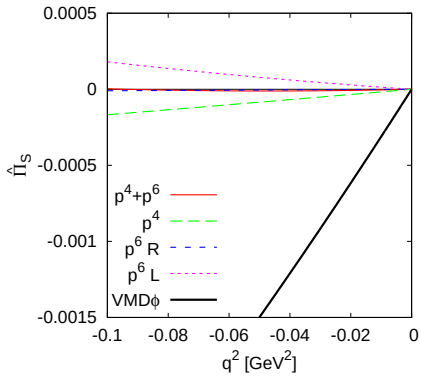

Figure 5: The subtracted two-point function $\hat{\Pi}_S(q^2)$. Plotted are the p^4 contribution of (18) labeled p^4, the parts of the higher order contribution: the pure two-loop contribution labeled p^6 R and the p^6 contribution from one-loop graphs labeled p^6 L as well as their sum. The pure LEC contribution is estimated by (33) with he mass of the ϕ.

an estimate for the contribution when including the photon coupling to strange quarks. I.e. we add the terms coming from Π_{US} and Π_S in (23).

The loop contributions satisfy the relations shown in (28) with corrections starting earliest at p^8. Alternatively we can write the first relation as

$$\Pi'_{\pi^+} + 2\Pi'_{UD} + \Pi'_{US} = 0\,, \tag{36}$$

this, together with the ratios shown in Fig. 4 and the second relation in (28), shows that we can expect the extra contributions to be quite small with the possible exception of the pure LEC contribution.

The pure LEC contribution is estimated to only apply to the connected part and so contributes only to Π_S. Given that the ϕ mass is significantly larger than the ρ-mass we will for that part need to include this difference. A first estimate is simply by using (33) with m_V now the ϕ-mass of $m_\phi = 1020$ MeV. We will call this VMDϕ in the remainder.

The estimate we include for Π_S includes both connected and disconnected contributions. We would need to go to partially quenched ChPT to obtain that split-up generalizing the methods of [6].

Fig. 5 shows the different contributions to $\hat{\Pi}_S$. We did not plot $\hat{\Pi}_{US}$ since the relations (28) imply that the p^4, p^6L and p^6R are exactly $-1/2$ the contributions for $\hat{\Pi}_S$ and in our estimate the pure LEC part for $\hat{\Pi}_{US}$ vanishes. The contributions are much smaller than those of the connected light quark contribution shown in Fig. 2. One remarkable effect is the very strong cancellation between the p^4 and p^6 effects give an almost zero loop contribution.

8 Comparison with lattice and other data

For comparing with lattice and phenomenological data we can use the Taylor expansion around $q^2 = 0$ from our expressions and the same coefficients evaluated from experimental data or via the time moment analysis on the lattice [25].

We expand the functions as

$$\hat{\Pi}(q^2) = \Pi_1 q^2 - \Pi_2 q^4 + \cdots \tag{37}$$

The signs follow from the fact that the lattice expansion is defined in terms of $Q^2 = -q^2$ and the usual lattice convention for Π has the opposite sign of ours. The coefficients, obtained by fitting an eight-order polynomial to the ranges shown in the plots, are given in Table 1.

[26] is from an analysis of experimental data. [27] are preliminary numbers from the BMW collaboration and we have removed the charm quark contribution from their numbers. These numbers are not corrected for finite volume. For [25, 28] we have taken the numbers from their configuration 8, which has physical pion masses and multiplied by 9/5 for the latter to obtain Π_{π^+}. Our estimates are in reasonable agreement for the connected contribution. For the disconnected contribution, our results are higher but of a similar order.

There have been many more studies of the muon $g-2$ on the lattice and in particular a number of studies of the disconnected part. However, their results are often not presented in a form that we can easily compare to. From our numbers above we expect the disconnected contribution to be a few % and of the opposite sign of the connected contribution. [19] finds $-0.15(5)\%$, much smaller than we expect, [29] finds about -1.5% which is below but of the same order as our estimate.

The same comment applies to studies of the strange contribution, e.g. [30] finds a contribution of about 7% of the light connected contribution which is in reasonable agreement with our estimate.

9 Summary and conclusions

We have calculated in two- and three-flavour ChPT all the neutral two-point functions in the isospin limit including the singlet vector current. We have extended the ratio of $-1/2$ (or $-1/10$ for the electromagnetic current) of [6] to a large part of the higher order loop corrections. We used the nonet estimates of LECs to set the new constants for the singlet current equal to zero and then provided numerical estimates for the disconnected and strange quark contributions.

We find that the disconnected contribution is negative and a few % of the connected contribution, the main uncertainty being the new LECs which we estimated to be zero. A similar estimate for the strange quark contribution has a large cancellation between p^4 and p^6 leaving our rather uncertain estimate of the LECs involved as the main contribution.

Reference	Π_A	Π_1 (GeV^{-2})	Π_2 (GeV^{-4})
sum	$\hat{\Pi}_{EM}$	0.0853	−0.204
[26]	Π_{EM}	0.0990(7)	−0.206(2)
[27]	$\hat{\Pi}_{EM}$	0.0972(2)(1)	−0.166(6)(3)
Π^{VMD}	$\hat{\Pi}_{\pi^+}$	0.0967	−0.166
p^4	$\hat{\Pi}_{\pi^+}$	0.0240	−0.086
p^6 R	$\hat{\Pi}_{\pi^+}$	0.0031	−0.014
p^6 L	$\hat{\Pi}_{\pi^+}$	0.0287	−0.066
sum	$\hat{\Pi}_{\pi^+}$	0.153	−0.328
[27]	$\hat{\Pi}_{\pi^+}$	0.1657(16)(18)	−0.297(10)(05)
[28]	Π_{π^+}	0.1460(22)	−0.2228(65)
p^4	$\hat{\Pi}_{UD}$	−0.0116	0.043
p^6 R	$\hat{\Pi}_{UD}$	−0.0015	0.007
p^6 L	$\hat{\Pi}_{UD}$	−0.0147	0.032
sum	$\hat{\Pi}_{UD}$	−0.0278	0.082
[27]	$\hat{\Pi}_{UD}$	−0.015(2)(1)	0.046(10)(04)
$\Pi^{VMD\phi}$	$\hat{\Pi}_S$	0.0314	−0.030
p^4	$\hat{\Pi}_S$	0.0017	−0.001
p^6 R	$\hat{\Pi}_S$	0.0001	0.000
p^6 L	$\hat{\Pi}_S$	−0.0013	−0.005
sum	$\hat{\Pi}_S$	0.0319	−0.035
[27]	$\hat{\Pi}_S$	0.0657(1)(2)	−0.0532(1)(3)
[25]	$\hat{\Pi}_S$	0.06625(74)	−0.0526(11)

Table 1: The Taylor expansion coefficients of $\hat{\Pi}$ of [25, 26, 27, 28] and a comparison with our estimates.

Acknowledgements

This work is supported in part by the Swedish Research Council grants contract numbers 621-2013-4287 and 2015-04089 and by the European Research Council (ERC) under the European Union's Horizon 2020 research and innovation programme (grant agreement No 668679).

References

[1] G. W. Bennett *et al.* [Muon g-2 Collaboration], Phys. Rev. D **73** (2006) 072003 [hep-ex/0602035].

[2] F. Jegerlehner and A. Nyffeler, Phys. Rept. **477** (2009) 1 [arXiv:0902.3360 [hep-ph]].

[3] G. D'Ambrosio, M. Iacovacci, M. Passera, G. Venanzoni, P. Massarotti and S. Mastroianni, EPJ Web Conf. **118** (2016).

[4] T. Blum, Phys. Rev. Lett. **91** (2003) 052001 [hep-lat/0212018].

[5] H. Wittig, *plenary talk at lattice 2016*.

[6] M. Della Morte and A. Juttner, JHEP **1011** (2010) 154 [arXiv:1009.3783 [hep-lat]].

[7] J. Bijnens and J. Relefors, to be published.

[8] C. Bouchiat, L. Michel J. Phys. Radium, 22 (1961) 121

[9] L. Durand, Phys. Rev. **128** (1962) 441.

[10] S. Weinberg, Physica A **96** (1979) 327.

[11] J. Gasser and H. Leutwyler, Annals Phys. **158** (1984) 142.

[12] J. Gasser and H. Leutwyler, Nucl. Phys. B **250** (1985) 465.

[13] J. Bijnens, G. Colangelo and G. Ecker, JHEP **9902** (1999) 020 [arXiv:hep-ph/9902437].

[14] J. Bijnens, G. Colangelo and G. Ecker, Annals Phys. **280** (2000) 100 [arXiv:hep-ph/9907333].

[15] P. Herrera-Siklody, J. I. Latorre, P. Pascual and J. Taron, Nucl. Phys. B **497** (1997) 345 [hep-ph/9610549].

[16] S. Z. Jiang, F. J. Ge and Q. Wang, Phys. Rev. D **89** (2014) no.7, 074048 [arXiv:1401.0317 [hep-ph]].

[17] E. Golowich and J. Kambor, Nucl. Phys. B **447** (1995) 373 [hep-ph/9501318].

[18] G. Amoros, J. Bijnens and P. Talavera, Nucl. Phys. B **568** (2000) 319 [hep-ph/9907264].

[19] B. Chakraborty, C. T. H. Davies, J. Koponen, G. P. Lepage, M. J. Peardon and S. M. Ryan, Phys. Rev. D **93** (2016) no.7, 074509 [arXiv:1512.03270 [hep-lat]].

[20] J. Bijnens and G. Ecker, Ann. Rev. Nucl. Part. Sci. **64** (2014) 149 [arXiv:1405.6488 [hep-ph]].

[21] J. Bijnens and P. Talavera, JHEP **0203** (2002) 046 [hep-ph/0203049].

[22] G. Ecker, J. Gasser, A. Pich and E. de Rafael, Nucl. Phys. B **321** (1989) 311.

[23] G. Ecker, J. Gasser, H. Leutwyler, A. Pich and E. de Rafael, Phys. Lett. B **223** (1989) 425.

[24] M. Golterman, K. Maltman and S. Peris, Phys. Rev. D **90** (2014) 074508 [arXiv:1405.2389 [hep-lat]].

[25] B. Chakraborty *et al.* [HPQCD Collaboration], Phys. Rev. D **89** (2014) 114501 [arXiv:1403.1778 [hep-lat]].

[26] M. Benayoun, P. David, L. DelBuono and F. Jegerlehner, arXiv:1605.04474 [hep-ph].

[27] K. Miura, *Talk at lattice 2016*.

[28] B. Chakraborty, C. T. H. Davies, P. G. de Oliviera, J. Koponen and G. P. Lepage, arXiv:1601.03071 [hep-lat].

[29] T. Blum *et al.*, Phys. Rev. Lett. **116** (2016) 232002 [arXiv:1512.09054 [hep-lat]].

[30] T. Blum *et al.* [RBC/UKQCD Collaboration], JHEP **1604** (2016) 063 [arXiv:1602.01767 [hep-lat]].

Paper v

LU TP 16-51
September 2016

Vector two point functions in finite volume using partially quenched chiral perturbation theory at two loops

Johan Bijnens and Johan Relefors

Department of Astronomy and Theoretical Physics, Lund University,
Sölvegatan 14A, SE 223-62 Lund, Sweden

Abstract

We calculate vector-vector correlation functions at two loops using partially quenched chiral perturbation theory including finite volume effects and twisted boundary conditions. We present expressions for the flavor neutral cases and the flavor charged case with equal masses. Using these expressions we give an estimate for the ratio of disconnected to connected contributions for the strange part of the electromagnetic current. We give numerical examples for the effects of partial quenching, finite volume and twisting and suggest the use of different twists to check the size of finite volume effects. The main use of this work is expected to be for lattice QCD calculations of the hadronic vacuum polarization contribution to the muon anomalous magnetic moment.

1 Introduction

The hadronic contribution to the correlation function between two electromagnetic currents is known as the hadronic vacuum polarization (HVP). An important application of the HVP is in the prediction of the anomalous magnetic moment of the muon, muon $g-2$. The muon $g-2$ is defined by

$$a_\mu = \frac{g_\mu - 2}{2} \tag{1}$$

where g_μ, the gyromagnetic ratio, is one of the best measured quantities in physics. The experimental value from [1, 2, 3, 4] is

$$a_\mu = 11659208.9(5.4)(3.3)10^{-10}. \tag{2}$$

This value is around 3 standard deviations away from the SM prediction, where the precise tension depends on which prediction is used, see [5] for a review and [6] for more recent discussions. A new experiment at Fermilab aims to improve the uncertainty in the experimental measurement to 0.14 ppm [7] and there are even more ambitious reductions in the uncertainty discussed in [8]. However, in order to take full advantage of the reduced experimental errors the theoretical prediction must also be improved.

The theoretical prediction is usually divided into a pure QED, an electroweak and a hadronic contribution

$$a_\mu = a_\mu^{\text{QED}} + a_\mu^{\text{EW}} + a_\mu^{\text{had}}. \tag{3}$$

The main uncertainty in current predictions come from the hadronic part. This part can be divided into lowest order, higher orders and light-by-light contributions;

$$a_\mu^{\text{had}} = a_\mu^{\text{LO-HVP}} + a_\mu^{\text{HO-HVP}} + a_\mu^{\text{HLbL}}. \tag{4}$$

The first and last term dominate the uncertainty. For a nice overview of the different contributions and their uncertainties, see Fig. 19 in [9]. In the following we focus on the first term which is related to the HVP.

$a_\mu^{\text{LO-HVP}}$ can be determined in several ways. One way is to use dispersion relations to relate $a_\mu^{\text{LO-HVP}}$ to $\sigma(e^+e^- \to \text{hadrons})$ or $\sigma(\tau \to \nu_\tau + \text{hadrons})$. There is some tension between the two determinations [4]. This highlights the need for other ways of determining the HVP contribution to the muon $g-2$. One way forward is using lattice QCD[1].

In lattice QCD, the HVP is evaluated at Euclidean momentum transfer [11]. A complication is that the most important contributions to $a_\mu^{\text{LO-HVP}}$ are with Euclidean $Q^2 \simeq m_\mu^2 \simeq (106\text{ MeV})^2$. The contributions from different momentum regions are discussed in Fig. 3 of [12]. Simulating with periodic boundary conditions around $Q^2 \simeq m_\mu^2$ would require much larger volumes than presently available and there are also complications around $Q^2 \simeq 0$.

[1] A recent proposal on the experimental side is given in [10].

There are a number of proposals how these difficulties can be overcome. The use of partially twisted boundary conditions to allow continuous variation of momenta was given in [13, 14], see also [15]. This is only possible for the connected parts of the HVP and there is an added complication in that the cubic symmetry of the lattice is further reduced [16, 17, 18]. Some other recent proposals and calculations are given in [19, 20, 21, 22, 23, 24, 25]. The present status of lattice QCD determinations of hadronic contributions to the muon $g-2$ was outlined in [26].

In this paper we focus on effects from finite volume, partially twisted boundary conditions and partial quenching (PQ) using PQ chiral perturbation theory (PQChPT). Finite volume effects for the HVP were studied in [27] where they found that chiral perturbation theory (ChPT) gives a good description of the finite volume effect already at leading order, which is p^4 in this case. Here we calculate general vector two point functions in PQChPT in finite volume, that is both the finite volume correction and the infinite volume part, with twisted boundary conditions at p^6. Previous results in ChPT with twisted boundary conditions at p^4 were given in [18, 27]. We also point out that the finite volume corrections may be estimated by using different twist angles at the same q^2 in the same ensemble. Note that we use Minkowski space conventions.

In [13, 28] the ratio of disconnected to connected contributions for various contributions to the HVP were discussed. Here we extend the analysis to order p^6 to the ratio for the strange quark contribution to the electromagnetic current. We use the assumption of vector meson dominance (VMD) for the ϕ meson (VMDϕ) for the pure LEC contribution in PQChPT .

This paper is organized as follows. In section 2 we introduce the vector two point function in finite volume with twisted boundary conditions. Section 3 gives a brief introduction to PQChPT with twisted boundary conditions. Our main results, the expressions for the one and two point functions to order p^6 in PQChPT are introduced in section 4. There we also present the p^4 expressions. The expressions at p^6 are given in the appendix where the integral notation used is also introduced. In section 5 we discuss the ratio of disconnected to connected contributions in PQChPT , extending the analyses in [13, 28]. In section 6 we estimate the ratio of disconnected to connected contributions to the strange part of the electromagnetic current. We then present some numerical examples and a way to estimate finite volume effects using lattice data in section 7. Finally we conclude in section 8.

2 VV correlation function

We define the vector two point function as

$$\Pi^{\mu\nu}_{ab}(q) = i\int d^4x \exp(iq\cdot x)\left\langle T\left(j^{\mu}_{a}(x)j^{\nu\dagger}_{b}(0)\right)\right\rangle \tag{5}$$

with a, b indicating which currents are being considered. In cases where $a = b$ we use

$$\Pi^{\mu\nu}_{a}(q) \equiv \Pi^{\mu\nu}_{ab}(q), \quad a = b. \tag{6}$$

We define the electromagnetic current as

$$j^{\mu}_{EM} = \frac{2}{3} j^{\mu}_{U} - \frac{1}{3} j^{\mu}_{D} - \frac{1}{3} j^{\mu}_{S} \tag{7}$$

where

$$j^{\mu}_{U} = \bar{u}\gamma^{\mu}u, \qquad j^{\mu}_{D} = \bar{d}\gamma^{\mu}d, \qquad j^{\mu}_{S} = \bar{s}\gamma^{\mu}s. \tag{8}$$

In order to be able to apply twisted boundary conditions for the connected part of various two point functions we will also define the off diagonal vector current

$$j^{\mu}_{\pi^+_v} = \bar{d}\gamma^{\mu}u. \tag{9}$$

The combination of two electromagnetic currents can be written as

$$j^{\mu}_{EM} j^{\nu\dagger}_{EM} = \frac{1}{9}\left(4 j^{\mu}_{U} j^{\nu\dagger}_{U} + j^{\mu}_{D} j^{\nu\dagger}_{D} + j^{\mu}_{S} j^{\nu\dagger}_{S} - 4 j^{\mu}_{U} j^{\nu\dagger}_{D} - 4 j^{\mu}_{U} j^{\nu\dagger}_{S} + 2 j^{\mu}_{D} j^{\nu\dagger}_{S}\right). \tag{10}$$

We do not consider the corresponding two point functions one by one. Instead we use the fact that in PQChPT we can keep the masses of the valence quarks arbitrary and calculate only one connected and one disconnected two point function. We denote these by

$$\Pi^{\mu\nu}_{\pi^+_v} \qquad \text{and} \qquad \Pi^{\mu\nu}_{XY}, \tag{11}$$

where $X, Y \in U, D, S$ with $X \neq Y$. These can then be used to construct all the possible two point functions. The finite volume correction for the connected parts of $\Pi^{\mu\nu}_{EM}$ calculated at arbitrary momentum transfer using twisted boundary conditions can be estimated from $\Pi^{\mu\nu}_{\pi^+_v}$. As it stands, $\Pi^{\mu\nu}_{\pi^+_v}$ with isospin in the valence sector is related to the connected part of $\Pi^{\mu\nu}_{U}$ but, setting the up and down valence quark masses to the strange quark mass, the connected part of $\Pi^{\mu\nu}_{S}$ can also be accessed. In this way the expressions are more general than the notation might imply. This is enough for calculating the connected part of the HVP with twisted boundary conditions.

There are constraints on the form factors following from the Ward identity

$$\partial_{\mu}\bar{q}_i\gamma^{\mu}q_j = i\left(m_i - m_j\right)\bar{q}_i q_j. \tag{12}$$

We only consider currents with same-mass quarks in which case the right hand side is zero and the current is conserved. In infinite volume this leads to the relation

$$\partial_{\mu}\Pi^{\mu\nu}_{ab} = 0. \tag{13}$$

For the case of the electromagnetic current this also follows from gauge invariance. In a Lorentz invariant framework any two point function constructed from conserved currents can be written as

$$\Pi^{\mu\nu}_{ab} = \left(q^{\mu}q^{\nu} - q^2 g^{\mu\nu}\right)\Pi_{ab}(q^2). \tag{14}$$

The quantity which is needed for the calculation of the muon $g-2$ is the subtracted quantity

$$\hat{\Pi}_{ab}(q^2) = \Pi_{ab}(q^2) - \Pi_{ab}(0) \tag{15}$$

where $a = b = EM$.

In finite volume, (13) doesn't hold for off-diagonal currents. In this case we get instead

$$i\partial_\mu \left\langle T\left\{ j^\mu_{\pi_v^+}(x) j^{\nu\dagger}_{\pi_v^+}(0) \right\} \right\rangle = \delta^{(4)}(x) \left\langle \bar{d}\gamma^\nu d - \bar{u}\gamma^\nu u \right\rangle . \tag{16}$$

The right hand side contains vacuum expectation values (VEVs) of flavor neutral vector currents which are non-zero due to broken Lorentz symmetry. Broken Lorentz symmetry also means that the decomposition (14) can not be used. In our results we use the parameterization (note that Π_{1ab} has no factor of q^2 in front)

$$\Pi^{\mu\nu}_{ab} = q^\mu q^\nu \Pi_{0ab}(q) - g^{\mu\nu}\Pi_{1ab}(q) + \Pi^{\mu\nu}_{2ab}(q). \tag{17}$$

This split is not unique but provides a useful way to organize results. Expressions given in this form reduce to (14) in the infinite volume limit. The Ward identity for $\Pi^{\mu\nu}_{\pi^+{}_v}$ following from (16) is

$$q^2 q^\nu \Pi_{0\pi_v^+}(q) - q^\nu \Pi_{1\pi_v^+}(q) + q_\mu \Pi^{\mu\nu}_{2\pi_v^+}(q) = \left\langle \bar{u}\gamma^\nu u - \bar{d}\gamma^\nu d \right\rangle . \tag{18}$$

For $\Pi^{\mu\nu}_{XY}$ we obtain instead

$$q^2 q^\nu \Pi_{0XY}(q) - q^\nu \Pi_{1XY}(q) + q_\mu \Pi^{\mu\nu}_{2XY}(q) = 0. \tag{19}$$

We have used these Ward identities to verify both our analytical expressions and numerical programs.

3 Partially quenched ChPT and twisted boundary conditions

The low energy effective field theory for the lightest pseudoscalar mesons is ChPT [29, 30, 31]. One way to parameterize the mesons in ChPT is

$$U = \exp\left(i\sqrt{2}\frac{M}{F_0} \right), \; M = \begin{pmatrix} \frac{\pi^0}{\sqrt{2}} + \frac{\eta}{\sqrt{6}} & \pi^+ & K^+ \\ \pi^- & -\frac{\pi^0}{\sqrt{2}} + \frac{\eta}{\sqrt{6}} & K^0 \\ K^- & \bar{K}^0 & -\frac{2\eta}{\sqrt{6}} \end{pmatrix}, \tag{20}$$

where F_0 is the pion decay constant in the chiral limit. The trace of M, corresponding to the singlet η, is removed due to the anomaly. To include partial quenching in ChPT we keep the trace of M and include a mass term for the singlet η which can be sent to infinity at a later stage [32].

M is then redefined as

$$M = \begin{pmatrix} U & \pi^+ & K^+ \\ \pi^- & D & K^0 \\ K^- & \bar{K}^0 & S \end{pmatrix}, \tag{21}$$

where U, D, S are flavor neutral mesons with quark content $\bar{u}u, \bar{d}d, \bar{s}s$ respectively. It is then possible to interpret the indices of M as flavor indices. Flavor indices can then be followed in Feynman diagrams using a double line notation for the mesons. Flavor lines forming loops are summed over all flavors and correspond to sea flavors, and lines which are connected with external mesons have fixed flavor content corresponding to valence flavors. Setting the masses of mesons with valence-valence, sea-valence or sea-sea meson different incorporates partial quenching. The method of following flavor lines is known as the quark flow method [33, 34, 35].

The lowest order Lagrangian with a singlet η mass term is

$$\mathcal{L} = \frac{F_0^2}{4} \left\langle D_\mu U D^\mu U^\dagger \right\rangle + \frac{F_0^2}{4} \left\langle \chi U^\dagger + U \chi^\dagger \right\rangle + \frac{m_0^2}{3} \left(U + D + S \right)^2, \tag{22}$$

where $\langle \ldots \rangle$ denotes the trace of $\ldots$ in flavor space and

$$D_\mu U = \partial_\mu U - i r_\mu U + i U l_\mu, \qquad \chi = 2B_0(s + ip) \tag{23}$$

with r_μ, l_μ, s, p external fields or sources. F_0 is the pion decay constant in the chiral limit and B_0 is related to the scalar quark condensate. The external sources will be used for incorporating quark masses, interactions with external photons and to generate Green functions of all our two point functions.

Quark masses are included by setting

$$s = \begin{pmatrix} m_u & 0 & 0 \\ 0 & m_d & 0 \\ 0 & 0 & m_s \end{pmatrix}, \tag{24}$$

where valence masses should be used for a fixed index on s and sea masses should be used for a summed index on s. External photons are introduced by

$$v_\mu = l_\mu = r_\mu = e A_\mu \begin{pmatrix} 2/3 & 0 & 0 \\ 0 & -1/3 & 0 \\ 0 & 0 & -1/3 \end{pmatrix}, \tag{25}$$

where A_μ is the external photon field and e is the electromagnetic charge.

In order to calculate two point functions such as Π_{UU}, we need to use

$$v_\mu = V_\mu \begin{pmatrix} 1 & 0 & 0 \\ 0 & 0 & 0 \\ 0 & 0 & 0 \end{pmatrix} \tag{26}$$

where V_μ is an external vector field. The standard ChPT Lagrangian assumes that the matrix v_μ is traceless which is not the case here. Including the trace of v_μ leads to additional terms in the Lagrangian. As explored in Ref. [28] these extra terms do not couple to mesons until $\mathcal{O}(p^6)$, or $\mathcal{O}(p^4)$ via the Wess-Zumino-Witten (WZW) term. For the two point function, two such vertices are needed. There is then no contribution to the finite volume correction until $\mathcal{O}(p^8)$. The $\mathcal{O}(p^6)$ terms do influence the infinite volume expressions and are needed in order to render these finite. The $\mathcal{O}(p^4)$ and $\mathcal{O}(p^6)$ Lagrangians can be found in [30, 31] and [36, 37], respectively.

The main extra complication from the singlet η mass term is that the propagator for diagonal mesons becomes rather involved. After the limit $m_0 \to \infty$ is taken the propagator between an $a\bar{a}$ and $b\bar{b}$ meson is

$$\mathcal{D}_{ab} = \frac{i\delta_{ab}}{p^2 - m_a^2} - \frac{i}{3}\frac{(p^2 - m_1^2)(p^2 - m_2^2)(p^2 - m_3^2)}{(p^2 - m_a^2)(p^2 - m_b^2)(p^2 - m_{\pi^0}^2)(p^2 - m_\eta^2)} \tag{27}$$

where $m_{1,2,3}$ are sea quark masses. For numerical integration we evaluate integrals with this propagator using the residue notation given in [38]. However, in the analytical expressions we keep $\mathcal{D}_{ab}$ intact, see Appendix A.

For a quark q in a box with length L, twisted boundary conditions are defined by

$$q(x^i + L) = \exp(i\theta_q^i) q(x^i) \tag{28}$$

where θ_q^i is the twist angle in the i direction. The twist of the anti quark follow from complex conjugation. The allowed momenta in direction i of the quark are then

$$p^i = \frac{2\pi}{L} n + \frac{\theta_q^i}{L}, \qquad n \in \mathbb{Z}. \tag{29}$$

The momentum of the quark can be continuously varied by varying the twist angle.

In [39], ChPT with twisted and partially twisted boundary conditions was developed, where partial twisting means that the twist on valence and sea quarks are different. The twist of a $\bar{q}'q$ meson is

$$\phi_{\bar{q}'q}(x^i + L) = \exp(i(\theta_q^i - \theta_{\bar{q}}^i))\phi_{\bar{q}'q}(x^i). \tag{30}$$

Diagonal mesons have zero twist and charge conjugate mesons have opposite twists of one another.

Loop integrals are replaced by sums over allowed momenta in finite volume. We regulate our integrals using dimensional regularization giving that we replace

$$\int \frac{d^d k}{(2\pi)^d} \to \int_V \frac{d^d k}{(2\pi)^d} = \int \frac{d^{d-3}k}{(2\pi)^{d-3}} \sum_{\vec{k} = \frac{2\pi}{L}\vec{n} + \frac{\vec{\theta}}{L}} \tag{31}$$

where we have collected the twist angles θ^i in a vector $\vec{\theta}$. We also use the four vector notation $\theta^\mu = (0, \vec{\theta})$.

An important consequence of twisted boundary conditions is that the summation in (31) is not symmetric around zero, which gives

$$\int_V \frac{d^d k}{(2\pi)^d} \frac{k^\mu}{k^2 - m^2} \neq 0. \tag{32}$$

This is a consequence of the fact that twisted boundary conditions break the cubic symmetry of the lattice. The way we evaluate integrals in finite volume is described in Appendix A.

4 Analytical results

In this section we give expressions for the vector one point and two point functions at p^4. The expressions at p^6 are given in Appendix B since they are rather long. We denote the p^4 part of a quantity X by $X^{(4)}$ and the p^6 part is denoted by $X^{(6)}$. The results for $\Pi^{\mu\nu}_{XY}$ assume no twist while results for $\Pi^{\mu\nu}_{\pi_v^+}$ and $\langle \bar{q}\gamma^\mu q\rangle$ are the partially twisted ones. The $\Pi^{\mu\nu}_{\pi_v^+}$ result assumes that the two valence quarks have the same mass, which is enough for HVP. The more general result with different mass valence quarks is considerably longer. Note that the results contain implicit sums over sea quarks. A term containing both $\mathcal{S}$ and $\mathcal{S}'$ has two implicit sums, a term containing only $\mathcal{S}$ has one implicit sum and a term with no sea quark mentioned has no implicit sum.

The results in Appendix B contain both the finite volume correction and the infinite volume part. For a quantity X we denote this by $X^{\mathcal{V}}$. If we would write these out separately the infinite volume part would be a bit shorter but the finite volume correction would be much longer. To achieve this compact expression we write every integral in finite volume as the sum of the finite part of the infinite volume integral after renormalization plus the finite volume correction. Symbolically we use notation where the part of an integral A which remains after renormalization is written as

$$A^{\mathcal{V}} = \bar{A} + A^V \tag{33}$$

This is described in more detail in Appendix A. Note that for this to work all products of the form $1/\epsilon \times \epsilon$ must cancel, otherwise the parts with A^ϵ would contribute. We have checked this cancellation explicitly. We have of course also checked that all divergencies cancel, except those that need to be absorbed in the new LECs involving the singlet vector current.

The full expression written explicitly in terms of infinite volume and finite volume integrals is obtained by expanding the expressions below and in Appendix B using (33) and the corresponding expressions for the other integrals. In order to access the finite volume corrections any term containing no finite volume integral should be dropped. The infinite volume result is obtained by removing all finite volume integrals.

4.1 $\Pi^{\mathcal{V}\mu\nu}_{\pi^+_v}$ at p^4

$$\begin{aligned}
\Pi^{\mathcal{V}(4)}_{0\pi^+_v}(q) &= 4B^{\mathcal{V}}_{21}(m^2_{u\mathcal{S}}, m^2_{\mathcal{S}d}, q) - 4B^{\mathcal{V}}_{1}(m^2_{u\mathcal{S}}, m^2_{\mathcal{S}d}, q) + B^{\mathcal{V}}(m^2_{u\mathcal{S}}, m^2_{\mathcal{S}d}, q) \\
\Pi^{\mathcal{V}(4)}_{1\pi^+_v}(q) &= -4B^{\mathcal{V}}_{22}(m^2_{u\mathcal{S}}, m^2_{\mathcal{S}d}, q) + A^{\mathcal{V}}(m^2_{u\mathcal{S}}) + A^{\mathcal{V}}(m^2_{d\mathcal{S}}) \\
\Pi^{\mathcal{V}(4)\mu\nu}_{2\pi^+_v}(q) &= 4B^{\mathcal{V}\mu\nu}_{23}(m^2_{u\mathcal{S}}, m^2_{\mathcal{S}d}, q) - 2q^\nu B^{\mathcal{V}\mu}_{2}(m^2_{u\mathcal{S}}, m^2_{\mathcal{S}d}, q) - 2q^\mu B^{\mathcal{V}\nu}_{2}(m^2_{u\mathcal{S}}, m^2_{\mathcal{S}d}, q)
\end{aligned} \tag{34}$$

4.2 $\Pi^{\mathcal{V}\mu\nu}_{XY}$ at p^4

$$\begin{aligned}
\Pi^{\mathcal{V}(4)}_{0XY}(q) &= -4B^{\mathcal{V}}_{21}(m^2_{XY}, m^2_{XY}, q) + 4B^{\mathcal{V}}_{1}(m^2_{XY}, m^2_{XY}, q) - B^{\mathcal{V}}(m^2_{XY}, m^2_{XY}, q) \\
\Pi^{\mathcal{V}(4)}_{1XY}(q) &= 4B^{\mathcal{V}}_{22}(m^2_{XY}, m^2_{XY}, q) - 2A^{\mathcal{V}}(m^2_{XY}) \\
\Pi^{\mathcal{V}(4)\mu\nu}_{2XY}(q) &= -4B^{\mathcal{V}\mu\nu}_{23}(m^2_{u\mathcal{S}}, m^2_{\mathcal{S}d}, q)
\end{aligned} \tag{35}$$

4.3 $\langle \bar{q}\gamma^\mu q\rangle^{\mathcal{V}}$ at p^4

$$\langle \bar{q}\gamma^\mu q\rangle^{\mathcal{V}(4)} = 2A^{\mu\mathcal{V}}(m^2_{q\mathcal{S}}) \tag{36}$$

5 Connected versus disconnected

In Ref. [28] we presented arguments for the ratio of disconnected to connected contributions to vector two point functions relevant to HVP. The basic observation used was that the singlet vector current does not couple to mesons until $\mathcal{O}(p^6)$, or $\mathcal{O}(p^4)$ through the WZW term. In this section we outline how PQ changes the conclusions in that paper.

To discuss the singlet vector current couplings in PQ QCD we need to briefly introduce the supersymmetric formulation of PQ QCD. In this formulation there are three quarks for every single quark in standard QCD. There are two fermionic quarks with different masses, these are the sea and valence quarks. The third quark is a boson with the same mass as the valence quark. Sea quark contributions are associated with closed quark loops. The fermionic and bosonic valence quark closed loop contributions cancel since they contribute with opposite signs. Using correlators formed from valence quarks then leads to PQ QCD.

The singlet vector current in the supersymmetric formulation is

$$V^\mu_s = j^\mu_U + j^\mu_D + j^\mu_S + j^\mu_{\tilde{U}} + j^\mu_{\tilde{D}} + j^\mu_{\tilde{S}} + j^\mu_1 + j^\mu_2 + j^\mu_3, \tag{37}$$

where U, D, S indicate valence quarks, $\tilde{U}, \tilde{D}, \tilde{S}$ indicate ghost quarks which cancel normal valence quark loops and $1, 2, 3$ indicate sea quarks. A general feature of two point functions in the PQ theory is then that

$$\Pi_{U\tilde{U}} = -\Pi^D_{UU}, \quad \text{and} \quad \Pi_{\tilde{U}} = -\Pi^C_{UU} + \Pi^D_{UU}, \tag{38}$$

where the superscripts, C and D, indicate the connected and disconnected part respectively. This follows from the observation that any normal quark loop gives a minus sign whereas bosonic quark loops don't. The connected (disconnected) part of any two point function contains one (two) quark loops which gives the above relations. All other quark loops are in common between the quark and ghost quark currents.

We now turn to the issue of the ratio between disconnected and connected two point functions. For any two point function Π_{ab} we denote the part which contains only vertices with no coupling to the singlet vector current by Π'_{ab}. Π'_{ab} contains, but is not limited to, diagrams which contain vertices only from the p^2 and p^4 Lagrangians, with the exception of the WZW term. The property that there is no coupling to the singlet vector current gives in the two flavor case

$$\Pi'_{U(U+D+\tilde{U}+\tilde{D}+1+2)} = 0. \tag{39}$$

Using (38) and working in the isospin limit gives

$$\frac{\Pi'_{U1}}{\Pi'_{\pi^+}} = -\frac{1}{2}. \tag{40}$$

Changing $1 \to D$ gives the unquenched result from [28]. The PQ theory gives a relation between the connected part with external valence quarks and the disconnected part with one external valence quark and one external sea quark.

Similarly, the three flavor case in the isospin limit gives the relation

$$\frac{\Pi'_{U1}}{\Pi'_{\pi^+}} = -\frac{1}{2} - \frac{\Pi'_{U3}}{2\Pi'_{\pi^+}}. \tag{41}$$

6 Disconnected and connected for the strange quark contribution

The expressions given in section 4 and the numerical results presented below are with lowest order masses. For this reason, low energy constants related to mass corrections appear in the two point functions. In this and the following section we have used as input for the lowest order masses and decay constant

$$m_\pi = 135 \text{ MeV}, \qquad m_K = 495 \text{ MeV}, \qquad F_\pi = 92.2 \text{ MeV}. \tag{42}$$

For the LECs we use the values of [40]:

$$\begin{aligned} &L_4^r = 0.3 \times 10^{-3}, \quad L_5^r = 1.0 \times 10^{-3}, \quad L_6^r = 0.1 \times 10^{-3} \quad \mu = 770 \text{ MeV}, \\ &L_8^r = 0.5 \times 10^{-3}, \quad L_9^r = 5.9 \times 10^{-3}, \quad L_{10}^r = -3.8 \times 10^{-3}, \end{aligned} \tag{43}$$

where μ is the renormalization scale.

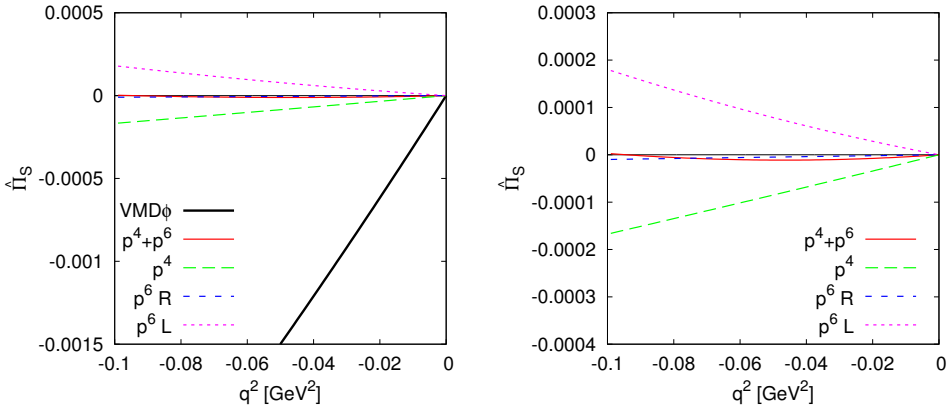

(a) (b)

Figure 1: (a) The different contributions to $\hat{\Pi}_S(q^2)$. The p^4 calculation, the pure two-loop part, p^6R, the p^6 part depending on the p^4 LECs, p^6L, and the pure LEC contribution as estimated in [28] using ϕ-dominance, $VMD\phi$. (b) The different loop contributions only, i.e. the $VMD\phi$ contribution not included, with the same vertical scale as used in Fig. 2 but with a different range.

In our earlier work [28] we estimated the ratio of disconnected to connected contributions for the two point functions with the up and down quark part of the electromagnetic currents. In addition, we estimated the size of the contributions from the strange quark electromagnetic current, $\hat{\Pi}_S$, and the mixed strange quark– up-down quarks, $\hat{\Pi}_{US}$. The latter is purely disconnected. We did not estimate the size of the disconnected contribution for the strange case since in [28] we used standard ChPT in the isospin conserving case which did not allow us to do that. Here we calculated the contributions using PQChPT so we can now estimate separately the connected and disconnected part.

The arguments for $\Pi'_{US} = (-1/2)\Pi'_S$ as given in [28] and in section 5 remain valid and we obtain the same ratios here.

In Fig. 1(a) we show the results as obtained in our earlier work for $\hat{\Pi}_S(q^2)$ but here in terms of lowest order masses. It should be remembered that the pure LEC contribution, i.e. tree level diagrams with no loops, is estimated by ϕ-meson exchange and only contributes to $\hat{\Pi}_S$ and not to $\hat{\Pi}_{US}$. For the loop contributions the relation $\hat{\Pi}_{US} = (-1/2)\hat{\Pi}_S$ as derived in [28] holds. There is a large cancellation between the p^4 and p^6 contributions and the final result is very much dominated by the pure LEC contribution as estimated by ϕ-exchange. In Fig. 1(b) we show the loop contributions with a smaller scale. For ease of comparison the vertical scale is the same as used in Fig. 2 but with a different range.

In Fig. 2 the loop contributions for the connected, (a), and disconnected, (b), parts are shown. It is clear that there is no simple ratio here as for the up-down case but in all

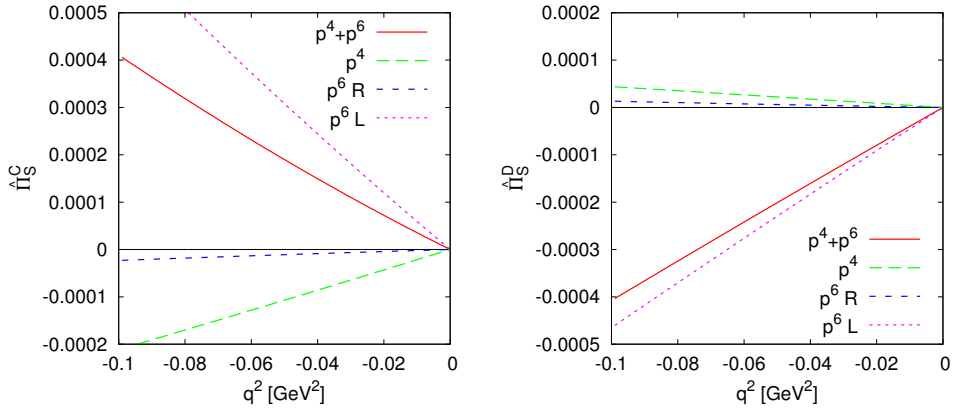

(a) (b)

Figure 2: (a) The different contributions to the connected part, $\hat{\Pi}_S^C(q^2)$. The p^4 calculation, the pure two-loop part, p^6R, and the p^6 part depending on the p^4 LECs, p^6L. The pure LEC contribution as estimated by $VMD\phi$ is not shown. (b) The different contributions to the disconnected part $\hat{\Pi}_S^D(q^2)$. The $VMD\phi$ contribution is zero for this case.

cases the disconnected contribution is of opposite sign to the connected one and there are significant cancellations.

The conclusion here is that the disconnected contribution is of order -15% of the total strange quark contribution with a sizable error. The error is both due to the large p^6 contribution and the uncertainty on the $VMD\phi$ estimate. The total strange quark contribution is by far dominated by the $VMD\phi$ part because even if individual loop contributions are of order 20%, there are large cancellations making the total strange quark contributions from the loops very small.

7 Numerical size of finite volume corrections

In this section we give numerical estimates of the finite volume effects for vector two point functions and vacuum expectation values. In particular we address the questions of convergence of the finite volume corrections and the effects of using different twist angles for determining finite volume effects from lattice data. Note that we treat the time direction as infinite. The numerical input is the same as in section 6 except the we have added

$$m_\pi L = 4\,. \tag{44}$$

As discussed in [15, 18], with twisted boundary conditions the vector currents can get a vacuum expectation value. The one loop result in standard ChPT was worked out in

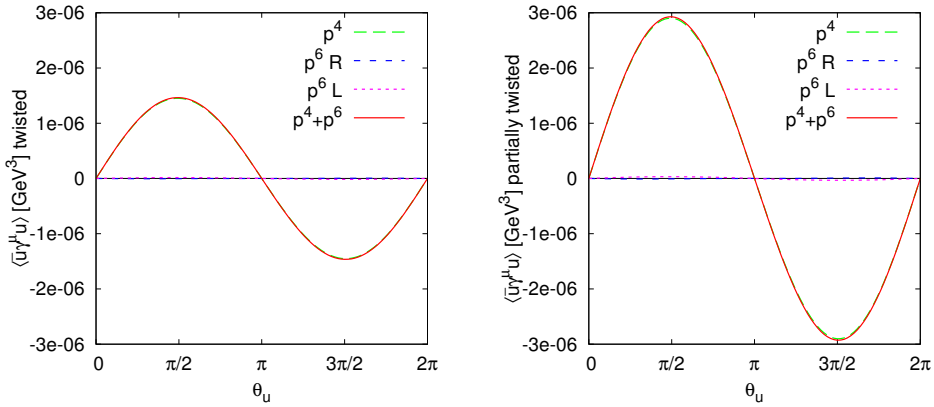

(a) (b)

Figure 3: (a) The vacuum expectation value $\langle \bar{u}\gamma^\mu u\rangle$ with the up valence and sea quark twisted with $\theta_u = (0, \theta, 0, 0)$. (b) Same but only the up valence quark twisted. In both cases the x-component or $\mu = 1$ is plotted, the others vanish.

[18]. Here we add the two loop results as well as partial quenching and twisting. The formulas (36) and (64) are fully general but we present numerics here for the case where up and down masses are the same and sea and valence masses equal. To put the numbers in perspective we can compare with the results for the scalar vacuum expectation value. The finite volume corrections here are taken with zero twist using the results of [41]

$$\begin{aligned} \langle \bar{u}u\rangle &= -\,1.2\ 10^{-2}\ \mathrm{GeV}^{-3}, & \langle \bar{u}u\rangle^V (p^4) &= -\,2.4\ 10^{-5}\ \mathrm{GeV}^{-3}, \\ \langle \bar{u}u\rangle^V (p^6 R) &= 4.5\ 10^{-7}\ \mathrm{GeV}^{-3}, & \langle \bar{u}u\rangle^V (p^6 L) &= -\,1.2\ 10^{-7}\ \mathrm{GeV}^{-3}., \end{aligned} \tag{45}$$

In Fig. 3(a) we plotted the result for $\langle \bar{u}\gamma^\mu u\rangle$ for $\theta_u = (0, \theta, 0, 0)$ for the fully twisted case, i.e. both the sea and valence up quarks are twisted. In Fig. 3(b) we plot with the same twist angle but for the partially twisted case, only the up valence quark is twisted. The finite volume corrections are roughly an order of magnitude smaller than for the scalar case in (45), but the same pattern is there. The p^6 corrections are very small. The partially twisted case is almost exactly a factor of two larger than the fully twisted case. The effects are strongly dominated by the pion loops and for these the difference at p^4 is exactly a factor of two. The vacuum expectation value $\langle \bar{d}\gamma^\mu d\rangle$ with the up quark fully twisted and no twist on the down quark is almost exactly minus $\langle \bar{u}\gamma^\mu u\rangle$. Again it is exactly minus for the pion loops only. For the partially twisted up quark $\langle \bar{d}\gamma^\mu d\rangle$ vanishes since then no active quark has twist.

We now turn to the two point functions. In the finite volume case we cannot simply present the combination $\hat{\Pi}(q^2)$ since the subtraction of zero is not well defined, after all $\Pi^{\mu\nu}(q = 0) \neq 0$. The relevant two point function to use with twisted boundary conditions

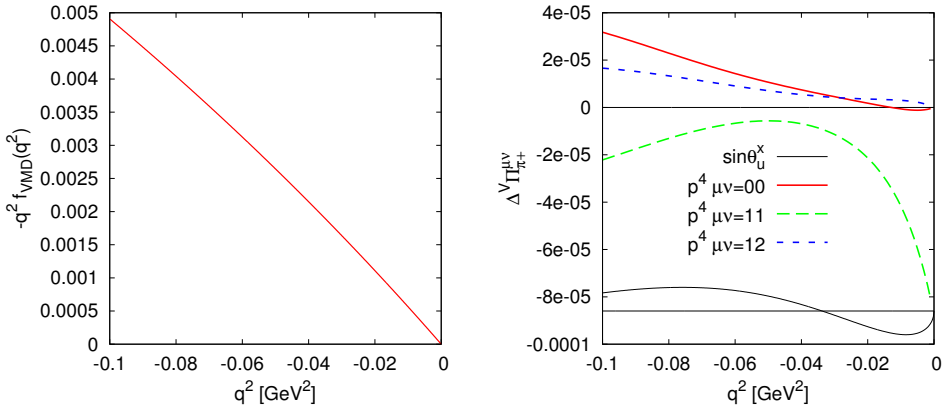

(a) (a)

Figure 4: (a) $-q^2 f_{\rm VMD}(q^2)$ as a function of q^2. This together with (47) and (48) can be used to judge the relative size of the finite volume effects in the following figures. (b) The finite volume corrections at p^4 for the spatially symmetric case. The lower straight line indicates zero around which $\sin\theta_u^x$ oscillates.

is the connected light part, Π_{π^+}. In the following we only twist the up quark. We also put the up and down masses equal and sea and valence masses the same.

There is essentially no numerical difference between the fully twisted (both valence and sea up quark twisted) and partially twisted cases. We therefore present only the partially twisted case in the plots. The Ward identity is fulfilled in both cases but the right hand side of (18) gets the same numerical value in the fully twisted case from both the up and down vacuum expectation value, and in the partially twisted case only from the up vacuum expectation value.

In order to show the size of the finite volume corrections we can compare with the naive VMD estimate. This corresponds to

$$\Pi^{\mu\nu}_{\pi^+}\big|_{\rm VMD} = (q^\mu q^\nu - g^{\mu\nu})\,\frac{4F_\pi^2}{m_V^2 - q^2} = (q^\mu q^\nu - g^{\mu\nu})\, f_{\rm VMD}(q^2) \tag{46}$$

with $m_V = 770$ MeV. When we choose $q = (0, \sqrt{-q^2}, 0, 0)$ we have

$$\Pi^{00} = -\Pi^{22} = -\Pi^{33} = -q^2 f_{\rm VMD}(q^2) \tag{47}$$

and all others zero. Instead for $q = (0, \sqrt{-q^2/3}, \sqrt{-q^2/3}, \sqrt{-q^2/3})$ we have that

$$\Pi^{00} = -\,q^2 f_{\rm VMD}(q^2) \qquad \Pi^{ii} = \frac{2}{3} q^2 f_{\rm VMD}(q^2) \qquad \Pi^{ij}\big|_{i\neq j} = -\,\frac{1}{3} q^2 f_{\rm VMD}(q^2) \tag{48}$$

with the others zero. We have plotted $-q^2 f_{\rm VMD}(q^2)$ in Fig. 4(a).

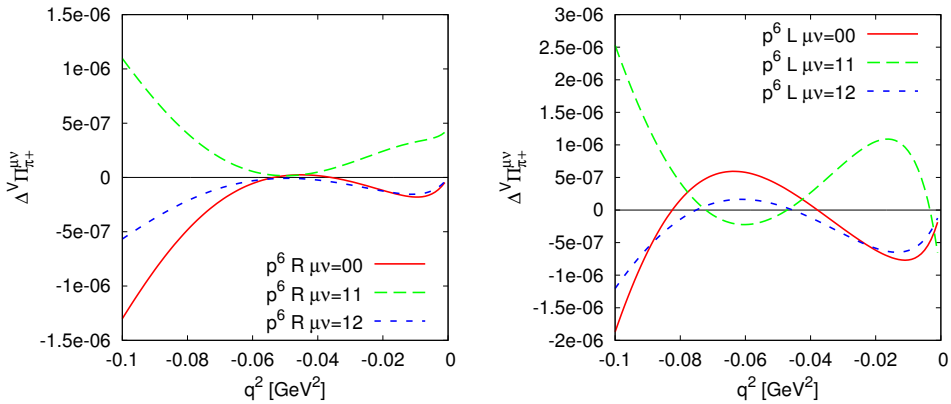

(a) (a)

Figure 5: The parts of the finite volume corrections at p^6 for the spatially symmetric case(a) p^6R (b) p^6L.

We can now present the finite volume corrections. First we take the spatially symmetric twisted case. Here we use $\theta_u = q/L$ with $q = (0, \sqrt{q^2/3}, \sqrt{q^2/3}, \sqrt{q^2/3})$. The p^4 corrections are shown in Fig. 4(b). $\Pi^{\mu\nu}(q = 0) \neq 0$ is clearly visible. The relative size of the correction compared to the VMD estimate is in the few % range (except of course at $q^2 = 0$ where it becomes infinite). Note that here we have $\Pi^{11} = \Pi^{22} = \Pi^{33}$, $\Pi^{01} = \Pi^{02} = \Pi^{03} = 0$ and $\Pi^{12} = \Pi^{13} = \Pi^{23}$. In [27] they found that lowest order ChPT gives a good description of finite volume effects already at leading order (p^4). If this is the case, then the higher order corrections should turn out to be small, in contrast to the infinite volume case where they can be significant, see [28]. In Fig. 5 we plot the two parts of the finite volume correction for Π_{π^+} at order p^6. We find that the correction is small, supporting the conclusion of [27]. The bottom curves in Fig. 4(b) and 6 show $\sin(\theta_u^x)$ allowing to judge the type of twisting effects expected.

In Fig. 6(a) we show the full (p^4+p^6) finite volume correction for the spatially symmetric case. The p^4 result is included with thin dashed lines for comparison. Using the same twist angle in all spatial directions is common in lattice calculations of the HVP. It gives the possibility to average over several directions reducing the statistical error. However, the finite volume corrections do depend on how the twisting is done. We could have chosen to twist only in the x-direction. In that case we have $\theta_u = q/L$ with $q = (0, \sqrt{q^2}, 0, 0)$ and $\Pi^{22} = \Pi^{33}$ and all elements with $\mu \neq \nu$ vanish. The full $(p^4 + p^6)$ finite volume corrections for this case are shown in Fig. 6(b). Again, the p^4 results are included with thin dashed lines.

Comparing the two halves of Fig. 6 we see quite different finite volume corrections. This can be used to test the size of the finite volume corrections using only lattice data by

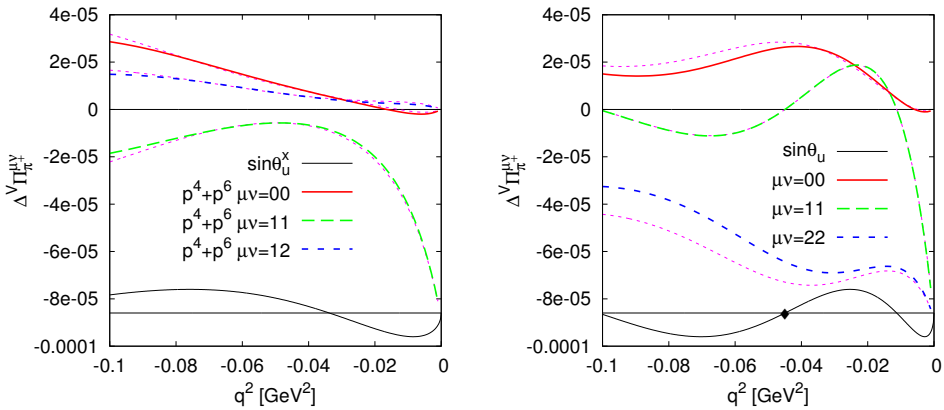

(a) (b)

Figure 6: The finite volume corrections adding p^4 and p^6. The p^4 correction is shown as the thin dashed line where each thin line should be associated with the closest thick line. The lower straight line indicates zero around which $\sin\theta_u^x$ oscillates. (a) The spatially symmetric case (b) Twisting only the x-direction. The diamond indicates a q^2 accessible with periodic boundary conditions.

using two different ways of twisting that should reduce to the same q^2. This would also constitute a test of our predictions for the finite volume corrections. The quantity we will use for this is the average of the spatial diagonal components

$$\overline{\Pi} = \frac{1}{3}\sum_{i=1,2,3} \Pi^{ii}\,. \tag{49}$$

The finite volume corrections to $\overline{\Pi}$ are shown in Fig. 7. In (a) we show the p^4 result and in (b) the sum of the p^4 and p^6 results. There is a good convergence and the difference between spatially symmetric twisting and twisting only in the x-direction is of similar size as the actual correction over a sizable range of q^2. This difference can thus be used to test the finite volume corrections using the same underlying set of configurations without having to resort to tricks like reweighting [42]. That the curves for the two cases coincide for $q^2 = 0$ is clear since then the twists vanish fully for both cases.

8 Conclusion

In this paper we have calculated the vector one and two point functions at p^4 and p^6 using PQChPT in finite volume with twisted boundary conditions. We have calculated one connected and one disconnected two point function. In PQChPT this is all that is

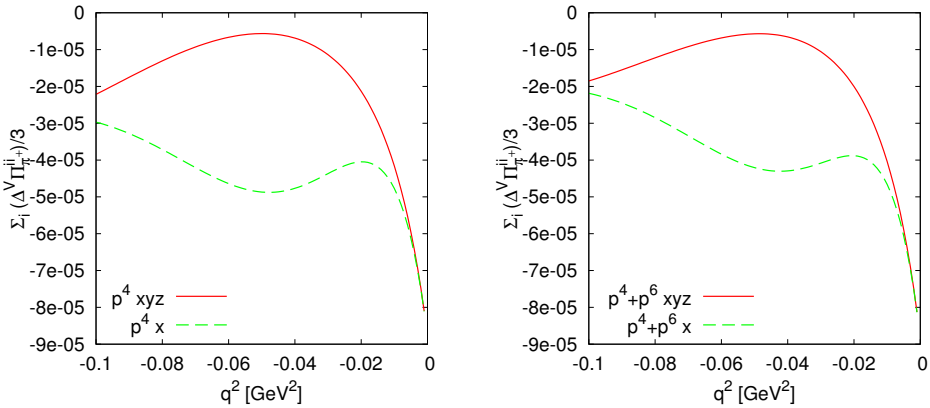

(a) (b)

Figure 7: The finite volume corrections to the spatial average as defined in (49). xyz is the spatially symmetric twisting and x twisting only in the x-direction. (a) p^4 (b) Sum of p^4 and p^6.

needed to obtain all vector two point functions. The connected two point function was calculated by considering a flavor charged current with equal masses. The disconnected two point function was calculated using two neutral currents with different flavors.

Extending the work of [13] and our work in [28] we have used the PQ expressions to give a numerical estimate of the ratio of disconnected to connected contributions for the strange quark part of the electromagnetic current. Using VMD for the ϕ meson to estimate the pure LEC contribution we obtain a ratio of about -15%.

We have also looked at the effects from finite volume and twisted boundary conditions. The p^6 contributions to the finite volume corrections are small when compared with the p^4 contributions which supports the conclusion of [27]. We also point out that the difference between estimates using different twist angles at the same physical point can be used to estimate the finite volume corrections.

A Integral notation

The loop integrals needed when calculating vector two point functions are

$$A^{\{,\mu,\mu\nu\}}\left((m^2)^n\right) = \frac{1}{i}\int_V \frac{d^dk}{(2\pi)^d}\frac{\{1,k^\mu,k^\mu k^\nu\}}{(k^2-m^2)^n} \tag{50}$$

$$B^{\{,\mu,\mu\nu,\mu\nu\alpha\}}\left((m_1^2)^{n_1},(m_2^2)^{n_2},q\right) = \frac{1}{i}\int_V \frac{d^dk}{(2\pi)^d}\frac{\{1,k^\mu,k^\mu k^\nu,k^\mu k^\nu k^\alpha\}}{(k^2-m_1^2)^{n_1}((q-k)^2-m_2^2)^{n_2}}.$$

When twisted boundary conditions are used the allowed momenta k in k^2-m^2 are indicated by the mass, e.g. allowed momenta in $k^2-m_{\pi^+}^2$ are the π^+ momenta, see [18]. The integrals above contain both the finite volume and infinite volume contributions. Exemplifying with A and suppressing all arguments, we split the integrals according to

$$\begin{aligned} A &= \frac{C_A}{\bar{\epsilon}} + A^{\mathcal{V}} + \epsilon A^{\epsilon} + \mathcal{O}(\epsilon^2), \\ \frac{1}{\bar{\epsilon}} &= \frac{1}{\epsilon} + \ln(4\pi) + 1 - \gamma. \end{aligned} \tag{51}$$

The constant C_A is the coefficient of $1/\bar{\epsilon}$ and differs from integral to integral. We renormalize our expressions using the ChPT version of $\overline{MS}$ where parts proportional to $1/\bar{\epsilon}$ cancel. $A^{\mathcal{V}}$ then contains the part of the infinite volume integral which remains after renormalization plus the finite volume correction. We express this as

$$A^{\mathcal{V}} = \bar{A} + A^V \tag{52}$$

where $\bar{A}$ is the infinite volume part and A^V is the finite volume correction.

The infinite volume part of the integrals, including the residues of the poles, can be found from [43] using that the higher pole integrals can be obtained by derivatives with respect to the masses. Methods for evaluating the finite volume correction, as well as expressions for some of the integrals, can be found in [39, 44, 18]. In [18] we gave explicit expressions, in terms of Jacobi theta functions, for the finite volume corrections to all of the integrals except for $B^{\mu\nu\alpha}\left((m_1^2)^{n_1},(m_2^2)^{n_2},q\right)$. The expression for the finite volume correction to $B^{\mu\nu\alpha}\left((m_1^2)^{n_1},(m_2^2)^{n_2},q\right)$ is

$$\begin{aligned} B^{V\mu\nu\alpha}\left((m_1^2)^{n_1},(m_2^2)^{n_2},q\right) =& \frac{\Gamma(n_1+n_2)}{\Gamma(n_1)\Gamma(n_2)}\int dx(1-x)^{n_1-1}x^{n_2-1}\times\Big(\\ & A^{v\mu\nu\alpha}((\tilde{m}^2)^{n_1+n_2}) \\ & +x(\delta^\mu_\rho\delta^\nu_\sigma q^\alpha + \delta^\mu_\rho q^\nu\delta^\alpha_\sigma + q^\mu\delta^\nu_\rho\delta^\mu_\sigma)A^{V\rho\sigma}((\tilde{m}^2)^{n_1+n_2}) \\ & +x^2(\delta^\mu_\rho q^\nu q^\alpha + q^\mu\delta^\nu_\rho q^\alpha + q^\mu q^\nu\delta^\alpha_\rho)A^{V\rho}((\tilde{m}^2)^{n_1+n_2}) \\ & +x^3 q^\mu q^\nu q^\alpha A^V((\tilde{m}^2)^{n_1+n_2})\Big) \end{aligned} \tag{53}$$

where

$$\tilde{m}^2 = (1-x)m_1^2 + xm_2^2 - x(1-x)q^2 \tag{54}$$

and the integrals on the right hand side should be evaluated with the twist angle

$$\vec{\tilde{\theta}} = \vec{\theta} - x\vec{q}. \tag{55}$$

In the actual results we have split the integrals as

$$\begin{aligned} B^{\mu\nu\alpha} &= q^\mu q^\nu q^\alpha B_{31} + (g^{\mu\nu}q^\alpha + g^{\mu\alpha}q^\nu + g^{\nu\alpha}q^\mu)B_{32} + B_{33}^{\mu\nu\alpha} \\ B^{\mu\nu} &= q^\mu q^\nu B_{21} + g^{\mu\nu}B_{22} + B_{23}^{\mu\nu} \\ B^{\mu} &= q^\mu B_1 + B_2^\mu \\ A^{\mu\nu} &= g^{\mu\nu}A_{22} + A_{23}^{\mu\nu} \end{aligned} \tag{56}$$

where all arguments are suppressed.

The diagonal integral introduced in (27) can in principle be split up using the residue notation of [38] so that all integrals are of the form (50). This leads to longer and more difficult to read expressions and we keep the diagonal propagator intact using notation such as

$$A(\mathcal{D}_{ab}) = \frac{1}{i}\int_V \frac{d^dk}{(2\pi)^d}\left(\frac{\delta_{ab}}{p^2-m_a^2} - \frac{1}{3}\frac{(p^2-m_1^2)(p^2-m_2^2)(p^2-m_3^2)}{(p^2-m_a^2)(p^2-m_b^2)(p^2-m_{\pi^0}^2)(p^2-m_\eta^2)}\right). \tag{57}$$

The residue notation is used in the numerical evaluations needed in section 7.

B Analytical results

In this appendix we present the analytical expressions for vector two point functions and one point functions at p^6 in PQChPT in finite volume with twisted boundary conditions. The expressions contain both the infinite volume part and the finite volume correction, see section 4, where the p^4 expressions are presented, and Appendix A.

B.1 $\Pi_{XY}^{\mathcal{V}\mu\nu}$ at p^6

$$\begin{aligned}
&F_0^2\Pi_{0XY}^{\mathcal{V}(6)} = \qquad (58)\\
&+(B^{\mathcal{V}}(m_{XY}^2,m_{XY}^2,q) - 4B_1^{\mathcal{V}}(m_{XY}^2,m_{XY}^2,q) + 4B_{21}^{\mathcal{V}}(m_{XY}^2,m_{XY}^2,q))q^2\\
&\quad\times(4L_9^r - \frac{1}{2}B_1^{\mathcal{V}}(m_{X\mathcal{S}}^2,m_{X\mathcal{S}}^2,q) - \frac{1}{2}B_1^{\mathcal{V}}(m_{Y\mathcal{S}}^2,m_{Y\mathcal{S}}^2,q))\\
&+2(B^{\mathcal{V}}(m_{XY}^2,(m_{XY}^2)^2,q) - 4B_1^{\mathcal{V}}(m_{XY}^2,(m_{XY}^2)^2,q) + 4B_{21}^{\mathcal{V}}(m_{XY}^2,(m_{XY}^2)^2,q))\\
&\quad\times(16m_{XY}^2m_{\mathcal{SS}}^2L_6^r - 8m_{XY}^2m_{\mathcal{SS}}^2L_4^r + m_{XY}^2A^{\mathcal{V}}(\mathcal{D}_{XY})\\
&\qquad + 16m_{XY}^4L_8^r \quad - 8m_{XY}^4L_5^r))\\
&\quad+4q^2B_{21}^{\mathcal{V}}(m_{XY}^2,m_{XY}^2,q)\times(B_{21}^{\mathcal{V}}(m_{X\mathcal{S}}^2,m_{X\mathcal{S}}^2,q) + B_{21}^{\mathcal{V}}(m_{Y\mathcal{S}}^2,m_{Y\mathcal{S}}^2,q))\\
&\quad-2q^2B_{21}^{\mathcal{V}}(m_{X\mathcal{S}}^2,m_{X\mathcal{S}}^2,q)\times(B_1^{\mathcal{V}}(m_{XY}^2,m_{XY}^2,q) - B_1^{\mathcal{V}}(m_{Y\mathcal{S}}^2,m_{Y\mathcal{S}}^2,q))\\
&\quad-4q^2B_{21}^{\mathcal{V}}(m_{Y\mathcal{S}}^2,m_{Y\mathcal{S}}^2,q)B_{21}^{\mathcal{V}}(m_{X\mathcal{S}}^2,m_{X\mathcal{S}}^2,q)\\
&\quad-2q^2B_{21}^{\mathcal{V}}(m_{Y\mathcal{S}}^2,m_{Y\mathcal{S}}^2,q)\times(B_1^{\mathcal{V}}(m_{XY}^2,m_{XY}^2,q) - B_1^{\mathcal{V}}(m_{X\mathcal{S}}^2,m_{X\mathcal{S}}^2,q))\\
&\quad-\frac{q^2}{2}B_1^{\mathcal{V}}(m_{XY}^2,m_{XY}^2,q)\times(B^{\mathcal{V}}(m_{X\mathcal{S}}^2,m_{X\mathcal{S}}^2,q) + B^{\mathcal{V}}(m_{Y\mathcal{S}}^2,m_{Y\mathcal{S}}^2,q))\\
&\quad-3q^2B_1^{\mathcal{V}}(m_{Y\mathcal{S}}^2,m_{Y\mathcal{S}}^2,q)B_1^{\mathcal{V}}(m_{X\mathcal{S}}^2,m_{X\mathcal{S}}^2,q)\\
&\quad+q^2B^{\mathcal{V}}(m_{Y\mathcal{S}}^2,m_{Y\mathcal{S}}^2,q)\times(B_1^{\mathcal{V}}(m_{X\mathcal{S}}^2,m_{X\mathcal{S}}^2,q) + \frac{1}{4}B^{\mathcal{V}}(m_{XY}^2,m_{XY}^2,q))\\
&\quad+q^2B^{\mathcal{V}}(m_{X\mathcal{S}}^2,m_{X\mathcal{S}}^2,q)\times(B_1^{\mathcal{V}}(m_{Y\mathcal{S}}^2,m_{Y\mathcal{S}}^2,q) + \frac{1}{4}B^{\mathcal{V}}(m_{XY}^2,m_{XY}^2,q))\\
&\quad-\frac{1}{2}q^2B^{\mathcal{V}}(m_{Y\mathcal{S}}^2,m_{Y\mathcal{S}}^2,q)B^{\mathcal{V}}(m_{X\mathcal{S}}^2,m_{X\mathcal{S}}^2,q) - 8A^{\mathcal{V}}(m_{XY}^2)(L_9^r + L_{10}^r)
\end{aligned}$$

$$
\begin{aligned}
&F_0^2\Pi_{1XY}^{\mathcal{V}(6)} = \\
&8m_{XY}^2(B_{22}^{\mathcal{V}}(m_{XY}^2,(m_{XY}^2)^2,q) - \frac{1}{4}A^{\mathcal{V}}((m_{XY}^2)^2)) \\
&\times(-16m_{\mathcal{SS}}^2L_6^r + 8m_{\mathcal{SS}}^2L_4^r - A^{\mathcal{V}}(\mathcal{D}_{XY}) - 16m_{XY}^2L_8^r + 8m_{XY}^2L_5^r) \\
&+2(A^{\mathcal{V}}(m_{X\mathcal{S}}^2) - A^{\mathcal{V}}(m_{XY}^2)) \times B_{22}^{\mathcal{V}}(m_{Y\mathcal{S}}^2,m_{Y\mathcal{S}}^2,q) \\
&+2(A^{\mathcal{V}}(m_{Y\mathcal{S}}^2) - A^{\mathcal{V}}(m_{XY}^2)) \times B_{22}^{\mathcal{V}}(m_{X\mathcal{S}}^2,m_{X\mathcal{S}}^2,q) \\
&+(A^{\mathcal{V}}(m_{X\mathcal{S}}^2) + A^{\mathcal{V}}(m_{Y\mathcal{S}}^2)) \times(-2B_{22}^{\mathcal{V}}(m_{XY}^2,m_{XY}^2,q) + A^{\mathcal{V}}(m_{XY}^2)) \\
&+4(B_{22}^{\mathcal{V}}(m_{X\mathcal{S}}^2,m_{X\mathcal{S}}^2,q)B_{22}^{\mathcal{V}}(m_{XY}^2,m_{XY}^2,q) + B_{22}^{\mathcal{V}}(m_{Y\mathcal{S}}^2,m_{Y\mathcal{S}}^2,q)B_{22}^{\mathcal{V}}(m_{XY}^2,m_{XY}^2,q) \\
&\quad - B_{22}^{\mathcal{V}}(m_{Y\mathcal{S}}^2,m_{Y\mathcal{S}}^2,q)B_{22}^{\mathcal{V}}(m_{X\mathcal{S}}^2,m_{X\mathcal{S}}^2,q)) \\
&-A^{\mathcal{V}}(m_{Y\mathcal{S}}^2)A^{\mathcal{V}}(m_{X\mathcal{S}}^2) \\
&-16B_{22}^{\mathcal{V}}(m_{XY}^2,m_{XY}^2,q)L_9^rq^2 - 8A^{\mathcal{V}}(m_{XY}^2)L_{10}^rq^2
\end{aligned}
\tag{59}
$$

$$
\begin{aligned}
&F_0^2\Pi_{2XY}^{\mathcal{V}(6)\mu\nu} = \\
&-4(B_{22}^{\mathcal{V}}(m_{XY}^2,m_{XY}^2,q) - \frac{1}{2}A^{\mathcal{V}}(m_{XY}^2)) \times(B_{23}^{\mathcal{V}\mu\nu}(m_{X\mathcal{S}}^2,m_{X\mathcal{S}}^2,q) + B_{23}^{\mathcal{V}\mu\nu}(m_{Y\mathcal{S}}^2,m_{Y\mathcal{S}}^2,q)) \\
&-4(B_{22}^{\mathcal{V}}(m_{X\mathcal{S}}^2,m_{X\mathcal{S}}^2,q) - \frac{1}{2}A^{\mathcal{V}}(m_{X\mathcal{S}}^2)) \times(B_{23}^{\mathcal{V}\mu\nu}(m_{XY}^2,m_{XY}^2,q) - B_{23}^{\mathcal{V}\mu\nu}(m_{Y\mathcal{S}}^2,m_{Y\mathcal{S}}^2,q)) \\
&-4(B_{22}^{\mathcal{V}}(m_{Y\mathcal{S}}^2,m_{Y\mathcal{S}}^2,q) - \frac{1}{2}A^{\mathcal{V}}(m_{Y\mathcal{S}}^2)) \times(B_{23}^{\mathcal{V}\mu\nu}(m_{XY}^2,m_{XY}^2,q) - B_{23}^{\mathcal{V}\mu\nu}(m_{X\mathcal{S}}^2,m_{X\mathcal{S}}^2,q)) \\
&+16q^2L_9^rB_{23}^{\mathcal{V}\mu\nu}(m_{XY}^2,m_{XY}^2,q) \\
&+8m_{XY}^2B_{23}^{\mathcal{V}\mu\nu}(m_{XY}^2,(m_{XY}^2)^2,q) \\
&\times(16m_{\mathcal{SS}}^2L_6^r - 8m_{\mathcal{SS}}^2L_4^r + A^{\mathcal{V}}(\mathcal{D}_{XY}) + 16m_{XY}^2L_8^r - 8m_{XY}^2L_5^r) \\
&-4B_{23}^{\mathcal{V}\beta\mu}(m_{X\mathcal{S}}^2,m_{X\mathcal{S}}^2,q)B_{23}^{\mathcal{V}\beta\nu}(m_{XY}^2,m_{XY}^2,q) \\
&-4B_{23}^{\mathcal{V}\beta\nu}(m_{Y\mathcal{S}}^2,m_{Y\mathcal{S}}^2,q)B_{23}^{\mathcal{V}\beta\mu}(m_{XY}^2,m_{XY}^2,q) \\
&+4B_{23}^{\mathcal{V}\beta\mu}(m_{X\mathcal{S}}^2,m_{X\mathcal{S}}^2,q)B_{23}^{\mathcal{V}\beta\nu}(m_{Y\mathcal{S}}^2,m_{Y\mathcal{S}}^2,q)
\end{aligned}
\tag{60}
$$

B.2 $\Pi_{\pi_v^+}^{\mathcal{V}\mu\nu}$ at p^6

$$
\begin{aligned}
&F_0^2\Pi_{0\pi_v^+}^{\mathcal{V}(6)} = \\
&2(A^{\mathcal{V}}(m_{xx}^2) - A^{\mathcal{V}}(m_{xy}^2)) \\
&\times(-m_{xx}^2B^{\mathcal{V}}((m_{xx}^2)^2,m_{xy}^2,q) + 4m_{xx}^2B_1^{\mathcal{V}}((m_{xx}^2)^2,m_{xy}^2,q) \\
&\quad - 4m_{xx}^2B_{21}^{\mathcal{V}}((m_{xx}^2)^2,m_{xy}^2,q) - B^{\mathcal{V}}(m_{xx}^2,m_{xy}^2,q) + 2B_1^{\mathcal{V}}(m_{xx}^2,m_{xy}^2,q)) \\
&+m_{\mathcal{S}x}^2(B^{\mathcal{V}}(m_{x\mathcal{S}}^2,(m_{\mathcal{S}y}^2)^2,q) + B^{\mathcal{V}}((m_{x\mathcal{S}}^2)^2,m_{\mathcal{S}y}^2,q) - 4B_1^{\mathcal{V}}(m_{x\mathcal{S}}^2,(m_{\mathcal{S}y}^2)^2,q)
\end{aligned}
\tag{61}
$$

$$
\begin{aligned}
&- 4B_1^{\mathcal{V}}((m_{x\mathcal{S}}^2)^2, m_{\mathcal{S}y}^2, q) + 4B_{21}^{\mathcal{V}}(m_{x\mathcal{S}}^2, (m_{\mathcal{S}y}^2)^2, q) + 4B_{21}^{\mathcal{V}}((m_{x\mathcal{S}}^2)^2, m_{\mathcal{S}y}^2, q)) \\
&\times (-16m_{\mathcal{S}'\mathcal{S}'}^2 L_6^r + 8m_{\mathcal{S}'\mathcal{S}'}^2 L_4^r - 16m_{\mathcal{S}x}^2 L_8^r + 8m_{\mathcal{S}x}^2 L_5^r - A^{\mathcal{V}}(\mathcal{D}_{x\mathcal{S}})) \\
&+ 4(A^{\mathcal{V}}(m_{x\mathcal{S}}^2) + A^{\mathcal{V}}(m_{y\mathcal{S}}^2)) \times ((L_{10}^r + L_9^r) + \frac{1}{8}B^{\mathcal{V}}(m_{x\mathcal{S}'}^2, m_{\mathcal{S}'y}^2, q)) \\
&+ B_{2\beta}^{\mathcal{V}}(m_{x\mathcal{S}}^2, m_{\mathcal{S}y}^2, q) \\
&\times (B_2^{\mathcal{V}\beta}(m_{x\mathcal{S}'}^2, m_{\mathcal{S}'y}^2, q) + 2q^\beta B_1^{\mathcal{V}}(m_{x\mathcal{S}'}^2, m_{\mathcal{S}'y}^2, q) - 4q^\beta B_{21}^{\mathcal{V}}(m_{x\mathcal{S}'}^2, m_{\mathcal{S}'y}^2, q)) \\
&+ B_{2\beta}^{\mathcal{V}}(m_{x\mathcal{S}'}^2, (m_{\mathcal{S}'y}^2)^2, q) \times (A^{\mathcal{V}\beta}(m_{y\mathcal{S}}^2) - A^{\mathcal{V}\beta}(m_{\mathcal{S}'\mathcal{S}}^2)) \\
&+ B_{2\beta}^{\mathcal{V}}((m_{x\mathcal{S}'}^2)^2, m_{\mathcal{S}'y}^2, q) \times (A^{\mathcal{V}\beta}(m_{x\mathcal{S}}^2) - A^{\mathcal{V}\beta}(m_{\mathcal{S}'\mathcal{S}}^2)) \\
&- 4q^\beta(A_\beta^{\mathcal{V}}(m_{x\mathcal{S}}^2) - A_\beta^{\mathcal{V}}(m_{\mathcal{S}'\mathcal{S}}^2)) \times (B_{21}^{\mathcal{V}}((m_{x\mathcal{S}'}^2)^2, m_{\mathcal{S}'y}^2, q) - B_{31}^{\mathcal{V}}((m_{x\mathcal{S}'}^2)^2, m_{\mathcal{S}'y}^2, q)) \\
&- 4q^\beta(A_\beta^{\mathcal{V}}(m_{y\mathcal{S}}^2) - A_\beta^{\mathcal{V}}(m_{\mathcal{S}'\mathcal{S}}^2)) \times (2B_{21}^{\mathcal{V}}(m_{x\mathcal{S}'}^2, (m_{\mathcal{S}'y}^2)^2, q) - B_{31}^{\mathcal{V}}(m_{x\mathcal{S}'}^2, (m_{\mathcal{S}'y}^2)^2, q)) \\
&+ (q^2 - 2m_{xx}^2)(B^{\mathcal{V}}(m_{xx}^2, m_{xy}^2, q) - 2B_1^{\mathcal{V}}(m_{xx}^2, m_{xy}^2, q))^2 \\
&+ 2B_{21}^{\mathcal{V}}(m_{x\mathcal{S}}^2, m_{\mathcal{S}y}^2, q) \\
&\times (-8L_9^r q^2 + 4q^2 B_1^{\mathcal{V}}(m_{x\mathcal{S}'}^2, m_{\mathcal{S}'y}^2, q) - A^{\mathcal{V}}(m_{x\mathcal{S}'}^2) + A^{\mathcal{V}}(m_{y\mathcal{S}'}^2) - 2q^2 B_{21}^{\mathcal{V}}(m_{x\mathcal{S}'}^2, m_{\mathcal{S}'y}^2, q)) \\
&+ q^2 B_1^{\mathcal{V}}(m_{x\mathcal{S}}^2, m_{\mathcal{S}y}^2, q) \times (16L_9^r + 2B^{\mathcal{V}}(m_{x\mathcal{S}'}^2, m_{\mathcal{S}'y}^2, q) - 3B_1^{\mathcal{V}}(m_{x\mathcal{S}}^2, m_{\mathcal{S}y}^2, q)) \\
&+ 5q^\beta B_1^{\mathcal{V}}(m_{x\mathcal{S}'}^2, (m_{\mathcal{S}'y}^2)^2, q) \times (A_\beta^{\mathcal{V}}(m_{y\mathcal{S}}^2) - A_\beta^{\mathcal{V}}(m_{\mathcal{S}'\mathcal{S}}^2)) \\
&+ q^\beta B_1^{\mathcal{V}}((m_{x\mathcal{S}'}^2)^2, m_{\mathcal{S}'y}^2, q) \times (A_\beta^{\mathcal{V}}(m_{x\mathcal{S}}^2) - A_\beta^{\mathcal{V}}(m_{\mathcal{S}'\mathcal{S}}^2)) \\
&- B^{\mathcal{V}}(m_{x\mathcal{S}}^2, m_{\mathcal{S}y}^2, q) \times (4L_9^r q^2 + A^{\mathcal{V}}(m_{y\mathcal{S}'}^2) + \frac{q^2}{2}B^{\mathcal{V}}(m_{x\mathcal{S}'}^2, m_{\mathcal{S}'y}^2, q)) \\
&- q^\beta B^{\mathcal{V}}(m_{x\mathcal{S}'}^2, (m_{\mathcal{S}'y}^2)^2, q) \times (A_\beta^{\mathcal{V}}(m_{y\mathcal{S}}^2) - A_\beta^{\mathcal{V}}(m_{\mathcal{S}'\mathcal{S}}^2))
\end{aligned}
$$

$$
\begin{aligned}
&F_0^2 \Pi_{1\pi_v^+}^{\mathcal{V}(6)} = \qquad (62) \\
&+ (A^{\mathcal{V}}(m_{xx}^2) - A^{\mathcal{V}}(m_{xy}^2)) \\
&\times (8m_{xx}^2 B_{22}^{\mathcal{V}}((m_{xx}^2)^2, m_{xy}^2, q) - 2m_{xx}^2 A^{\mathcal{V}}((m_{xx}^2)^2) + A^{\mathcal{V}}(m_{xy}^2) - A^{\mathcal{V}}(m_{xx}^2)) \\
&+ 4m_{\mathcal{S}x}^2(B_{22}^{\mathcal{V}}(m_{x\mathcal{S}}^2, (m_{\mathcal{S}y}^2)^2, q) + B_{22}^{\mathcal{V}}((m_{x\mathcal{S}}^2)^2, m_{\mathcal{S}y}^2, q) \\
&\quad - \frac{1}{4}A^{\mathcal{V}}((m_{x\mathcal{S}}^2)^2) - \frac{1}{4}A^{\mathcal{V}}((m_{y\mathcal{S}}^2)^2)) \\
&\times (16m_{\mathcal{S}'\mathcal{S}'}^2 L_6^r - 8m_{\mathcal{S}'\mathcal{S}'}^2 L_4^r + 16m_{\mathcal{S}x}^2 L_8^r - 8m_{\mathcal{S}x}^2 L_5^r + A^{\mathcal{V}}(\mathcal{D}_{x\mathcal{S}})) \\
&+ 4L_{10}^r q^2 (A^{\mathcal{V}}(m_{x\mathcal{S}}^2) + A^{\mathcal{V}}(m_{y\mathcal{S}}^2) \\
&- 4q^\beta(A_\beta^{\mathcal{V}}(m_{x\mathcal{S}}^2) - A_\beta^{\mathcal{V}}(m_{\mathcal{S}'\mathcal{S}}^2))B_{32}^{\mathcal{V}}((m_{x\mathcal{S}'}^2)^2, m_{\mathcal{S}'y}^2, q) \\
&+ 4q^\beta(A_\beta^{\mathcal{V}}(m_{y\mathcal{S}}^2) - A_\beta^{\mathcal{V}}(m_{\mathcal{S}'\mathcal{S}}^2)) \times (B_{22}^{\mathcal{V}}(m_{x\mathcal{S}'}^2, (m_{\mathcal{S}'y}^2)^2, q) - B_{32}^{\mathcal{V}}(m_{x\mathcal{S}'}^2, (m_{\mathcal{S}'y}^2)^2, q)) \\
&+ 2B_{22}^{\mathcal{V}}(m_{x\mathcal{S}}^2, m_{\mathcal{S}y}^2, q) \times (8L_9^r q^2 + A^{\mathcal{V}}(m_{x\mathcal{S}'}^2) + A^{\mathcal{V}}(m_{y\mathcal{S}'}^2) - 2B_{22}^{\mathcal{V}}(m_{x\mathcal{S}'}^2, m_{\mathcal{S}'y}^2, q)) \\
&- 8L_9^r q^\beta(A_\beta^{\mathcal{V}}(m_{x\mathcal{S}}^2) - A_\beta^{\mathcal{V}}(m_{y\mathcal{S}}^2)) - A^{\mathcal{V}}(m_{y\mathcal{S}}^2)A^{\mathcal{V}}(m_{x\mathcal{S}'}^2) \\
&+ A^{\mathcal{V}\beta}((m_{x\mathcal{S}'}^2)^2) \times (A_\beta^{\mathcal{V}}(m_{x\mathcal{S}}^2) - A_\beta^{\mathcal{V}}(m_{\mathcal{S}'\mathcal{S}}^2)) \\
&+ A^{\mathcal{V}\beta}((m_{y\mathcal{S}'}^2)^2) \times (A_\beta^{\mathcal{V}}(m_{y\mathcal{S}}^2) - A_\beta^{\mathcal{V}}(m_{\mathcal{S}'\mathcal{S}}^2))
\end{aligned}
$$

$$
\begin{aligned}
&F_0^2\Pi^{\mathcal{V}(6)\mu\nu}_{2\pi_v^+} = \qquad (63)\\
&2(A^{\mathcal{V}}(m_{xx}^2) - A^{\mathcal{V}}(m_{xy}^2))\\
&\times (2m_{xx}^2 q^\mu B_2^{\mathcal{V}\nu}((m_{xx}^2)^2, m_{xy}^2, q) + q^\mu B_2^{\mathcal{V}\nu}(m_{xx}^2, m_{xy}^2, q)\\
&\quad - m_{xx}^2 B_{23}^{\mathcal{V}\mu\nu}((m_{xx}^2)^2, m_{xy}^2, q) + (\mu \leftrightarrow \nu))\\
&- 2m_{\mathcal{S}x}^2(+B_2^{\mathcal{V}\nu}(m_{x\mathcal{S}}^2, (m_{\mathcal{S}y}^2)^2, q)q^\mu + B_2^{\mathcal{V}\nu}((m_{x\mathcal{S}}^2)^2, m_{\mathcal{S}y}^2, q)q^\mu\\
&\ - B_{23}^{\mathcal{V}\mu\nu}(m_{x\mathcal{S}}^2, (m_{\mathcal{S}y}^2)^2, q) - B_{23}^{\mathcal{V}\mu\nu}((m_{x\mathcal{S}}^2)^2, m_{\mathcal{S}y}^2, q) + (\mu \leftrightarrow \nu))\\
&\times (-16m_{\mathcal{S}'\mathcal{S}'}^2 L_6^r + 8m_{\mathcal{S}'\mathcal{S}'}^2 L_4^r - 16m_{\mathcal{S}x}^2 L_8^r + 8m_{\mathcal{S}x}^2 L_5^r - A^{\mathcal{V}}(\mathcal{D}_{x\mathcal{S}})\\
&+ (A^{\mathcal{V}\beta}(m_{y\mathcal{S}}^2) - A^{\mathcal{V}\beta}(m_{\mathcal{S}'\mathcal{S}}^2))\\
&\times (\delta_\beta^\nu q^\mu B^{\mathcal{V}}(m_{x\mathcal{S}'}^2, m_{\mathcal{S}'y}^2, q) - 3\delta_\beta^\nu q^\mu B_1^{\mathcal{V}}(m_{x\mathcal{S}'}^2, m_{\mathcal{S}'y}^2, q) + 8\delta_\beta^\nu q^\mu L_9^r\\
&\quad + 2\delta_\beta^\nu q^\mu B_{21}^{\mathcal{V}}(m_{x\mathcal{S}'}^2, m_{\mathcal{S}'y}^2, q) - \delta_\beta^\nu B_2^{\mathcal{V}\mu}(m_{x\mathcal{S}'}^2, m_{\mathcal{S}'y}^2, q) - 2\delta_\beta^\nu q^\mu B_{22}^{\mathcal{V}}(m_{x\mathcal{S}'}^2, (m_{\mathcal{S}'y}^2)^2, q)\\
&\quad + 4\delta_\beta^\nu B_{32}^{\mathcal{V}}(m_{x\mathcal{S}'}^2, (m_{\mathcal{S}'y}^2)^2, q)q^\mu + 2q^\beta B_{23}^{\mathcal{V}\mu\nu}(m_{x\mathcal{S}'}^2, (m_{\mathcal{S}'y}^2)^2, q)\\
&\quad - 2q^\mu B_{23\beta}^{\mathcal{V}\nu}(m_{x\mathcal{S}'}^2, (m_{\mathcal{S}'y}^2)^2, q) + 2B_{33\beta}^{\mathcal{V}\nu\mu}(m_{x\mathcal{S}'}^2, (m_{\mathcal{S}'y}^2)^2, q) + (\mu \leftrightarrow \nu))\\
&+ (A^{\mathcal{V}\beta}(m_{x\mathcal{S}}^2) - A^{\mathcal{V}\beta}(m_{\mathcal{S}'\mathcal{S}}^2))\\
&\times (\delta_\beta^\nu q^\mu B_1^{\mathcal{V}}(m_{x\mathcal{S}'}^2, m_{\mathcal{S}'y}^2, q) - 2\delta_\beta^\nu q^\mu B_{21}^{\mathcal{V}}(m_{x\mathcal{S}'}^2, m_{\mathcal{S}'y}^2, q) - 8\delta_\beta^\nu q^\mu L_9^r\\
&\quad - 2\delta_\beta^\nu B_{22}^{\mathcal{V}}((m_{x\mathcal{S}'}^2)^2, m_{\mathcal{S}'y}^2, q)q^\mu + 4\delta_\beta^\nu q^\mu B_{32}^{\mathcal{V}}((m_{x\mathcal{S}'}^2)^2, m_{\mathcal{S}'y}^2, q)\\
&\quad - 2B_{23\beta}^{\mathcal{V}\nu}((m_{x\mathcal{S}'}^2)^2, m_{\mathcal{S}'y}^2, q)q^\mu + 2B_{33\beta}^{\mathcal{V}\nu\mu,}((m_{x\mathcal{S}'}^2)^2, m_{\mathcal{S}'y}^2, q) + (\mu \leftrightarrow \nu))\\
&+ (A_\mu^{\mathcal{V}}(m_{x\mathcal{S}}^2) - A_\mu^{\mathcal{V}}(m_{\mathcal{S}'\mathcal{S}}^2))\\
&\times (B_1^{\mathcal{V}}(m_{x\mathcal{S}'}^2, m_{\mathcal{S}'y}^2, q)q^\nu - 2B_{21}^{\mathcal{V}}(m_{x\mathcal{S}'}^2, m_{\mathcal{S}'y}^2, q)q^\nu - 8q^\nu L_9^r)\\
&+ 4B_{23}^{\mathcal{V}\beta\mu}(m_{x\mathcal{S}'}^2, m_{\mathcal{S}'y}^2, q)B_{23}^{\mathcal{V}\beta\nu}(m_{x\mathcal{S}}^2, m_{\mathcal{S}y}^2, q)\\
&+ B_{23}^{\mathcal{V}\mu\nu}(m_{x\mathcal{S}}^2, m_{\mathcal{S}y}^2, q)\\
&\times (8B_{22}^{\mathcal{V}}(m_{x\mathcal{S}'}^2, m_{\mathcal{S}'y}^2, q) - 2A^{\mathcal{V}}(m_{x\mathcal{S}'}^2) - 2A^{\mathcal{V}}(m_{y\mathcal{S}'}^2) - 16L_9^r q^2)\\
&- 2(B_{23}^{\mathcal{V}\beta\nu}(m_{x\mathcal{S}}^2, m_{\mathcal{S}y}^2, q)B_{2\beta}^{\mathcal{V}}(m_{x\mathcal{S}'}^2, m_{\mathcal{S}'y}^2, q)q^\mu + (\mu \leftrightarrow \nu))\\
&+ 2q^\alpha B_{2\beta}^{\mathcal{V}}(m_{x\mathcal{S}}^2, (m_{\mathcal{S}y}^2)^2, q)\\
&\times (\delta_\beta^\nu q^\mu A_\alpha^{\mathcal{V}}(m_{y\mathcal{S}'}^2) - \delta_\beta^\nu q^\mu A_\alpha^{\mathcal{V}}(m_{\mathcal{S}\mathcal{S}'}^2) + (\mu \leftrightarrow \nu))\\
&+ B_{2\beta}^{\mathcal{V}}(m_{x\mathcal{S}}^2, m_{\mathcal{S}y}^2, q)\\
&\times (-B_2^{\mathcal{V}\mu}(m_{x\mathcal{S}'}^2, m_{\mathcal{S}'y}^2, q)\delta_\beta^\nu q^2 + \delta_\beta^\nu B^{\mathcal{V}}(m_{x\mathcal{S}'}^2, m_{\mathcal{S}'y}^2, q)q^\mu q^2\\
&\quad - 3\delta_\beta^\nu B_1^{\mathcal{V}}(m_{x\mathcal{S}'}^2, m_{\mathcal{S}'y}^2, q)q^\mu q^2 + 2\delta_\beta^\nu B_{21}^{\mathcal{V}}(m_{x\mathcal{S}'}^2, m_{\mathcal{S}'y}^2, q)q^\mu q^2\\
&\quad - 2\delta_\beta^\nu B_{22}^{\mathcal{V}}(m_{x\mathcal{S}'}^2, m_{\mathcal{S}'y}^2, q)q^\mu + \delta_\beta^\nu A^{\mathcal{V}}(m_{y\mathcal{S}'}^2)q^\mu - \delta_\beta^\nu A^{\mathcal{V}\mu}(m_{y\mathcal{S}'}^2)\\
&\quad + \delta_\beta^\nu A_\mu^{\mathcal{V}}(m_{\mathcal{S}\mathcal{S}'}^2) + 8\delta_\beta^\nu q^\mu L_9^r q^2 + (\mu \leftrightarrow \nu))\\
&+ 2B_{2\beta}^{\mathcal{V}}(m_{xx}^2, m_{xy}^2, q)(q^2 - 2m_{xx}^2)\\
&\times (\delta_\beta^\nu B_2^{\mathcal{V}\mu}(m_{xx}^2, m_{xy}^2, q) + 2\delta_\beta^\nu q^\mu B_1^{\mathcal{V}}(m_{xx}^2, m_{xy}^2, q) - q^\mu B^{\mathcal{V}}(m_{xx}^2, m_{xy}^2, q) + (\mu \leftrightarrow \nu))
\end{aligned}
$$

B.3 $\langle \bar{q}\gamma^\mu q\rangle^{\mathcal{V}}$ at p^6

$$
\begin{aligned}
&\langle \bar{q}\gamma^\mu q\rangle^{\mathcal{V}(6)} = \\
&A^{\mathcal{V}\mu}(m^2_{q\mathcal{S}})\left(A^{\mathcal{V}}(m^2_{q\mathcal{S}'}) - 2A^{\mathcal{V}}_{22}((m^2_{q\mathcal{S}'})^2)\right) \\
&+ 2m^2_{q\mathcal{S}}A^{\mathcal{V}\mu}((m^2_{q\mathcal{S}})^2)(16m_{\mathcal{S}'\mathcal{S}'}L^r_6 - 8m_{\mathcal{S}'\mathcal{S}'}L^r_4 + A^{\mathcal{V}}(\mathcal{D}_{q\mathcal{S}}) + 16m^2_{q\mathcal{S}}L^r_8 - 8m^2_{q\mathcal{S}}L^r_5) \\
&- A^{\mathcal{V}\mu}(m_{\mathcal{S}\mathcal{S}'})\left(A^{\mathcal{V}}(m^2_{q\mathcal{S}}) - 2A^{\mathcal{V}}_{22}((m^2_{q\mathcal{S}})^2)\right) \\
&- 2A^{\mathcal{V}\beta\mu}_{23}((m^2_{q\mathcal{S}'})^2)\left(A^{\mathcal{V}}_\beta(m^2_{q\mathcal{S}}) - A^{\mathcal{V}}_\beta(m_{\mathcal{S}'\mathcal{S}})\right)
\end{aligned}
\tag{64}
$$

References

[1] G. W. Bennett *et al.* [Muon g-2 Collaboration], Phys. Rev. Lett. **89** (2002) 101804 [Erratum-ibid. **89** (2002) 129903] [hep-ex/0208001].

[2] G. W. Bennett *et al.* [Muon g-2 Collaboration], Phys. Rev. Lett. **92** (2004) 161802 [hep-ex/0401008].

[3] G. W. Bennett *et al.* [Muon G-2 Collaboration], Phys. Rev. D **73** (2006) 072003 [hep-ex/0602035].

[4] J. Beringer *et al.* [Particle Data Group Collaboration], Phys. Rev. D **86** (2012) 010001.

[5] F. Jegerlehner and A. Nyffeler, Phys. Rept. **477** (2009) 1 [arXiv:0902.3360 [hep-ph]].

[6] G. D'Ambrosio, M. Iacovacci, M. Passera, G. Venanzoni, P. Massarotti and S. Mastroianni, EPJ Web Conf. **118** (2016).

[7] R. M. Carey, K. R. Lynch, J. P. Miller, B. L. Roberts, W. M. Morse, Y. K. Semertzides, V. P. Druzhinin and B. I. Khazin *et al.*, FERMILAB-PROPOSAL-0989.

[8] H. Iinuma [J-PARC New g-2/EDM experiment Collaboration], J. Phys. Conf. Ser. **295** (2011) 012032.

[9] T. P. Gorringe and D. W. Hertzog, Prog. Part. Nucl. Phys. **84** (2015) 73 [arXiv:1506.01465 [hep-ex]].

[10] C. M. Carloni Calame, M. Passera, L. Trentadue and G. Venanzoni, Phys. Lett. B **746** (2015) 325 [arXiv:1504.02228 [hep-ph]].

[11] T. Blum, Phys. Rev. Lett. **91** (2003) 052001 [hep-lat/0212018].

[12] M. Della Morte, B. Jager, A. Juttner and H. Wittig, JHEP **1203** (2012) 055 [arXiv:1112.2894 [hep-lat]].

[13] M. Della Morte and A. Juttner, JHEP **1011** (2010) 154 [arXiv:1009.3783 [hep-lat]].

[14] A. Juttner and M. Della Morte, PoS LAT **2009** (2009) 143 [arXiv:0910.3755 [hep-lat]].

[15] C. Aubin, T. Blum, M. Golterman and S. Peris, Phys. Rev. D **88** (2013) no.7, 074505 [arXiv:1307.4701 [hep-lat]].

[16] D. Bernecker and H. B. Meyer, Eur. Phys. J. A **47** (2011) 148 [arXiv:1107.4388 [hep-lat]].

[17] T. Blum *et al.* [RBC/UKQCD Collaboration], JHEP **1604** (2016) 063 [arXiv:1602.01767 [hep-lat]].

[18] J. Bijnens and J. Relefors, JHEP **1405** (2014) 015 [arXiv:1402.1385 [hep-lat]].

[19] G. Bali and G. Endrődi, Phys. Rev. D **92** (2015) no.5, 054506 [arXiv:1506.08638 [hep-lat]].

[20] X. Feng, S. Hashimoto, G. Hotzel, K. Jansen, M. Petschlies and D. B. Renner, Phys. Rev. D **88** (2013) 034505 [arXiv:1305.5878 [hep-lat]].

[21] B. Chakraborty *et al.* [HPQCD Collaboration], Phys. Rev. D **89** (2014) no.11, 114501 doi:10.1103/PhysRevD.89.114501 [arXiv:1403.1778 [hep-lat]].

[22] E. de Rafael, Phys. Lett. B **736** (2014) 522 [arXiv:1406.4671 [hep-lat]].

[23] C. A. Dominguez, K. Schilcher and H. Spiesberger, arXiv:1605.07903 [hep-ph].

[24] S. Bodenstein, C. A. Dominguez, K. Schilcher and H. Spiesberger, Phys. Rev. D **88** (2013) 014005 [arXiv:1302.1735 [hep-ph]].

[25] M. Golterman, K. Maltman and S. Peris, Phys. Rev. D **90** (2014) 074508 [arXiv:1405.2389 [hep-lat]].

[26] H. Wittig, *plenary talk at lattice 2016.*

[27] C. Aubin, T. Blum, P. Chau, M. Golterman, S. Peris and C. Tu, Phys. Rev. D **93** (2016) 054508 [arXiv:1512.07555 [hep-lat]].

[28] J. Bijnens and J. Relefors, arXiv:1609.01573 [hep-lat].

[29] S. Weinberg, Physica A **96** (1979) 327.

[30] J. Gasser and H. Leutwyler, Annals Phys. **158** (1984) 142.

[31] J. Gasser and H. Leutwyler, Nucl. Phys. B **250** (1985) 465.

[32] S. R. Sharpe and N. Shoresh, Phys. Rev. D **64** (2001) 114510 [hep-lat/0108003].

[33] S. R. Sharpe, Phys. Rev. D **41** (1990) 3233. doi:10.1103/PhysRevD.41.3233

[34] S. R. Sharpe, Phys. Rev. D **46** (1992) 3146 [hep-lat/9205020].

[35] C. W. Bernard and M. F. L. Golterman, Phys. Rev. D **46** (1992) 853 doi:10.1103/PhysRevD.46.853 [hep-lat/9204007].

[36] J. Bijnens, G. Colangelo and G. Ecker, JHEP **9902** (1999) 020 [arXiv:hep-ph/9902437].

[37] J. Bijnens, G. Colangelo and G. Ecker, Annals Phys. **280** (2000) 100 [arXiv:hep-ph/9907333].

[38] C. Aubin and C. Bernard, Phys. Rev. D **68** (2003) 034014 [hep-lat/0304014].

[39] C. T. Sachrajda and G. Villadoro, Phys. Lett. B **609** (2005) 73 [hep-lat/0411033].

[40] J. Bijnens and G. Ecker, Ann. Rev. Nucl. Part. Sci. **64** (2014) 149 [arXiv:1405.6488 [hep-ph]].

[41] J. Bijnens and K. Ghorbani, Phys. Lett. B **636** (2006) 51 [hep-lat/0602019].

[42] A. Bussone, M. Della Morte, M. Hansen and C. Pica, arXiv:1609.00210 [hep-lat].

[43] J. Bijnens and P. Talavera, JHEP **0203** (2002) 046 [hep-ph/0203049].

[44] J. Bijnens, E. Boström and T. A. Lähde, JHEP **1401** (2014) 019 [arXiv:1311.3531 [hep-lat]].